THE DEVELOPMENT OF A NARROW-SLOT LARGE SCALE ELECTROPHORETIC SEPARATOR

A THESIS PRESENTED FOR THE
DEGREE OF DOCTOR OF PHILOSOPHY
IN CHEMICAL ENGINEERING
IN THE
UNIVERSITY OF CANTERBURY

by

S.R. VAUGHAN

1980

ACKNOWLEDGEMENTS

I would like to thank my supervisor Professor Roger Keey for his thoughtful guidance of this project. Roger's ability to stand back and see the bigger picture has been of immense help on the occasions when the work was becoming bogged down in detail. His readiness to discuss and analyse matters at short and irregular notice has been of tremendous value.

I would also like to especially thank Mr Colin Campbell, without whose extraordinary skill and patience this project would never have become a working reality. Other members of the Department of Chemical Engineering technical staff have also been of assistance from time to time and their help in finding solutions to peculiar problems, often at very short notice, is gratefully acknowledged. In particular I would like to thank Messrs Gordon Gray and Warrick Earl for their work on the electronics for this project. Numerous staff and postgraduate students from this and other departments have contributed suggestions for this work and these comments have been greatly appreciated.

My parents, while not always understanding what was going on, have given great moral support throughout this work and this has been a great strength to me. I would also like to thank the Principal and staff of Christchurch College, where, during the latter part of this work I was Senior Tutor, for putting up with my sometimes peculiar working hours.

The financial assistance of the Medical Research Council of New Zealand in the form of a postgraduate scholarship is gratefully acknowledged, as is the funding for materials and

equipment provided by the University Grants Committee. I would also like to thank Professor A.M. Kennedy for finding additional funds to keep this work going.

Last, but by no means least, I wish to thank Mrs Christine McEntee for doing such a superb job of typing this thesis.

CONTENTS

LIST OF FIGURES

LIST OF PLATES

ABSTRACT

This study investigates the concept of a narrow-slot electrophoretic separator from both the theoretical and practical standpoints. The study develops a theoretical model for mass transfer in a narrow-slot electrophoretic separator by use of the differential balance equations and the theory of electrokinetic processes. A numerical solution technique is evolved for the differential equation resulting from these theoretical considerations and the expected concentration profiles in a narrow-slot separator are presented.

These solutions, combined with studies of hydrodynamic, thermal and electrical stability criteria for flow in the narrow-slot separator are used as a basis for the design and development of a prototype narrow-slot electrophoretic separator of commercial scale (throughput of order between 10^{-5} and 10^{-6} kg s^{-1}). While further development remains to be done on this device, particularly with regard to the selection of membrane materials; qualitative agreement between the theory and operation of the narrow-slot cell for single solutes has been obtained.

CHAPTER 1: INTRODUCTION

1.1 Background and Scope

1.1.1 The Purification of Biological Materials

Continuing advances in fields as diverse as medical science, industrial chemical synthesis, vaccine production, biochemical research, treatment of wastes and production of fuel from biomass have led to steadily increasing demands for larger quantities of biologically active and bio-synthesised substances. As a topical example, the drug inferon is produced in a culture containing considerable cellular and protein material, of which most must be removed in order to produce a final product of high activity (W1). A more extensive list of potential separations of cellular material is given by Vanderhoff and Van Oss (V1).

In New Zealand's situation of high productivity of animal- and plant-derived products and long distances from markets, the production of high-purity biochemicals makes sense. For instance, while in the longer term insulin production will probably use tailored micro-organisms, in the near future the New Zealand meat industry will provide an attractive source of animal derived insulin. Presently the processing of pancreas to remove insulin is done outside New Zealand. The advantages of local processing of such substances increase directly with the increased cost of transport fuel. Further to this, Vanderhoff and Van Oss point out that the insulin-producing micro-organisms will require purification to similar standards (V1).

1.1.2 Difficulties Encountered in the Separation and Purification of Biological Materials

The handling of biological materials is complicated

by the extreme environmental sensitivity of these substances, especially when compared with common organic chemicals. Biological substances are sensitive to heat, chemical environment (pH, the presence of specific substances such as heavy metal ions etc.) and to a lesser extent, mechanical action and radiation frequency and intensity. Further, the risk of cross-contamination by other micro-organisms, particularly in the case of living cells, is a constraint on the conditions of processing of such substances.

While to some extent dependent on the particular substance under consideration, in general, proteins and cellular material cannot tolerate temperatures much in excess of $30^{o}C$ or less than $0^{o}C$. (Except in the particular case of quick freezing for preservation.) Living cells can exist in environments of widely differing pH, but generally are adapted to a particular pH and changing the pH of their surroundings has a detrimental effect. Similarly proteins and like substances are denatured by chemical changes induced in their structure by pH changes. Cellular material is also damaged by solutions of very high or very low ionic strength because of osmotic pressure differences across the cell walls.

Further chemically related constraints are imposed by the sensitivity of biological compounds to phenolics, halogen-containing compounds, (particularly halogenated hydrocarbons), quarternary ammonium compounds, heavy metal ions and, to a lesser extent, alcohols. In most cases, these substances react chemically with proteins in the structure, causing varying degrees of denaturing. In general, radiation of frequencies higher than those of visible light will cause varying amounts of destruction to biological materials. There is also some evidence (N2) that high shear rates such as those caused by prolonged exposure to

high-speed, high-pressure pumping will damage cell structures and break down the long-chain molecules of proteins. In the case of cellular material, extremes of pressure, especially when applied rapidly, cause decay of the structure.

Thus separation and purification of biological materials are limited to comparatively mild physical and chemical conditions. This constraint rules out many traditional separation processes where even moderate heat, pressure or fluid velocities might be used.

1.1.3 Electrophoresis as a Separative and Purifying Tool

As previously stated, any device for the separation and/or purification of biological materials must necessarily do so under mild physical and chemical conditions. Electrophoresis, which takes advantage of the different responses of macro-molecules and suspended substances to a steady electric field in a dilute ionic solution, can normally be performed within the limits required by such substances.

Briefly, electrophoretic separations depend on differences in speed and direction of movement of differing particles under the influence of an electric field. These differences result from the interactions of the surface charge of the particles with the imposed electric field and the ionic species in solution. (In this context, "particles" should be taken to include dissolved macro-molecules and suspended solids as well as cellular organisms.) The result of electrophoresis is that, some time after the electric field has been applied to a homogenous mixture of components, the faster migrating species will be further displaced than the slower. In certain cases, components of the original mixture may have moved in different

directions (Figure 1.1). If the system is in continuous flow at right angles to the plane of Figure 1.1, these flows can be split at one end of the device and the separated streams taken away (Figure 1.2).

Potentially electrophoresis therefore offers a number of advantages for this class of separation:

(i) Chemically mild conditions pertain in the carrier solution - normally a buffer at a low concentration and a pH appropriate to the substances being separated;

(ii) Separations that can be performed at low to ambient temperature may be satisfactory;

(iii) The separation is at atmospheric or near atmospheric pressure;

(iv) With suitable materials of construction, an electrophoretic separator can be totally enclosed and still permit observation of the separation;

(v) Since bulk flow through the separator must necessarily be laminar, there is no extreme mechanical action on the solute.

However, electrophoresis has some significant drawbacks which must be overcome before the process can be used on any significant scale. These disadvantages are:

(i) The presence of a direct current field implies the passage of a current through the solution resulting in ohmic heating; this has two effects:-

(a) The solution may reach a sufficiently high temperature to damage the substances being purified;

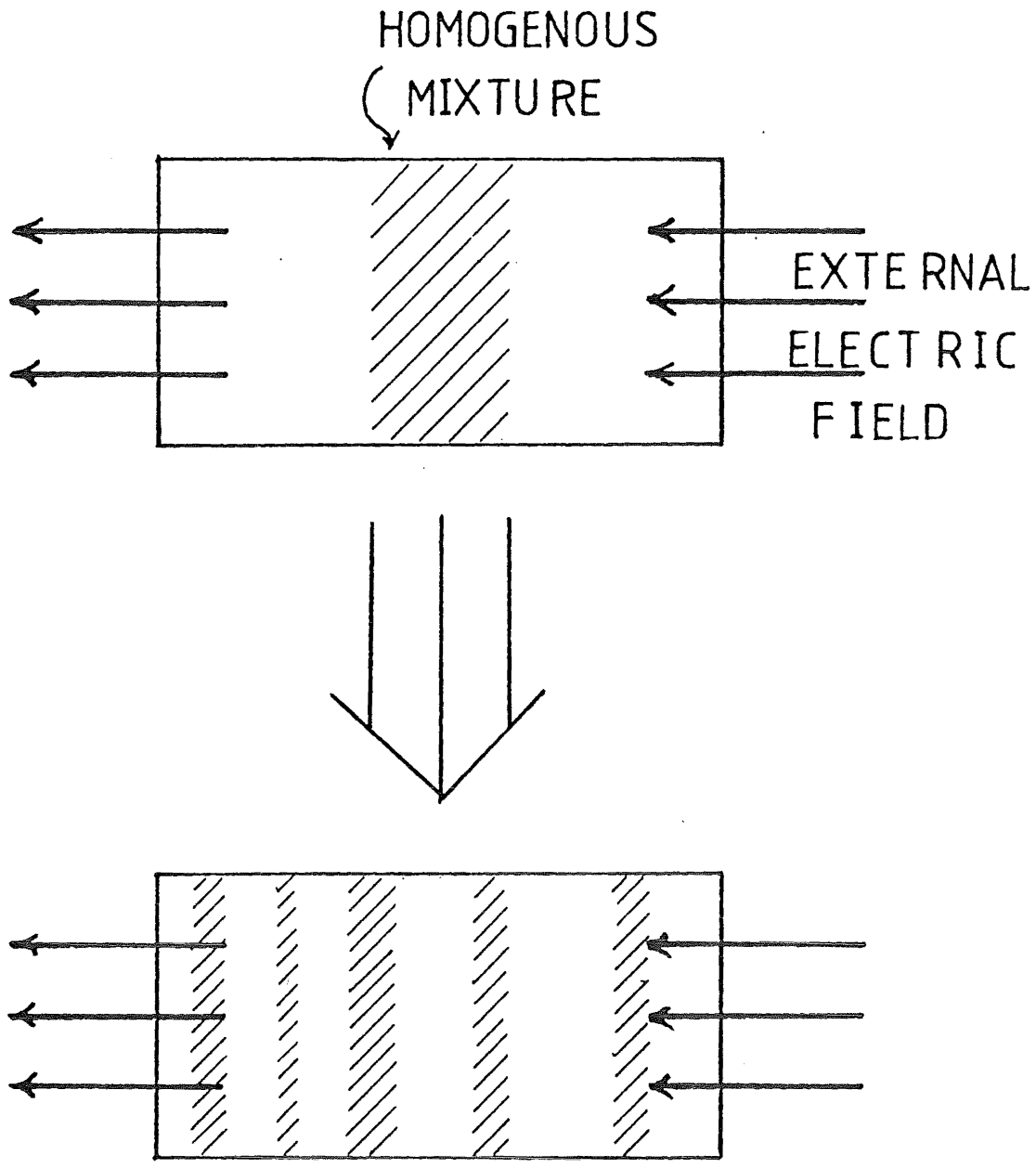

FIGURE 1.1 ELECTROPHORESIS PRINCIPLE

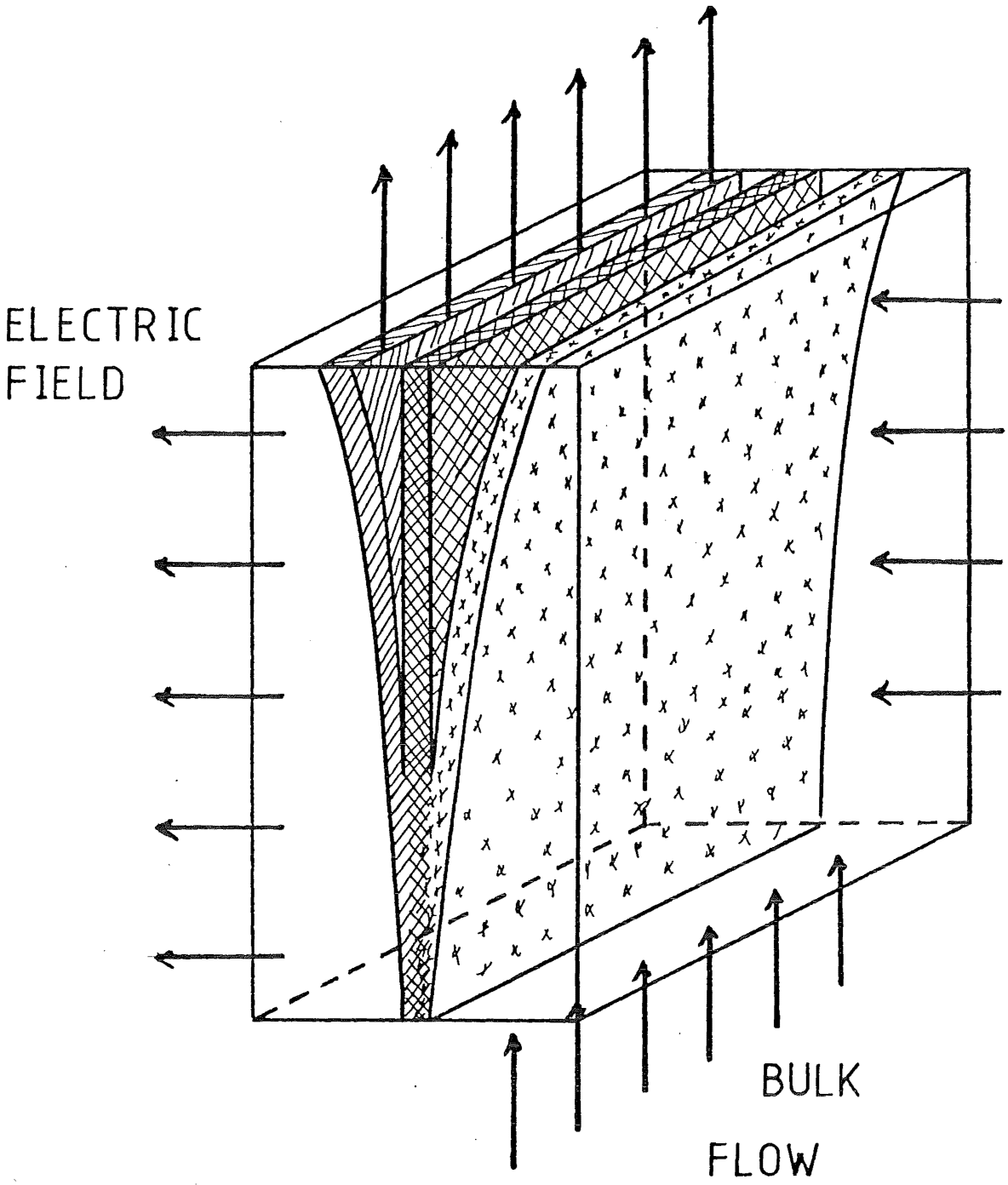

FIGURE 1.2 CONTINUOUS-FLOW ELECTROPHORESIS

(b) Temperature differences in the solution may cause hydraulic disturbances in the solution being treated with remixing of the separated components;

(ii) The electrophoretic velocities of most substances of interest are very small and their differences are smaller still, leading to comparatively long separation times;

(iii) If the electric field is increased to counter this last problem the inadequacy of the charge carriers in the solution for carrying the increased current by ionic drift may result in electrically induced turbulence; this again remixes the separated components;

(iv) The electric field must be introduced into the separator in some way. This usually involves metal/solution interfaces with consequent pH changes, gas evolution and polarisation effects when the field is operating; therefore some way must be found to isolate these phenomena from the separation while maintaining a high electric field in the separating zone;

(v) Electroosmotic effects tend to distort fluid-flow profiles near non-electrically conducting surfaces when an electric field is present; these effects will also distort the flow of the separated components (Figure 1.3).

1.1.4 Proposal for Narrow-Slot Continuous-Flow Electrophoresis

A concept proposed by Arcus (A2) overcomes many of the difficulties listed above. In this concept the separator is made extremely narrow, in relation to its depth and length, in the plane of the electric field (Figure 1.4). This geometry has a number of advantages.

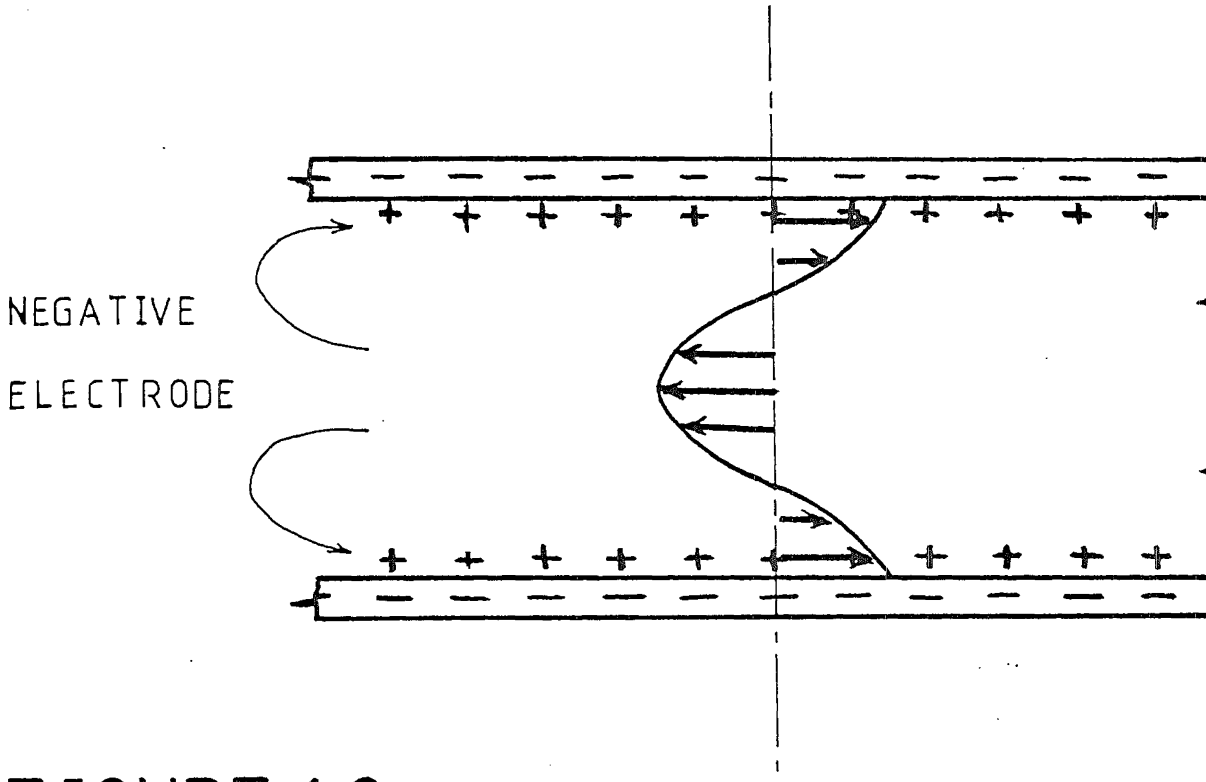

FIGURE 1.3 ELECTROOSMOTIC VELOCITY PROFILE
(for the case of impermeable electrodes)

The single most important feature of this concept is that the solute components move over a comparatively short distance in order to be separated. This allows either a shortened time of exposure to the electric field or a decreased field, or both. A number of important consequences follow from this. Firstly, ohmic heating of the solution is minimised because of the lower current intensity and shorter current path. Secondly, the electric field strength can more readily be kept below the point at which electrically induced turbulence is precipitated. Thirdly, this geometry permits the faces of the separating region to act as heat sinks to reduce further heating effects.

Further inspection of this geometry reveals more subtle advantages. The device is capable of increase in depth limited only by the strength and stability of the materials of construction. As shown in Figure 1.4, the throughput of the proposed device increased linearly with depth. Another consequence of the high depth-to-width ratio is that the non-conducting surfaces in contact with the solution present a relatively small area to them. This minimises changes in electroosmotic flow across the depth of the device giving the minimum possible distortion of the separated streams from this cause. Since laminar flow must be maintained in the separating zone of the device, as components are deflected away from the centre of the stream by the imposed electric field, their separation is enhanced by entering a region of lower velocity (Figure 1.5). This effect is similar to Taylor's dispersion in cylindrical ducts (T1). The result in this case is to enhance the separative capability of the device.

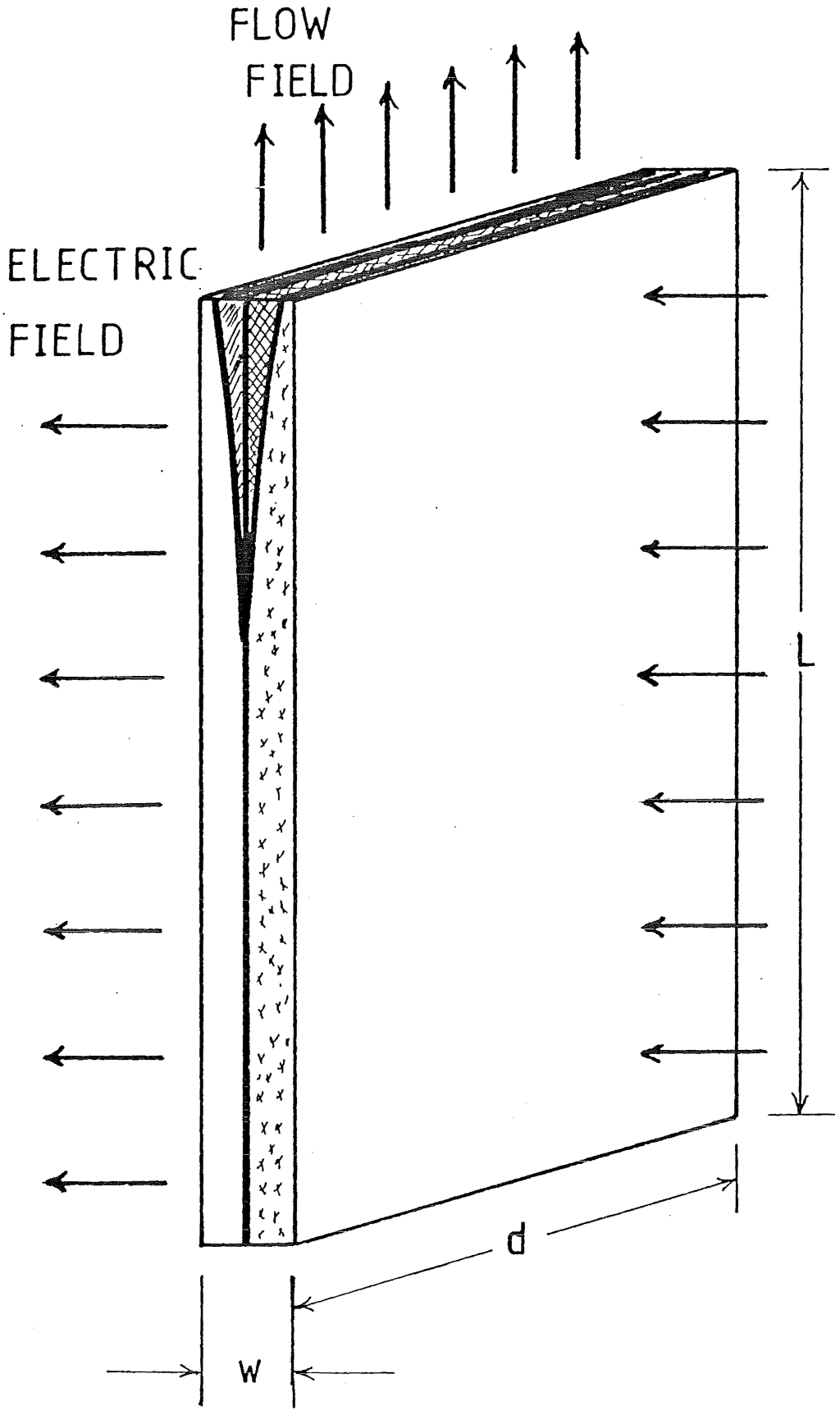

FIGURE 1.4 NARROW-SLOT ELECTROPHORESIS

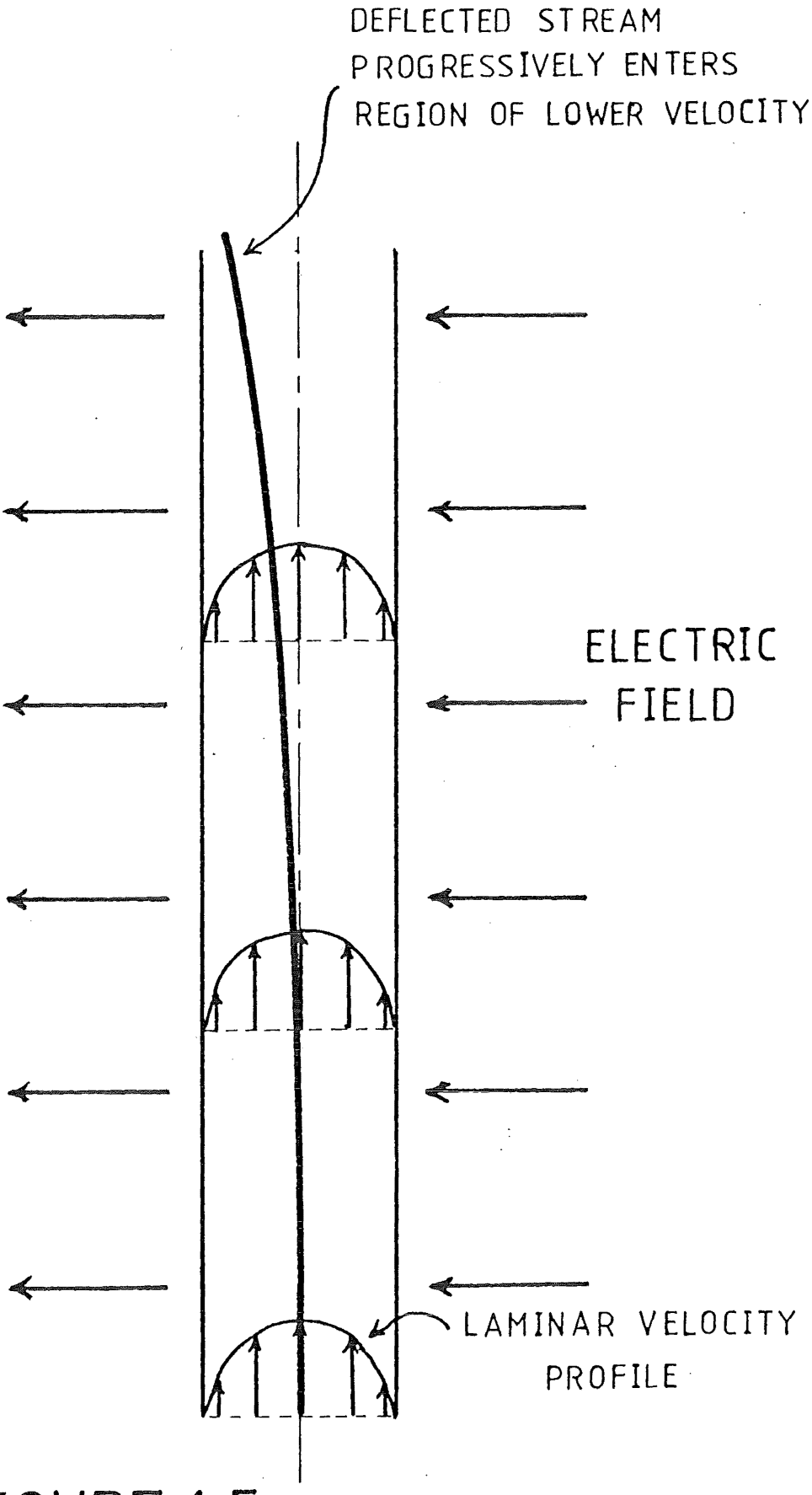

FIGURE 1.5 THE EFFECT OF VELOCITY PROFILE

Typically prospective materials for electrophoretic separation are handled as dilute dispersions in the carrier buffer. Thus the solution densities are little different from those of the carrier buffer solutions. Consequently this geometry can be arranged so that the solutions are flowing vertically upward. Therefore the density gradient in the device (a result of ohmic heating) extends from high values at the bottom to lower values at the top with the result that the stability of the flow is aided by this density gradient.

However, the narrow-slot geometry of the proposal results in very large 'electrode' surfaces. Clearly these cannot be metal/solution interfaces, as chemical changes and physical disturbances would disturb the flow of the solutions, causing remixing of the components, and possibly cause chemical damage to sensitive materials. It is therefore necessary to remove this activity from the separating zone and yet retain a sufficiently high electric-field gradient across the separating zone. The proposal thus requires separate electrode chambers isolated from the separating zone (Figure 1.6). The recent development of ultrafiltration membranes in large sheets enables a barrier to be formed which is permeable to ions but will not (with suitable support) transmit mechanical disturbances or permit the passage of the solute components beyond the walls of the separating zone. A barrier of this type also permits buffer solutions of higher concentrations than those in the separating zone to be used in the electrode chambers. This latter has the effect of lowering the total electrical resistance of the device. The solution in the outer (electrode) chambers can then be circulated through de-entrainment vessels to remove evolved gases and then through a cooling device to remove excess heat before being remixed and fed back to the separator.

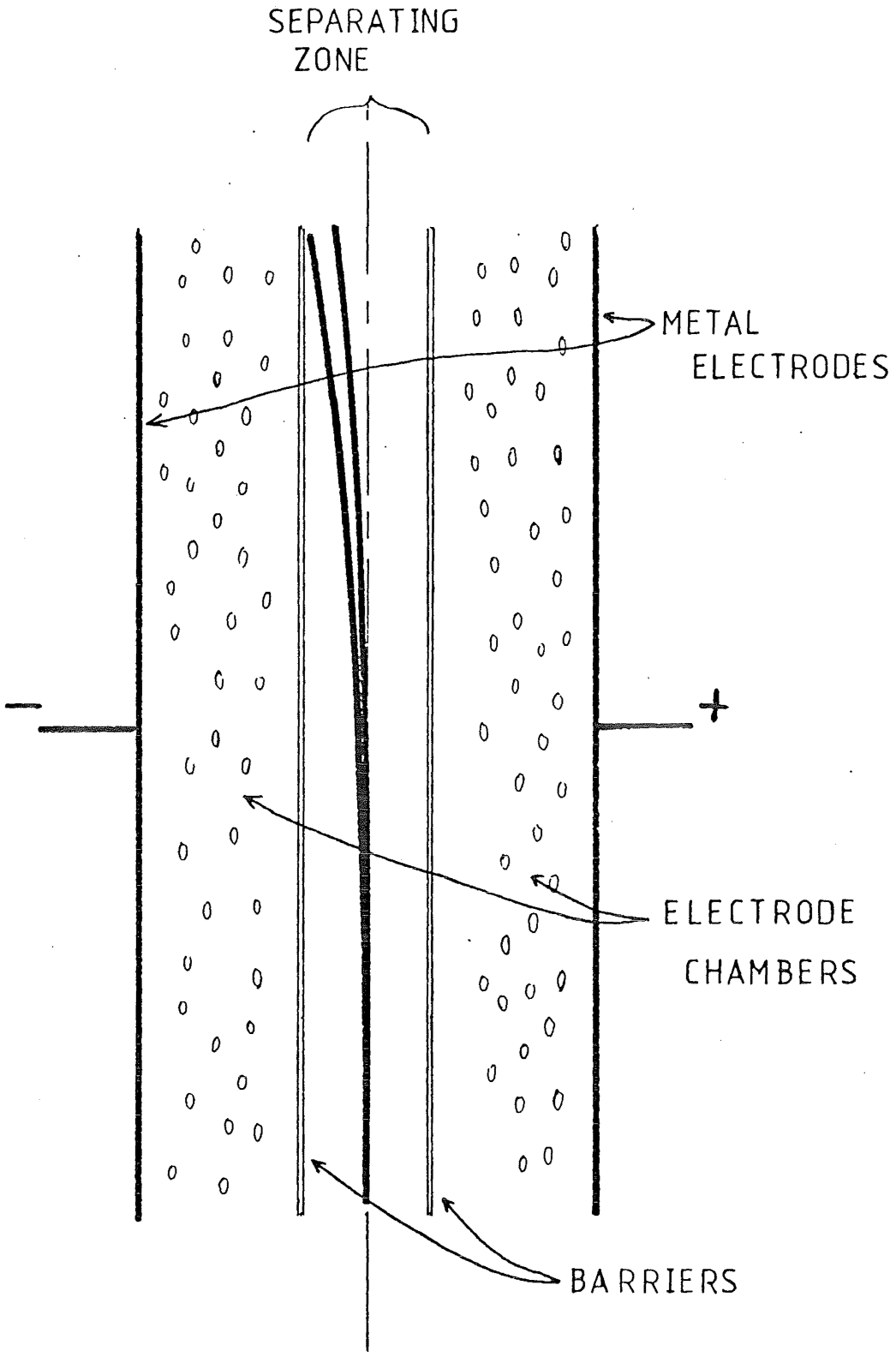

FIGURE 1.6 BARRIER POSITIONS FOR NARROW-SLOT CELL

1.1.5 Objectives of This Work

The object of this study is to develop the above concept into a workable device to separate materials in quantities of commercial interest. This includes a theoretical investigation of the mass- and heat-transfer phenomena involved and the investigation of the parameters (electrical, mechanical, hydrodynamic and electrokinetic) affecting electrophoresis that relate to this concept. The results of these theoretical investigations are to be used to design, construct, and test an electrophoretic separator based on the narrow-slot free-flow concept.

1.2 Electrokinetics

1.2.1 Introduction

The first recorded observations of electrokinetic phenomena appear to be those of Reuss (R2). Reuss observed that an aqueous dispersion of clay particles moved toward the positive electrode when these were under the influence of an electric field. He further observed that, if a potential difference was maintained across an immobilised plug of wet clay, there was a flow of water from one side to the other. These phenomena, respectively electrophoresis and electro-osmosis, are in fact manifestations of the same type of solid-liquid interaction.

In investigating this latter effect, Quinke (Q1) showed that the passage of liquid through a porous plug or a fine non-conducting capillary induced a potential difference. This converse of electro-osmosis is known as the streaming potential. Quinke (Q1) further showed that the direction of flow is not necessarily that of the current flow in the fluid. This led to the hypothesis that these effects were caused by charge separation at the solid-liquid boundary. Dorn (D2) later observed

that, when suspended particles settle through a liquid, a potential gradient is generated in the direction of motion. This effect, known as sedimentation potential or Dorn effect, was also explicable in terms of the charge separation hypothesis.

In the case of clay particles, Si^{4+} ions in the crystal lattice may be replaced by Al^{3+} ions. The particles as a whole now carry a negative charge with respect to the solution. Similarly, some crystal structures absorb cations and anions preferentially and to differing extents, thus leaving a nett charge on both the particle and the surrounding solution. A third mechanism occurs with solids containing carboxyl or similar dissociatable groups. Dissociation depends on pH, composition of the carrier solution and ionic strength. This mechanism is of major importance in the case of polyelectrolytes and protein-containing substances (including living cells). Fourthly, adsorption of surfactant ions onto particulate surfaces will normally charge the particle with all or part of the charges of the surfactant.

Clearly, whenever a solid as part of a fixed surface or a suspended particle carries a nett charge, the solution next to it carries a charge of the same magnitude and opposite sign. However, the charges in solution are mobile and hence conform themselves to a balance between minimum electrostatic energy and maximum entropy. These two sets of charges, one in the solution and one on the solid constitute the electrical double layer.

1.2.2 Theory of the Diffuse Double Layer

The theory of the diffuse double layer was developed independently by Gouy (G4, G5) and Chapman (C2). This theory assumes all ions to be point charges which are acted on by

electrostatic forces and thermal movement within the liquid. This combination of forces leads to a Boltzman distribution of charges of the form:

$$N_i = N_{i\infty} \exp(-Z_i e\phi/kT) \qquad 1.1$$

where N_i = number of ions of species i per unit volume at distance from the solid surface;

$N_{i\infty}$ = number of ions at a large distance from the solid surface;

ϕ = electric potential at some distance from the surface;

e = electronic charge;

k = Boltzman constant;

T = absolute temperature;

Z_i = charge number of species i;

The situation represented by this relation is depicted schematically in Figure 1.7.

The space charge density is also therefore a function of distance x. This space charge density is given by:

$$\rho_e = \Sigma_i N_i Z_i e \qquad 1.2$$

If the solution contains only one symmetrical electrolyte, then:

$$\rho_e = Z e(N_+ - N_-) \qquad 1.3$$

Substituting equation 1.1 into equation 1.3, one finds:

$$\rho_e = -2 Z e N \sinh[\frac{Ze\phi}{kT}] \qquad 1.4$$

A further relationship between the variables x, ϕ and ρ_e is given by the Poisson equation:

$$\underset{\sim}{\nabla}.(\underset{\sim}{\nabla}\phi) = \underset{\sim}{\nabla}^2\phi = -\rho_e/\varepsilon \qquad 1.5$$

where ε is the electric permitivity of the solution.

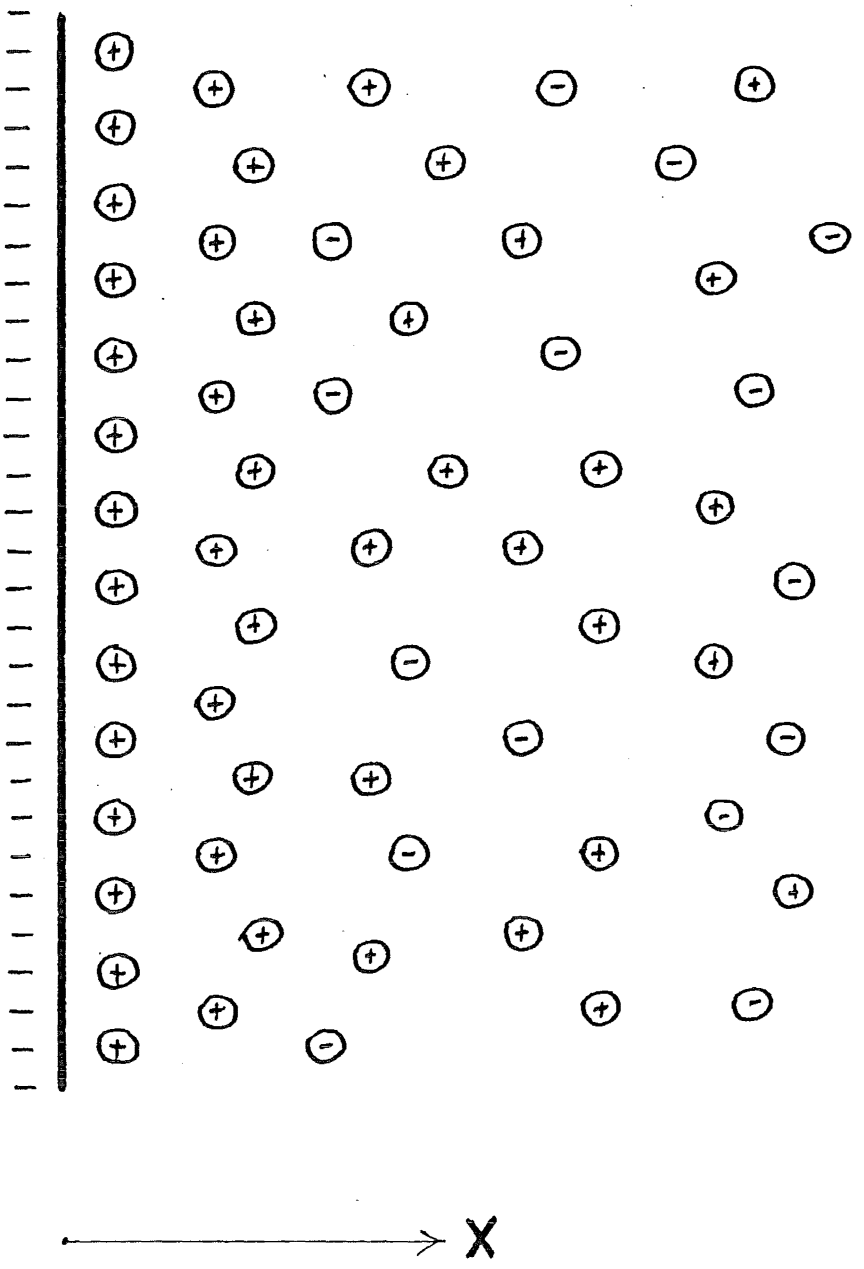

FIGURE 1.7 The distribution of ions at a charged solid surface.

Combination of equations 1.1 and 1.5 gives the Poisson-Boltzman equation which is the basis of the Gouy-Chapman theory:

$$\underset{\sim}{\nabla}^2\phi = \left(\frac{2ZeN}{\varepsilon}\right) \sinh\left[\frac{Ze\phi}{kT}\right] \qquad 1.6$$

For low potentials where

$$\sinh\left[\frac{Ze\psi}{kT}\right] \simeq \frac{Ze\psi}{kT} \quad \left(\text{i.e. } \phi \lesssim \frac{25}{Z}\ \text{mV}\right),$$

this relation becomes:

$$\underset{\sim}{\nabla}^2\phi = \left(\frac{2Ne^2Z^2}{\varepsilon kT}\right)\phi = \kappa^2\phi \qquad 1.7$$

which is the linearisation used in the Debye-Huckel theory for electrolyte solutions.

The quantity κ is of some importance as $\frac{1}{\kappa}$ (which has units of length) may be regarded as the thickness of the double layer; sometimes known as the Debye length.

1.2.3 The Poisson-Boltzman Equation for Flat Plates

For an infinite flat plate with a constant potential over its surface, the Poisson-Boltzman equation can be written:

$$\frac{d^2\phi}{dx^2} = \frac{2ZeN}{\varepsilon} \sinh\left(\frac{Ze\phi}{kT}\right) \qquad 1.8$$

where the x coordinate is perpendicular to the plate.

Equation 1.8 can be integrated twice to give the potential-distance relationship for a flat plate. Using the boundary conditions:

$$\phi = 0 \text{ and } \frac{d\phi}{dx} = 0 \quad \text{at } x = \infty$$

one finds on the first integration:

$$\frac{d\phi}{dx} = -\left(\frac{8NkT}{\varepsilon}\right)^{\frac{1}{2}} \sinh\left(\frac{Ze\phi}{2kT}\right) \qquad 1.9$$

The second integration requires the condition that $\phi = \phi_0$ at $x = 0$, where ϕ_o is the surface potential on the plate. The result

$$\tanh\left(\frac{Ze\phi}{4kT}\right) = \tanh\left(\frac{Ze\phi_0}{4kT}\right) \exp(-\kappa x) \qquad 1.10$$

is then the general solution to the Poisson-Boltzman equation for flat plates. For the special case of $Ze\phi_0/4kT << 1$, the approximation $\tan h x \simeq x$ can be used and hence equation 1.10 can be written:

$$\phi = \phi_0 \exp(-\kappa x) \qquad 1.11$$

for the case of small surface potentials.

From these results the surface charge density σ_0 may be related to the surface potential ϕ_0 as follows.

The surface charge density is exactly balanced by the charge in solution.

$$\therefore \sigma_0 = -\int_0^\infty \rho_e \, dx \qquad 1.12$$

Substituting 1.5 into 1.12 and assuming no charge variation in the y or z directions, one gets:

$$\sigma_0 = \varepsilon \int_0^\infty \frac{d^2x}{dx^2} \, d \qquad 1.13$$

$$= -\varepsilon \left(\frac{d\phi}{dx}\right)_{x=0}$$

and on inserting 1.9, equation 1.13 yields:

$$\sigma_0 = \varepsilon (8 \, N \, \varepsilon \, kT)^{\frac{1}{2}} \sinh\left(\frac{Ze\phi_0}{2kT}\right) \qquad 1.14$$

which for small ϕ_0 becomes:

$$\sigma_0 \simeq \varepsilon \, \kappa \, \phi_0 \qquad 1.15$$

This is the required relationship between the surface charge density σ and the surface potential ϕ_0.

1.2.4 The Poisson-Boltzman Equation for Spheres

For spheres equation 1.6 can be written as:

$$\frac{1}{r^2}\frac{d}{dr}\left(r^2\frac{d\phi}{dr}\right) = \left(\frac{2ZeN}{\varepsilon}\right)\sinh\left(\frac{Ze\phi}{kT}\right) \qquad 1.16$$

This relationship cannot be solved analytically except for the special case of linearisation at low surface potential. In this case, the solution is:

$$\phi = \phi_0\left(\frac{a}{r}\right)\exp[-\kappa(r - a)] \qquad 1.17$$

where r = distance from the centre of the sphere;
and a = radius of the sphere.

On comparing equation 1.17 and equation 1.11, it can be seen that for large κa the double layer around a spherical particle can be equated to that for a flat plate. Further, it can be shown that from the above expression (1.17) the total surface charge Q for a spherical particle of low surface potential has the value:

$$Q = 4\pi\varepsilon a(1 + \kappa a)\phi_0 \qquad 1.18$$

But, since $Q = 4\pi a^2\sigma_0$ for $\kappa a >> 1$, equation 1.18 reduces to the corresponding equation for a flat plate.

For the case of high surface potential, numerical solutions are required for equation 1.16. Such solutions have been evaluated by Loeb et al. (L3) for a wide range of situations. Overbeek and Bijsterbosch (O1) present a number of graphical comparisons between these results and those for flat plates.

1.2.5 The Poisson-Boltzman Equation for Cylinders

While a number of proteins, cells and like materials may be treated as spheres, a far greater number of such substances more closely resemble charged long chains. Thus the geometry of

many of these materials is more closely approximated by a long thin cylinder. For cylinders, on ignoring end effects and assuming $\phi = \phi(r)$ only, equation 1.7 becomes:

$$\frac{d}{dr}\left[\frac{1}{r}\frac{d}{dr}(r\phi)\right] = \kappa^2\phi \qquad 1.19$$

Again, this relationship is not amenable to analytical solution and so numerical solutions or approximations are required. Philip and Wooding (P4) have devised an approximate technique which they have shown to give sufficient accuracy to be useable for predicting electro-kinetic effects such as electrophoresis.

1.2.6 Modifications to the Poisson-Boltzman Equation

The diffuse double-layer theory outlined above assumes both point charges and ions in free solution of zero radius. Obviously neither of these assumptions is strictly correct. Firstly, the finite size of ions prevent them from approaching closer than their ionic radii to the surface and, secondly, ions often interact with the surface chemically, such as through specific adsorption. These possibilities were first pointed out by Stern (S8) and later modified by Grahame (G2).

The result of these effects is that the surface charge is compensated for by the sum of the charges in the diffuse layer and in the closer Stern layer (Figure 1.8). A somewhat more detailed discussion of the theories involved in these models is given by Overbeek and Lijklema (O2).

1.2.7 Slipping Planes in Electrokinetics

All electrokinetic phenomena deal with tangential relative motion between a solid and the surrounding liquid. It is thus of considerable importance to know the position of the slipping plane between the two phases. While no unequivocal

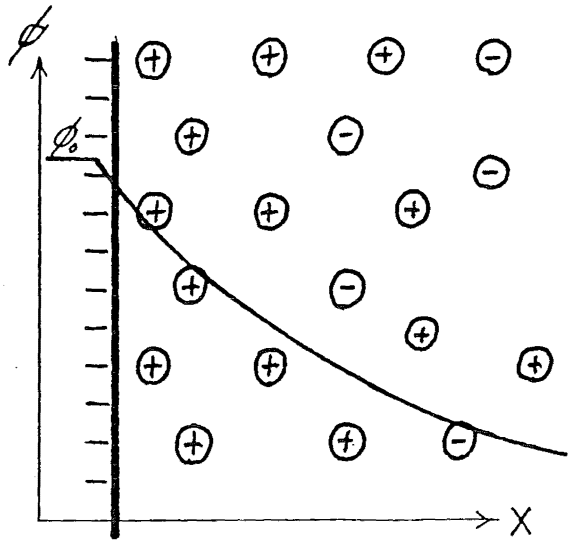

(i) No specific adsorption

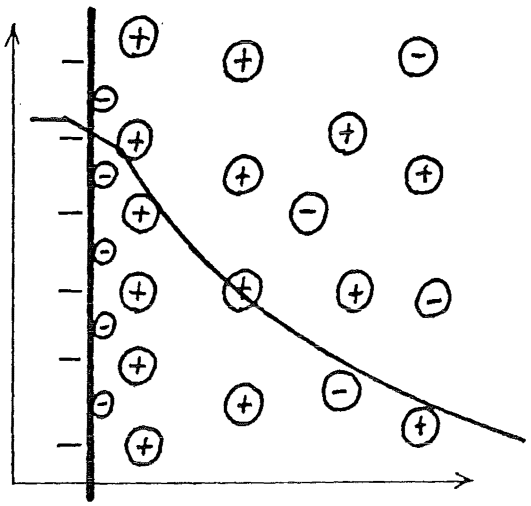

(ii) Weak specific adsorption of anions

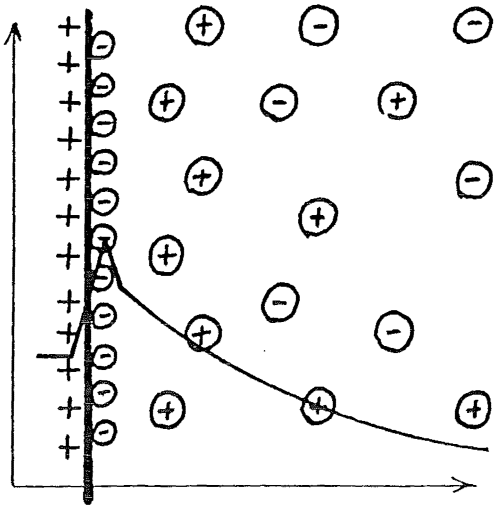

(iii) Strong specific adsorption of anions

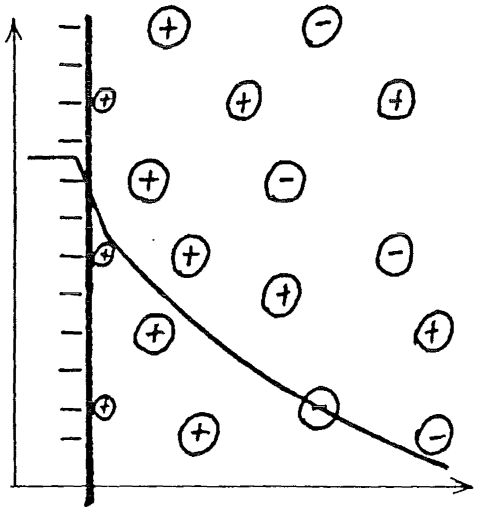

(iv) Weak specific adsorption of cations

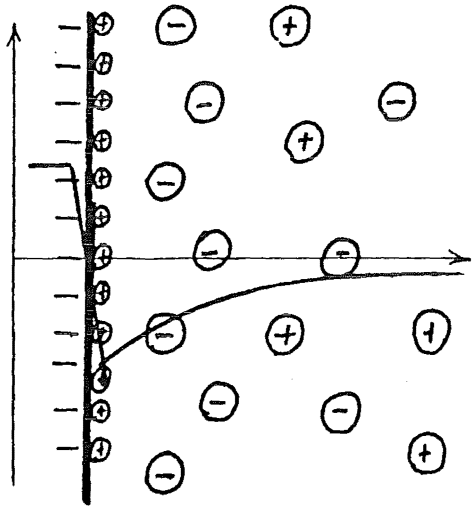

(v) Strong specific adsorption of cations

FIGURE 1.8 Specific adsorption effects

answer can be given to this problem, it would appear from the work of Lyklema (L5) that the slipping plane corresponds to the outer surface of the closer Stern layer. This being so, the potential at the slipping plane (or zeta-potential) can be equated to the potential at the surface of the Stern layer.

This implies that the zeta-potential is sensitive to changes in surface charge, ionic strength and like quantities. So, it would appear, are the parameters used to describe electrokinetic phenomena, thus giving some justification for using double-layer theory as a basis for discussing electrokinetic phenomena.

1.3 Theory of Electrophoresis

1.3.1 Introduction

The simplest possible picture of electrophoretic transport would suggest that the velocity of the particle under consideration could be predicted by balancing the electric force on the particle against the friction against the medium:

$$U = \frac{QE}{f} \qquad 1.20$$

Or, introducing the mobility, m, one has:

$$m = \frac{U}{E} = \frac{Q}{f} \qquad 1.21$$

However there are two other important effects. Firstly, the countercharge in the solution is comparatively close to the particle and it is subject to a force equal and opposite to the electric force on the particle. Hydrodynamic interaction transmits a substantial fraction of this force to the particle and this electrophoretic retardation may reduce the mobility of the particle by several orders of magnitude. Secondly, since the particle and

countercharge move in opposite directions and a finite time is required to replace the counterions in the double layer, the double layer is distorted. This distortion, called the relaxation effect, produces an electric field opposed to the imposed field about the particle, resulting in a reduction in mobility by as much as a half. These effects are shown schematically in Figure 1.9.

Most of the problems involved in the theory of electrophoresis concern the quantifying of these two effects.

The following discussion is initially limited to spherical particles in the absence of relaxation effects; that is to say, the double layer around the particle is treated as being undisturbed. The extensions of the theory to account for the effects of relaxation and to particles of other shapes are added later in the section.

1.3.2 Spherical Particles with a Thick Double Layer

Consider a small particle with a thick and diffuse double layer which resultingly has little effect on the electric field (Figure 1.10). In this case, the forces acting on the particle at steady state may be written as:

i) The force of the electric field on the charged particle:

$$F_1 = QE \qquad 1.22$$

ii) The hydrodynamic friction on the particle as it moves through the fluid:

$$F_2 = -6\pi\mu aU \qquad 1.23$$

where μ = dynamic viscosity of the fluid

and U = velocity of the particle;

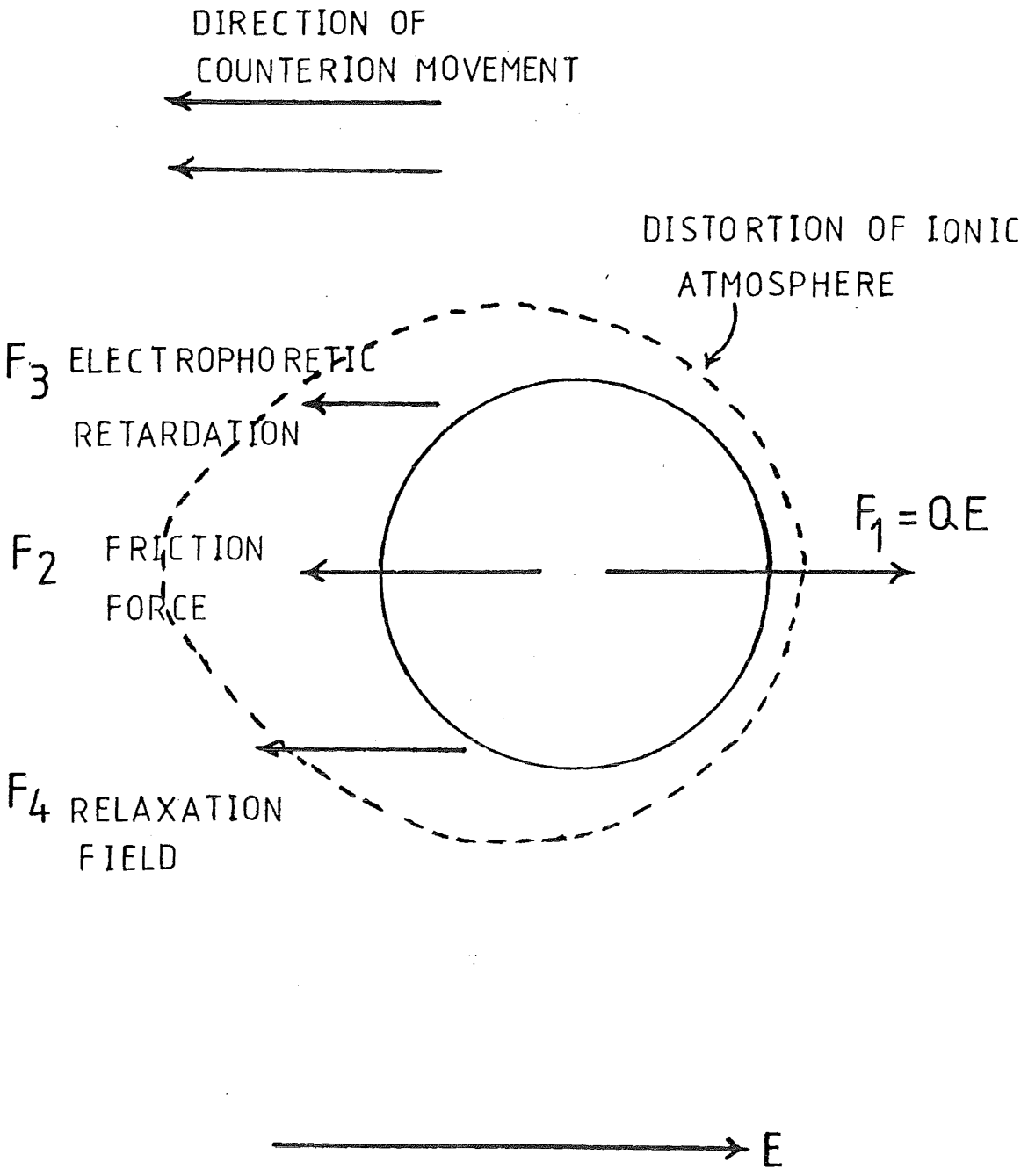

FIGURE 1.9 Forces on a particle in electrophoresis

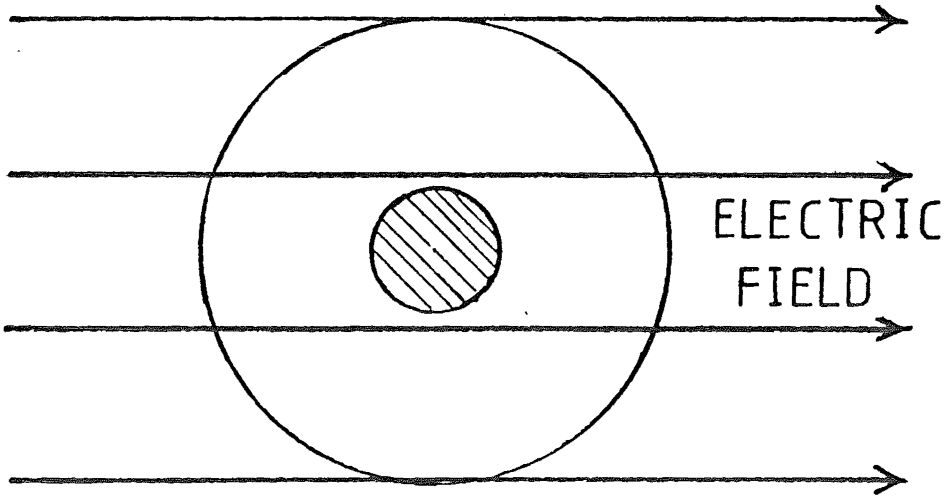

FIGURE 1.10 DIFFUSE DOUBLE LAYER

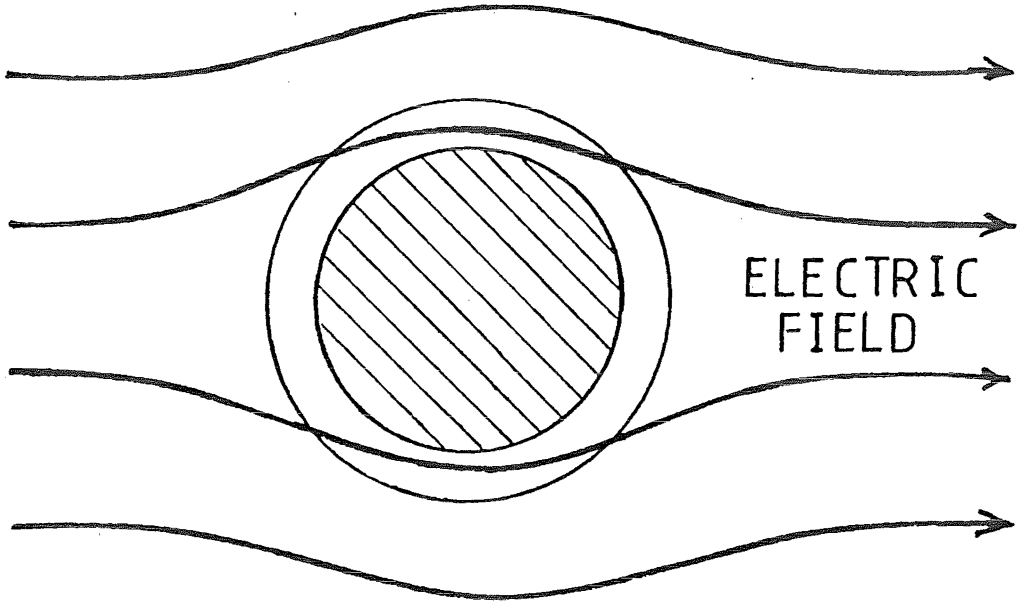

FIGURE 1.11 THIN DENSE DOUBLE LAYER

iii) Electrophoretic retardation caused by the interaction between the motion of the countercharge in the double layer and the particle:

$$F_3 = E(\varepsilon\zeta a - Q) \qquad 1.24$$

where ε = electric permitivity of the fluid
and ζ = potential of the particle at the surface of shear.

By summing these forces and equating to zero, one gets, in conjunction with equation 1.21:

$$m = \frac{\zeta\varepsilon}{6\pi\mu} \qquad 1.25$$

Thus the mobility of a particle is proportional only to the zeta-potential and the solution properties. Equation 1.25 is, in fact, the classic result of Huckel (H8).

1.3.3 Spherical Particles with a Thin Double Layer

The other extreme case of electrophoretic behaviour is that for a relatively large particle with a thin dense double layer. In this case, considered first by von Smoluchowski (V6), the electric field is considerably distorted by the double layer (Figure 1.11). Here the ions in the double layer are in an electric field smaller than in the previous case and so provide a less effective resistance to movement of the particle; that is, less electrophoretic retardation. Under these conditions, Poisson's equation may be used to evaluate the electrophoretic mobility. This equation is written in the form:

$$\frac{d}{dx}(\varepsilon \frac{d\phi}{dx}) = -4\pi\rho_e \qquad 1.26$$

where x is the distance from the surface of shear.

Von Smoluchowski's integration of this equation gives, with the potential at the surface of shear set equal to ζ:

$$m = \frac{\zeta\varepsilon}{4\pi\mu} \qquad 1.27$$

to describe the mobility.

1.3.4 The General Relation Between Mobility and ζ-Potential

The two equations 1.25 and 1.26 were reconciled by Henry (H5) who showed that these two expressions were extremes of a more general equation containing a term involving the thickness of the double layer and the radius of the particle;

$$m = \frac{\zeta\varepsilon}{6\pi\mu} f(\kappa a) \qquad 1.28$$

Henry found that for $\kappa a > 300$, $f(\kappa a) = 1.5$ and for $\kappa a < 1$, $f(\kappa a) = 1.0$. These limits allow the general equation to revert to the Huckel or von Smoluchowski forms for the appropriate cases. Henry's paper contains a plot of $^2/_3 f(\kappa a)$ and an analytical expression for this function.

1.3.5 Relaxation Effects

The above expressions assume a spherically symmetrical double layer. However, as noted previously, such is not the case in some instances. Figure 1.12 shows schematically the form of the relaxation field. This field can be thought of as the result of a 'tail' of ions behind the moving particle and a 'compression' of the ionic atmosphere in front of it.

Extensive calculations by Booth (B13), Overbeek (O3), and later Weirsema et al (W3) have given tables of mobilities, including the relaxation effect for various electrolytes. The reader is referred to these sources for detailed sets of these values. However, it is worth noting the following conditions under which relaxation is not significant:

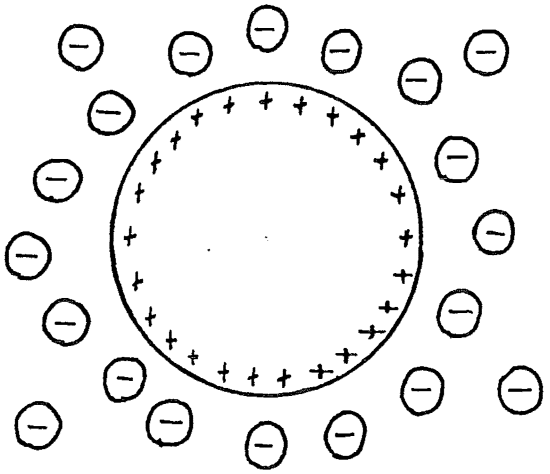

NO FIELD APPLIED: SYMMETRICAL DOUBLE LAYER

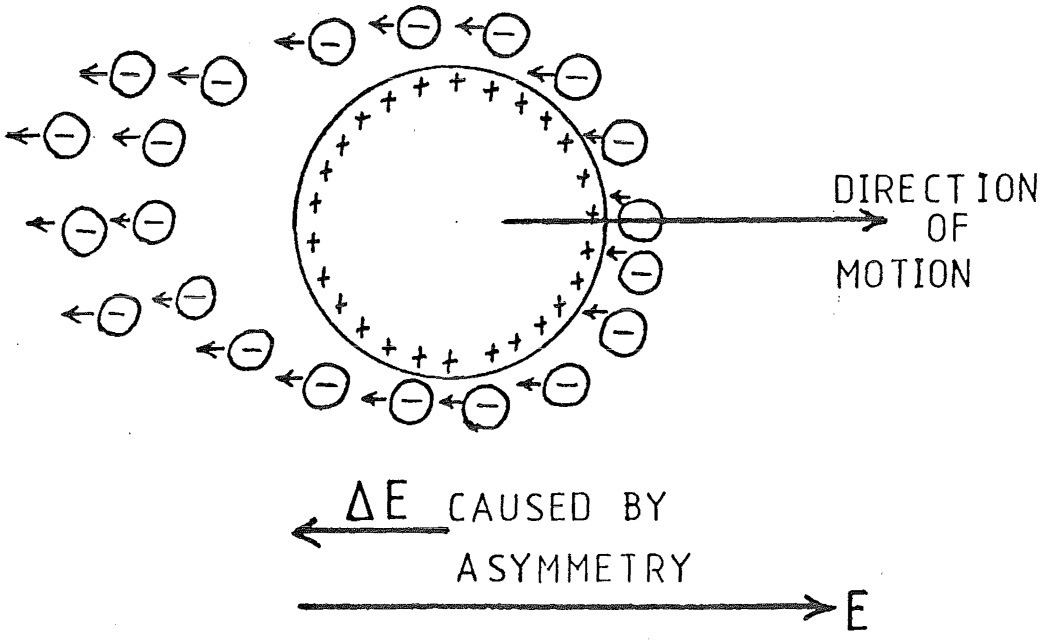

FIGURE 1.12 RELAXATION

i) When ζ-potentials are low (<25mV), electrophoresis is also slow and so the double layer is little disturbed;

ii) The double layer is thick and very diffuse (i.e. $\kappa a \to \infty$, in practice $\kappa a > 25$);

iii) The double layer is thin and dense (i.e. $\kappa a < 0.1$).

1.3.6 Particles of Shapes Other Than Spherical

1.3.6.1 Cylindrical Particles: Long thin cylinders may serve as reasonable approximations to the real shapes of some cells, viruses and polyelectrolytes. Henry (H5) examined the case of cylinders and, neglecting relaxation, he showed that for cylinders parallel to the field von Smoluchowski's equation (1.26) applied. Cylinders perpendicular to the field have a situation similar to that of Figure 1.11 but the resulting mobility is dependent on κa. At low κa von Smoluchowski's equation holds but at high κa the value of the mobility is half this. By averaging the contributions over all possible orientations de Keizer, Van der Drift and Overbeek (K1) have shown:

$$m_{(\text{average cylinders})} = \frac{1}{3} m_{(\text{parallel})} + \frac{2}{3} m_{(\text{perpendicular})} \quad 1.29$$

Some work has been done on relaxation effects for cylinders (S9) but there are, to date, no complete published results.

1.3.6.2 Particles of Arbitrary Shape: In general simple interpretations of electrokinetic behaviour for particles of arbitrary shape are possible only in the case of very low or very high values of κ (i.e. electrolyte concentration). If the largest linear dimension of the particle is very much less than $\frac{1}{\kappa}$ ionic atmosphere effects are very small and hence the mobility is found by summing the friction (viscous) and electrical forces and equating to zero. The friction effects can usually be found

from sedimentation data. If on the other hand the smallest local radius of curvature of the particle is very much larger than $\frac{1}{\kappa}$ then the von Smoluchowski relation (equation 1.26) again applies. Overbeek (04) has shown that in this instance relaxation effects are small. However electrophoretic retardation may be significant.

1.3.7 Optimisation of Electrophoretic Separations

The major importance of the theory summarised in the foregoing elements of this section is to establish a framework for maximising the efficiency of electrophoretic separations.

From the above theory the following conclusions can be noted.

i) Electrophoretic mobility is nearly proportional to ζ-potential (with some corrections for relaxation).

ii) For higher values of κa the mobility becomes less sensitive to ζ-potential.

iii) ζ-potentials increase in less than direct proportion to particle charge and are strongly influenced by κ.

iv) Size and shape of particles have a relatively minor influence on mobility for a given surface charge density.

v) Mobility is affected by temperature mainly through its effect on solution properties (particularly μ and ε).

vi) Particle charges are influenced by pH, ion activity and type, and sometimes by adsorption of particular ions (e.g. surfactants).

Electrophoretic separations are dependent on the mobility differences of the species being separated and therefore where possible conditions should be manipulated to maximise such differences.

Moderate to low ionic strengths are preferable, not only from the point of view that high ionic strengths mean lower absolute mobilities but also high ionic strengths imply high electric currents with attendant thermal problems. Selection of pH or ion activity at a point where surface charge (and hence ζ-potential) change rapdily will normally result in greater mobility differences (for example in the region of pKa of an acid or base group on a protein). Further lowering ionic strengths will tend to further increase ζ-potentials but relaxation effects tend to become more significant also. Hence mobility increases are less than might be expected. Such lower ionic strengths do have the added advantage of lower currents and so lessened heating effects but denaturing of biological substances may occur at very low ionic strengths.

From the above it can be seen that electrokinetic theory can be used to make qualitative assessments of the parameters for optimising electrophoretic separations.

1.4 Electroosmosis

1.4.1 Introduction

In general, when a conducting fluid is placed in contact with a fixed non-conducting surface a double layer is formed. Thus, when an electric field is applied to this combination, the resulting conditions are analogous to those for electrophoresis, but in this case the surface is fixed so that

the fluid rather than the solid is forced to move by the electric force. This effect is known as electroosmosis and is almost invariably present in electrophoretic separators as the conditions for these two phenomena are identical. In reality, both are manifestations of the same basic electrokinetic process.

1.4.2 Electroosmosis and the Double Layer

In a manner analogous to electrophoresis (see preceeding section), the steady state in electroosmosis implies a balance between electrical and frictional forces. Consequently, for a flat plane parallel to the electric field, with the x ordinate at right angles to the plane, the balance may be written:

$$E\rho_e = \mu \frac{d^2U}{dx^2} \qquad 1.30$$

which yields, on substituting the appropriate form of Poisson's equation (1.26) into this relationship.

$$\frac{-\varepsilon E}{4\pi} \frac{d^2\phi}{dx^2} = \mu \frac{d^2U}{dx^2} \qquad 1.31$$

When one performs the indicated double integration on this relationship, given that:

in the bulk fluid at $x = \infty$. $\frac{d\phi}{dx} = 0$

and $\phi_\infty = 0$

and $\frac{dU}{dx} = 0$;

and at the slipping plane,

$\phi = \zeta$

and $U = 0$;

the relationship is given for the electroosmotic velocity far from the wall:

$$U_{os} = \frac{E\varepsilon\zeta}{4\pi\mu} \qquad 1.32$$

Equation 1.32 is the classic result of Overbeek (05) and the consequences of this relationship are discussed in greater depth by him.

1.4.3 Electroosmosis in Closed Tubes

Of paramount importance in electrophoresis devices is the electroosmotic velocity profile in the device since the real velocity of a particle in such a device is given by:

$$U = U_{el} + U_{os} \qquad 1.33$$

at any position in the device. The effects of varying electroosmotic velocity with radius for a closed tube are best illustrated by the results of the Apollo 16 experiments in free-flow electrophoresis (M6). Micale, Vanderhoff, and Snyder (ibid) showed that the bullet-shaped profiles observed in these experiments are the direct consequence of electroosmosis in the polycarbonate tubes used. These authors showed that evaluation of the appropriate fluid-mechanical relationships, in conjunction with the condition that the tube is closed, yields:

$$U = U_{os}\left(\frac{2r^2}{a^2} - 1\right) \qquad 1.34$$

where U = fluid velocity,

r = radius,

and a = radius of the tube.

The resulting velocity profile is of the form shown in Figure 1.3; note in particular that there is flow in both directions.

1.4.4 Electroosmosis in Open Tubes

In contrast to the electroosmotically generated velocity profiles in closed tubes, those in open tubes are unimodal and unidirectional (see Figure 1.13). In a detailed

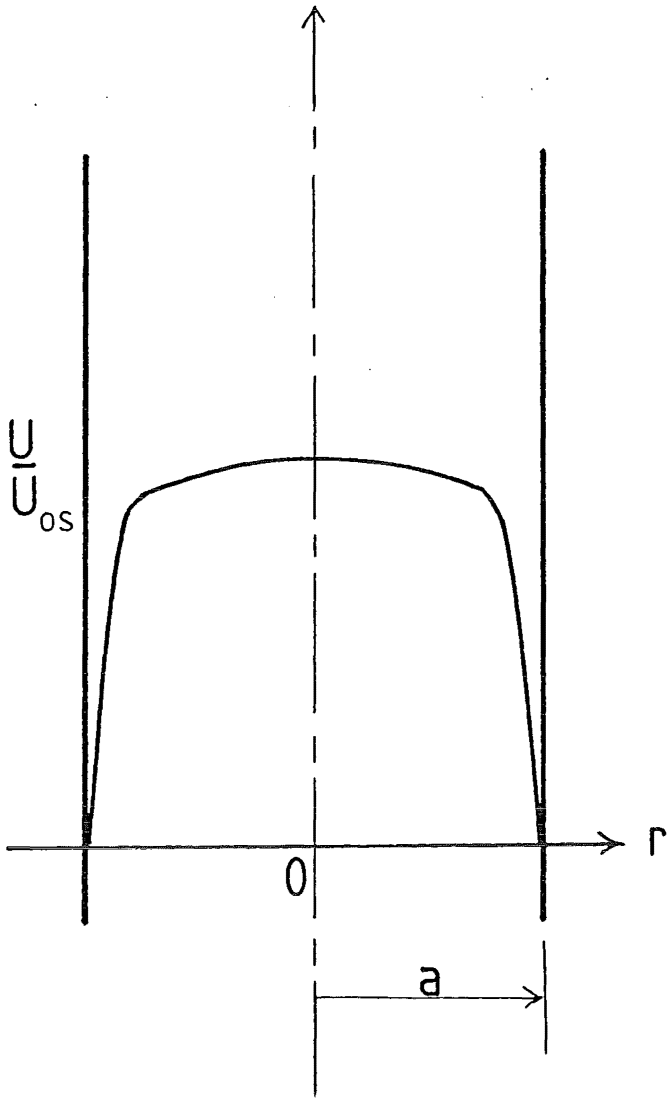

FIGURE 1.13 Electroosmotic velocity for an open ended tube.

analysis of electroosmotic effects in circular ducts, Nee (N1) shows, by evaluation of the required fluid-mechanical and electrokinetic relationships, that for a 'rough-walled' tube (i.e., for the condition of no slip at the wall) the following equation represents the expected velocity profile in an open-ended tube of radius a:

$$U(r) = U_{os}\left(1 - \frac{\cosh \kappa r}{\cosh \kappa a}\right) \qquad 1.35$$

Equation 1.35 applies for dilute ionic solutions and therefore U_{os} is evaluated by the use of equation 1.32. As shown in Figure 1.13, the significance of this result from the point of view of an electrophoretic separator lies in the fact that there is no recirculation of fluid (i.e., U is nowhere negative). It is further worth noting that the velocity profile closely approximates that for plug flow, particularly for values of $\frac{r}{a}$ less than approximately 0.8.

1.4.5 Electroosmosis in Rectangular Ducts

As might be expected from the foregoing sections, the form of the velocity profile in electroosmosis in a duct of rectangular cross-section is influenced by the permeability or 'openness' of the electrode faces of the duct. The analysis of Strickler and Sacks (S11) shows that in general the velocity profile for a duct of rectangular cross-section and depth 2d will be given by:

$$U = \left(\frac{3}{2} U_{os} - \frac{3}{4} \frac{Q_x}{d}\right)\left(\frac{y^2}{d^2} - 1\right) + U_{os} \qquad 1.36$$

where Q_x is the nett flow through the electrode walls per unit electrode height (see Figure 1.14(i)). This equation is not strictly correct for a real system as it assumes that the velocity at the wall is U_{os}, whereas Nee (N1) shows that U_{os} is normally

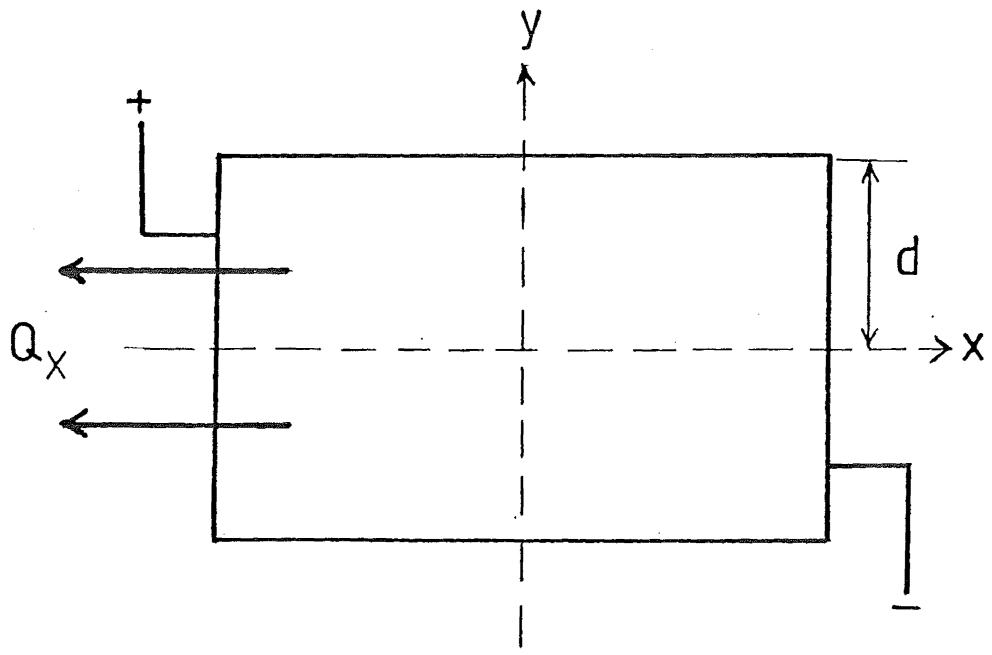

(i) COORDINATE SYSTEM FOR EQUATION 1.36

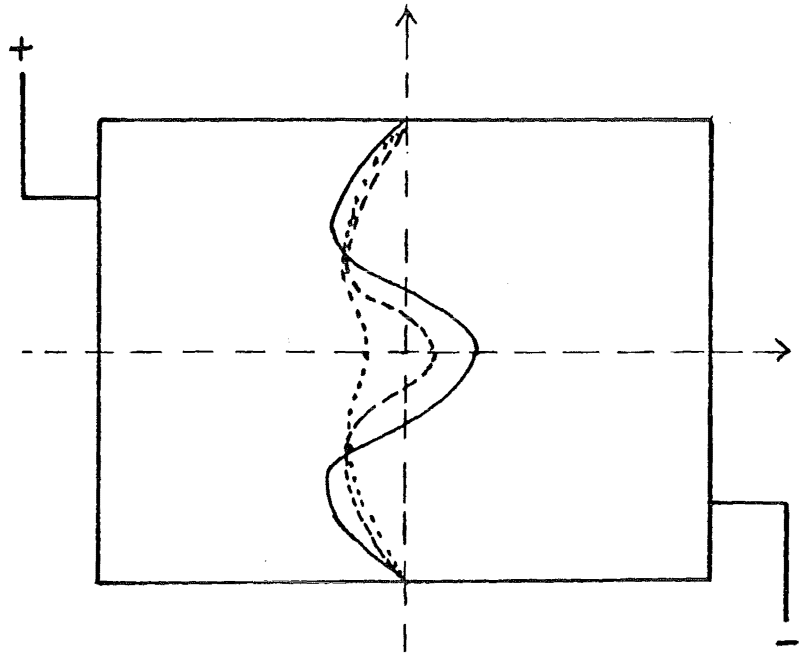

(ii) VELOCITY PROFILES FOR VARIOUS DEGREES OF PERMEABILITY OF THE ELECTRODES

(·····> – · – · – > ——)

FIGURE 1.14 Electroosmosis in rectangular ducts

zero at the wall and attains its full value at some finite distance from the wall.

Inspection of equation 1.36 shows that if

$$Q_x = 2\,U_{os}\,d \qquad 1.37$$

then the velocity profile is flat (i.e. plug flow). For other values of Q_x, the general form of the profile is shown in Figure 1.14(ii). Note that equation 1.36 takes no account of the ratio of channel depth to width. The equation of Komagata,

$$U = U_{os}\left(1 - \frac{3}{2}\left(1 - \frac{y^2}{d^2}\right)\left(1 - \frac{192}{5K}\right)^{-1}\right) \qquad 1.38$$

quoted by Vanderhoff and Micale (V7), does. In equation 1.38, K is the ratio of channel width to channel depth (i.e. $K = \frac{w}{d}$ in the notation of Figure 1.4). Since in a narrow-slot electrophoretic separator K is very small, the electroosmotically induced velocity profile is extremely flat. Or, expressed another way, the effect of the parabolic term in equation 1.38 is very small. Efforts to locate the original source of this reference have been unsuccessful and so it is impossible to determine what, if any, limiting assumptions apply to equation 1.38.

As a further note, it is worth pointing out that experiments by Micale and Vanderhoff (ibid) show generally smaller electroosmotic velocities for flow in channels constructed from acrylic-type plastics than those in glass capillaries. However, these results are dependent on the buffer system chosen, and so great care should be shown in extrapolating the results from them.

1.5 Electrophoretic Separation Methods and Devices

1.5.1 Introduction

As has already been remarked upon, the early observations of Reuss (R2) were the precursors to electrophoresis devices and techniques. Almost 100 years later Picton and Linder (P7) and Hardy (H4) placed this work on a more quantitative footing by attempting to classify substances by their electrophoretic properties. From this and similar work it became apparent that electrophoresis was a potentially important tool for both the separation and characterisation of biomolecules. Work on the basis of these early devices continued in the 1920's and 1930's until a number of developments gave rise to two distinct trends in evolving techniques: moving-boundary electrophoresis and zone electrophoresis.

1.5.2 Moving Boundary Electrophoresis

The classic work of Tiselius, first described in 1937 (T3), still remains the major contribution in this field. The Tiselius U-tube apparatus (shown schematically in Figure 1.15) enabled control of current, pH, heating effects, ion types and concentrations and a constant density solution. Thus, for the first time, true 'free solution' electrophoresis could be studied. The movement of the zone boundaries in the Tiselius apparatus could be studied using Schlieren optics to track the refractive index gradients along the arms of the device.

Preparative work was also possible, but only the two components at the 'ends' of the separation could be recovered. This last feature is the most serious drawback of the moving boundary method as only a limited number of components could be recovered pure. For a full discussion of the Tiselius cell the

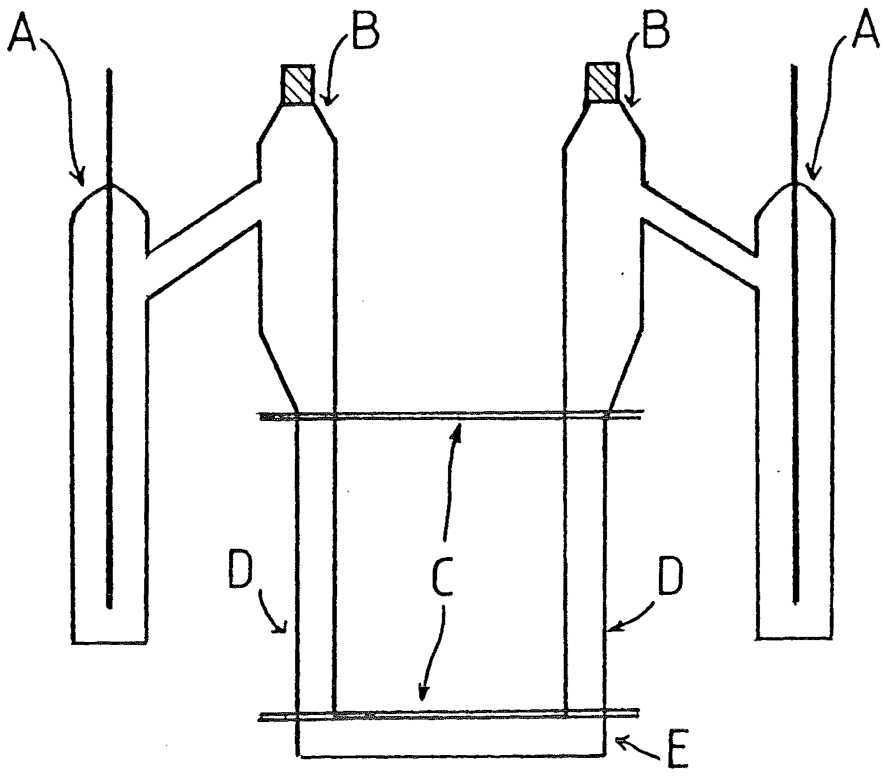

A ELECTRODE CHAMBERS B BUFFER RESERVIORS
C SLIPPING PLANES TO ENABLE SECTIONS D AND E
TO BE SEPARATED HORIZONTALLY

(a) SCHEMATIC OF CELL

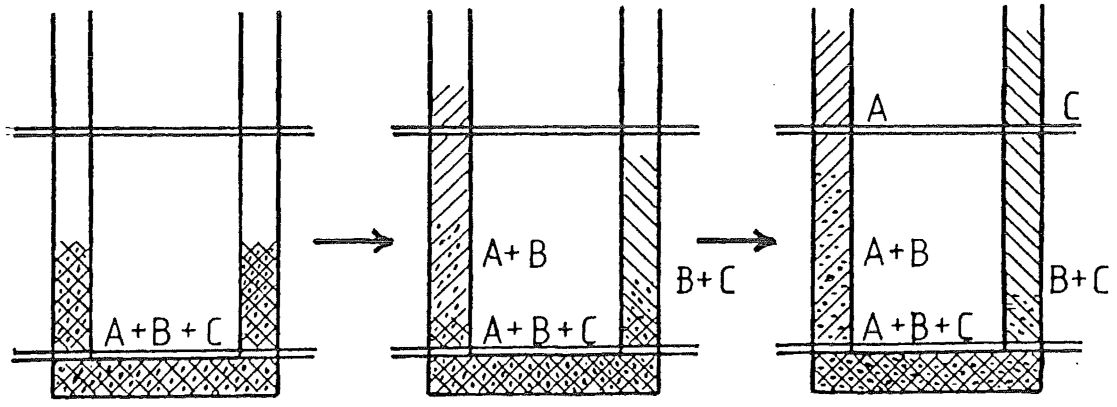

(b) PRINCIPLE OF OPERATION

FIGURE 1.15 TISELIUS CELL

reader is referred to Longsworth (L4).

1.5.3 Micro-electrophoresis

In a limited number of cases where the species to be considered are true suspended solid particles rather than dissolved macro-molecules, direct visual measurement of the speed of individual particles is possible. This is particularly so for observation of bacteria or living cells.

The device commonly used for this work today is the micro-electrophoresis cell developed by Abramson (A1) which can normally be placed directly on a microscope stage (Figure 1.16). With this type of device, the particulate motion can be observed individually during electrophoresis and hence free solution mobilities of specific particles may be determined using very small quantities of material. However, there are complications. Micro-electrophoresis tubes are normally made from glass, and so are relatively fragile and highly susceptible to electro-osmotic effects; this latter problem is increased by the small dimensions of the device. While convection can normally be avoided by careful choice of current densities and illuminating methods, settling of particles with densities different from the supporting buffer is a problem. Further, the method is clearly of little use for preparative work.

An excellent review of the theoretical and practical aspects of micro-electrophoresis is given by Brinton and Laufer (B14). More recent work by van Oss and Fike (V3) has shown that some of the problems of the method may be overcome by the use of special modifications to the basic cell intended to give plug-flow electro-osmosis.

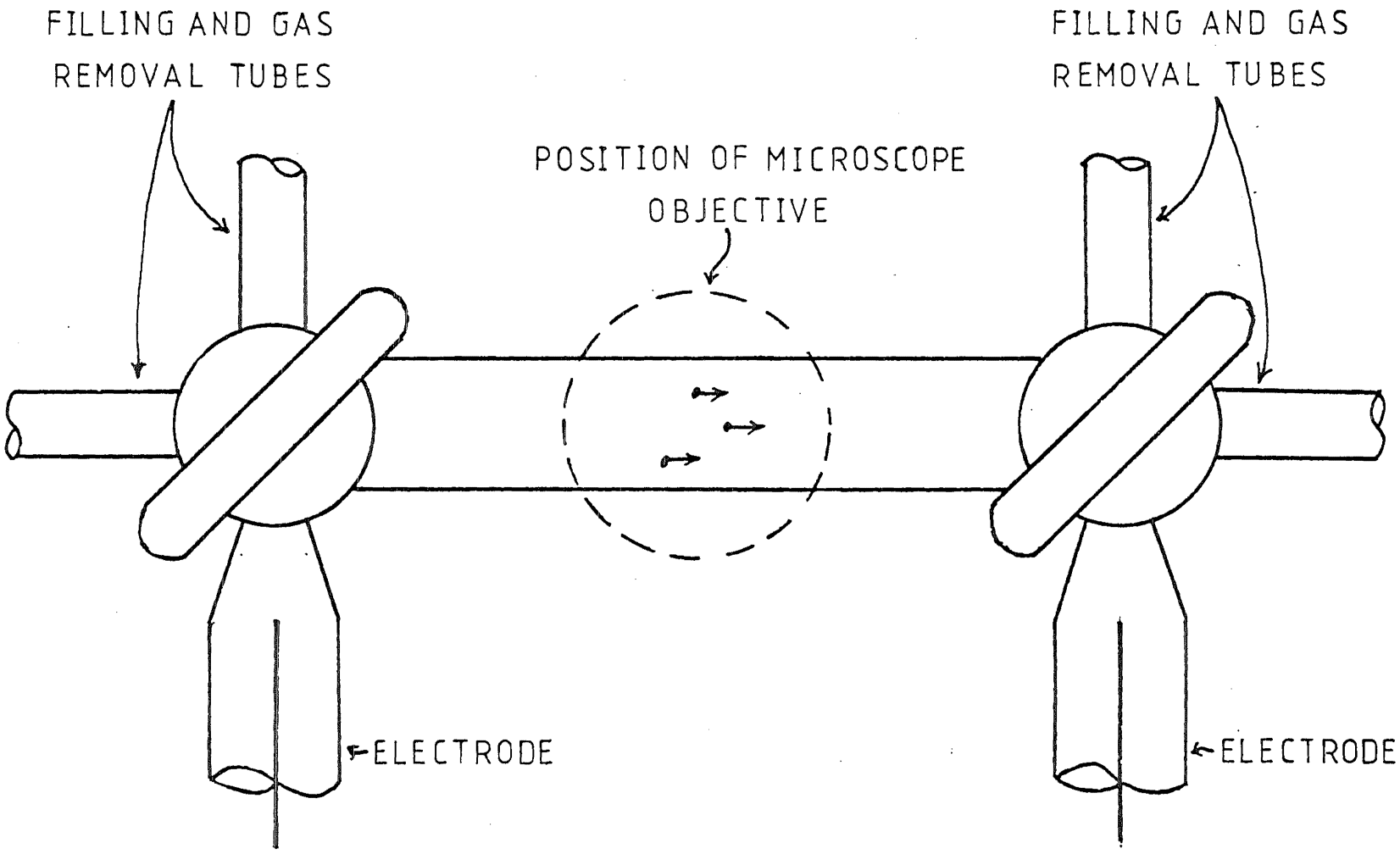

FIGURE 1.16 MICRO-ELECTROPHORESIS CELL

1.5.4 Paper Electrophoresis

The development of paper chromatography in the 1940's gave a considerable stimulus to the parallel use of paper as a support medium to stabilise electrophoretic separations. Such paper-based separations belong to the class of techniques collectively known as zone electrophoresis which is illustrated schematically in Figure 1.1. While this technique was first demonstrated by Köenig (K3), the real development of this method did not occur until highly pure chromatography papers became available in the late 1940's and early 1950's (K7).

Figure 1.17 shows schematically the commonest set-up for simple paper electrophoresis. The sample to be analysed is 'spotted' on the centre of the paper and the current switched on. Since the structure of the paper greatly slows the motion of the components being separated, the separations are extremely slow - 24 hours for a single run not being uncommon. However, balanced against this, the separated component bands are stabilised by the paper so that sharp definition of the components and a high level of reproducibility are possible. Thus this method is favoured for analytical purposes.

In the above form, the preparative capacity of paper electrophoresis is clearly extremely limited. However, a series of developments, culminating in the device designed by Grassman and Hannig (G3) and commercially available as the Elphor V separator, led to usable small-scale preparative capability. In this device, the paper is suspended vertically and the feed substance flows, in a background buffer stream, vertically downward through the paper while the electric field is applied horizontally across it. The process has an extremely

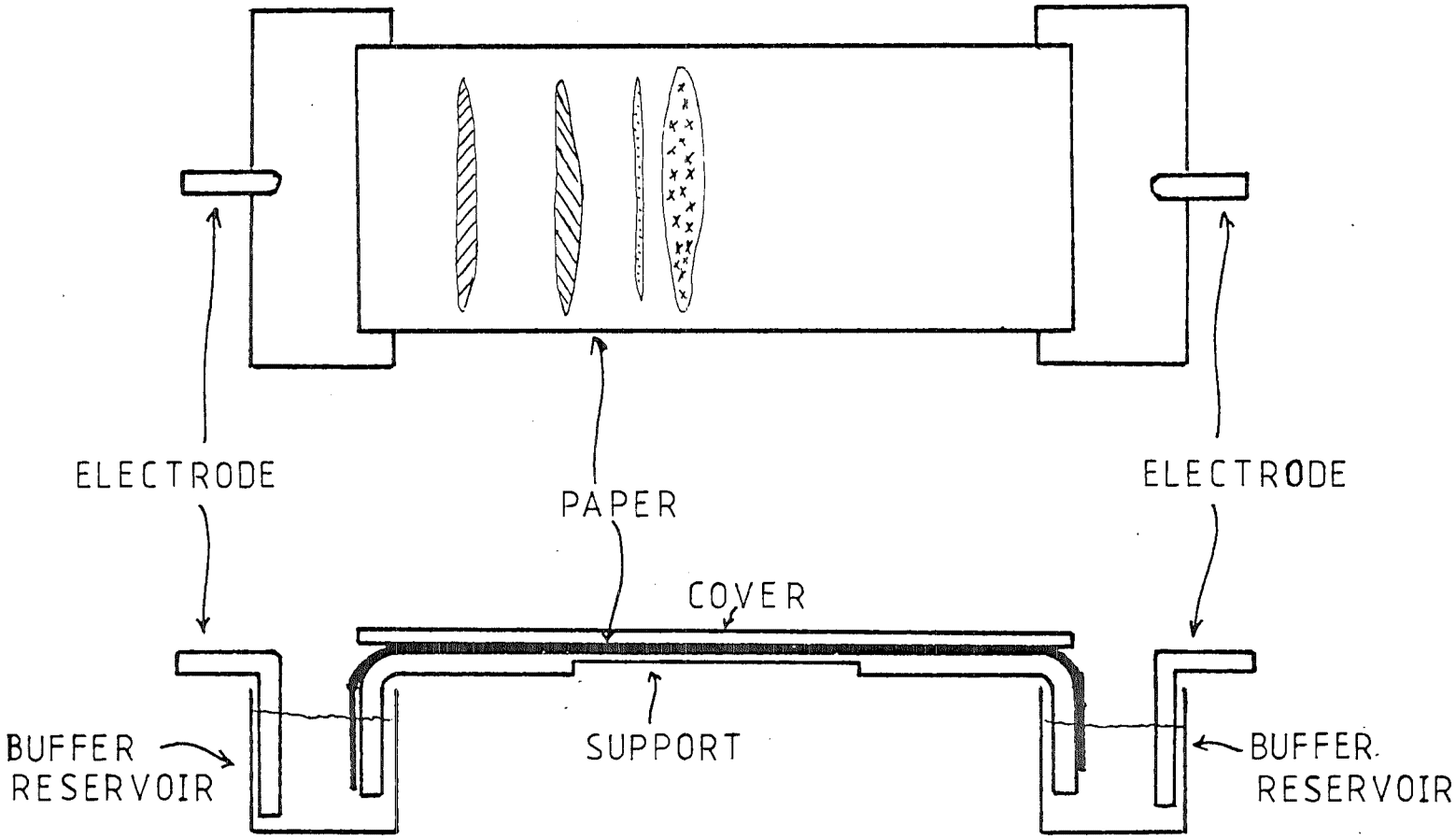

FIGURE 1.17 PAPER ELECTROPHORESIS CELL

high resolution, but the continuous-flow operation is extremely slow; typically the separation of proteins in a 2 ml blood sample taking upwards of 36 hours.

A full review of paper electrophoresis techniques is presented by Wunderly (W5).

1.5.5 Zone Electrophoresis in Various Support Media

Following from the techniques developed for paper supports, this class of electrophoresis has steadily been extended to the use of numerous other supports with the object of increasing throughput and/or resolution. A by-no-means exhaustive list of these substances includes powdered cellulose, granular starch, polyvinyl chloride resins, diatomaceous earths, asbestos, agar gels, and more recently crosslinked dextrans and polyacrylamide.

The principles involved in separations in these media are basically similar to those used in paper electrophoresis. However, these materials may be packed into a variety of different shapes. Hence, slab-like, semi-cylindrical and cylindrical geometries are used. For a more detailed examination of the various techniques and materials available in this area, the reader is referred to Kunkel and Trautman (K8), Bloemendal (B10), Smith (S6), and Gianazza and Righetti (G1).

In general, these techniques emphasise high resolution at the expense of throughput. For example, polyacrylamide gels are widely used as diagnostic tools for the identification of particular proteins in pathological investigations. These substances have the effect of increasing resolution due to the selectivity of their pore structures. A further refinement of these techniques is to perform electro-

phoresis in one direction on a sample and then, on the same support, thin layer chromatography at right angles to the direction of electrophoresis. The resulting 'fingerprint' is extremely useful for diagnostic purposes. However, the quantities separated are insignificantly small.

On a more useful scale for preparative purposes, Vermeulen et al. (V4) report successful separations in an annular bed packed with glass or polystyrene beads. Their paper describes simple separations at rates of 0.1 to 1 kg per hour. However problems were encountered with thermal and electro-osmotic effects.

1.5.6 Special Analytical Techniques

For laboratory applications, a small-scale cylindrical type of batch separator has been devised. The apparatus, shown schematically in Figure 1.18, takes advantage of the fact that an artificially imposed density gradient in a fluid will remain stable even in the presence of small temperature differences. Such density gradients are normally constructed using a concentration gradient of substances such as sucrose, dextran, polyelectrolytes of high molecular weight or colloidal silica. The separation is performed in the central tube, leaving a series of bands of separated components along the length of the density gradient. These can then be removed, one at a time, by filling the tube from below. Full details of a typical density-gradient electrophoresis set up are given by Boltz and Todd (B12).

Still higher resolutions can be provided by isotachophoresis. In this technique, boundaries between zones of different ionic type (either anion or cation with a common counterion) are created in the solution. The sample to be

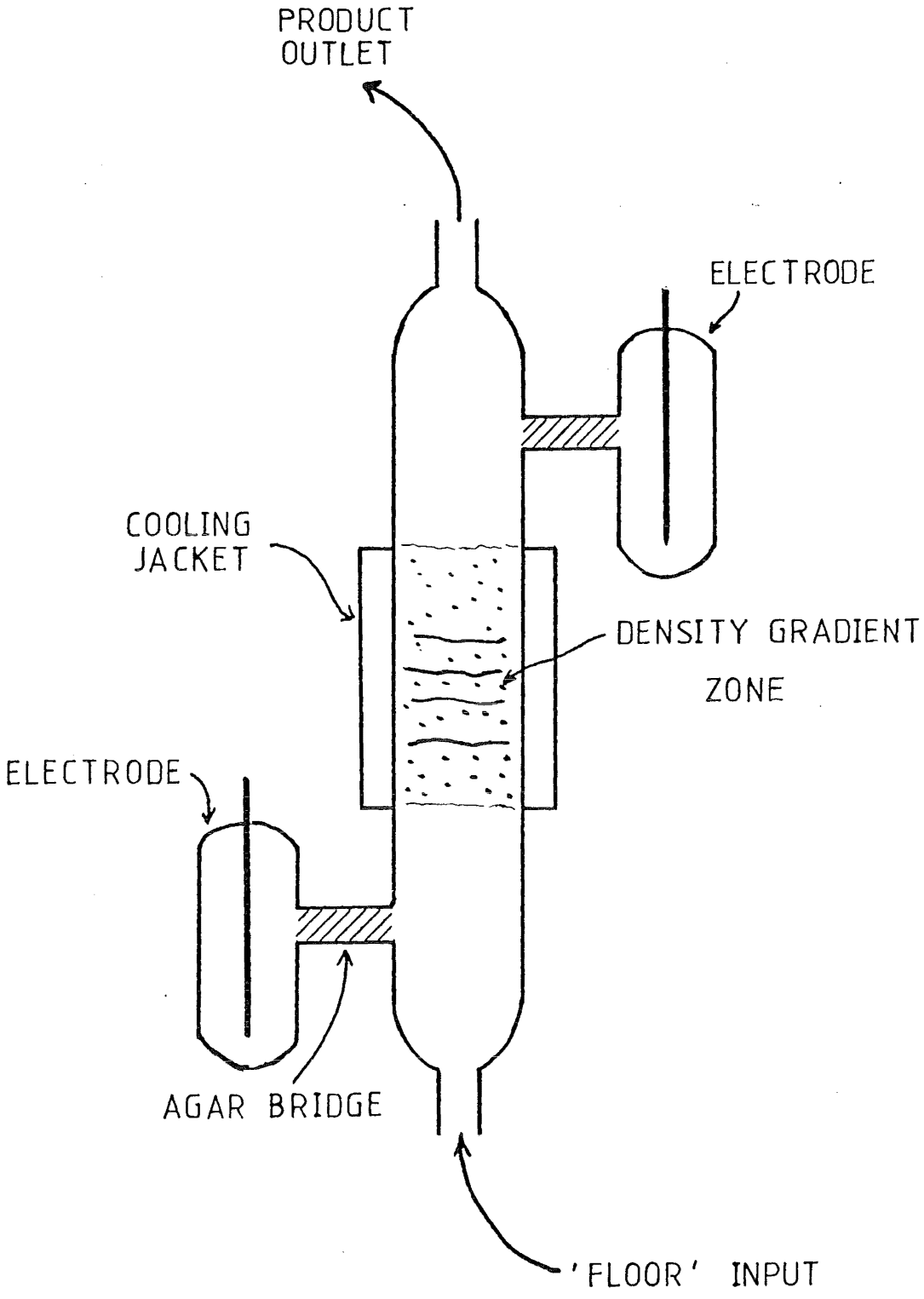

FIGURE 1.18 DENSITY GRADIENT CELL

separated is then placed between these two ionic types and the field applied. The resulting 'steps' in the field gradient caused by the boundaries thus sharpen the resolution of the separated species to a very high degree. The operation of this process is detailed, with an outline of the theory, by Bier and Allgyer (B4).

For extremely high resolutions, the properties of a series of polyamide-derived compounds collectively known as carrier ampholytes is utilised. These compounds are capable of forming continuous pH gradients under the influence of an electric field. Introduction of proteins to such a pH field results in the migration of each type until the pH is reached at which it no longer has a surface charge. This pH (known as the isoelectric point) is a characteristic of each protein and hence the separate types are extremely finely resolved or focussed by this principle. A review of the theory and current practice of this isoelectric focussing procedure was recently published by Righetti (R3). A recent trend has been to combine these high-resolution techniques with gel-support media, particularly the newer types of polyacrylamide gel (C3).

1.5.7 Electrodecantation

Investigation by Pauli in the early 1920's (P1) into the use of electrodialysis to purify colloids led to the observation that after the passage of a direct current a colloid solution formed two distinct layers; one at the bottom containing most of the colloid and one at the top with little or no colloid. This result was explained by Blank and Valko (B9). They observed that the colloids migrated toward one of the semi-permeable membranes separating the electrodes from the centre in the Pauli cell. Here the concentration of colloids formed a sinking layer of greater density.

The original Pauli single-compartment cell later evolved into the multiple-membrane equipment shown in Figure 1.19. This type of equipment was used in the electrodecantation of latex for the rubber industry (M8) (where the latex particles floated rather than sank), and later for concentration of aqueous polytetrafluoroethylene (D3).

1.5.8 Forced Flow Electrophoresis

Bier (B3) has produced a device for large-scale single component separations. One cell of this device is shown in Figure 1.20. In this device, the electric field is applied across the two outer semi-permeable membranes. The solution being fractionated is forced through the filter between the membranes, while the electric field forces (in this case, negatively charged) species in the opposite direction. Correct adjustment of the flow, electric field strength, and the draw-off rate from the bottom left permits only positively charged or isoelectric species to flow from the right-hand outlet. This type of device has been used both for electrophoretic recovery of single components and for electrically aided filtration (H1).

1.5.9 Endless Belt Continuous Electrophoresis

Simultaneous work by Kolin (K4, K5) and Hjerten (H7) showed that a particle suspended in a fluid may be stabilised by either rotating the vessel containing the fluid or causing the fluid itself to trace an annular path (Figure 1.21). As shown in the diagram, the rotation of the fluid causes the suspended particle to oscillate relative to the vessel about a mean central point.

This observation led to the development of an extremely elegant device for free-zone electrophoresis. The

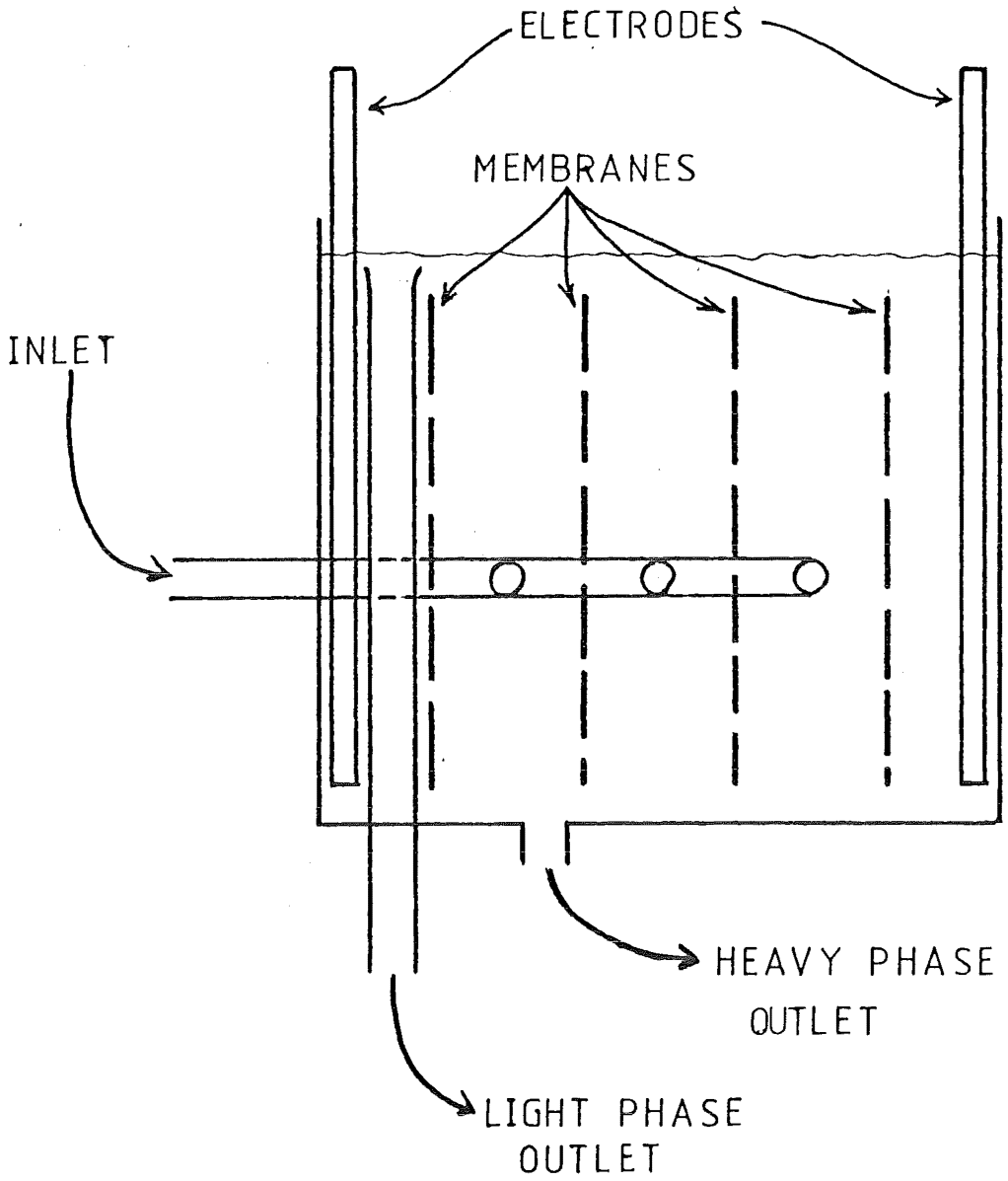

FIGURE 1.19 MULTI-COMPARTMENT ELECTRO-DECANTER

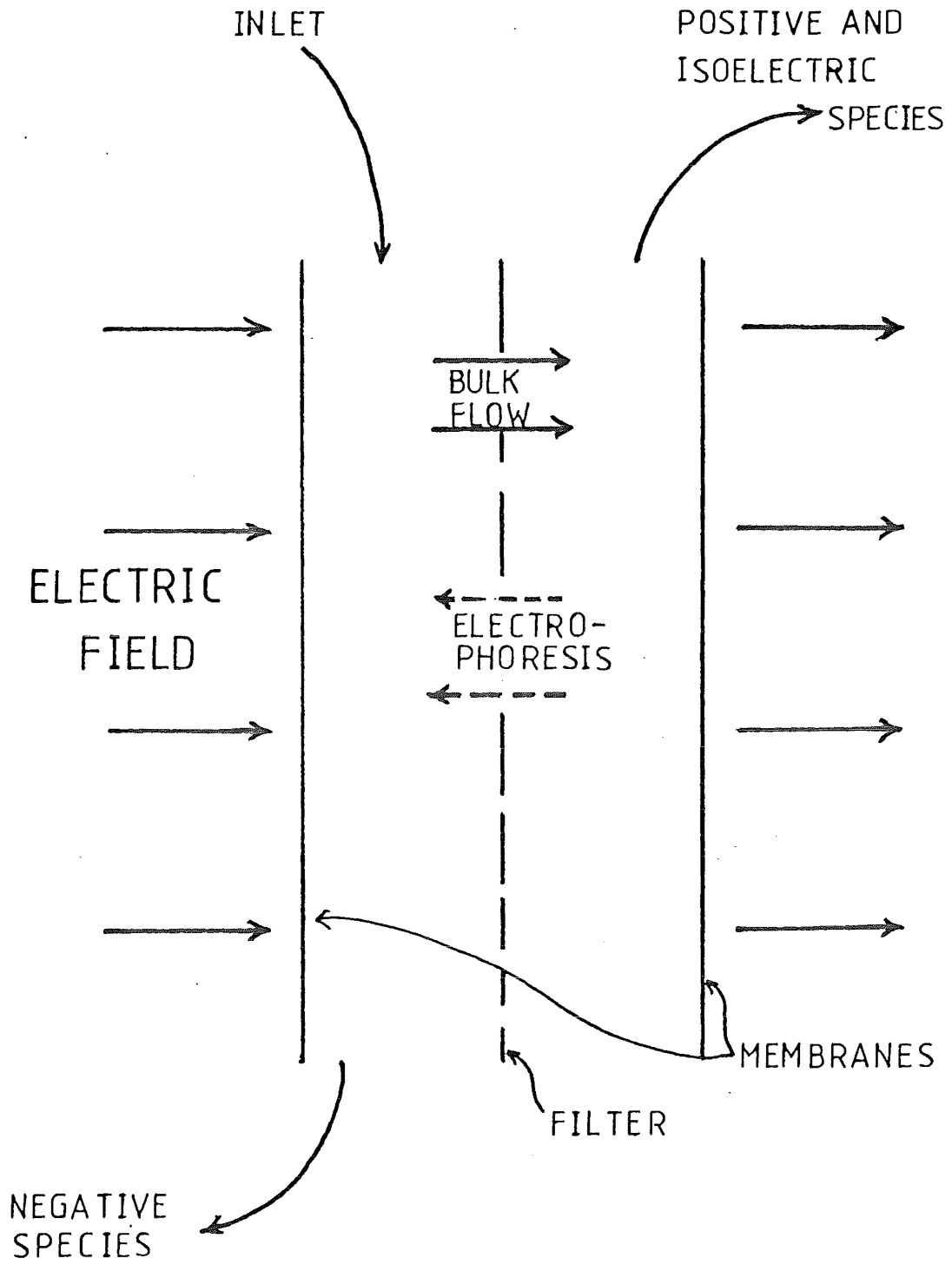

FIGURE 1.20 BIER CELL

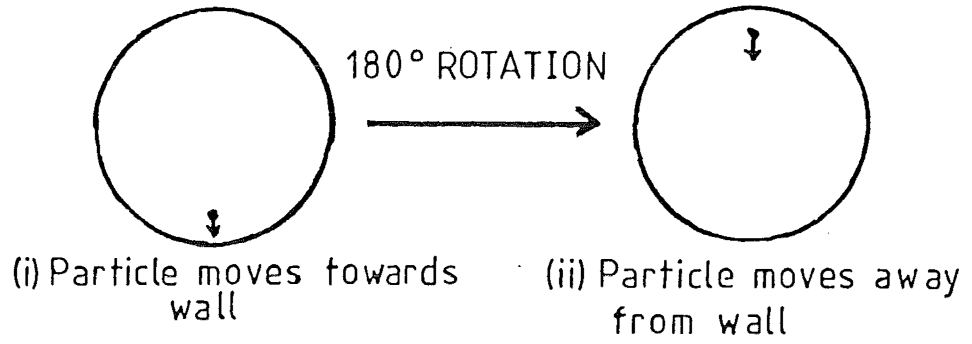

(a) PARTICLE STABILISATION

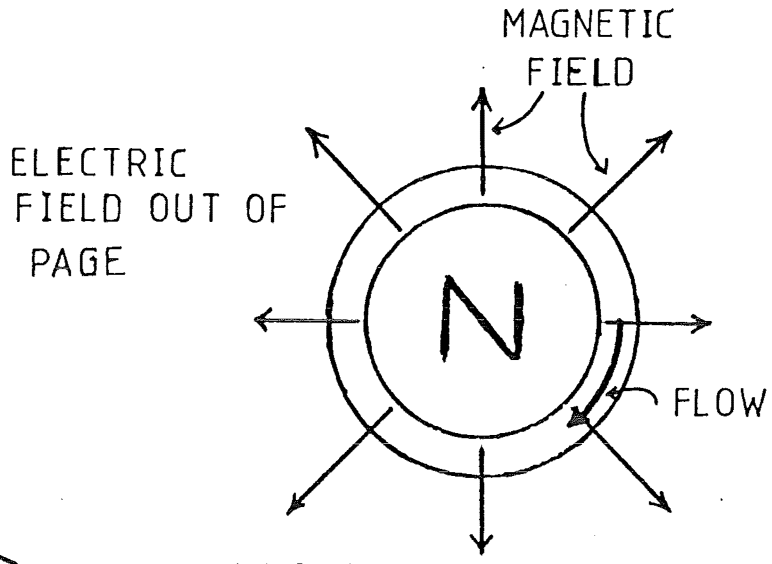

(b) FLOW PRINCIPLE

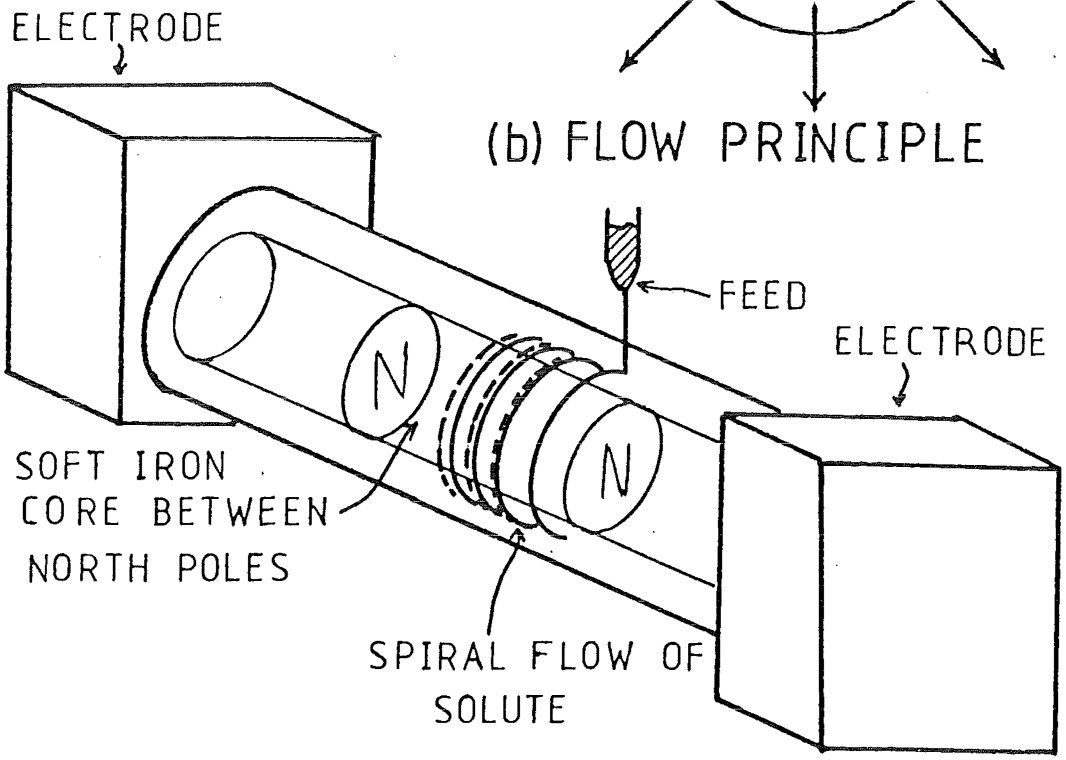

(c) SEPARATOR

FIGURE 1.21 'ENDLESS BELT' CELL

principal elements of this device are represented schematically in Figure 1.21. The central ion core sandwiched between two magnetic north poles provides a radially outward magnetic field which interacts with the longitudinal electric field between the two electrode compartments to give a circumferential fluid flow. The longitudinal electric field provides an electrophoretic force moving particles injected at a suitable point along the annular cylindrical space. The result is a spiral flow of each component, each spiral with a different pitch. These flows can be removed by the use of suitable sampling tubes or the pitches photographed to provide mobility data. This device has undergone considerable development since its conception and a summary of this development can be found in Kolin (K6).

1.5.10 Free Flow Zone Electrophoresis Devices

Probably the first free-flow zone electrophoresis device proposed was that of Philpot (P5) in 1940. However, this device was never entirely successful as the separation depended on the maintenance of a complex vertical density gradient across a horizontal flow. Philpot subsequently transferred his work to AERE Harwell and rethought the entire concept of the device.

This revised device consists of a rotating outer cylinder with a static inner cylinder forming an annular space across which the electric field is radially applied (Figure 1.22). The solute then travels vertically upward with radial electrophoretic migration of each component in a stabilising shear gradient induced by rotation of the outer electrode (P6). Subsequently, this device was developed as a preparative laboratory separator by the Harwell Biochemistry Group (M3).

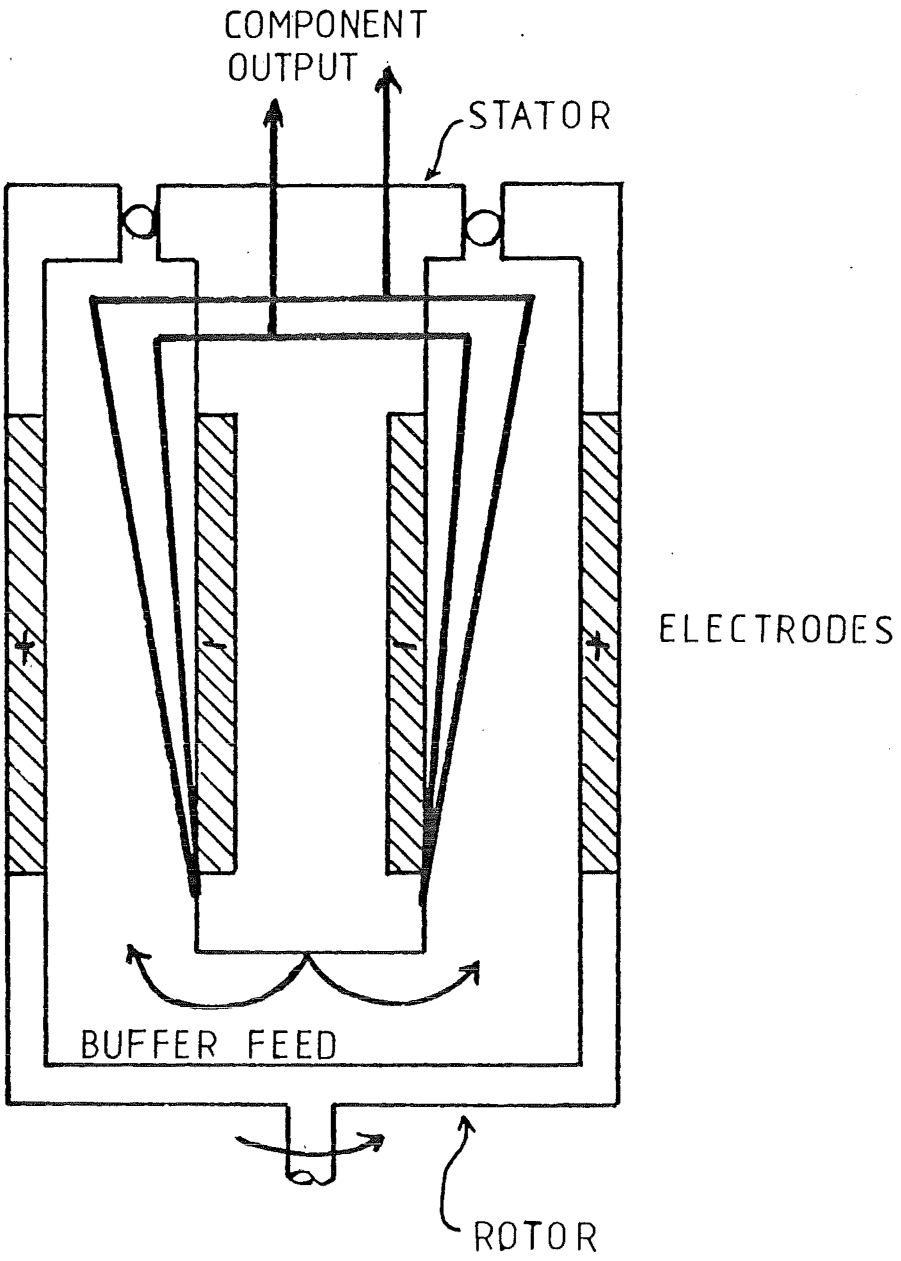

FIGURE 1.22 VELOCITY GRADIENT STABILIZED CELL

The other major direction of development of continuous-flow zone electrophoresis was a vertical downflow cell developed independently by Hannig et al. (H2) and Strickler and co-workers (S10). Both of these devices are narrow rectangular slab-shaped cells, with the electrodes at the narrower of the two pairs of faces (Figure 1.23). Cooling is supplied on the larger (non-electrode) faces of the cells. These devices are capable of high resolution, but because of the shallowness of the cell their preparative capacity is limited (typical throughputs are in the range 1-200 microlitres per minute). This configuration also suffers from electro-osmotic effects because of the large area of non-conducting cell wall in contact with the solution. In spite of these drawbacks, both devices are capable not only of high-resolution preparative separations, but also of direct measurement of free solution mobilities. A summary of the theoretical relationships describing the operation of these devices is given by Vanderhoff et al. (V2).

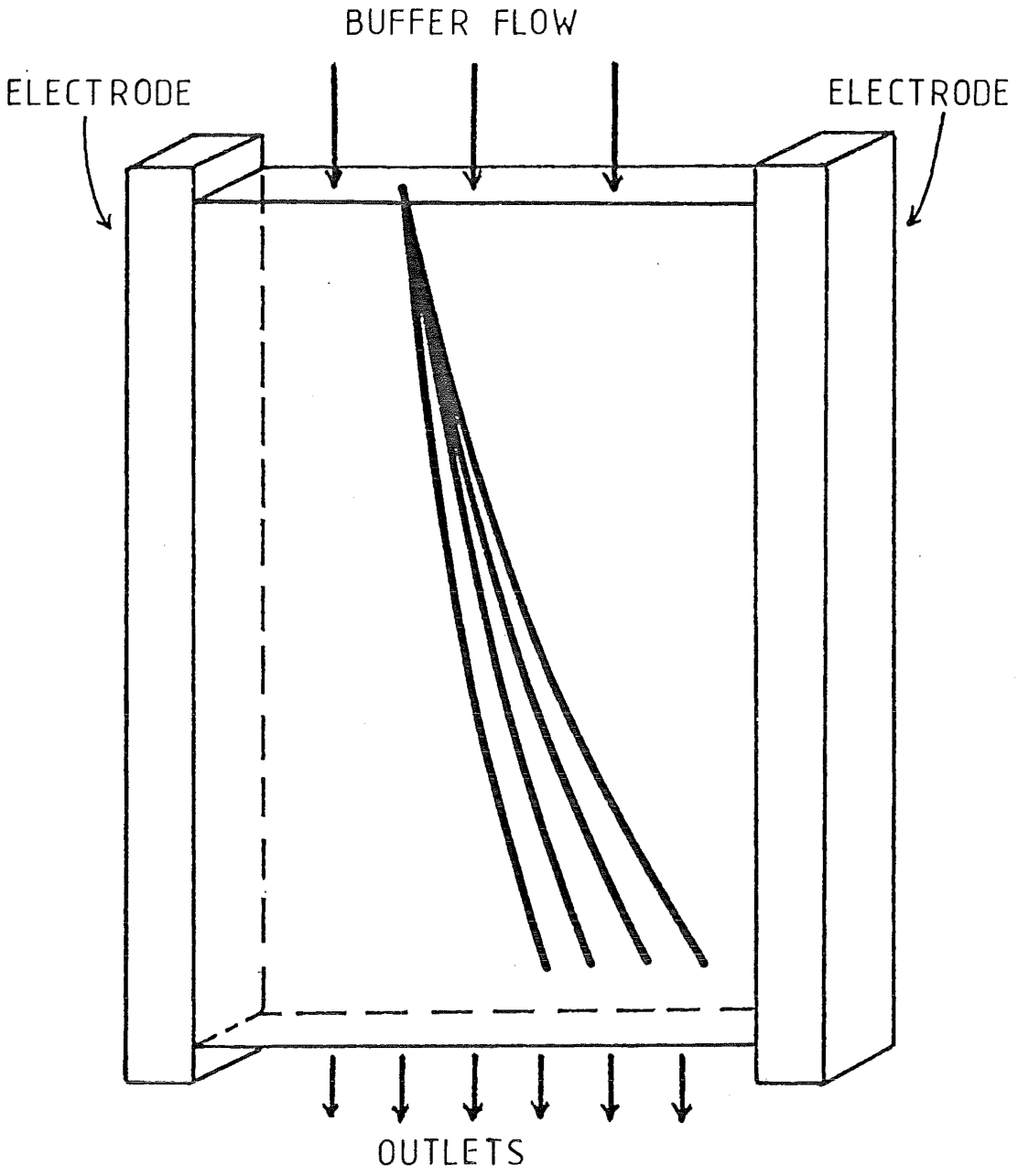

FIGURE 1.23 FREE SOLUTION DOWNFLOW CELL

2. PRELIMINARY STUDIES

2.1 Purpose of Preliminary Studies

2.1.1 Fundamentals

The concept of a free-flow, narrow-slot, electrophoresic separator outlined in section 1.1.5 requires highly stable flow conditions in the separating zone in order to operate successfully (see figures 1.4 and 1.6). Therefore, to investigate the practicability of the concept, the potential sources of destabilising forces must be investigated. Further, there must clearly exist conditions under which the flow in the separating zone can be maintained stable for useful periods of time in order for the concept to be a practical proposition.

From preliminary examination of the concept, it can be seen that fluid-dynamic, thermal, and electric-field effects are present and the operating envelope of the device must lie in an area where none of these effects will give rise to flow instabilities.

2.1.2 Fluid Dynamics

The primary condition of no remixing of separated streams, on which free-flow electrophoresis depends, can only be met with fully developed laminar flow throughout the separator. (It may be reasonably expected that no slip will occur at the solid boundaries of the separating channel; therefore plug flow is discarded as unrealistic.) Further, provision is required to introduce the feed components to the correct portion of the narrow slot and separately remove the transferred substances. The geometry of the device should also minimise, and if possible eliminate, settling of the solute components which may have

densities different from those of the carrier stream.

2.1.3 Thermal Stability

The electric field fundamental to electrophoresis implies the passage of current which in turn means resistive heating. The operation of the device is thus constrained to a heating rate less than that which will create temperature differences high enough to cause thermal convection. Qualitatively this involves a balance of flowrate, heat loss by conduction and resistive heat generation.

2.1.4 Electric Field Effects

Observations made by Brown (B15) in 1964 showed that high direct current electric fields induced swirling motion in dielectric liquids. These observations were later extended and put on a theoretical footing by Hewish and Brignal (H6) and Atten and Moreau (A3). This latter work is of interest in the case of electrophoresis as it involves external electric fields applied to solutions, rather than space-charge limited fields (i.e. fields resulting from charges within the liquid.)

From this series of papers, it appears that there is some upper limiting electric-field strength above which turbulence is induced in free liquids. This represents a limit for the field strengths useable in continuous-flow electrophoresis.

Electroosmosis has been discussed in the previous chapter (section 1.4). As is pointed out, electroosmosis has the effect of distorting flow profiles in electrophoresic separations.

2.2 Fluid Dynamics

2.2.1 Introduction

As remarked previously, the Arcus narrow-slot electrophoretic separator requires the formation and maintenance of fully developed laminar flow through a rectangular duct with a large depth-to-width ratio (Figure 1.4). Thus geometries are required for entrance and exit regions which meet this requirement. The entrance region must also enable the introduction of a feed layer surrounded by buffer streams without discontinuities being caused in the flow where these streams merge. Similarly, the exit must permit partitioning of a number of narrow sections across the width of the stream, with each section retaining the full depth of the separator (Figure 2.1). The concept also requires the maintenance of fully developed laminar flow in a rectangular duct of constant cross-section in the presence of small density differences across the width of the flow.

2.2.2 Entrance Geometry

It can be shown that, for the boundary layer in Newtonian flow over a flat plate (W4),

$$\rho\left(\frac{\partial U_x}{\partial t} + U_x \frac{\partial U_x}{\partial x} + U_y \frac{\partial U_y}{\partial y}\right) = -\frac{\partial P}{\partial x} + \mu \frac{\partial^2 U_x}{\partial y^2} \qquad 2.1$$

where x is a dimension parallel and y a distance normal to the plate. Since there is a no-slip condition at the surface (i.e. $U_x = U_y = 0$ at $y = 0$), equation 2.1 becomes (for steady-state behaviour)

$$\mu \frac{\partial^2 V_x}{\partial y^2}\Big|_{y=0} = \frac{dP}{dx} \qquad 2.2$$

If $\frac{dP}{dx}$ is zero or negative, the second derivative of velocity is also zero or negative. Far from the plate the second

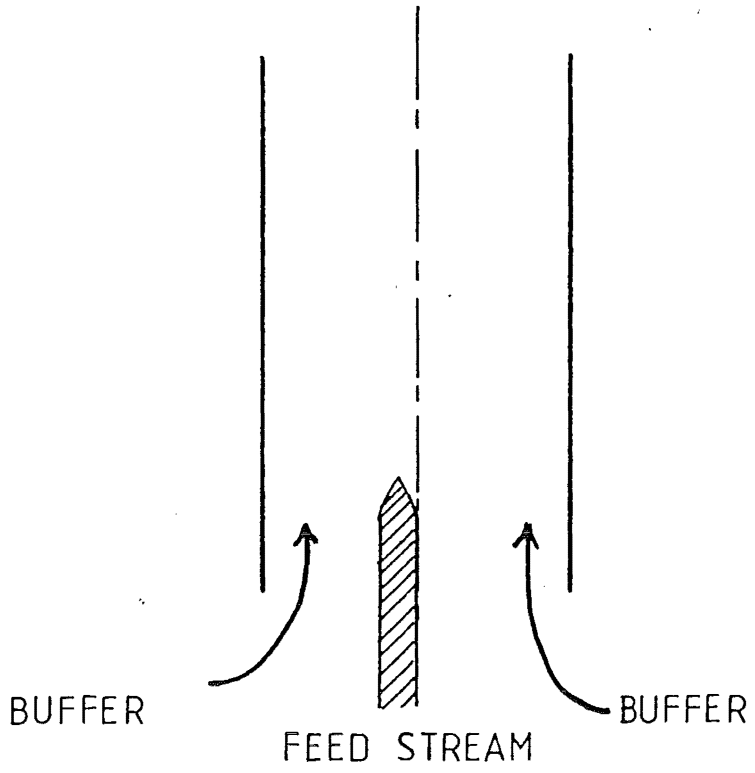

(a) Entrance Requirements

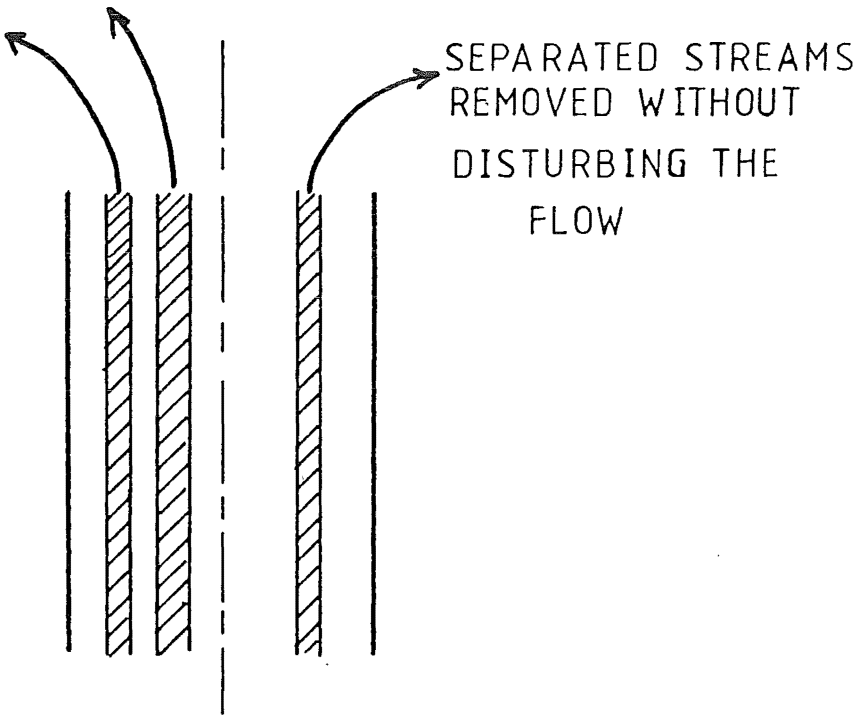

(b) Exit Requirements

FIGURE 2.1 ENTRANCE AND EXIT REQUIREMENTS

derivative of velocity must also be zero. For both these cases, inspection of the appropriate curves of velocity and velocity gradient as a function of y (W4) shows that the velocity gradient at the wall is continuous and without a point of inflection. Resultingly, flow under these circumstances is stable; that is, there is no boundary-layer separation. Further, since in a converging channel the velocity increases in the direction of convergence, the pressure decreases in the same direction. Thus, flow in a converging channel, formed by two converging flat plates between parallel walls, is unconditionally stable provided the velocity increase is not sufficient to induce turbulent flow.

Thus it can be seen that a continuously converging channel will maintain laminar flow into a narrow parallel-sided duct. By extension of this principle, a number of converging channels merging into a common converging channel will sustain laminar flow, provided there are no eddying effects from the separation of flow from the inner channel walls at the plane where the channels merge. In practice, this last condition can be met if the ends of these inner walls are sharp knife-edges and flow is sufficiently slow.

2.2.3 Exit Geometry

At the end of the narrow-slot separating zone, there will be a number of flat sheets of components flowing parallel to each other but extremely close together (see Figure 1.4). In order to complete the mass-transfer process, these flows must be separated physically for recovery: that is to say, the outlet stream must be split into separate streams that are led to separate collecting vessels.

Due to the narrowness of the separating zone, there will be inadequate room to insert the required number of flow splitters directly across the width of the zone. However, problems are presented by fitting a diverging section of the same depth as the separating zone to accommodate these flow splitters. Such a diverging section will give rise to decelerating flow and hence a positive pressure gradient in the direction of flow. By equation 2.2, the second derivative of velocity therefore becomes positive at the wall. However, the condition that $\frac{\partial^2 V_x}{\partial y^2}\Big|_{y=\infty} = 0$ still holds. Inspection of the curves of velocity and its derivatives as a function of distance from the wall (W4) shows that a point of inflection in the velocity gradient occurs. This implies zero velocity at some distance from the wall and hence boundary-layer separation causing eddying and the resulting break-down of laminar flow. Such a situation is clearly unacceptable.

Consideration of the above arguments shows that it is necessary to both broaden the flow in order to insert collector slots and at the same time maintain laminar flow throughout. This latter condition demands constant or increasing velocity. To meet these requirements, the geometry shown in Figure 2.2 is proposed. As shown, this geometry diverges in the plane of separation, but converges at right-angles to this plane (i.e. the depth decreases). Since the cross-sectional area of the proposed geometry decreases, accelerating and hence stable flow is retained while permitting the output to be split and the components collected separately.

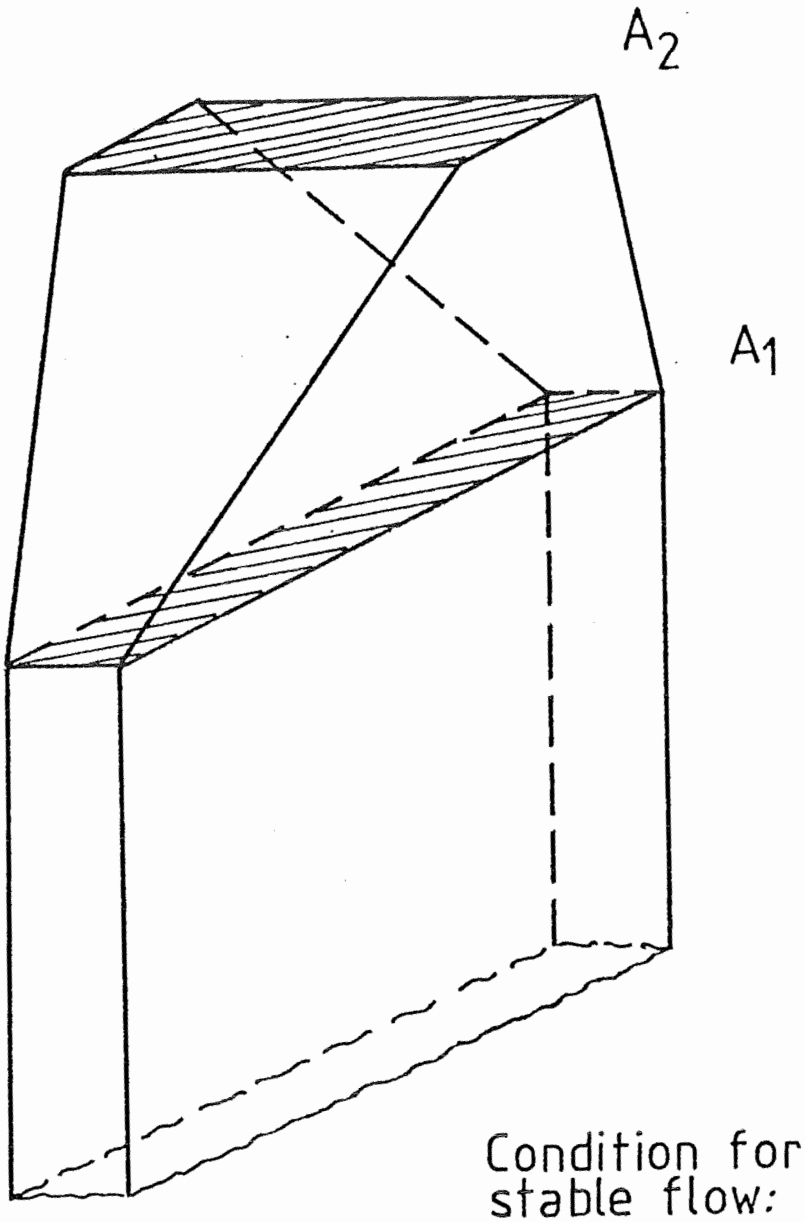

FIGURE 2.2 OUTLET GEOMETRY

2.2.4 Fluid Flow in the Narrow Slot

The projected form of the narrow-slot electrophoresic separator assumes that the separating zone is a narrow, but relatively deep, rectangular cell of constant cross-sectional area. The relatively great depth-to-width ratio enables the flow in this section to be considered using the two-dimensional model shown in Figure 2.3. Thus, given fully developed laminar flow into the duct and in the absence of externally imposed disturbances, it is reasonable to expect stable laminar flow to be maintained in the duct. For the moment the question of the destabilising influences of external forces and density gradients due to solute components is ignored. These effects are the subject of the remaining sections of this chapter.

2.2.5 Preliminary Fluid-Flow Test Device

On the basis of the above reasoning, the test cell shown in Figure 2.4 was buit. This device was designed to provide some experimental experience of the hydrodynamics of the narrow-slot proposal. The cell was fed water from three constant-head tanks and the flow through the cell visualised by the addition of a small amount of B.D.H. Laboratories brilliant green dye to one stream. The resulting traces were photographed through an orange filter. Flowrates through the test cell were measured by timing the collection of a volume of the outflow in a calibrated vessel.

The resulting images were related to the Reynolds number for flow through the centre section of the device.

$$Re = \frac{DU\rho}{\mu} \qquad 2.3$$

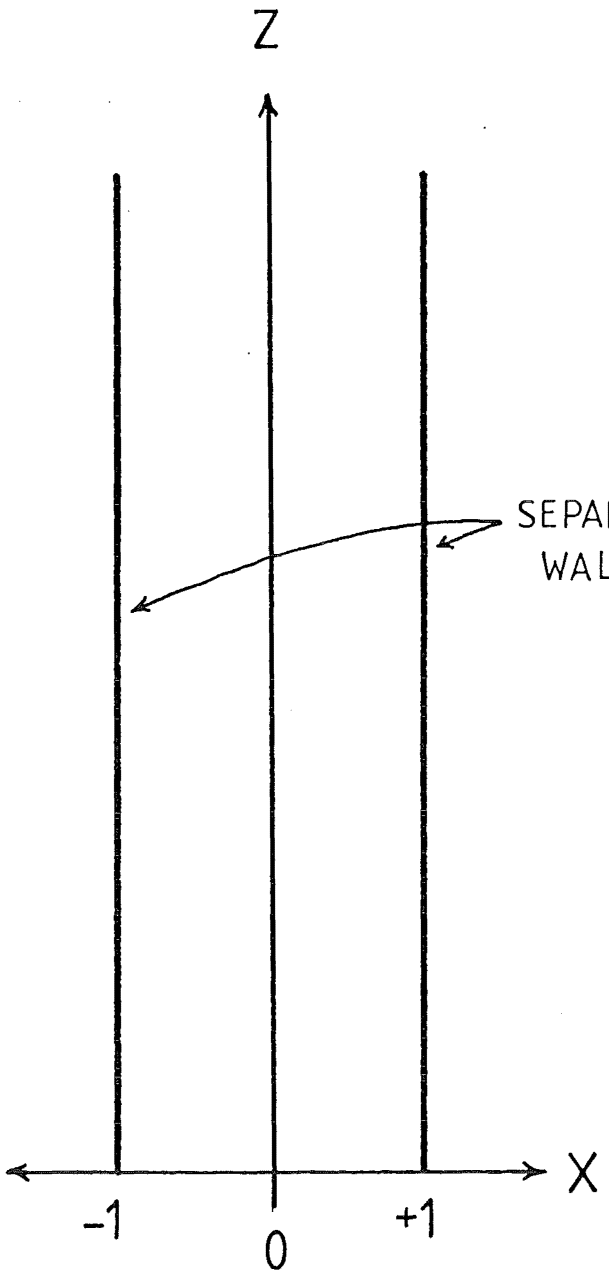

FIGURE 2.3 COORDINATE SYSTEM FOR NARROW-SLOT SEPARATOR

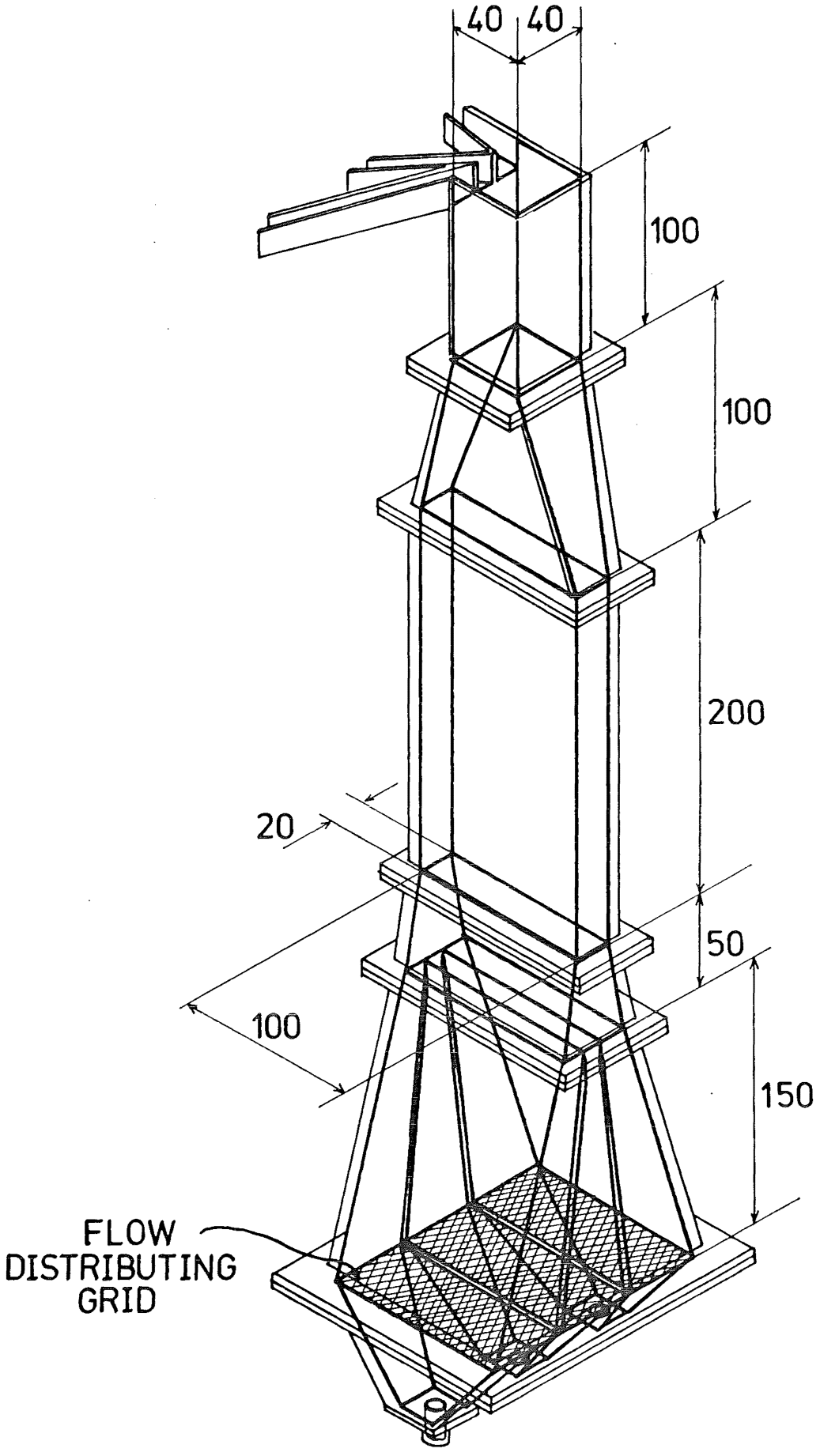

FIGURE 2.4 FLUID DYNAMIC TEST CELL

(ALL DIMENSIONS IN mm)

where D = mean hydraulic diameter of the centre section

$$= \frac{4 \times (\text{cross sectional area})}{\text{wetted perimeter}}$$

$$= \frac{4 \times w \times d}{2(w + d)} \qquad \text{(see Figure 1.4)}$$

and

U = mean velocity of flow through the rectangular duct

$$= \frac{\text{volume collected}}{\text{time of collection}} \times (\text{cross-sectional area of centre section})$$

and ρ = fluid density

and μ = fluid viscosity

The properties of water at $20^{o}C$ were used.

The results of these observations are shown in plates 2.1 - 2.3. While the observations from these experiments are not totally quantitative in defining the regimes for flow stability, the experiments suggest the following conclusions.

i) At extremely low flows (Reynolds number in the range 10-30), it was very difficult to establish stable flow (plate 2.1). This was considered to be due to the effect of the micro-turbulence-creating grids used to provide sufficient pressure drop at the inlet to permit laminar flow to form across the full width of the inlet ducts (see Figure 2.4).

ii) At Reynolds numbers in the range 100-250, well-defined stable flow was observed (Plate 2.2).

iii) At Reynolds numbers of approximately 400, wavelike disturbances were observed in the flow (pate 2.3). This type of disturbance was thought to be caused by instabilities in the flow at the knife edges where the three streams combined at the inlet.

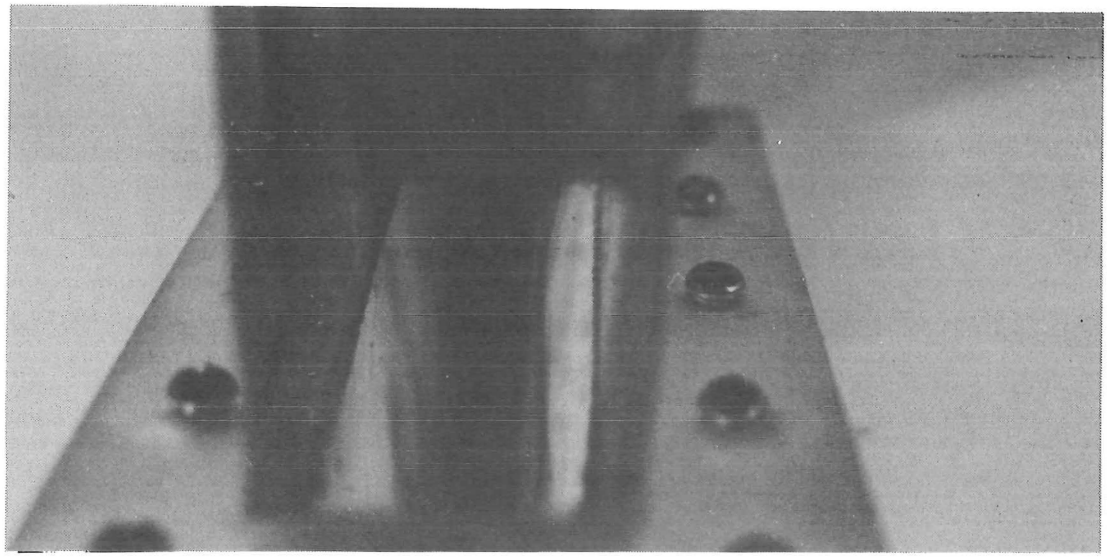

(iii) Outlet

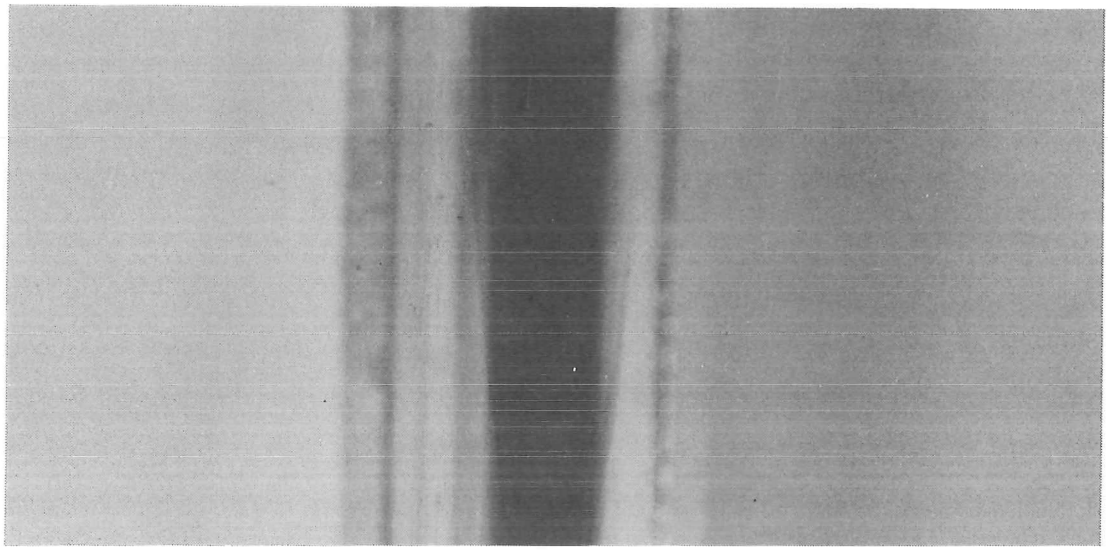

(ii) Centre

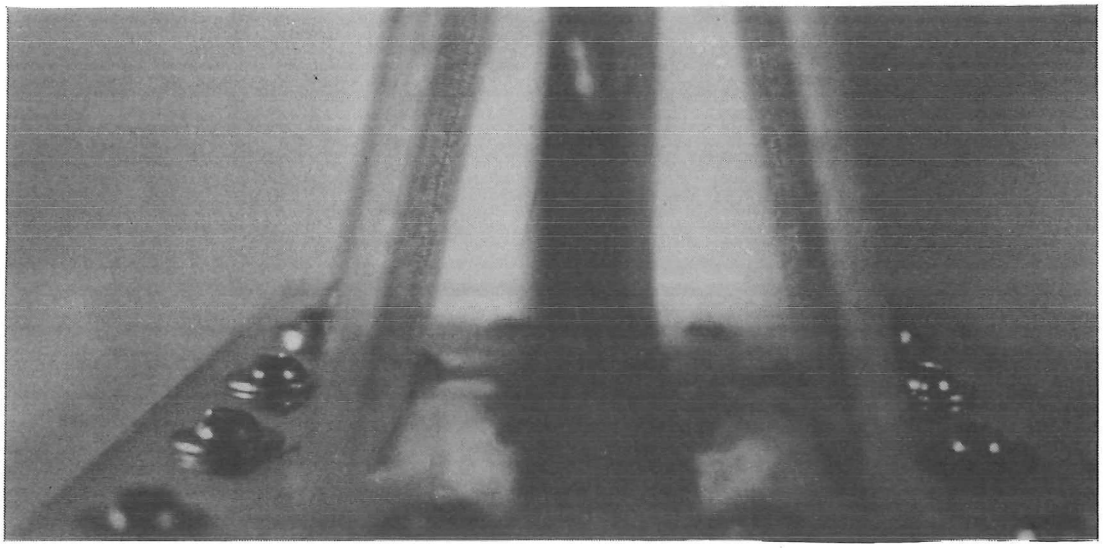

(i) Inlet

Plate 2.1: Flow through fluid dynamic test cell at Re = 16.

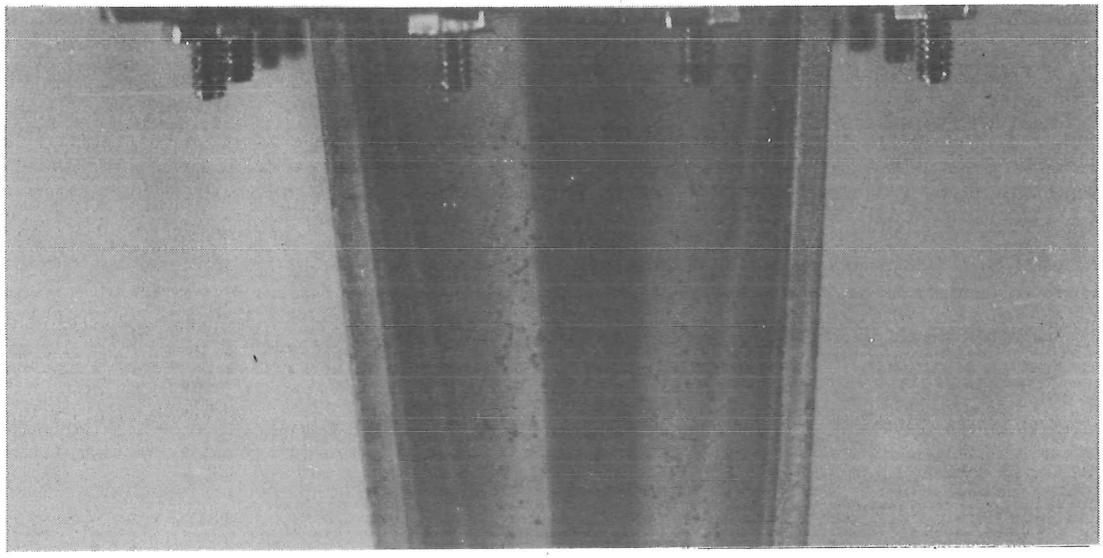

(iii) Outlet

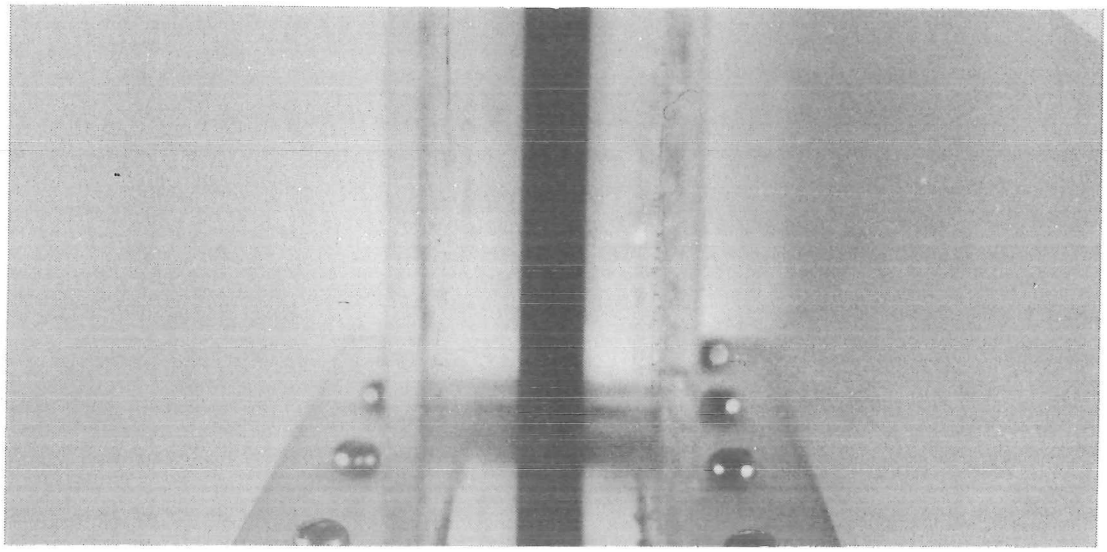

(ii) Centre

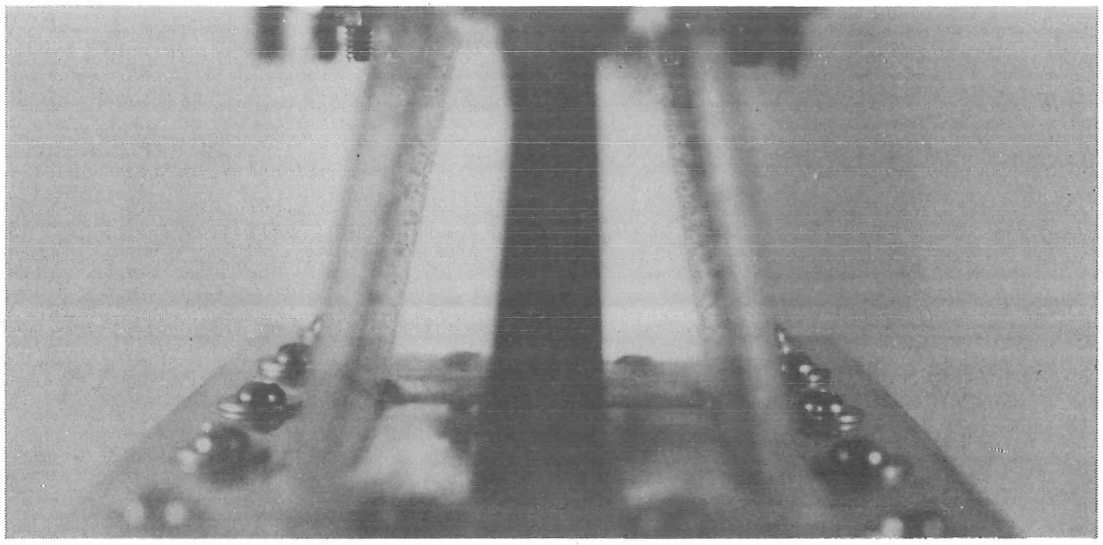

(i) Inlet

Plate 2.2: Flow through fluid dynamic test cell at Re = 140

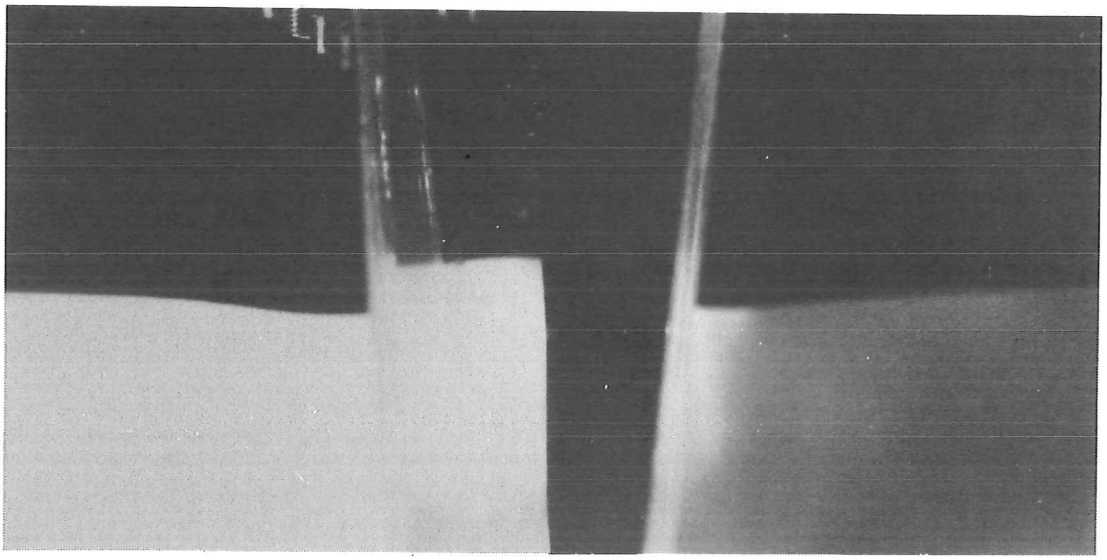

(iii) Outlet

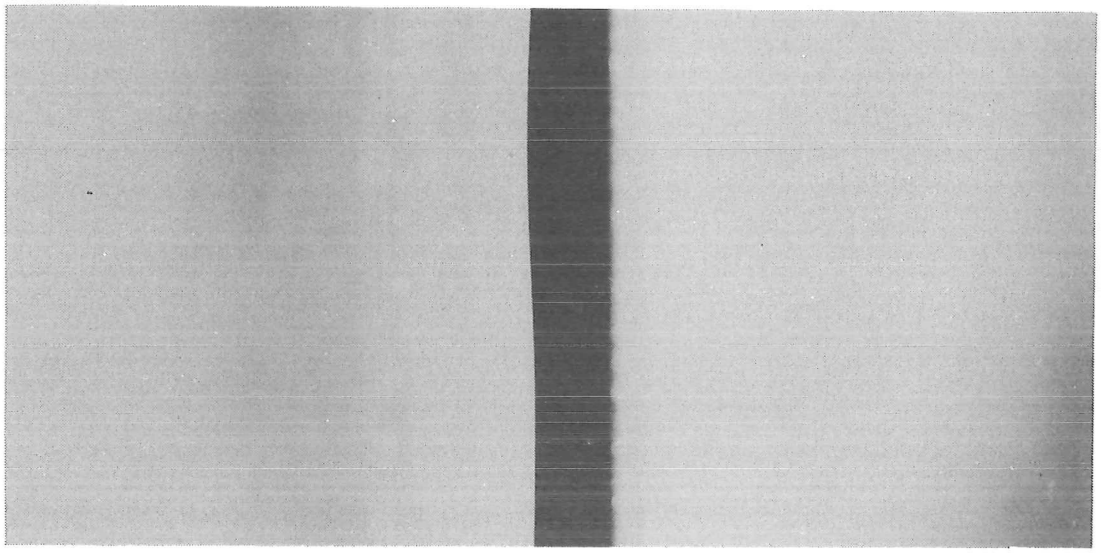

(ii) Centre

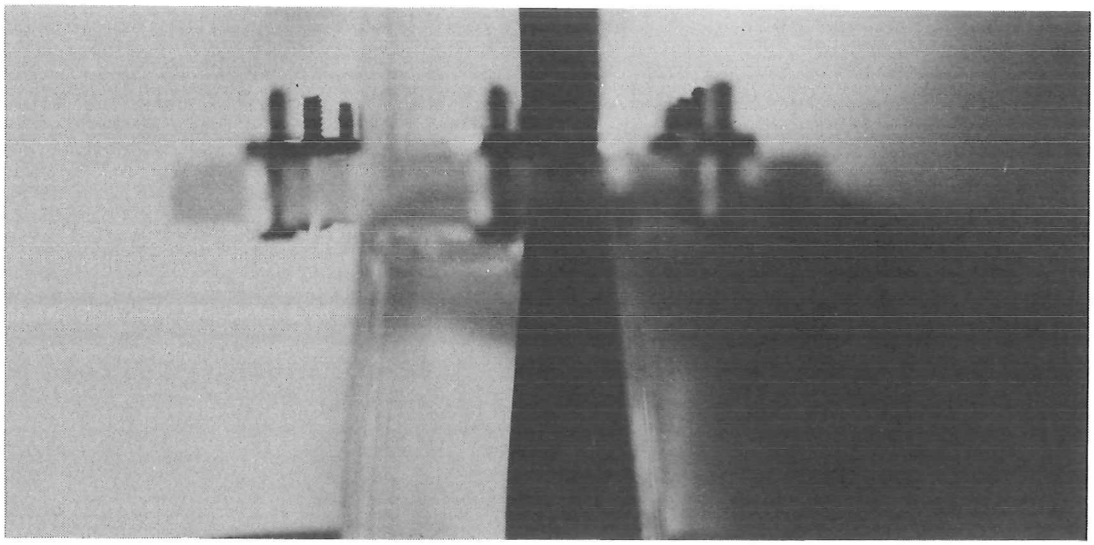

(i) Inlet

Plate 2.3: Flow through fluid dynamic test cell at Re = 400.

iv) In general, stable flow was maintained in the outlet throat, confirming the hypothesis about the stabilising effect of this geometry.

On the basis of these observations, it was concluded that stable flow in a cell with the geometry outlined above could be maintained, at least over the range $100 < Re < 200$, for waterlike solutions.

2.3 Theoretical Stability Analysis

2.3.1 Concept

In order to examine the instabilities likely to result from the electric field and fluid property gradients in the narrow-slot electrophoresis concept the appropriate differential balance conservation equations are used. These equations are written in the appropriate form for the geometry of this device and subjected to small perturbations, with the object of finding the conditions for which these perturbations are or are not damped.

The coordinate system used for this analysis is shown in Figure 2.5. This diagram also shows the forms of the gradients of the parameters of interest in their initial (undisturbed) state. The analysis is of the form of that of Turnbull (T7).

Note that this analysis does not deal with thermally induced disturbances.

2.3.2 Equations

Conservation of mass may be written in vector terms as the differential balance:

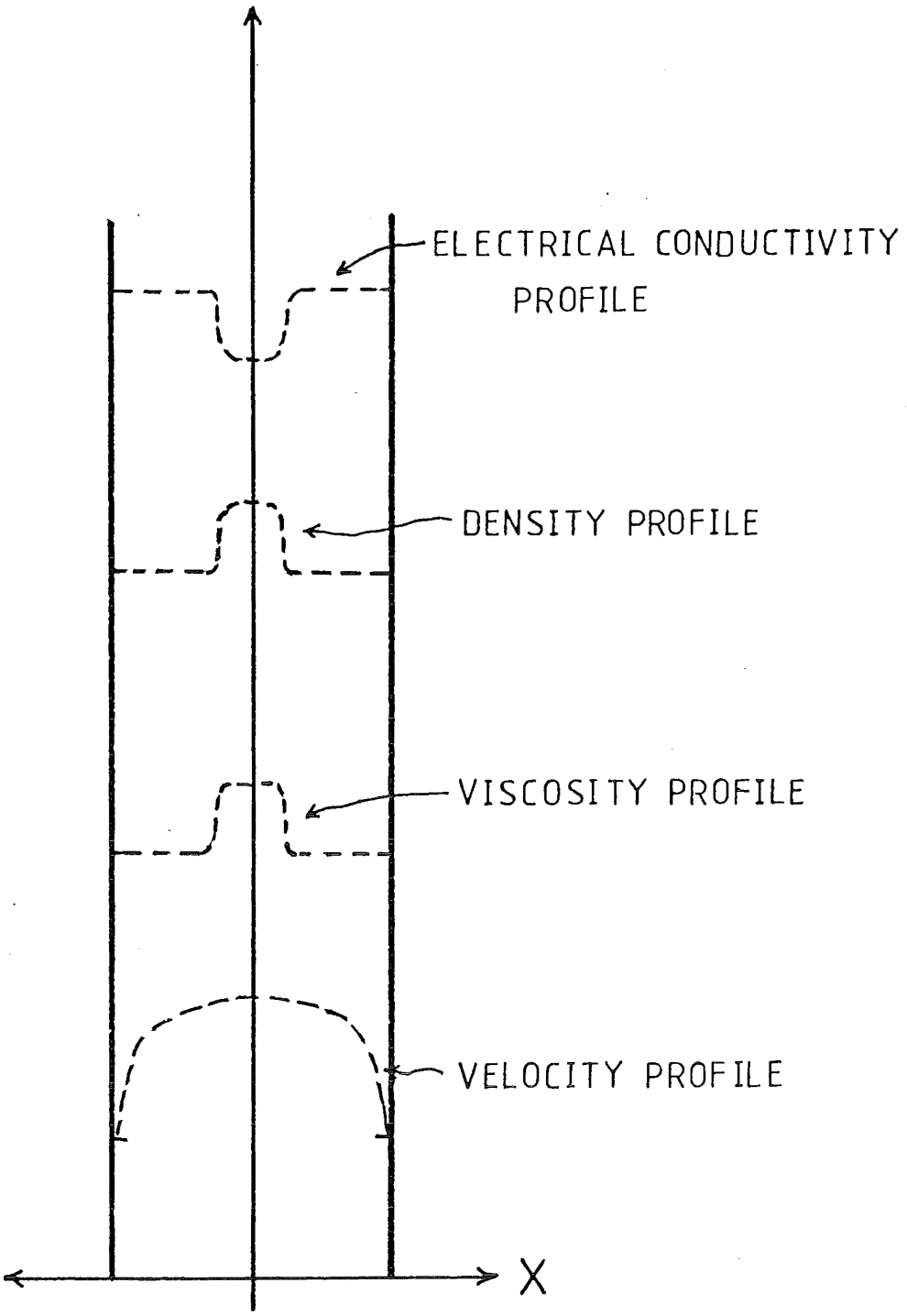

FIGURE 2.5 SOLUTION PROPERTY PROFILES FOR NARROW-SLOT SEPARATOR

$$\frac{\partial \rho}{\partial t} + \underset{\sim}{\nabla}.(\rho \underset{\sim}{U}) = 0 \qquad 2.4$$

Similarly conservation of momentum may be written as

$$\rho \frac{\underset{\sim}{\underset{\sim}{DU}}}{Dt} = -\nabla P + \rho g + \underset{\sim}{f}_e + \underset{\sim}{\nabla} . \underset{\sim}{\underset{\sim}{\tau}} \qquad 2.5$$

where the derivative following the motion is defined by

$$\frac{\underset{\sim}{D}}{Dt} = \frac{\partial}{\partial t} + \underset{\sim}{U}.\underset{\sim}{\nabla} \qquad 2.6$$

The differential energy balance may be written for this case as

$$\rho C_p \frac{\underset{\sim}{DT}}{Dt} = \underset{\sim}{\nabla}.(k\underset{\sim}{\nabla}T) + P_v + P_e \qquad 2.7$$

and the general expression for the electrical force on the fluid can be expressed as

$$\underset{\sim}{f}_e = e \underset{\sim}{E} - \tfrac{1}{2} \underset{\sim}{E}.\underset{\sim}{E}\nabla\varepsilon + \tfrac{1}{2}\underset{\sim}{\nabla}(\rho_e \frac{\partial \varepsilon}{\partial \rho_e} \underset{\sim}{E}.\underset{\sim}{E}) \qquad 2.8$$

In the above equations, the symbols have the following meanings:

ρ = fluid density

ρ_e = electric charge density

t = time

$\underset{\sim}{U}$ = velocity

$\underset{\sim}{g}$ = gravitational acceleration

$\underset{\sim}{f}_e$ = electric force on the fluid

$\underset{\sim}{\underset{\sim}{\tau}}$ = stress tensor

C_p = heat capacity (at constant pressure)

k = thermal conductivity

$\underset{\sim}{E}$ = electric field strength

P_v = viscous power dissipation

P_e = electric power dissipation

T = temperature

ε = electric permitivity

In addition, since the fluid is of low electrical conductivity, magnetic field effects can be neglected and so:

$$\underset{\sim}{\nabla} \times \underset{\sim}{E} = 0 \qquad 2.9$$

and

$$\underset{\sim}{\nabla} \times \varepsilon\underset{\sim}{E} = \rho_e \qquad 2.10$$

also

$$\frac{\partial \rho_e}{\partial t} + \underset{\sim}{\nabla} . \underset{\sim}{J} = 0 \qquad 2.11$$

where $\underset{\sim}{J}$ = the current vector.

Since the fluid is in motion, the current vector must include a specific term to account for the bulk convective flow of the charge-carrying species, viz.

$$\underset{\sim}{J} = \Lambda\underset{\sim}{E} + \rho_e \underset{\sim}{V} \qquad 2.12$$

where Λ = specific conductance of the fluid.

2.3.3 Linear Theory Perturbation Analysis

In order to test the stability of the narrow-slot system, the variables electric field, density, electric conductivity, and viscosity have small perturbations applied to them. The perturbed form of the equation is then tested to examine the cases for which these perturbations die out. This is done by taking the curl of the equation and examining the perturbed portion of the resulting relationship for the conditions which cause the amplitudes of the disturbances to decay to zero (Turnbull (T7)).

Perturbations are assumed to be wavelike, two-dimensional, and of the general form:

$$\rho' = \text{Real } [\hat{\rho}(x)(e^{j(\omega t - Kz)})] \qquad 2.13$$

where $\hat{\rho}$ is a complex amplitude, and K and ω are the wavelength and frequency respectively. Since the bulk flow through the cell is laminar and expected to be large with respect to flow induced by other forces, fluid properties are assumed to be retained by the fluid 'packets' as they move.

$$\text{Hence} \quad \frac{\underset{\sim}{D}(\mu + \mu')}{Dt} = 0 \qquad 2.14$$

$$\text{and} \quad \frac{\underset{\sim}{D}(\rho + \rho')}{Dt} = 0 \qquad 2.15$$

$$\text{and} \quad \frac{\underset{\sim}{D}(\Lambda + \Lambda')}{Dt} = 0 \qquad 2.16$$

For incompressible steady flow equation 2.4 reduces to:

$$\underset{\sim}{\nabla} \cdot \underset{\sim}{U} = 0 \qquad 2.17$$

Since the streamline-flow regime is the area of interest, the stream function may be utilised:

$$\Psi = -\underset{\sim}{\nabla} \times \underset{\sim}{U} \qquad 2.18$$

and, further, the partial derivative with respect to x may be expressed:

$$D = \frac{\partial}{\partial x} \qquad 2.19$$

Because the disturbances are two-dimensional waves, only the y component of the stream function is non-zero; this will be labelled ψ (amplitude $\hat{\psi}$). Furthermore since the electric field is irrotational and thus curl-free, it may be described by a potential function:

$$\underset{\sim}{E} = -\underset{\sim}{\nabla} \phi \qquad 2.20$$

Given these conditions, and on taking the curl of the momentum equation (2.5) and linearising, the relationship

below is arrived at. (This relationship includes the assumed form of the bulk-flow velocity profile; viz. $U_z = U(1 - x^2)$).

$$(j\omega\rho - \rho V(1 - x^2)jK)(D^2 - K^2)\hat{\psi} + (4xUjK\rho + D\rho U(1 - x^2)jK - D\rho j\omega)D + 2(UjK - D\rho jK\ 2x\ U)\hat{\psi} + 4U^2\ x(1-x^2)jK\hat{\rho}$$

$$= D\rho g + D\hat{\rho}g + \varepsilon E\ jK(D^2 - K^2)\hat{\phi} - \varepsilon D^2 EjK\hat{\phi} + 4UD\mu$$

$$+ 2D\mu(D^2 - K^2)D\hat{\psi} - D^2\mu(D^2 + K^2)\hat{\psi} + \mu(D^2 - K^2)\hat{\psi} + 2K^2Ux\hat{\mu} \qquad 2.21$$

On examining the electrical relationships, combination of equations 2.11 and 2.12 gives

$$\frac{\partial \rho_e}{\partial t} + \underset{\sim}{\nabla}.(\Lambda\underset{\sim}{E} + \rho_e \underset{\sim}{V}) = 0 \qquad 2.22$$

When equation 2.10 is incorporated, this equation yields:

$$\frac{\partial}{\partial t}(\underset{\sim}{\nabla}.\varepsilon\underset{\sim}{E}) + \underset{\sim}{\nabla}\Lambda.\underset{\sim}{E} + \Lambda\ \underset{\sim}{\nabla}.\underset{\sim}{E} + \underset{\sim}{\nabla}.[(\underset{\sim}{\nabla}.\varepsilon\underset{\sim}{E})\underset{\sim}{V}] = 0 \qquad 2.23$$

for which the curl can be taken and the resulting relationship linearised in a similar fashion to give:

$$(-j\omega\varepsilon - \Lambda + U(1 - x^2)jK)(D^2 - K^2)\hat{\phi} - D\Lambda D\hat{\phi} - jKD^2E\hat{\phi} + \Lambda DE = 0 \qquad 2.24$$

A number of procedures were tried to use these equations in evaluating the magnitudes of the electric-field and solution-property gradients at which oscillations in the stream function would first begin to grow with time. (That is, the flow becomes unstable). These attempts were unsuccessful; however, a number of qualitative conclusions could be drawn from these relationships.

2.3.4 Qualitative Conclusions from the Theoretical Stability Relationships

i) The vertical flow will necessarily become unstable after some time as a result of the horizontal density gradient and vertical gravity field. This is because the term $\nabla\rho \times \underset{\sim}{g}$ is always non-zero. This effect is expected to be hastened by perturbations in the density gradient.

ii) Small disturbances in the imposed electric field may initiate flow disturbances due to coupling between the stream function and the electric field.

iii) The magnitude of the fluid velocity through the cell may be expected to have some effect on the onset of turbulence, as may the specific conductance of the solution.

It would therefore appear that extreme care should be taken to stabilise flow through gradients of solution properties and the imposed electric field in a narrow-slot separator.

The following sections report on experimental investigations used to establish likely limits for thermal and electrical stability of the narrow-slot separator.

2.4 Experimental Investigation of Electroturbulence

2.4.1 Introduction

While the initial work in the area of electro-turbulence (H6, A3) was performed with dielectric liquids of small specific conductance, it was considered likely that aqueous solutions of low electrical conductivity would exhibit such behaviour. To investigate this, a two-part investigation

was undertaken to evaluate the criteria for the onset of electroturbulent phenomena in dilute buffer solutions. The first investigation, that of Sheppard (S2), examined the onset of electrically induced turbulence in static dilute buffer solutions. Tillman later extended this to include the effects of electroturbulence on a laminar velocity profile in a rectangular duct (T2).

2.4.2 Electroturbulence in Static Buffer Solutions

The experimental work of Sheppard (S2) was performed with a cell similar to that of Malkus and Veronis (M2). This cell consisted of a pair of flat electrodes with the fluid under test placed between them. In the case of the Sheppard apparatus, these electrodes were semi-permeable cellophane membranes, with the actual metal-solution interfaces outside these membranes. This was necessary in order to avoid the disturbances resulting from gas evolution at the metal-solution interfaces in this aqueous buffer solution. The solutions used in the study were aqueous sodium acetate and sodium propionate.

Sheppard's observations showed that for these substances electroturbulence was observed at electric fields ranging from 1.7 to 3.4 kVm^{-1}. However, as his report points out, observation of turbulence in the solution cannot be used to accurately predict the actual onset of electrically induced disturbances, as such disturbances must have grown to some finite size before they become observable. Sheppard, by means of a thin layer of oil on the surface of the solution, was able to show the cellular form of these disturbances and draw similarities between his observation and those of Malkus and Veronis (ibid).

The Sheppard report also suggested the possibility of plotting current against potential difference across the cell to detect the onset of turbulence. It would be expected that a plot of these variables would show a change in slope at the onset of electroturbulence due to the increased apparent conductance resulting from increased ion transfer by the turbulent motion. However, due to complicating effects such as gas evolution and polarisation at the metal-solution interfaces, Sheppard was unable to conclusively demonstrate this.

Theoretical studies based on those of Hewish and Brignal (H6) led Sheppard to suggest that there would exist a value of the electrical Raleigh number above which electroturbulence would be expected to occur. This electrical Raleigh number Ra_{el}, is given by:

$$Ra_{el} = \frac{\varepsilon \Delta\phi}{\mu m_i}$$

where $\Delta\phi$ = potential difference

and μ = solution dynamic viscosity

and m_i = mobility of the ions present

Sheppard's calculations led to the result that the critical value of the electrical Raleigh number was 161 and his experimental results supported this within the relatively large (up to 50%) experimental error. These results also suggested that this dimensionless group was in fact representative of the parameters involved in electroturbulence as, in particular, the phenomenon was found to be voltage rather than current dependent.

2.4.3 Electroturbulence in Buffer Solutions in Laminar Flow

Tillman (T2) extended the work of Sheppard to include the effects of a laminar flow field on the critical

values for the parameters affecting the onset of electroturbulence. Tillman used a cell similar to that used for the hydrodynamic studies (Figure 2.4). This cell used only a single inlet stream and had electrodes 70 x 70 mm inserted in the parallel-flow section of the device. These metal electrodes were isolated from the central stream by an arrangement of cellophane membranes similar to that used by Sheppard.

Tillman observed transitions to turbulent flow in this cell by plotting graphs of current against voltage and observing the point of first change of slope. These data were obtained by reading current and voltage values at the first instance when the needles on the appropriate meters came to rest. Attempts were also made to observe the onset of turbulence with dye tracers. However, electrophoretic motion of the dyes and the difficulty of injecting dyes into a single stream, made this difficult and the results inconclusive.

Tillman's observations showed that for low concentrations of electrolyte the critical voltage for the onset of turbulence was a decreasing function of Reynolds number, while at higher concentrations, the critical voltage was unaffected by the Reynolds number. These experiments also showed that this critical voltage was a decreasing function of buffer concentration at fixed Reynolds number. The current measured at the onset of turbulence was shown to increase with electrolyte concentration up to some limit determined by Reynolds number (see Figure 2.6).

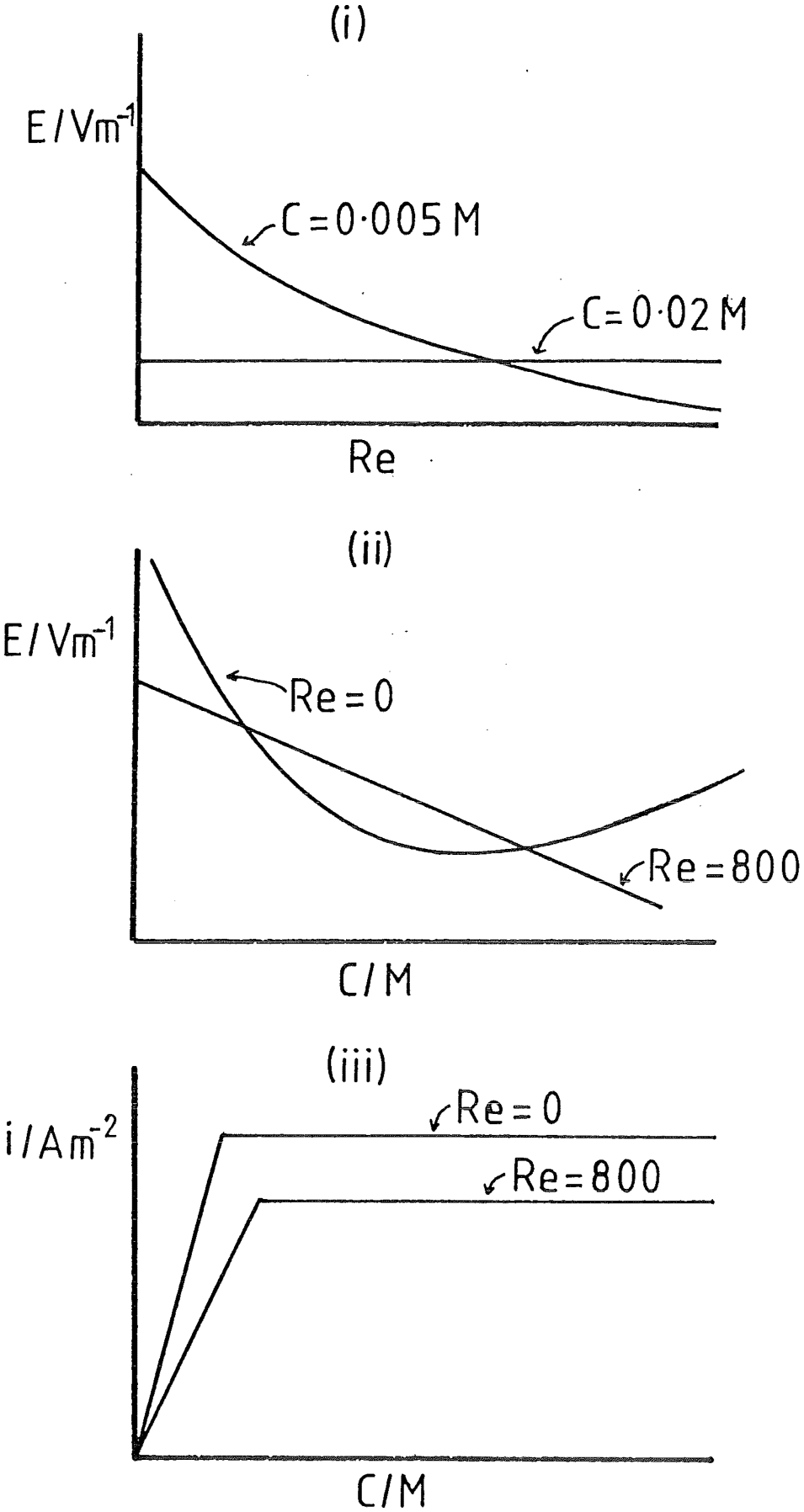

FIGURE 2.6 STABILITY RELATIONSHIPS FROM TILLMAN'S WORK

These results agreed qualitatively with the theory extended by Tillman from the work of LaCroix, Atten and Hopfinger (L1). This analysis suggests that the electrical Ralleigh number for the onset of turbulent flow is 100 rather than 161. At this lower value, Schneider and Watson (S1) observed stable hexagonal cells in a static fluid. Although this state of affairs is derived and observed for the space charge limited situation, Tillman hypothesised that cells of this type interact with laminar flow to produce instability. He further suggested that the effect of the flow could be accounted for by writing a relation of the form:

$$E_{critical(flow)} = (1 - \frac{Re}{Re_{critical}})E_{critical(static)} \quad 2.25$$

As can be seen from Figure 2.6(i), this trend is followed at low concentrations and low Reynolds numbers.

2.4.4 General Conclusions from the Electro-hydraulic Stability Experiments

i) These experiments confirm the existence of electro-turbulence for dilute buffer solutions.

ii) The observation of static fluids suggest that the criterion of Hewish and Brignall (H6) for the onset of electro-turbulence in fluids in electric fields not space-charge limited were applicable to dilute aqueous buffers.

iii) Observation of the current-voltage curves for an electric field applied to a dilute buffer in laminar flow showed that both flowrate and electric-field strength affected the onset of turbulence.

iv) Tillman (T2) suggested that a criterion of the form

$$E_{\text{critical flow}} = \left(1 - \frac{Re}{Re_{\text{critical}}}\right) E_{\text{critical(static)}}$$

could be applied to flowing dilute buffer solutions. $E_{\text{critical(static)}}$ may be arrived at from the criterion $Ra_{el} = 100$, that is

$$\frac{\varepsilon \Delta\phi}{\mu m_i} = 100$$

v) In the region of interest for electrophoretic separations (specific conductances of order 10^{-1} S m^{-1} and Reynolds numbers of order 100), electric fields are thus limited to values between 1.0 and 1.5 kVm^{-1}.

2.5 Temperature Profiles in the Separating Zone

2.5.1 Introduction

As already noted, the passage of an electric current necessarily gives rise to ohmic heating in the fluid through which it passes. This heating may induce disturbances in a flowing fluid due to bouyancy effects induced by temperature differences. In the case of electrophoresis, internal ohmic heating of the carrier buffer may also cause local temperatures to rise beyond the level where degradation of the components being separated occurs.

In order to investigate these phenomena, two approaches were used. Firstly, the likely form of the temperature profiles in a narrow-slot electrophoretic separator was evaluated using the appropriate differential energy balance. Secondly, an investigation was carried out to evaluate both experimentally and theoretically the conditions leading to the disturbance of laminar flow due to heating effects. This latter work was a B.E. project undertaken by a final-year student (B16) and is reported on in section 2.6. This section concerns the question of

temperature profiles in undisturbed laminar flow in a narrow rectangular duct.

2.5.2 Description of the Narrow-Slot Cell in Terms of the Differential Energy Balance

In its most general form, the differential balance energy (B6) may be written: (cf. equation 2.6)

$$\rho \bar{C}p \frac{\tilde{D}T}{Dt} = -\underset{\sim}{\nabla}.\underset{\sim}{q} - (\underset{\approx}{\tau}:\underset{\sim}{\nabla}.\underset{\sim}{U}) + \Sigma_i \underset{\sim}{j}_i \underset{\approx}{g}_i + \left(\frac{\partial \ln \bar{V}}{\partial \ln T}\right)_{P x_i} \frac{\tilde{D}P}{Dt}$$

$$+ \Sigma_i H_i(\underset{\sim}{\nabla}.\underset{\sim}{J}_i - \underset{\sim}{R}_i) \qquad 2.26$$

Let us consider this equation, term by term:

The left-hand side represents the rate of gain of energy for a fluid of constant density and heat capacity (i.e. for small temperature changes).

$\underset{\sim}{\nabla}.\underset{\sim}{q}$, the energy flux relative to the mass-averaged velocity of the fluid, can, in the case of a fluid of constant thermal conductivity, be written:

$$k \underset{\sim}{\nabla}^2 T$$

$\underset{\approx}{\tau}.\underset{\sim}{\nabla}.\underset{\sim}{U}$, the rate of viscous energy dissipation, is written for fluids of constant viscosity (again on the assumption of small temperature changes) as:

$$\mu \Phi_v$$

where Φ_v is made up of terms like $\left(\frac{\partial U_x}{\partial x}\right)^2$.

$\Sigma_i \underset{\sim}{j}_i \underset{\approx}{g}_i$ is the sum of all terms involving work done on the fluid by body forces. For dilute solutions in laminar flow at atmospheric pressure, gravitation is the only such body force. Therefore this term reduces to

$$\rho(\underset{\sim}{U}.\underset{\sim}{g}) \ .$$

Since the system under consideration is an incompressible liquid of constant physical properties,

$$\left(\frac{\partial \ln V}{\partial \ln T}\right)_{P_{xi}} \frac{\underset{\sim}{DP}}{Dt} = 0$$

In the narrow-slot electrophoretic separator, there is no chemical reaction, so the term $H_i(\underset{\sim}{\nabla}.\underset{\sim}{J}_i.R_i)$ reduces to the transport of the solute components multiplied by their enthalpies. The only such transport (with respect to the mass-averaged velocity of the system) is diffusion and electrophoresis; hence this term becomes:

$$H_i(D_i \underset{\sim}{\nabla}^2 C_i) + m_i(C_i \underset{\sim}{\nabla}^2\phi + \underset{\sim}{\nabla}.C_i.\underset{\sim}{\nabla}.\phi)$$

A further energy term must be added to account for resistive heating. This is expressed as:

$$\Sigma_i \phi^2 K_i x_i$$

This expression requires the definition of an electrical conductance per unit volume, instead of the customary conductance per unit length for fixed electrode cross-sectional area. This transformation is achieved by setting

$$K_i = \frac{C_i \Lambda_i}{l^2}$$

where C_i = concentration of species i

and Λ_i = specific conductance of species i

and l = distance between 'electrodes'

Thus equation 2.26 becomes

$$\rho Cp \frac{\underset{\sim}{DT}}{Dt} = -k \underset{\sim}{\nabla}^2 T - \mu\phi_v + \rho(\underset{\sim}{v}.\underset{\sim}{g}) + \Sigma_i \phi^2 K_i x_i$$

$$+ H_i(D_i \underset{\sim}{\nabla}^2 C_i + m_i(C_i \underset{\sim}{\nabla}^2\phi + \underset{\sim}{\nabla} C_i.\underset{\sim}{\nabla}\phi)) \qquad 2.27$$

for the narrow-slot electrophoretic separator.

Equation 2.27 can be reduced to dimensionless form by defining the following (starred) dimensionless quantities for the various deviations.

$$T^* = \frac{T - T_0}{T_1 - T_0}$$

$$\underset{\sim}{U}^* = \frac{\underset{\sim}{U}}{U}$$

$$t^* = \frac{tU}{D}$$

$$\underset{\sim}{\nabla}^* = \underset{\sim}{\nabla} D$$

$$\underset{\sim}{g}^* = \frac{\underset{\sim}{g}}{g}$$

$$\frac{\underset{\sim}{D}}{Dt^*} = \frac{D}{U}\frac{\underset{\sim}{D}}{Dt}$$

where the quantities T_0, D, U, t etc. are characteristic quantities of the system. This transforms equation 2.26 into;

$$\frac{DT^*}{Dt^*} = -\left(\frac{kD}{\rho Cp}\right)\nabla^{*2}T^* - \left(\frac{\mu U^2 D}{\rho Cp(T_1-T_0)}\right)\Phi_v^* + \left(\frac{U g D}{Cp(T_1-T_0)}\right)(\underset{\sim}{U}^*.\underset{\sim}{g}^*)$$

$$+ \left(\frac{\Sigma K_i x_1(\phi_1-\phi_0)^2}{\rho Cp(T_1-T_0)}\right)\phi^{*2} + \frac{H_i D_i D(C_1-C_0)}{\rho Cp(T_1-T_0)}\underset{\sim}{\nabla}^{*2}C_i^* + \frac{H_i m_i (C_1-C_0)(\phi_1-\phi_0)}{\rho Cp(T_1-T_0)}\nabla^{*2}\phi^*$$

$$+ \frac{H_i m_i (C_1-C_0)(\phi_1-\phi_0)}{\rho Cp(T_1-T_0)}\underset{\sim}{\nabla}^* C_i^* . \underset{\sim}{\nabla}^*\phi^* \qquad 2.28$$

which can be reduced to more manageable form by defining the following dimensionless groups:

$$Re = \frac{DU\rho}{\mu} \qquad \text{Reynolds number}$$

$$Pr = \frac{Cp\mu}{k} \qquad \text{Prandtl number}$$

$$Br = \frac{\mu U^2}{k(T_1-T_0)} \qquad \text{Brinkman number}$$

$$El = \frac{\mu}{m_i \Delta\phi\rho} \qquad \text{Electrophoresis number}$$

$$Sc = \frac{\mu}{D_i \rho} \qquad \text{Schmidt number}$$

$$H_E = \frac{(\varepsilon K_i x_i)(\Delta\phi)^2 D}{\rho U^3} \qquad \text{Electrical heating number}$$

$$H_{MT} = \frac{H_i (C_1 - C_0)}{\rho U^2} \qquad \text{Mass flux heat flow number}$$

$$Fr = \frac{U}{gD^2} \qquad \text{Froude number}$$

Use of these groups gives the following form of equation 2.28 (omitting the stars for clarity).

$$\frac{\underset{\sim}{DT}}{Dt} = \frac{1}{Pr\ Re} \underset{\sim}{\nabla}^2 T + \frac{Br}{Pr\ Re} \Phi_v + \frac{Br}{Pr\ Fr} \underset{\sim}{g}.\underset{\sim}{U} + \frac{Br\ H_E}{Pr} \phi^2$$

$$+ \frac{Br\ H_{MT}}{Pr\ Re\ Sc} \underset{\sim}{\nabla}^2 C_i + \frac{Br\ H_{MT}}{Pr\ El\ Re} (C_i \underset{\sim}{\nabla}^2 \phi + \underset{\sim}{\nabla} C_i . \underset{\sim}{\nabla}\phi) \qquad 2.29$$

This relates the energy effects in the narrow-slot separator under the above assumptions.

2.5.3 Order of Magnitude Analysis of Equation 2.28

Equation 2.28 may contain terms which, in terms of the overall relationship, are insignificantly small. If so, equation 2.28 can be simplified by omitting these terms before attempting a solution. The relative magnitude of each term is investigated by substituting reasonable numerical values of the various parameters into the dimensionless groups and comparing the resultant values of the coefficients for equation 2.29.

The parameters used in the analysis given below draw on work summarised earlier in this chapter and on the results of other workers in the area of electrophoresis (as referenced).

If waterlike transport and thermal properties are assumed for the bulk solution, then:

$$\rho = 10^{3} \text{ kg m}^{-3}$$

and $\mu = 10^{-3} \text{ Nsm}^{-2}$

and $Cp = 4.2 \text{ kJ kg}^{-1}\text{K}^{-1}$

and $k = 6 \times 10^{-4} \text{ kW m}^{-1} \text{ K}^{-1}$

therefore $Pr = 7.0$

For a 1 cm wide cell (i.e. D = 0.01 m), on assuming $Re = 100$,

then $U = 0.01 \text{ m s}^{-1}$

and hence $Fr = 10 \qquad (g = 9.8 \text{ m s}^{-2})$

and for a 'base' temperature difference of 1 K

$$Br = 1.7 \times 10^{-4}$$

If the diffusivity of macromolecules and small particles is of the same order as that of a particle 10 mm in diameter, then:

$$D = 10^{-10} \text{ m s}^{-1} \qquad \text{(reference W2)}$$

therefore

$$Sc = 10^{4}$$

Using the value given by Hertjen (H7) for the electrophoresis of *R. phycoerythm* in free solution

$$= 6 \times 10^{-9} \text{ m}^{2} \text{ s}^{-1} \text{ V}^{-1}$$

and on assuming $\Delta\phi = 10$ V,

$$El = 16$$

If the specific conductance of the bulk solution is of the order 10^{-3} S cm^{-1} and the concentration of this main charge carrier is 0.01 M or 10 moles m^{-3}, then, given that the contribution of the solute substance(s) to charge carrying is small, it follows that:

$$\Sigma K_i x_i = 100 \text{ S } m^{-3};$$

therefore,

$$H_E = 10^5.$$

Further, on assuming that the maximum concentration gradient is small (of order 0.01) and that the enthalpies of the substances transported are of order 10^4 kJ kg^{-1}, then;

$$H_{MT} = 10^3$$

Thus the order of magnitude of the coefficients of equation 2.28 are:

$$\frac{1}{Pr\ Re} \simeq 1.4 \times 10^{-3}$$

$$\frac{Br}{Pr\ Re} \simeq 2 \times 10^{-7}$$

$$\frac{Br}{Pr\ Fr} \simeq 2 \times 10^{-6}$$

$$\frac{Br\ H_E}{Pr} \simeq 2$$

$$\frac{Br\ H_{MT}}{Pr\ Re\ El} \simeq 2 \times 10^{-8}$$

and $$\frac{Br\ H_{MT}}{Pr\ Re\ El} \simeq 1 \times 10^{-5}$$

From this it can be seen that it is justifiable to simplify equation 2.28 to read:

$$\frac{\underset{\sim}{DT}}{Dt} = \frac{1}{Pr\ Re} \underset{\sim}{\nabla}^2 T + \frac{Br\ H_E}{Pr} \phi^2 \qquad 2.30$$

which describes the temperature profiles in the narrow-slot separator, when the appropriate boundary and initial conditions are included. This relationship (equation 2.30) indicates that for a realistically dimensioned system, only bulk flow, resistive heating and conduction are significant heat transport mechanisms.

2.5.4 Application of Equation 2.29 to the Narrow-Slot Separator

Since the narrow-slot separator has a high depth-to-width ratio, equation 2.29 can be used in two dimensional form to describe adequately the temperatures in this device. The coordinate system shown in Figure 2.3 will be used. This places the walls of the separating zone at $x = \pm 1$ and the zero of the coordinate system at the centre and entrance to the zone. The following assumptions (as well as those already used) are made for this system.

i) The only non-zero component of velocity is that in the z direction and this velocity is a function of x only.

Specifically $U_z = U(1 - x^2)$

where for this case of fully developed laminar flow U = 1.5 (B7).

ii) The electric field is assumed to be in the x direction only.

iii) Steady state is assumed.

iv) Thermal diffusion is assumed to be small with respect to heat transport by bulk flow of the fluid.

These conditions reduce equation 2.30 to:

$$U_z \frac{\partial T}{\partial z} = \frac{1}{Pr\ Re} \frac{\partial^2 T}{\partial x^2} + \frac{Br\ H_E}{Pr} \phi^2 \qquad 2.31$$

subject to the initial condition

$$T = 0 \quad \text{at } z = 0$$

$$-1 \leqslant x \leqslant 1.$$

That is, all the fluid enters at the same temperature, so that the dimensionless derivative in temperature is everywhere zero at the entrance.

The boundary condition used is that of constant wall temperature;

$$T_{wall} = T_B \qquad x = \pm 1$$

$$z \geqslant 0$$

The thermal relationships at the boundary may thus be written in dimensionless terms as

$$k \frac{dT}{dx} = h(T - T_B) \qquad 2.32$$

or

$$\frac{dT}{dx} = Nu(T - T_B) \qquad 2.33$$

where h = heat-transfer coefficient at the wall

and Nu = Nusselt number

$$= \frac{hD}{k}$$

An approximate Nusselt number may be obtained for this system from the Sieder and Tate correlation for laminar flow in tubes (S3).

$$Nu = 1.86(Re\ Pr\ D/l)^{1/3} \left(\frac{\mu_b}{\mu_0}\right)^{0.14} \qquad 2.34$$

where D = diameter

and l = length

and the viscosity ratio is that between bulk (b) and wall (0) values.

The mean hydraulic diameter is again used to represent D for this expression and, since temperature differences are assumed small,

$$\mu_b/\mu_0 = 1.$$

2.5.5 Solution of Equation 2.31

Inspection of equation 2.31 shows that it is of parabolic form with one non-constant coefficient (C1). This equation is solved numerically using the explicit Dufort-Frankel procedure (ibid). This procedure considers the separating chamber to be made up of a network of elements, as shown in Figure 2.7. On using this notation, the differential terms are put into finite-difference form as follows:

$$\frac{\partial T}{\partial z} \simeq \frac{T_{i\ n+1} - T_{i\ n-1}}{2\Delta z} \qquad 2.35$$

and

$$\frac{\partial^2 T}{\partial x^2} \simeq \frac{T_{i-1\ n+1} - T_{i\ n+1} - T_{i\ n} + T_{i+1\ n}}{(\Delta x)^2} \qquad 2.36$$

where the subscripts give the position of each value in the network. Carnahan, Luther and Wilkes (ibid) state that this method is second-order correct and stable for all values of the ratio $\Delta z/(\Delta x)^2$.

For the computation, the following values of step size were chosen:

$$\Delta x = 0.05$$

$$\Delta z = 0.25$$

thus permitting a relatively fine graduation of temperature values across the width of the model without excessive numbers of steps along the length of the model.

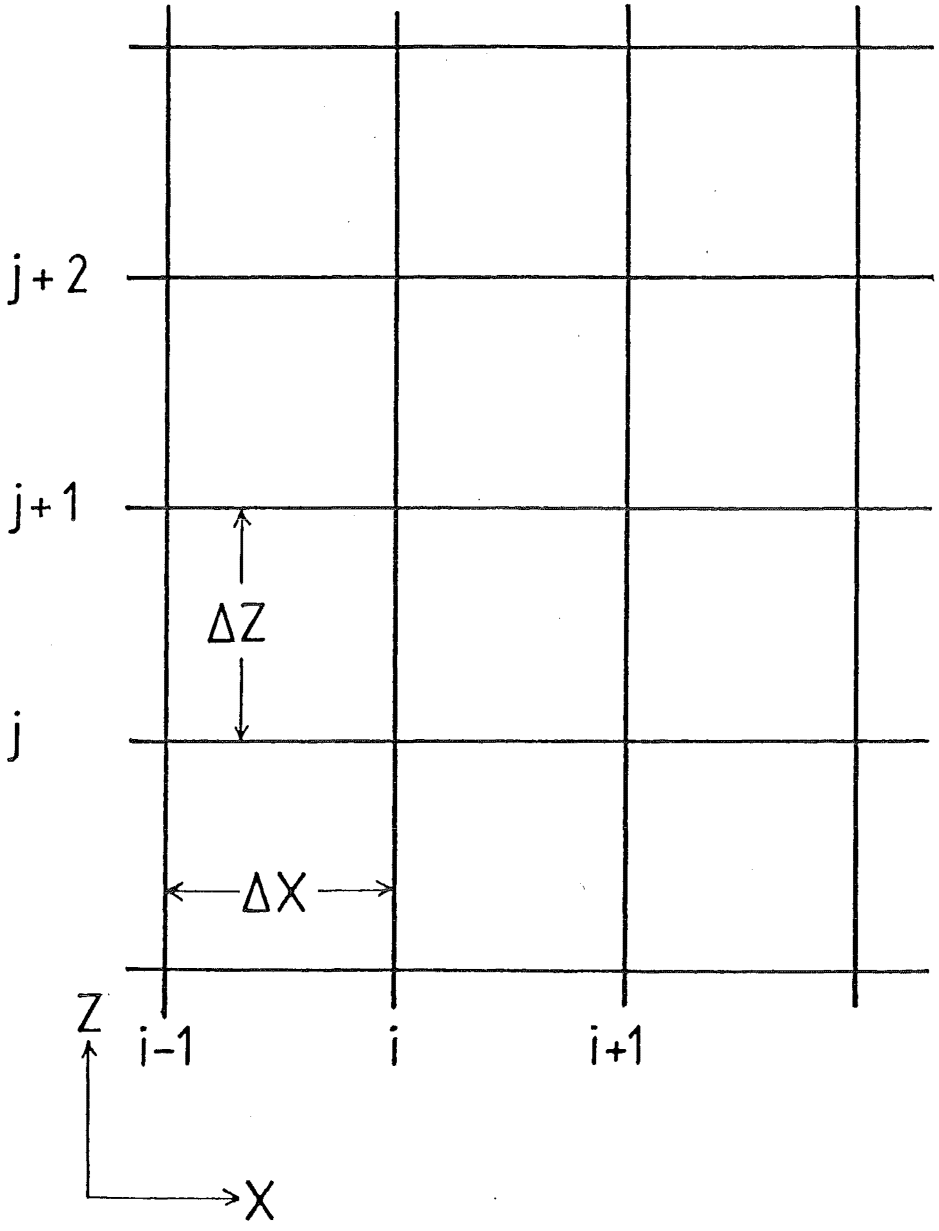

FIGURE 2.7 FINITE DIFFERENCE NETWORK FOR DUFORT-FRANKEL PROCEEDURE

Boundary conditions were incorporated into this method of solution by using the relationships;

$$\left.\frac{dT}{dx}\right|_0 = \frac{4T_{1j} - 3T_{0j} - T_{2j}}{2\Delta x} \qquad 2.37$$

and

$$\left.\frac{dt}{dx}\right|_N = \frac{4T_{N-1j} - 3T_{Nj} + T_{N-2j}}{2\Delta x}$$

where the subscripts 0 and N represent the first and last values across the network (i.e. at x = -1 and x = +1 respectively).

The program generated from these equations is given in Appendix (1). Results from this computation for the two boundary conditions given and at a specific conductance of 0.001 S cm^{-1} and a potential difference of 7.5 V are shown in Figure 2.8. The computations are on a dimensionless basis and the following values for the base parameters were used.

Base temperature difference = 10 K

Cell width = 5 mm

(i.e. base length = 0.025 m)

The thermal and transport properties of water at 20°C were used to give:

Re = 100

Pr = 6.8

Br = 3.33 x 10^{-6}

H_E = 1400

The dimensionless wall temperature was set equal to zero. The two boundary conditions used were:

i) No heat transfer at the wall, i.e. Nu = 0 (Figure 2.8(i)).

FIGURE 2.8(i) DIMENSIONLESS TEMPERATURE PROFILES FOR
$\Delta\phi = 7.5\,V$, $\Lambda = 0.1\,S\,m^{-1}$, $Re = 100$, $Nu = 0$

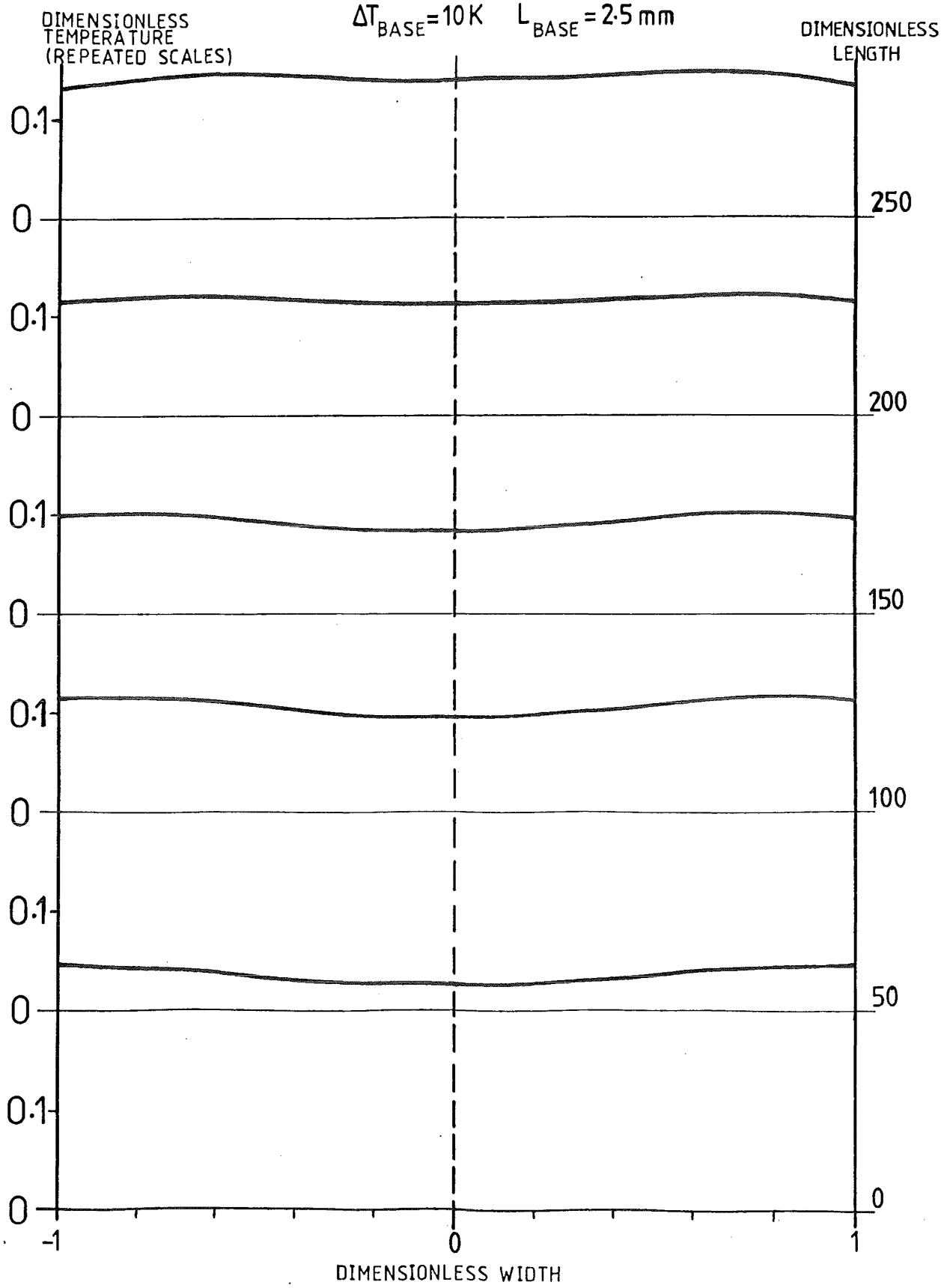

FIGURE 2.8 (ii) DIMENSIONLESS TEMPERATURE PROFILES FOR
$\Delta\emptyset$ = 7·5 V, Λ = 0·1 Sm^{-1}, Re = 100 , Nu = 4·44

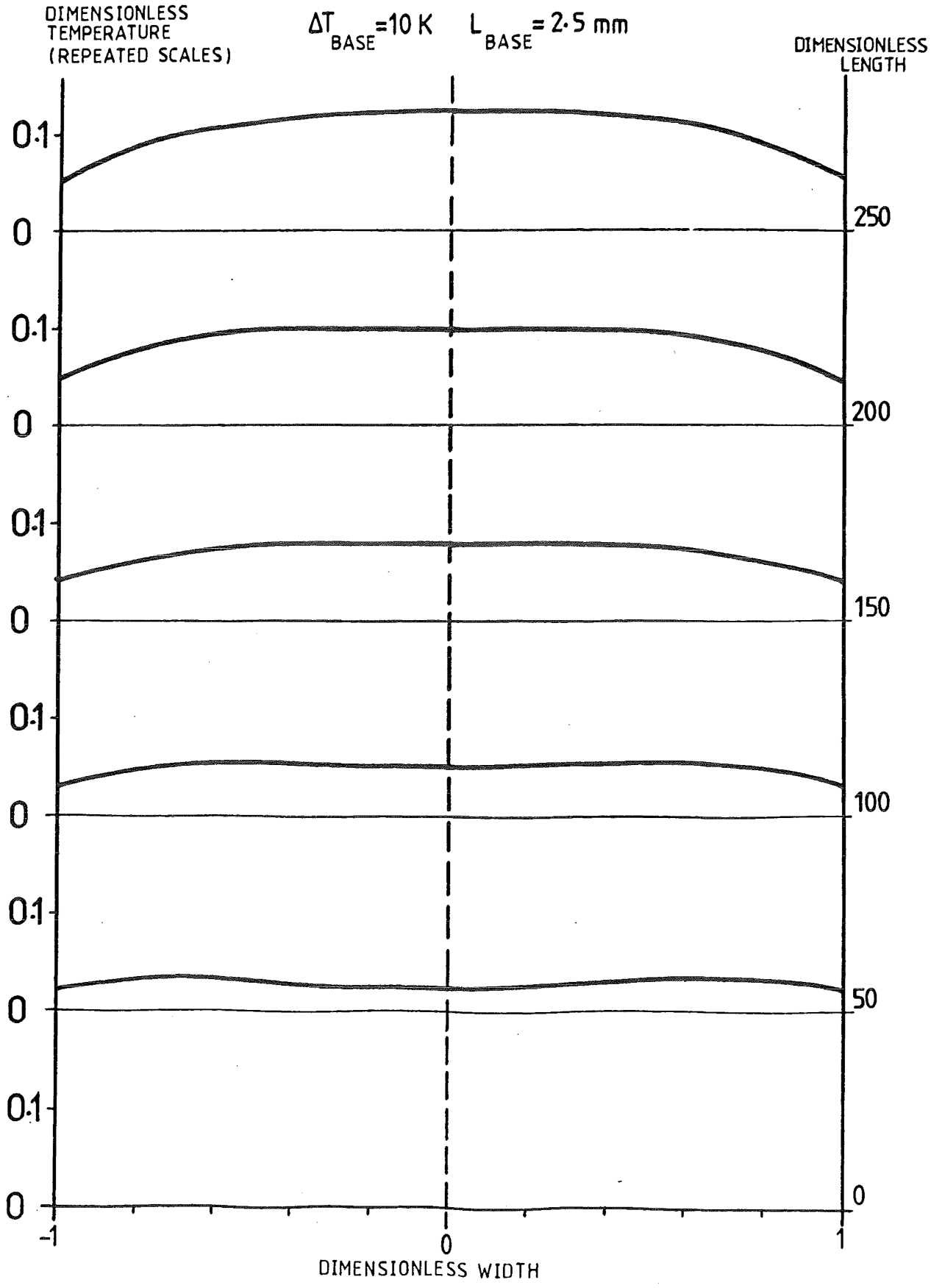

ii) Heat flux through the wall governed by a constant wall temperature (in accordance with equation 2.34; $Nu = 4.44$) (Figure 2.8(ii)).

As can be seen from these plots, the temperature profiles resulting from this model are nearly flat for the case of no heat flux at the walls, and increasingly parabolic for the case of constant wall temperature. In fact, Figure 2.8(ii) closely resembles the velocity profiles resulting from the development of laminar flow in a circular tube (B7). Thus it can be seen that for small temperature differences under these conditions the temperature profiles can be expected to reinforce the velocity profile. Following from this work, an investigation was undertaken by Buckenham (B16) to examine coupling between the fluid flow and temperature profiles.

2.6 Thermal Stability

2.6.1 Introduction

Historically the question of thermally induced instability in free-flow electrophoresis has been given a good deal of attention (see section 1.5 and section 1.5.10 in particular). It may be expected that the effects of thermally induced disturbances to the laminar flow through the narrow-slot separator will have similar effects to those already discussed for electroturbulence. Consequently the useful operating envelope of this device will necessarily be constrained by the limits imposed by conditions for the onset of thermal disturbances to the flow.

2.6.2 The Criteria of Metais and Eckert

Metais and Eckert (M5), by collection of experimental data for flow through pipes, have established a number of charts indicating the parameters for appropriate flow regimes for particular pipe orientations (i.e. vertical or horizontal). These charts plot Reynolds number against the parameter $GrPr\ \frac{D}{l}$ with each regime represented by an area on the chart. Where

$$Gr = \text{Grashoff number} = \frac{\rho^2 \beta g D^3 \Delta T}{\mu^2}$$

in which β is the coefficient of volume expansion of the fluid and the other symbols have their normal meanings. Note that in the above expression β and ρ are evaluated at the mean temperature of the fluid.

From the Metais and Eckert chart for flow in vertical pipes, for a Reynolds number of 100, the maximum value of the parameter $Gr\ Pr\ D/l$ for forced convection laminar flow is approximately 200.

$$\text{i.e. } Gr\ Pr\ D/l = 200$$

For a Prandtl number of 6.8 and assuming $D/l = 0.067$, this gives

$$Gr = 440$$

or

$$\frac{\rho \beta g D^3 \Delta T}{\mu^2} = 440$$

which gives;

$$\Delta T = 0.76\ K$$

for waterlike solutions at room temperature.

However these criteria are simplistic for a number of reasons. Firstly, the chart does not state whether the criteria for vertical flow apply to upward or downward flow. Secondly, the chart is intended to give flow regimes for use with heat-transfer correlations rather than predict stability limits. In fact, Metais and Eckert state the limits supplied by the chart are tentative, even for this purpose. This leads to the supposition that the results from these criteria could be in error by at least an order of magnitude.

2.6.3 The Experiments and Analysis of Buckenham

Buckenham (B16) set up a device based on the likely dimensions of a narrow-slot separator (viz a rectangular duct 1 cm x 10 cm x 1 m). This device was then used to examine the onset of thermally induced flow disturbances. Buckenham also set up equations relating flow and temperature for a two-dimensional model of this duct and theoretically examined the effects of differing heat-generation rates and flow rates on the expected velocity profile.

The Buckenham experiments were conducted by transferring heat inward through the deeper walls of the duct by circulating hot water in turbulent flow past these aluminum walls. It was expected that the observed behaviour would be similar to that of a heated stream with heat transfer to colder walls. A photograph of the typical results of this work is shown in Plate 2.4.

The work of Buckenham showed that the first form of disturbance to become apparent in upward laminar flow in a narrow rectangular slot was a form of vertical wave. Comparison between profiles photographed in the experimental duct and Buckenham's

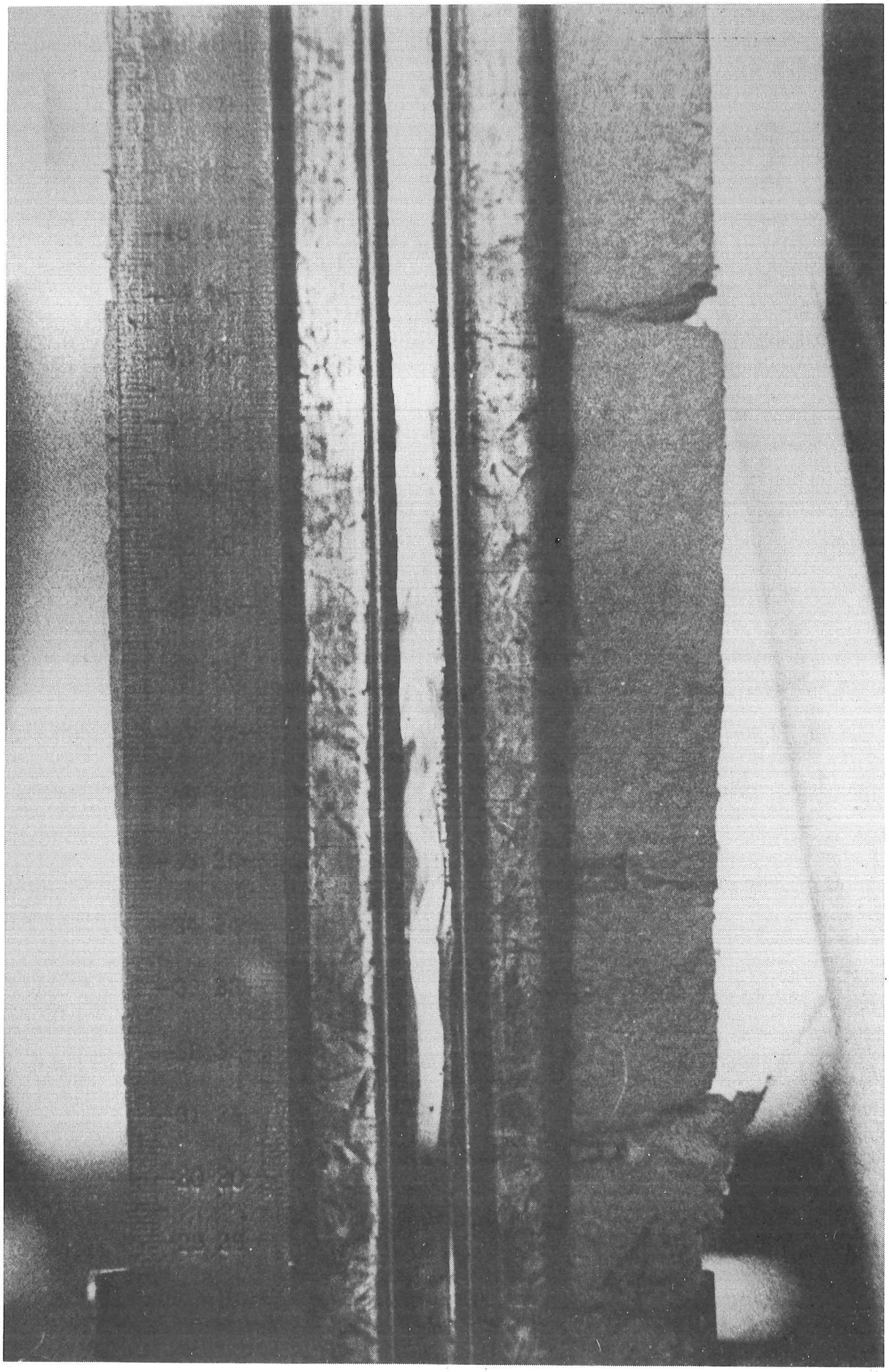

Plate 2.4: Thermally induced breakdown of laminar flow (after Buckenham)

theoretical calculations of the velocity profile for a given Reynolds number and heating rate indicated that the formation of this wave corresponded to a point of inflection in the velocity profile at some (small) finite distance from the wall. This result could be then used as a basis for the prediction of the onset of disturbances to the flow.

The Buckenham analysis did not exhaustively assess this criterion, but did indicate that, for a Reynolds number of approximately 100, an internal heat-generation rate exceeding 200 kW m^{-3} of duct volume precipitated flow disturbances. Buckenham also pointed out that, on a qualitative basis, the following conditions would contribute to the stabilisation of the flow against thermal effects:

i) The imposition of a positive wall temperature gradient in the direction of flow;

ii) Higher fluid viscosities;

iii) A decrease of the width of the duct in relation to its length and depth.

On taking 75% of Buckenham's figure for the limiting internal heat generation and assuming no conductive heat removal at the walls, a simple balance can be performed to give the order of magnitude of the voltage likely to produce thermal disturbances in a given solution.

Heat generation rate = electrical energy input

$$q = \Delta\phi I$$

$$= (\Delta\phi)^2(\Sigma_i K_i x_i)$$

as previously

$$\Sigma_i K_i x_i = 100 \text{ S m}^{-3}$$

$$\therefore (\Delta\phi)^2 = 2 \times 10^3$$

$$\text{or} \quad \Delta\phi = 45 \text{ V}$$

It would therefore appear that the performance of the narrow-slot electrophoresis separator is not limited by thermal considerations as the threshold voltage for electro-turbulence appears to be about one quarter of this value.

2.7 Conclusions From the Preliminary Work

2.7.1 Hydrodynamics

From the experiments performed with the preliminary hydrodynamic test cell, the most favourable geometry for a narrow-slot electrophoretic separator should be such that flow is either maintained at constant speed or accelerating throughout the device. This can be achieved by the use of a series of converging slots the full depth of the apparatus feeding a common converging channel into the main parallel-sided separating zone. Separated streams can then be recovered by way of a section diverging in the plane of separation and converging at right-angles to this and the plane of flow. Reynolds numbers in the range 100 - 200 apparently give stable flow in this geometry. Horizontal density differences across such a cell in a vertical position are likely to give rise to flow instabilities but the time constants for the evolution of these instabilities are likely to be long provided the density gradients are small.

2.7.2 Electro-hydraulics

From the work of Sheppard and Tillman (S2) (T2), the flow in a narrow-slot electrophoretic separator is likely to be affected by electroturbulence. The onset of this turbulence is likely to be predictable by the use of an expression of the form:

$$E_{critical(flow)} = E_{critical(static)}\left(1 - \frac{Re}{Re_{critical}}\right)$$

where the static critical electric field strength is given by the parameter

$$Ra_{el} = 100$$

For typical solution parameters (viz. low-concentration buffer solutions) and on assuming negligible effects from the electrical properties of separable solute materials, this indicates values of maximum permissible field strength of between 1.0 and 1.5 kV m^{-1}. From inspection of the terms of the expression written to describe the electrical stability of this system, it would appear that small local disturbances in the electric field of the solution properties may be expected to trigger electrohydraulic instability.

2.7.3 Thermal Effects

Investigation of the heat-transport differential balance for a narrow rectangular duct for small temperature differences suggests that the internal resistive heat generation with heat outflow at the walls will stabilise and possibly accentuate a laminar velocity profile in upflow. A more wide-ranging investigation by Buckenham (B16) showed that thermal instability effects would not be limiting in this device. Buckenham further pointed out that a positive wall-temperature gradient in the direction of upward flow and a very narrow duct both aid the stability of laminar flow.

3. DEVELOPMENT OF A THEORETICAL MODEL FOR THE NARROW-SLOT ELECTROPHORETIC SEPARATOR

3.1 Basis of the Model

3.1.1 Introduction

The concept of narrow-slot electrophoresis differs in a number of important aspects from previous free-flow electrophoretic methods. As briefly outlined in Chapter 1, this configuration has the potential to perform separations at a very much greater rate than other preparative electrophoresis devices. However the geometry inherent in the narrow-slot proposal introduces other effects. Since, as has been previously pointed out, the key to the concept is a large depth-to-width ratio (see Figure 3.1), the 'edge effects' due to the non-conductive faces become comparatively unimportant. Thus, the device can be effectively modelled by taking a two-dimensional 'slice' through the cell at right angles to both the electric field and the direction of flow (Figure 3.1(ii)).

However this configuration forces consideration of a number of effects which would be insignificant in devices of less extreme aspect ratio. Since transport is across a laminar velocity profile which has comparatively steep velocity gradients in the direction of the electric field, the interaction between the velocity field and the electrophoretic transport must be considered. On the other hand, since the non-conductive walls of the device are small in area, electroosmotic effects will be minimal. Electroosmotic effects will be further decreased by the presence of a stagnant zone adjacent to the non-conducting walls (Figure 3.2). The conductive walls of the separating zone are assumed to be completely impervious to solute.

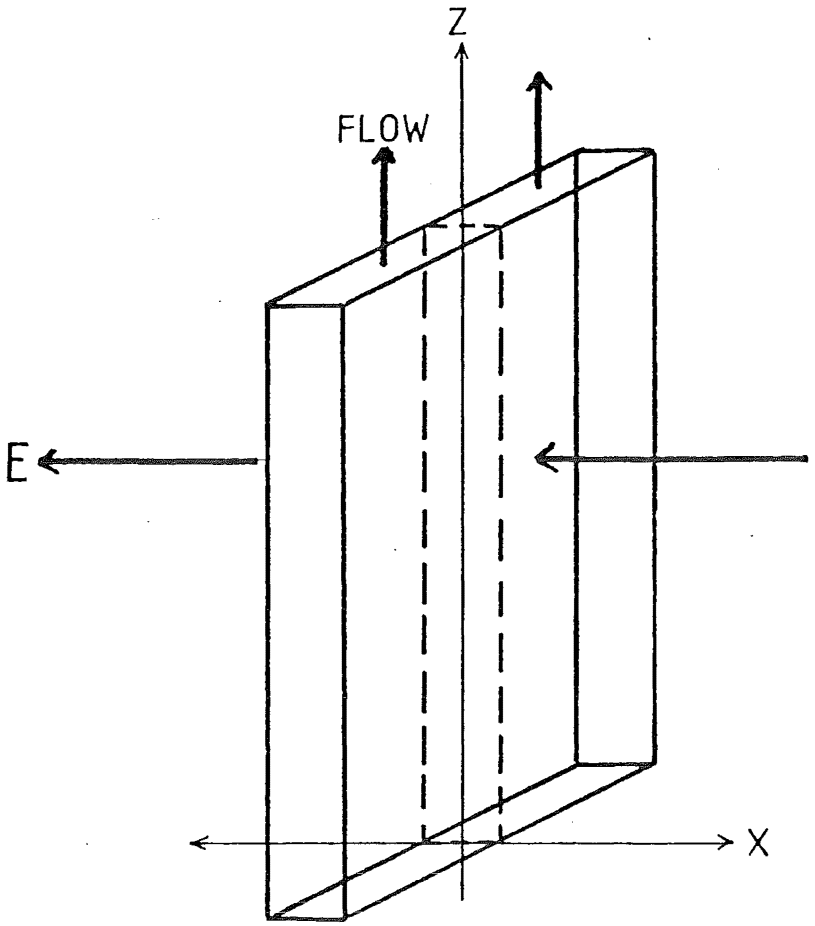

(i)

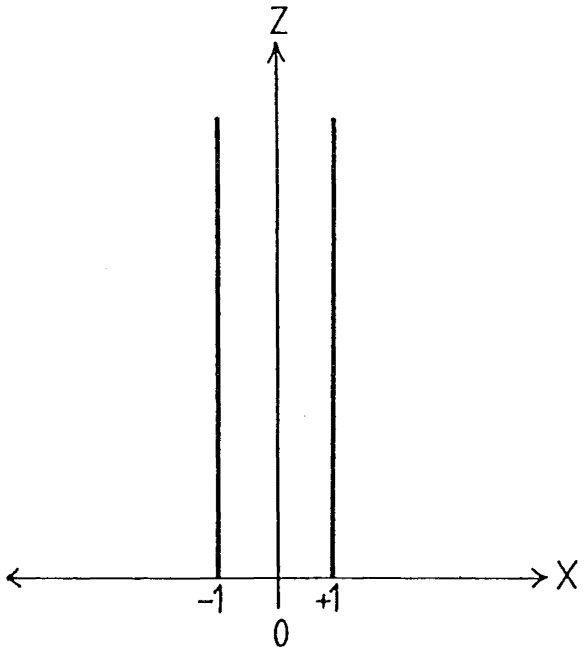

(ii)

FIGURE 3.1 RELATION OF COORDINATE SYSTEM TO THE NARROW-SLOT CELL

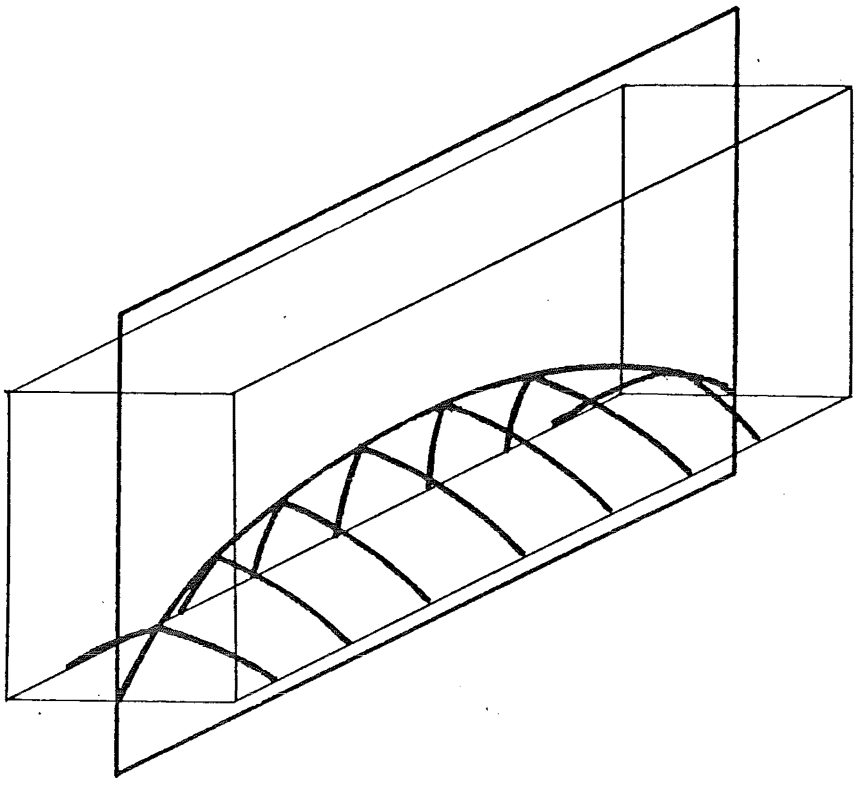

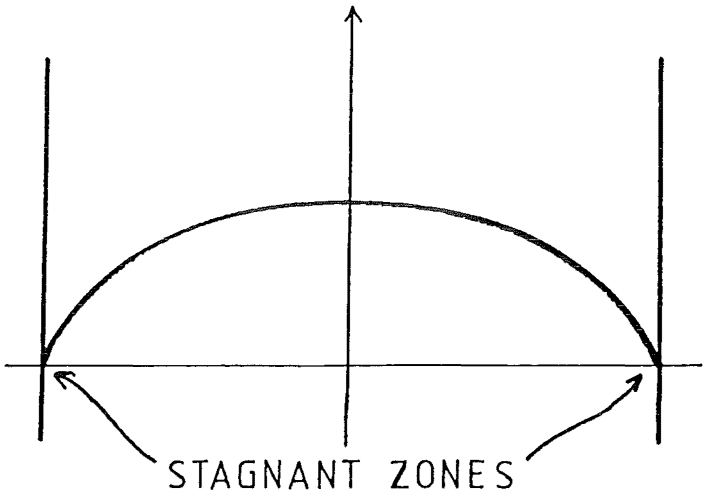

FIGURE 3.2 THREE DIMENSIONAL VELOCITY PROFILE IN THE NARROW-SLOT CELL

3.1.2 Electrophoretic Mobilities

As has been noted in section 1.3, the electrophoretic mobility of a substance is a function of a number of variables. Among the more significant of these are pH, ionic strength, background ion type, the presence or absence of surfactants and, to a lesser extent, temperature. The theoretical analysis that is the subject of this chapter assumes that the carrier solution for the electrophoretic separation performed in the narrow-slot cell has constant properties. Therefore, it follows that the above variables are held constant and so electrophoretic mobility can be treated as a constant parameter for each substance considered for the given conditions of the separation. This enables electrophoretic mobility to be treated as a constant in the differential mass balance equations used in this analysis.

3.1.3 Limits of the Model

The two-dimensional model of the narrow-slot electrophoresis process considers only the portion of a complete separator in which electrophoretic transport actually occurs. That is to say, it is assumed that it is possible to introduce and withdraw flows under conditions of fully-developed laminar flow in a continuous steady-state manner. The model also assumes a steady electric field independent of distance along the separator and having no time-dependent effects on the bulk flow through the device. For the purposes of the model, electro-osmosis is assumed to produce plug flow, that is electro-osmotic edge effects are ignored.

3.2 The Differential Balance Mass Transfer Equation

3.2.1 The General Relation

In its most general form, the differential mass

balance for a given system may be written;

$$\frac{\partial C_i}{\partial t} + \underset{\sim}{\nabla}.\underset{\sim}{N}_i = R_i \qquad 3.1$$

for any component i (B6).

For the particular case of an electrophoretic separator, no chemical reactions occur in the separating zone and the fluxes of the components of interest are the result of three causes only:

i) Bulk flow of the carrier solution;

ii) Molecular diffusion;

iii) Electrophoretic transport.

Since the solute species (i) is assumed to be in dilute solution, the flux term can be written;

$$N_i = -D_i \underset{\sim}{\nabla} C_i - m_i C_i \underset{\sim}{\nabla}\phi + C_i \underset{\sim}{U} \qquad 3.2$$

and therefore equation 3.1 can be written:

$$\frac{\partial C_i}{\partial t} + \underset{\sim}{\nabla}.(C_i \underset{\sim}{U}) = \underset{\sim}{\nabla}.(D_i \underset{\sim}{\nabla} C_i + m_i C_i \underset{\sim}{\nabla}\phi) \qquad 3.3$$

or

$$\frac{\partial C_i}{\partial t} + \underset{\sim}{\nabla} C_i . \underset{\sim}{U} + C_i(\underset{\sim}{\nabla}.\underset{\sim}{U}) = D_i \underset{\sim}{\nabla}^2 C_i + m_i C_i \underset{\sim}{\nabla}^2\phi + \underset{\sim}{\nabla} C_i . \underset{\sim}{\nabla}\phi \qquad 3.4$$

for dilute solutions.

3.2.2 Reduction of Equation 3.4 to Dimensionless Form

Using the transformations given below, equation 3.4 may be reduced to dimensionless form as shown. The following dimensionless variables can be defined:

$$\frac{\partial^*}{\partial t^*} = \frac{U}{D}\frac{\partial}{\partial t}$$

and $\underset{\sim}{\nabla}^* = D\underset{\sim}{\nabla}$

and $C_i^* = \dfrac{C_i - C_{i0}}{C_{i1}-C_{i0}}$

where $(C_{i1}-C_{i0})$ is some fixed concentration difference, say ΔC_i; further, let

$$\underset{\sim}{U}^* = \frac{\underset{\sim}{U}}{U}$$

and

$$\phi^* = \frac{\phi - \phi_0}{\phi_1 - \phi_0}$$

where $(\phi_1 - \phi_0)$ is some fixed potential difference, say $\Delta\phi$. Substitution of these relationships into equation 3.4 gives

$$\frac{U}{D}\Delta C_i \frac{\partial C_i^*}{\partial t^*} + \frac{\Delta C_i U}{D} C_i^* \underset{\sim}{\nabla}^*.\underset{\sim}{U}^* + \frac{\Delta C_i U}{D} \underset{\sim}{U}^*.\underset{\sim}{\nabla}^* C_i^* = \frac{\Delta C_i D_i}{D^2} \underset{\sim}{\nabla}^{*2} C_i^*$$

$$+ \frac{m_i \Delta\phi \Delta C_i}{D^2} \underset{\sim}{\nabla}^{*2}\phi^* + \frac{\Delta\phi\Delta C_i}{D^2} \underset{\sim}{\nabla}^* C_i^*.\underset{\sim}{\nabla}^*\phi^* \qquad 3.5$$

Dividing equation 3.5 through by the group $\dfrac{\Delta C_i U}{D}$ and defining the following dimensionless parameters,

Reynolds number $\quad Re = \dfrac{DU\rho}{\mu}$

Schmidt number $\quad Sc = \dfrac{\mu}{\rho D_i}$

Electrophoretic transport number $\quad El = \dfrac{\mu}{m_i \Delta\phi\rho}$

enables equation 3.5 to be rewritten (omitting the stars for clarity) as:

$$\frac{\partial C_i}{\partial t} + C_i \underset{\sim}{\nabla}.\underset{\sim}{U} + \underset{\sim}{U}.\underset{\sim}{\nabla} C_i = \frac{1}{Re\ Sc} \underset{\sim}{\nabla}^2 C_i + \frac{1}{Re\ El}(C_i \underset{\sim}{\nabla}^2\phi + \underset{\sim}{\nabla} C_i.\underset{\sim}{\nabla}\phi) \qquad 3.6$$

Since equation 3.6 is applied to a liquid system with an incompressible liquid, it follows that (B6):

$$\underset{\sim}{\nabla}.\underset{\sim}{U} = 0 \qquad 3.7$$

Further, since the system is assumed to be at steady state,

$$\frac{\partial C_i}{\partial t} = 0 \qquad 3.8$$

On imposing these two conditions on equation 3.6, it becomes

$$\underset{\sim}{U}.\nabla\underset{\sim}{C}_i = \frac{1}{Re\ Sc}\nabla^2\underset{\sim}{C}_i + \frac{1}{Re\ El}(C_i\nabla^2\phi + \nabla\underset{\sim}{C}_i.\nabla\phi) \qquad 3.9$$

which describes the general case of electrophoretic transport in a liquid at steady state.

3.2.3 Application of the Continuity Equation 3.9 to the Two-Dimensional Model

On using the coordinate system shown in Figure 3.1(ii), equation 3.9 may be expanded to read, in component form:

$$U_x\frac{\partial C_i}{\partial x} + U_z\frac{\partial C_i}{\partial z} = \frac{1}{Re\ Sc}\left(\frac{\partial^2 C_i}{\partial x^2} + \frac{\partial^2 C_i}{\partial z^2}\right) + \frac{1}{Re\ El}\left(C_i\frac{\partial^2\phi}{\partial x^2} + C_i\frac{\partial^2\phi}{\partial z^2}\right)$$

$$+ \frac{1}{Re\ El}\left(\frac{\partial C_i}{\partial x}\frac{\partial\phi}{\partial x} + \frac{\partial C_i}{\partial z}\frac{\partial\phi}{\partial z}\right) \qquad 3.10$$

If the following assumptions are made:

i) No bulk flow across the cell (i.e. $U_x = 0$);

ii) An electric field independent of z;

iii) A linear voltage gradient across the cell (i.e. in the x direction);

then equation 3.10 reduces to:

$$U_z\frac{\partial C}{\partial z} = \frac{1}{Re\ Sc}\left(\frac{\partial^2 C_i}{\partial x^2} + \frac{\partial^2 C_i}{\partial z^2}\right) + \frac{1}{Re\ El}\left(\frac{\partial C_i}{\partial x}\frac{\partial\phi}{\partial x}\right) \qquad 3.11$$

If the linear voltage gradient in the x direction is further assumed to have the same magnitude as $\Delta\phi$ in the expression,

$$\frac{1}{Re\ El} = \frac{m_i\Delta\phi}{DU}$$

then $\frac{\partial \phi}{\partial x}$ becomes unity. Also, if the effects of diffusion in the z direction are assumed to be small in comparison with bulk convective transport, then;

$$\frac{\partial^2 C_i}{\partial x^2} \simeq 0.$$

This assumption may be justified by considering typical values for the Reynolds and Schmidt numbers. For Re = 100 and $Sc = 10^4$ (see section 2.5) the product $ReSc$ is, in terms of system variables

$$Re\ Sc = \frac{DU}{D} = St$$

which is, in fact, the ratio of convective to diffusive transport. In this case,

$$Re\ Sc = 10^6$$

indicating that convective transport effects are expected to be very much larger than diffusive transport. Resultingly equation 3.11 becomes,

$$U_z \frac{\partial C_i}{\partial z} = \frac{1}{Re\ Sc} \frac{\partial^2 C_i}{\partial x^2} + \frac{1}{Re\ El} \frac{\partial C_i}{\partial x} \qquad 3.12$$

which, with suitable boundary and initial conditions, can be expected to describe electrophoretic transport in a narrow-slot separator. It is further worth noting that, in a similar fashion to the above, $Re\ El$ or the electrophoretic station number, is the ratio of convective to electrophoretic transport.

3.2.4 Boundary and Initial Conditions

The boundary conditions for equation 3.12 must match the physical condition that there is no transport of solute material through the 'electrode' walls of the separator. That is to say, the limits of the separating zone (at $x = \pm 1$

in Figure 3.1(ii)) represent perfect barriers to the solute components. Since there is assumed to be no bulk flow through the electrode walls of the separating zone, the only possible modes of transport for the solute are diffusion and electrophoresis. Therefore, in terms of the differential mass balance, the following condition must hold at the walls of the separating zone.

$$D_i \frac{\partial C_i}{\partial x} + m_i \Delta\phi \, C_i = 0 \qquad 3.13$$

Rewritten in dimensionless form this condition becomes:

$$\frac{1}{Re \; Sc} \frac{\partial C_i}{\partial x} + \frac{1}{Re \; El} C_i = 0 \qquad 3.14$$

at $x = \pm 1$

The initial conditions for equation 3.12 represent the shape of the concentration profile of the solute component(s) at the level at which they enter the separating zone. In this sense, the velocity profile may also be considered as an (invariant) initial condition. Since fully developed laminar flow is assumed, the velocity profile may be immediately written as:

$$U_z = U(1 - x^2) \qquad 3.15$$

where U is the ratio of maximum to mean velocity in the zone. For this rectangular duct, U = 1.5. This expression can be substituted directly into equation 3.12.

For simplicity in handling the numerical analysis of equation 3.12; the inlet concentration of the component under study is taken as unity. Since the solute is admitted as a fraction of the total width of the inlet the initial conditions for solute concentration may be written:

$$C_i = 1$$

for the region, $a \leq x \leq b$

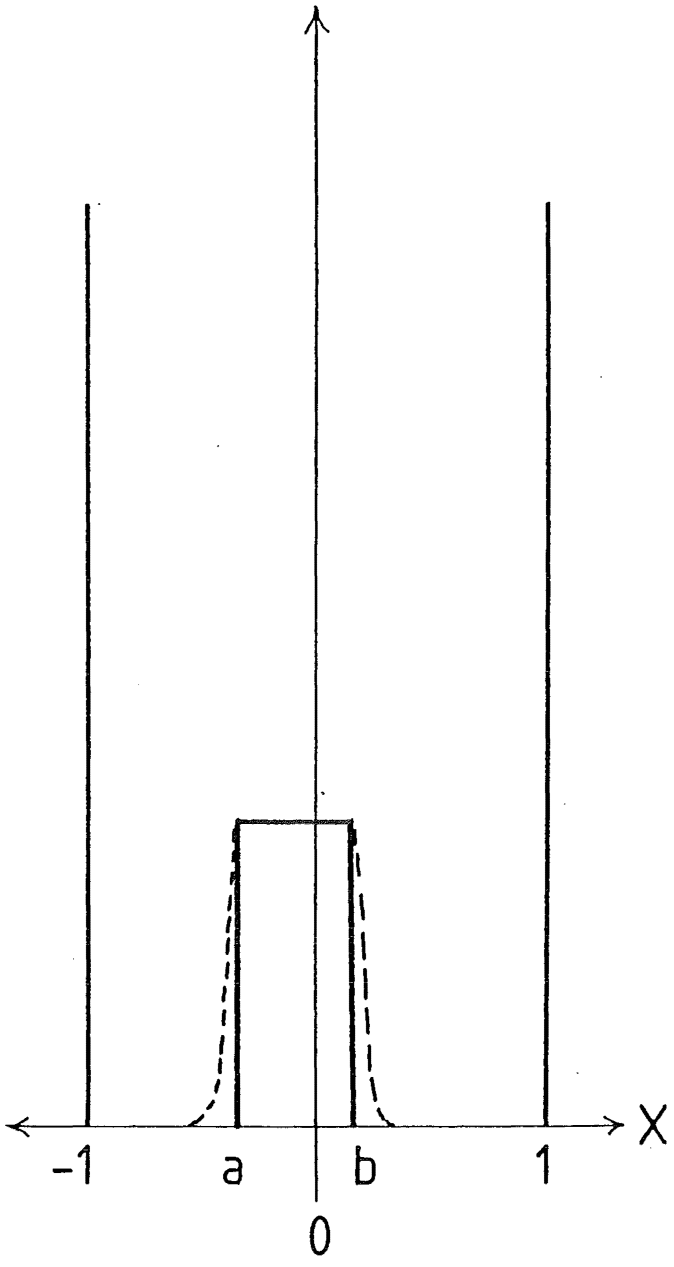

FIGURE 3.3 INPUT CONCENTRATION PROFILE

given $-1 \leqslant a < 1$, and $-1 < b \leqslant 1$

and

$$C_i = 0$$

for the zones $x < a$ and $x > b$

This situation is shown diagramatically in Figure 3.3 and may be considered mathematically as a pair of step functions at a and b. This condition was later modified to give a finite slope at a and b as a more realistic representation of the likely concentration profile (broken line in Figure 3.3).

3.3 Limiting Cases of Equation 3.12

3.3.1 Introduction

Equation 3.12 represents, for each component of an electrophoretic separation, the action of two forces on a system under conditions of steady-state flow. The relative magnitudes of these motive forces, namely electrophoresis and molecular diffusion, govern the type of differential equation equation 3.12 is, and hence the method of solution appropriate to this equation. The real case of the narrow-slot electrophoretic separator is likely to be represented by the situation where both forces are of significance (see below) and equation 3.12 cannot be further simplified in order to apply a 'standard form' method of solution. However, the limiting cases for the situations, where either molecular diffusion or electrophoresis is considered alone, are of interest in gauging the behaviour of the real system.

3.3.2 The Relative Magnitudes of Electrophoresis & Diffusion

An estimate of the relative significance of the various terms in equation 3.12 may be obtained by consideration of the magnitudes of the dimensionless groups involved. As a

basis a Reynolds number of 100 is used as the result of the preliminary hydraulic experiments suggest that at this value stable laminar flow can be maintained (section 2.2.5). As previously noted, Hertjen (H7) gives the following value for the mobility of *R. phycoerthym* in free solution.

$$m_i = 6 \times 10^{-9} \ m^2 \ S^{-1} \ V^{-1}$$

Assuming that this substance behaves like a 10mm spherical particle then it has a diffusivity of approximately (W2)

$$D_i = 10^{-10} \ m^2 \ S^{-1}$$

Further, on assuming an electric field of 10^3 Vm^{-1} (reasonable on the basis of the experiments of Tillman; see section 2.4), then the approximate magnitudes of the dimensionless groups are, if the solution has waterlike transport properties (valid for dilute solutions):

$$Re = 100$$
$$Sc = 10^4$$
$$El = 16$$

However, inspection of the variables involved in these dimensionless groups shows that the ratio Sc/El is a measure of the relative magnitudes of the electrophoretic and diffusive transport effects. For this case

$$Sc/El = \frac{m_i \Delta\phi}{D_i} = 6 \times 10^4$$

indicating that electrophoresis is more significant than diffusion.

However, in reality, this measure is rather too simplistic because, while electrophoresis may be viewed as a rate phenomenon, diffusion is dependent on local concentration

profiles as well as the magnitudes of the physical properties of the solution components. In the narrow-slot separator these gradients (and hence the value of the second derivative with respect to x) may be large.

3.3.3 The Behaviour of Equation 3.12 as z Tends to Infinity

In an infinitely long separating zone, a single component will eventually end up driven against one face of the separating chamber. In this state the only tendency for the substance to migrate from the given 'electrode' wall will be by diffusion down the concentration gradient at the wall. On expressing this condition mathematically, for as infinite distance from the entrance to the separating zone, equation 3.12 becomes:

$$\frac{1}{Re\ Sc}\frac{\partial^2 C_i}{\partial x^2} + \frac{1}{Re\ El}\frac{\partial C_i}{\partial x} = 0 \qquad 3.16$$

which is a second-order ordinary differential equation with constant coefficients, viz:

$$\frac{d^2 C_i}{dx^2} = \frac{-Sc}{El}\frac{dC_i}{dx} \qquad 3.17$$

which has the general solution,

$$C_i = A\exp[(-\frac{Sc}{El})x] + B \qquad 3.18$$

If migration occurs so that the solute substance accumulates at the 'electrode' wall, given by $x = -1$, then at this wall the boundary condition

$$\frac{dC_i}{dx} + \frac{Sc}{El}C_i = 0 \qquad 3.19$$

still holds. Applying this boundary condition to equation 3.17, one finds a solution of the form;

$$C_i = A\exp[(-\frac{Sc}{El})x] \qquad 3.20$$

where the constant A depends on the amount of solute material present and the solution applies only within the limits $-1 < x < 1$.

3.3.4 The Solution of Equation 3.12 for the Case of No Diffusion

If the diffusivity of the species being described by equation 3.12 is assumed to be zero, this equation reduces to:

$$U_z \frac{\partial C_i}{\partial z} = \frac{1}{Re\ El} \frac{\partial C_i}{\partial x} \qquad 3.21$$

or, expressed with the appropriate velocity profile;

$$U(1 - x^2)\frac{\partial C_i}{\partial z} = \frac{1}{Re\ El} \frac{\partial C_i}{\partial x} \qquad 3.22$$

subject to the boundary and initial conditions of section 3.2.4. Equation 3.22 is a first-order, quasi-linear hyperbolic equation and as such is amenable to solution by the method of characteristics (S4). Smith (ibid) gives a full discussion of the method of characteristics for solution of this class of equation. The basis of the method is the generation of a series of curves (in this case of z as a function of x) along which the value of the dependent variable (C_i) is given by some function of the independent variables.

Expressing equation 3.22 in the form necessary to evaluate the characteristic curves (cf. Smith (ibid)), one gets

$$\frac{dz}{U(1 - x^2)} = \frac{dx}{-(ReEl)^{-1}} \frac{dC_i}{0} \qquad 3.23$$

Therefore, the characteristic is described by

$$dz = dx[-U(Re\ El)(1 - x^2)] \qquad 3.24$$

or on integrating,

$$z = -U\ ReEl(x - \frac{x^3}{3}) + A \qquad 3.25$$

Moreover, since

$$\frac{dC_i}{0} = \frac{dx}{-(ReEl)^{-1}}$$

then C_i is constant along the characteristics given by equation 3.25.

The initial conditions are then introduced by the following procedure:

i) Selection of a particular value of x (say x_1) at $z = 0$;

ii) Substitution of these values into equation 3.25 to evaluate A.

The resulting curve then describes a line along which C_i retains the value given by the initial condition at the point,

$$x = x_1$$

and $$z = 0$$

In general, this procedure gives a series of curves of the form,

$$z = UReEl\left(\left(x_1 - \frac{x_1^3}{3}\right) - \left(x - \frac{x^3}{3}\right)\right) \qquad 3.26$$

along which C_i is constant.

Figure 3.4 shows a series of such curves plotted for different initial conditions using the fact that for fully-developed laminar flow U = 1.5 (B8). The curves in Figure 3.4(i) are plotted for the values Re = 100 and El = 16 which are assumed to be typical values for proteins (see section 3.3.2), while the curves in Figure 3.4(ii) are plotted for Re = 100 and El = 4. This latter value is derived from the mobility for titanium dioxide pigment given by Visca, Ardizzone and Formaro (V5).

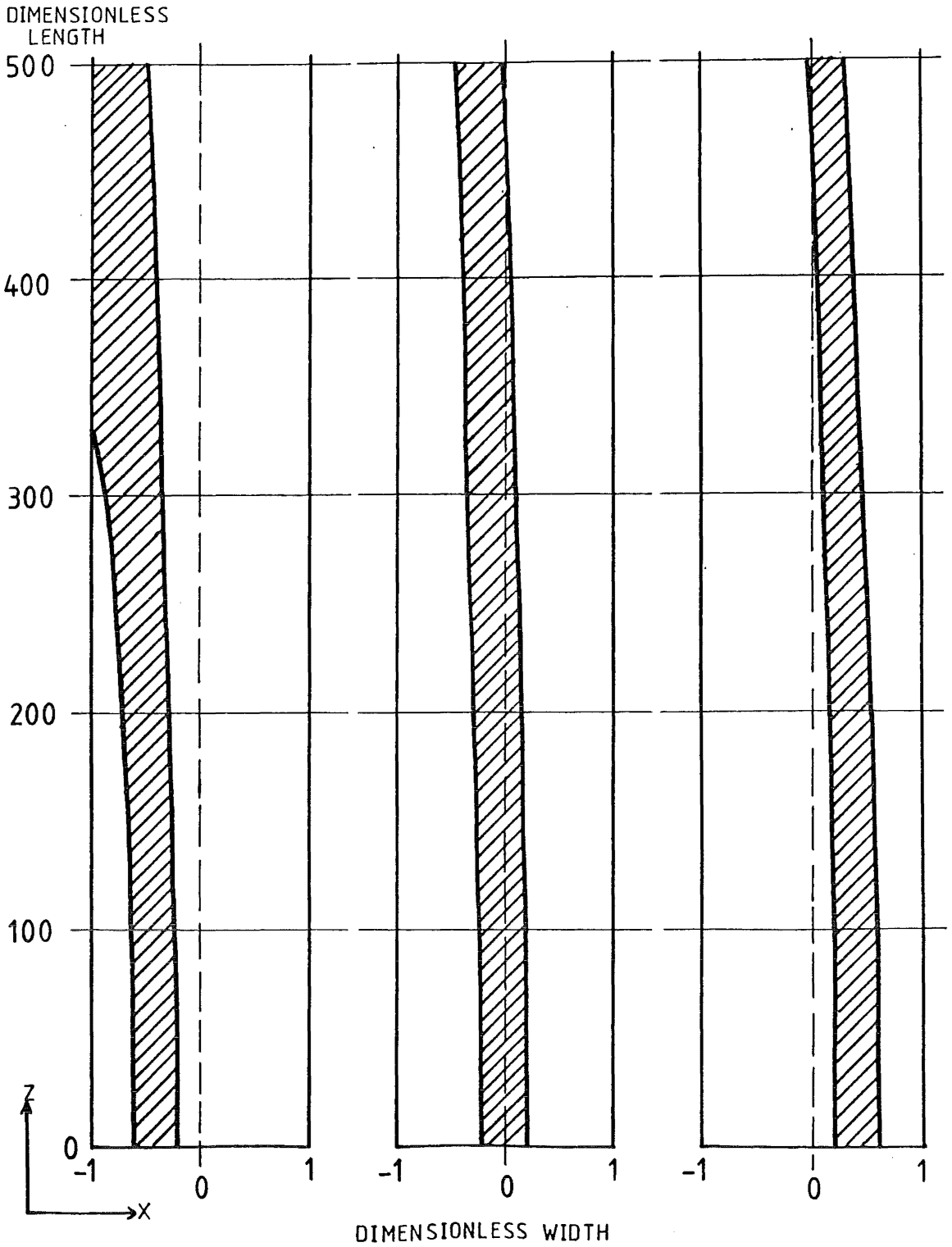

FIGURE 3.4(i) CHARACTERISTIC CURVES FOR EQUATION 3.26 FOR VARIOUS INITIAL CONDITIONS AT Re=100 & El=16 (approximate conditions for proteins)

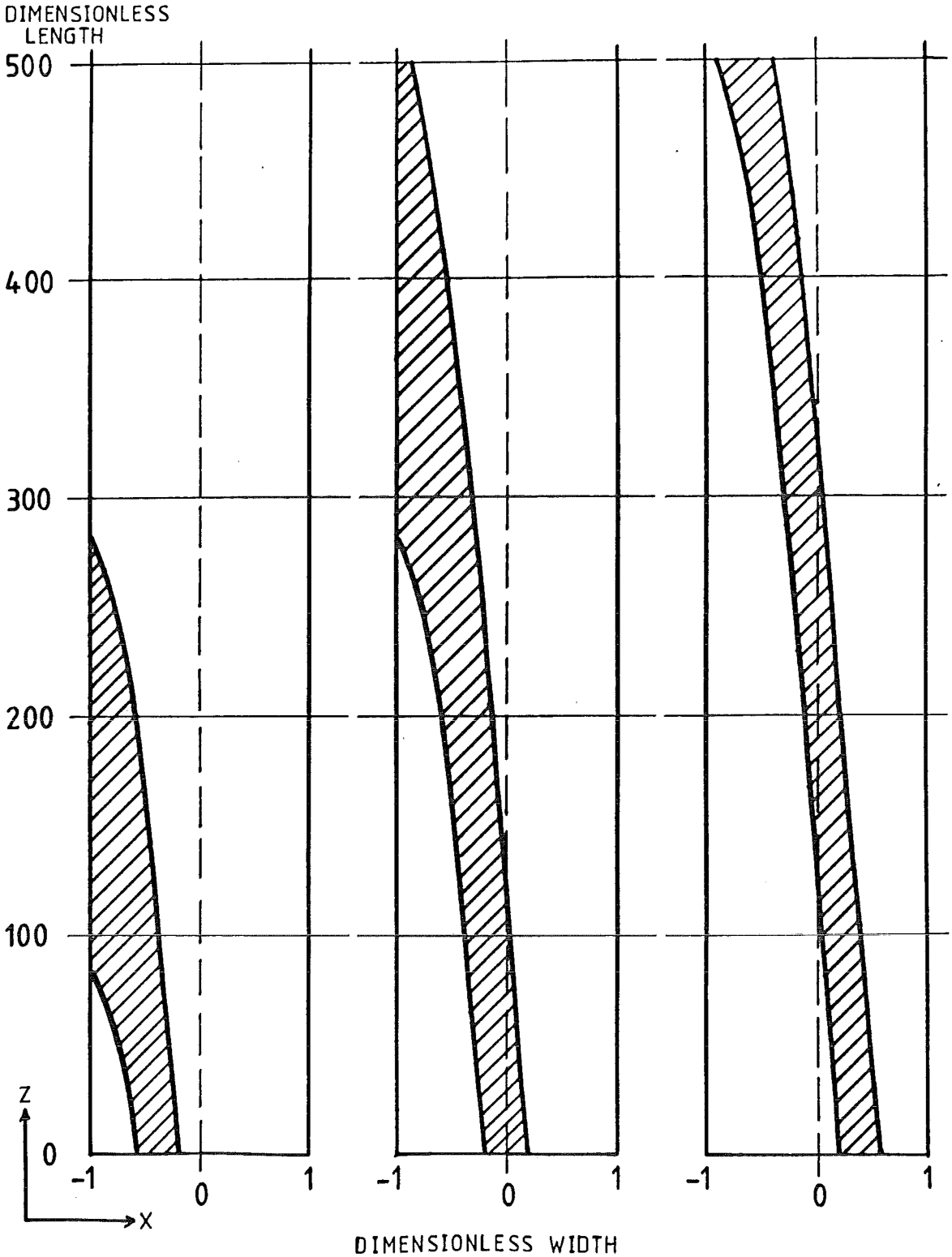

FIGURE 3.4(ii) CHARACTERISTIC CURVES FOR EQUATION 3.26 FOR VARIOUS INITIAL CONDITIONS AT Re=100 & El=4 (approximate conditions for pigments)

These curves demonstrate the sensitivity of the system to the value of El.

The boundary conditions in this case simply confine the characteristic curves to fixed limits and so this solution does not predict increases in the concentration at the wall after the curve reaches the wall. Intuitively, this is incorrect. Further, examination of the first curve in each series (Figures 3.4(i) and (ii)) shows that a second consequence of this approach is that conservation of mass is violated once the leading boundary of the concentration profile reaches the wall.

3.3.5 The Solution of Equation 3.12 for no Electrophoretic Transport

If there is no electrophoretic transport equation 3.12 reduces to:

$$U(1 - x^2)\frac{\partial C_i}{\partial x} = \frac{1}{Re\ Sc}\frac{\partial^2 C_i}{\partial x^2} \qquad 3.27$$

which is a parabolic partial differential equation with one non-constant coefficient. Equations of this type are amenable to solution by finite-difference numerical techniques (C1). In this particular case, equation 3.27 was solved using the Crank-Nicholson implicit procedure (ibid) which permits different step sizes in the x and z directions to be chosen (see Figure 3.5). Since this limiting case of the equation has no electrophoretic transport, the boundary condition can be reduced to:

$$D_i \frac{\partial C_i}{\partial x} = 0 \qquad 3.28$$

or more simply

$$\frac{\partial C_i}{\partial x} = 0 \ ;$$

that is to say, the concentration gradient at the wall is always zero.

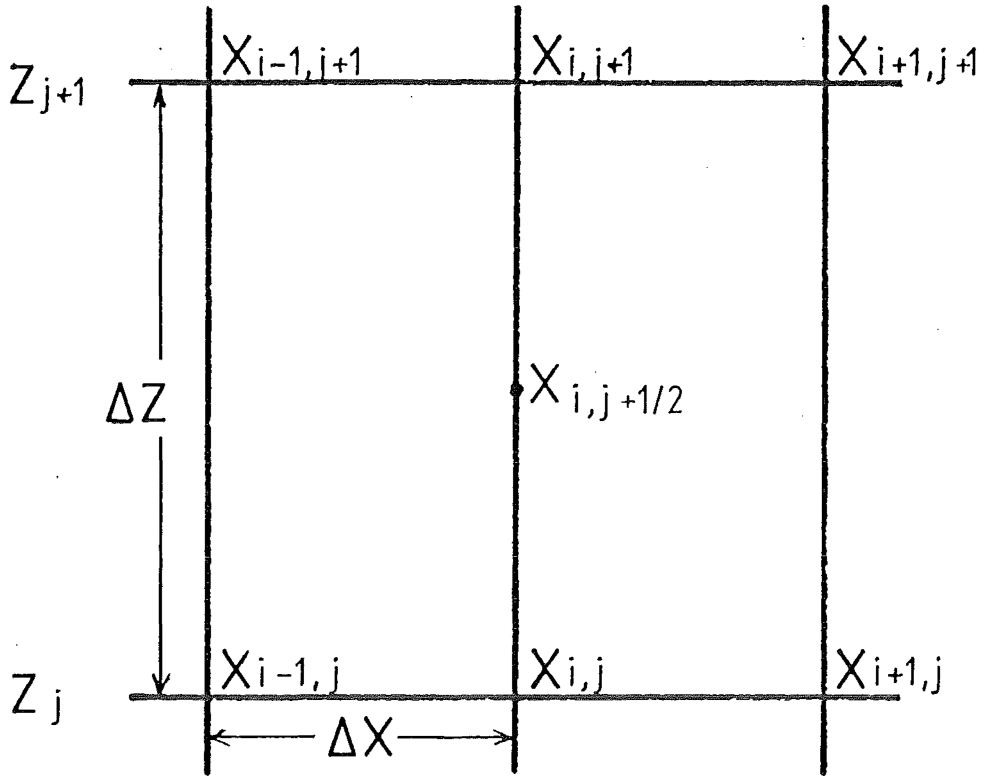

FIGURE 3.5 FINITE DIFFERENCE NETWORK FOR THE CRANK-NICHOLSON METHOD

The Crank-Nicholson method uses the following finite-difference approximations for the derivatives (ibid):

$$\frac{\partial C_i}{\partial z} \simeq \frac{C_{ij+1} - C_{ij}}{\Delta z} \qquad 3.29$$

$$\frac{\partial^2 C_i}{\partial x^2} = \tfrac{1}{2}\left[\frac{C_{i-1\,j+1} - 2C_{ij+1} + C_{ij-1}}{\Delta x^2}\right] + \tfrac{1}{2}\left[\frac{C_{i-1j} - 2C_{ij} + C_{ij-1}}{\Delta x^2}\right] \qquad 3.30$$

Similarly, the boundary conditions can be expressed by use of the approximations,

$$\left.\frac{\partial C_i}{\partial x}\right|_0 = \frac{3C_0 - 4C_1 + C_2}{2\Delta x} \qquad 3.31$$

$$\left.\frac{\partial C_i}{\partial x}\right|_N = \frac{3C_N - 4C_{N-1} + C_{N-2}}{2\Delta x} \qquad 3.32$$

where the subscripts 0 and N indicate that these values are the first and last points on the finite-difference grid, i.e. corresponding to $x = \pm 1$ in equation 3.12.

These approximations and boundary conditions were then used to write a FORTRAN program to provide concentration profiles given some initial profile. The program is discussed in full in section 3.4 which deals with the solution of equation 3.12 in its entirety by the use of a similar program. The output from this program is represented graphically in Figure 3.6 which shows the expected concentration profiles for diffusion only given $Re = 100$ and $Sc = 10^4$.

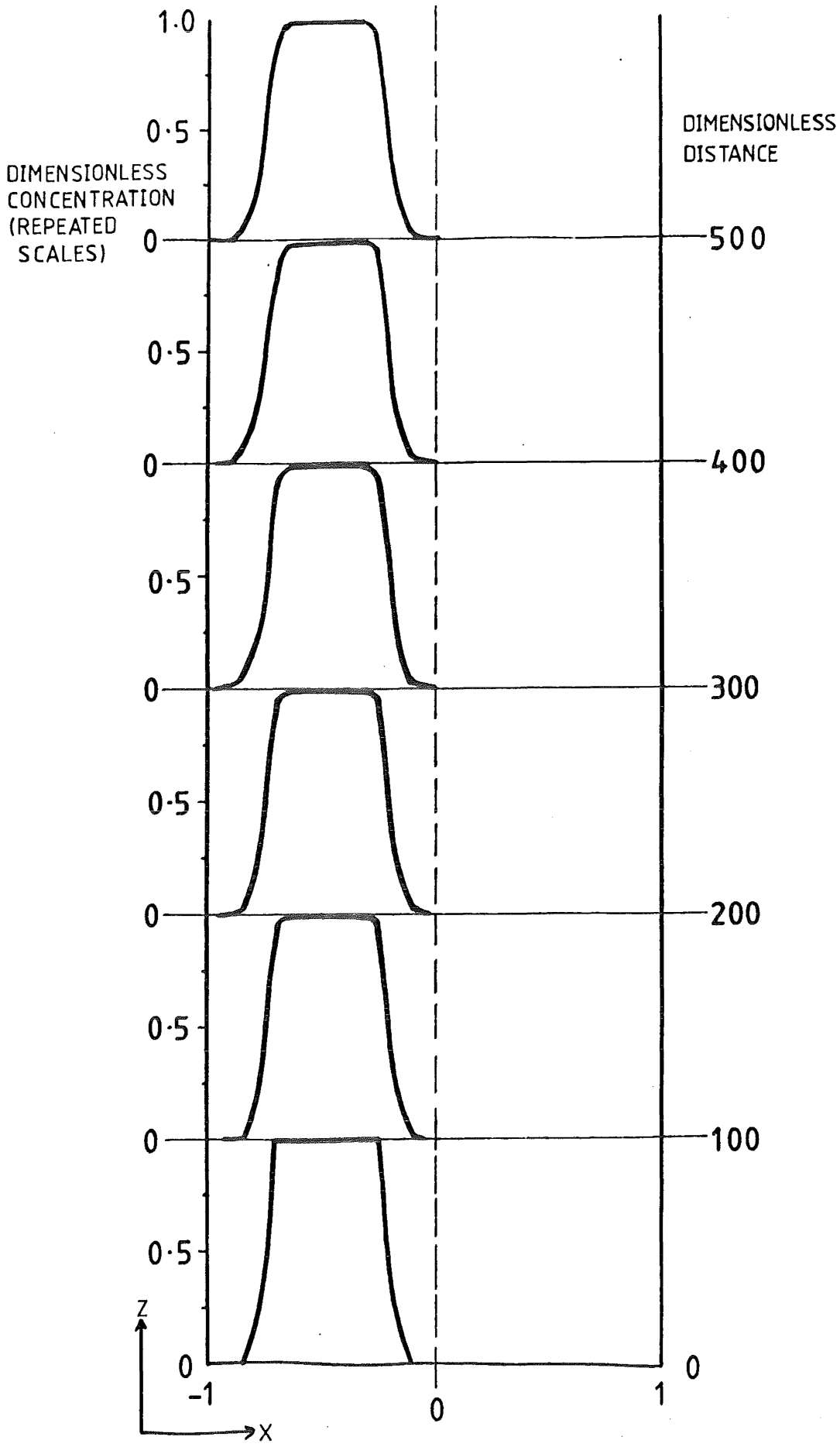

FIGURE 3.6(i) CONCENTRATION PROFILES IN NARROW SLOT FLOW FOR $Re=100$ & $Sc=10^4$

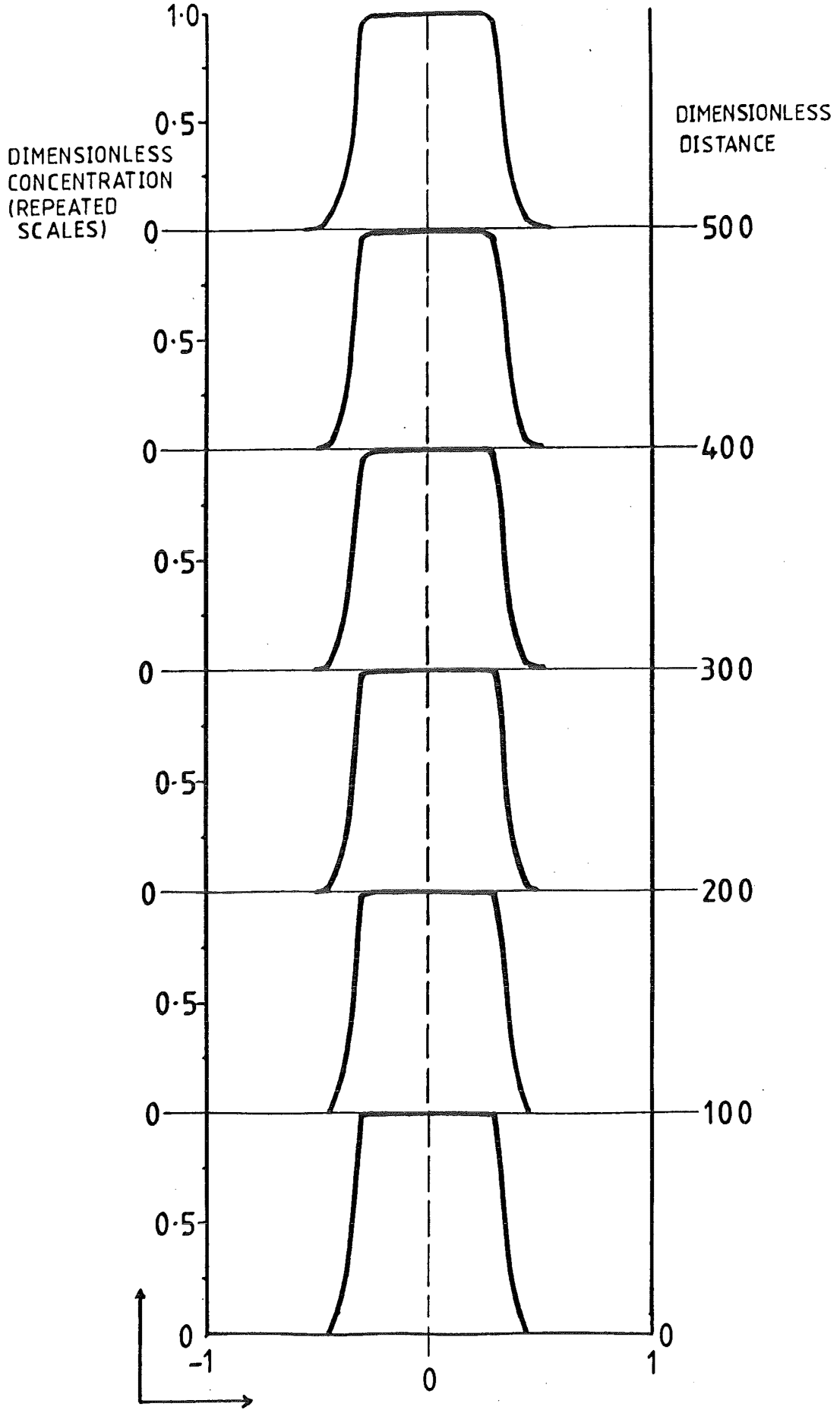

FIGURE 3.6(ii) CONCENTRATION PROFILES IN NARROW SLOT FLOW FOR Re=100 & $Sc=10^4$

3.4 Solution Methods for Equation 3.12

3.4.1 Classification of Equation 3.12

The central problem in finding a solution for equation 3.12 is classification of this equation in order to find an appropriate method of solution. The equation:

$$U_z \frac{\partial C_i}{\partial z} = \frac{1}{Re\ Sc} \frac{\partial^2 C_i}{\partial x^2} + \frac{1}{Re\ El} \frac{\partial C_i}{\partial x}$$

has both parabolic and hyperbolic elements. The relative magnitudes of these elements depend on the relative magnitudes of the coefficients of the terms on the right-hand side of the equation (see section 3.3.2). On this basis, the equation could be regarded as hyperbolic since, for values of practical interest, $\frac{1}{Re\ El}$ is larger than $\frac{1}{Re\ Sc}$. However, it is expected that the local concentration gradients in the narrow-slot separator will be relatively large so that the diffusive term cannot be written out of the relationship. Further, as has already been remarked, the use of characteristic curves, suggested by the use of the hyperbolic approximation for the solution of equation 3.12, does not give concentration profiles which obey mass conservation. The hyperbolic solution also does not give realistic behaviour of the solution to equation 3.12 at the boundaries. At these positions, the solution must show the general form of equation 3.20 at large z distances from the origin.

3.4.2 Solution of Equation 3.12 as Parabolic Equation

In spite of the dominance of the hyperbolic term, it was thought worthwhile to investigate the possibility of using the solution procedure for parabolic equations for equation 3.12. The method chosen was the Crank-Nicholson implicit procedure, as given by Carnahan, Luther and Wilkes (C1). An

implicit procedure was chosen because of the generally greater numerical stability of implicit procedures as opposed to explicit procedures.

Initially, the following finite-difference approximations were used to represent the differential terms:

$$\frac{\partial C_i}{\partial z} \simeq \frac{C_{ij+1} - C_{ij}}{\Delta z} \qquad 3.33$$

$$\frac{\partial^2 C_i}{\partial x^2} \simeq \tfrac{1}{2}\left[\frac{C_{i-1\ j+1} - 2C_{ij+1} + C_{i+1\ j+1}}{\Delta x^2}\right] + \tfrac{1}{2}\left[\frac{C_{i-1j} - 2C_{ij} + C_{i+1j}}{\Delta x^2}\right] \qquad 3.34$$

and

$$\frac{\partial C_i}{\partial x} \simeq \frac{C_{i+1j} - C_{ij}}{\Delta x} \qquad 3.35$$

where the subscript notation is that of Figure 3.5. These terms are all derived from Taylor series expansions about the appropriate points in Figure 3.5. As noted by Carnahan, Luther and Wilkes (C1), this particular series of approximations gives terms which are second-order correct in both the x and z directions for a parabolic differential equation. What effect the additional term has is by no means clear.

These approximations were then used with the boundary conditions represented by equation 3.28 to write a FORTRAN program for evaluation of the expected concentration profile with electrophoresis. This program, given in Appendix (2), involved the use of the Thomas recursive algorithm (S5) to solve the matrix network shown in Figure 3.7 which results from these equations.

$$3C_{1j+1} - 4C_{2j+1} + C_{3j+1} = 0$$

$$\left(-\frac{1}{2ReSc\Delta x^2}\right) C_{i-1\ j+1} + \left(\frac{U(1 - x_i^2)}{\Delta z} + \frac{1}{ReSc\Delta x^2}\right) C_{ij+1} + \left(\frac{-1}{2ReSc\Delta x^2}\right) C_{i+1\ j+1}$$

$$= \left(\frac{1}{2ReSc\Delta x^2}\right) C_{i-1j} + \left(\frac{U(1 - x_i^2)}{\Delta z} - \frac{1}{ReSc\Delta x^2} - \frac{1}{ReEl\Delta x}\right) C_{ij} + \left(\frac{1}{2ReEl\Delta x} - \frac{1}{2ReSc\Delta x^2}\right) C_{i+1j}$$

$$C_{N-2\ j+1} - C_{N-1\ j+1} + 3C_{Nj+1} = 0$$

Where $2 < i < N-1$ and j is the appropriate z 'level'

FIGURE 3.7: ORIGINAL CRANK-NICHOLSON NETWORK FOR EQUATION 3.12

The resulting profile was reasonable in terms of the limiting-case behaviour of the system (see sections 3.3.4 and 3.3.5) when the profile was not near the walls (i.e. at $x = \pm 1$). However there were several problems. Firstly, the transport due to electrophoresis was smaller than might be expected on the basis of Figure 3.4. Secondly the solute-concentration profiles did not build up as expected at the wall. Thirdly, attempts to use this program with solutes of high electrophoretic mobility (i.e. small magnitudes of El) led to the computation of negative concentrations at the sides of the input profile after a small number of steps in the procedure.

The problems encountered at the edges of the model, in particular at $x = -1$ (i.e. i = 1 in the network) for leftward electrophoretic transport, were due to the omission of part of the boundary condition. The full boundary condition (Equation 3.14) requires both electrophoretic transport and diffusion to be zero at the wall. It was further observed that the approximation for

$$\frac{\partial C_i}{\partial x}$$

$$\frac{\partial C_i}{\partial x} \simeq \frac{C_{i+1j} - C_{ij}}{\Delta x}$$

was, in fact, only first-order correct. The second-order correct term is, on the other hand:

$$\frac{\partial C_i}{\partial x} \qquad \frac{C_{i+1j} - C_{i-1j}}{2\Delta x} \qquad 3.36$$

which can be shown by Taylor expansion about the point given by the coordinates (i,j) in Figure 3.5

Substitution of these corrections into the program gave an algorithm which generated negative concentration values after the first pass of the method for all values of El tried. If the procedure was permitted to continue, waves in the concentration profile of increasing magnitude with increasing distance were produced even when extremely small step sizes and double-precision arithmetic were used (see Figure 3.8). From these computations, it was concluded that the Crank-Nicholson implicit method of solution was numerically unstable for equation 3.12.

3.4.3 Hybrid Methods

Since equation 3.12 could be regarded as a combination hyperbolic and parabolic differential equation it was considered that solving this equation would require a hybrid of the two methods appropriate to these two types. That is to say, a solution may be possible if the method of characteristics is used to provide a model of the electrophoresis 'shift' and a numerical technique appropriate to a parabolic equation is used to model diffusive effects. This raises the question, in which part of such a hybrid should the velocity term be contained? Inspection of the relative magnitudes of the dimensionless groups involved would suggest that the major effects in the system are those of bulk flow and electrophoresis (see section 3.3.2). This would suggest that the model should be of a form which utilises characteristic curves of the type used in section 3.3.5 (i.e. characteristics plotted on the basis of electrophoretic transport and the assumed velocity profile). On the other hand, at the microscopic level, electrophoresis is a linear effect; that is, the rate of transport is directly proportional to the voltage gradient, which for a linear gradient is linear. Thus, for the

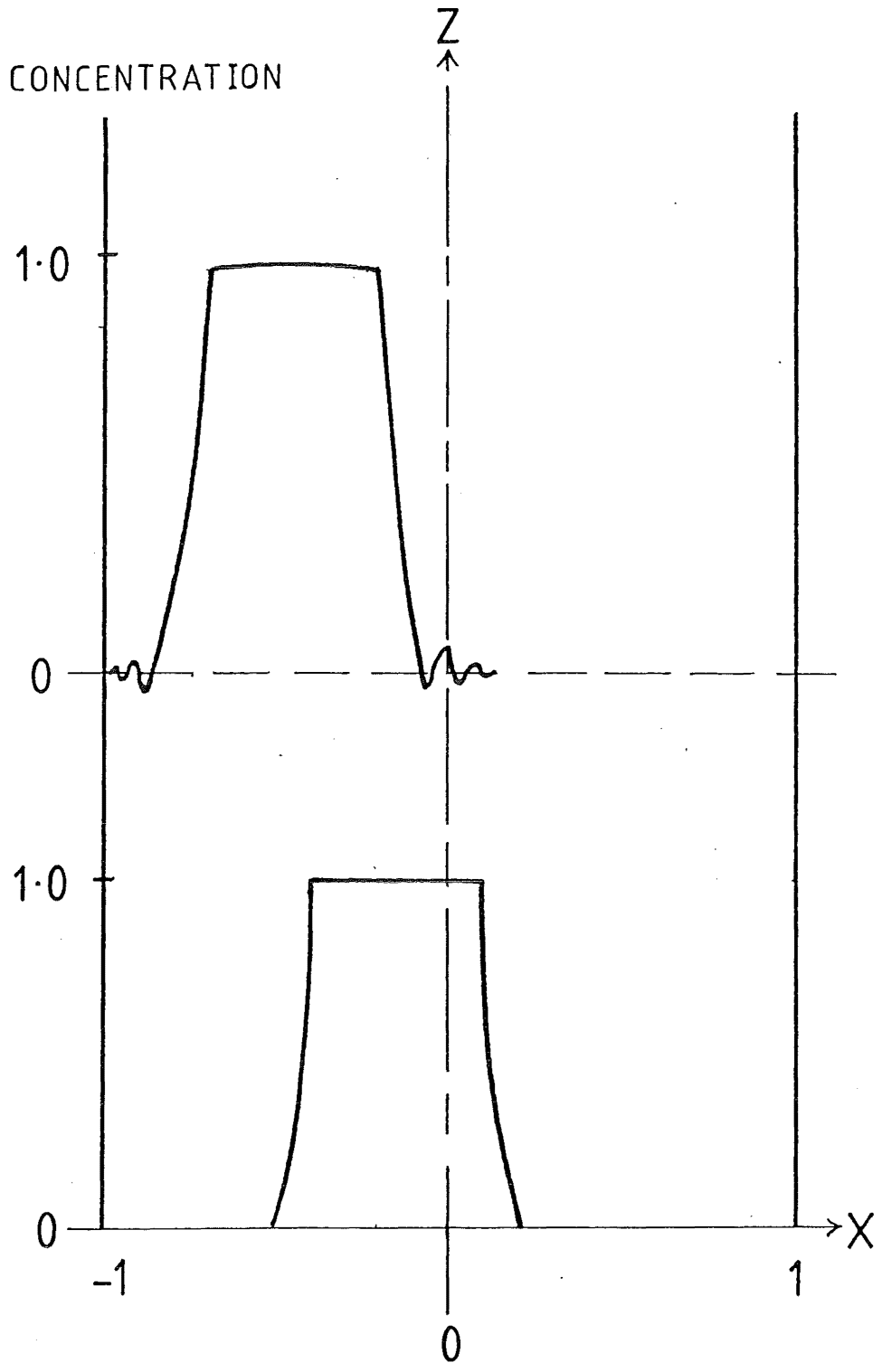

FIGURE 3.8 SKETCH OF NUMERICAL INSTABILITY IN THE CRANK-NICHOLSON METHOD OF SOLUTION OF EQUATION 3.12

small increments used for a finite-difference model, characteristics that are straight lines may better fit the behaviour of a real system. Resultingly, both models were tested and used to generate predicted concentration profiles.

3.4.3.1 The Linear Characteristics Model for Solution of Equation 3.12: Two adjacent rows of the finite-element network for solution of a parabolic differential equation may be considered as the basis for the solution of the whole network (see Figure 3.9(i)). The normal finite-difference solution technique utilises values at a level (or row) j of such a network, operates on these by way of the finite-difference form of the equation, and generates a row of values at j+1 (the so-called 'marching' solution (S5)). The method is always started with initial conditions (i.e. at j = 1) and the procedure is repeated as often as necessary in order to arrive at values at (in this case) positions further along the model in the z direction.

The hybrid method developed for equation 3.12 applies the shift based on the characteristic curve at the points on row j to give a new set of positions for the values at each point (i,j) at row j' (Figure 3.9(ii)). These values at the shifted positions are then used to calculate new magnitudes for the values at the positions on the original grid. If the shift is a linear one, as shown in Figure 3.9(ii), the new positions of the grid points are given by:

$$x_{ij}' = x_{ij} - \frac{\Delta z}{Re\ El} \qquad 3.37$$

and the new values for the concentration for 'level j' are given by:

$$C_{ij}' = C_{ij} + (C_{i+1j} - C_{ij}) \frac{\Delta z}{Re\ El} \qquad 3.38$$

as can be seen from examination of the geometry of Figure 3.9(ii).

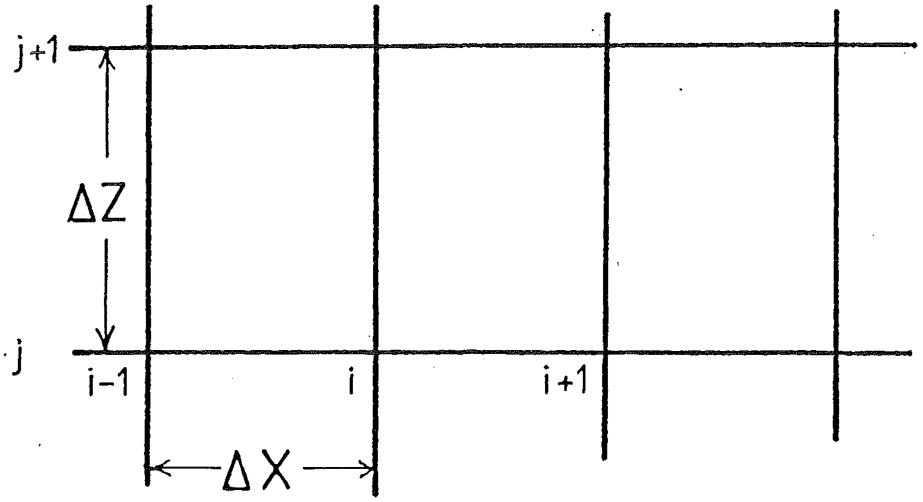

(i)

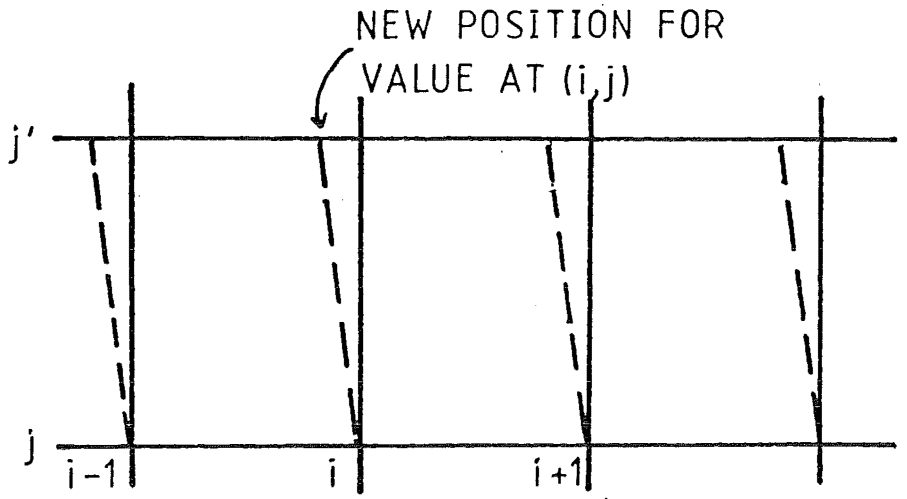

(ii)

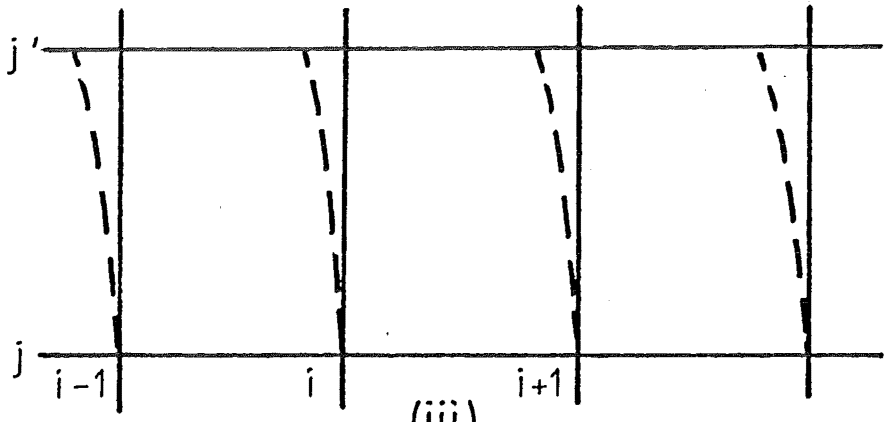

(iii)

FIGURE 3.9 NETWORKS FOR HYBRID METHOD

3.4.3.2 The Cubic Characteristics Model for the Solution of Equation 3.12: If the parabolic velocity profile is used to generate the characteristic curves to represent electrophoretic transport, the model becomes somewhat more complex. The same general procedure as that outlined in the previous section is used to proceed from step to step of the solution, but now the relationship between the concentrations at the grid points on row j and those on row j' is given by:

$$C_{ij}' = C_{ij} + (C_{i+1j}' - C_{ij})\frac{(x_{ij} - x_{ij}')}{\Delta x} \qquad 3.40$$

where x_{ij}' is evaluated by solving the cubic equation (cf. section 3.3.4):

$$x_{ij}' - \frac{x_{ij}'^3}{3} = x_{ij} - \frac{x_{ij}^3}{3} - \frac{\Delta z}{URe\mathcal{E}l} \qquad 3.41$$

That is to say, the shifts needed to translate values from row j to row j' are no longer constant or linear (see Figure 3.9(ii)). Thus each particular x_{ij} has a different x_{ij}' associated with it which is derived from the solution of equation 3.41. However, once this shift has been achieved, the same type of procedure can be applied to evaluate the effect of diffusion. But in this case, the Crank-Nicholson method is applied to

$$\frac{\partial C_i}{\partial z} = \frac{1}{Re\ Sc}\frac{\partial^2 C_i}{\partial x^2} \qquad 3.42$$

since the effect of the velocity profile has already been accounted for.

3.4.3.3 Boundary Conditions: As has been pointed out in section 3.3.4, the method of characteristics takes no account of the boundary conditions for equation 3.12. This leads to the requirement for a special form of the shift relation to model the no-flux condition at the wall boundary. A number of

procedures were tried in order to find an adequate analogue of the boundary condition (equation 3.14). The approach found most suitable was to decouple the two portions of the boundary condition so that the electrophoretic and diffusive effects could be treated separately. This was done by defining a further 'fictitious' grid point outside the standard pattern (see Figure 3.10), and using the characteristics-based shift procedure only up to the last normal grid point (i = 1 in Figure 3.10), about which point a special term of the form;

$$C_{1j}' = C_{1j} + C_{2j}\left(\frac{\Delta z}{Re\ El}\right) \qquad 3.43$$

was written. The boundary condition of no diffusion (essentially $\frac{\partial^2 C_i}{\partial x^2}\Big|_0 = 0$) was then applied between this value and that at the 'fictitious' boundary point (i = 0 in Figure 3.10). Further, the Δx increment between the points i = 1 and i = 0 was made very much smaller than the main grid-step size to minimise the effects of this modification on the remaining section of the concentration profile. For a full discussion of this practice of using fictitious points to incorporate boundary values the reader is referred to Smith (S5).

Inspection of Figure 3.4 shows that the method of characteristics does not give a mass-conservative solution to the equation as the concentration profile approaches the boundary. Similar problems occur for the hybrid solution method in spite of the use of a characteristic only over short distances (i.e. distances equal to the step size). In fact, the errors resulting from this procedure are cumulative leading to significant deviations from a mass balance for large z values. The one case where this does not occur is where Δx is exactly equal to the magnitude of the electrophoresis shift for a single step so that

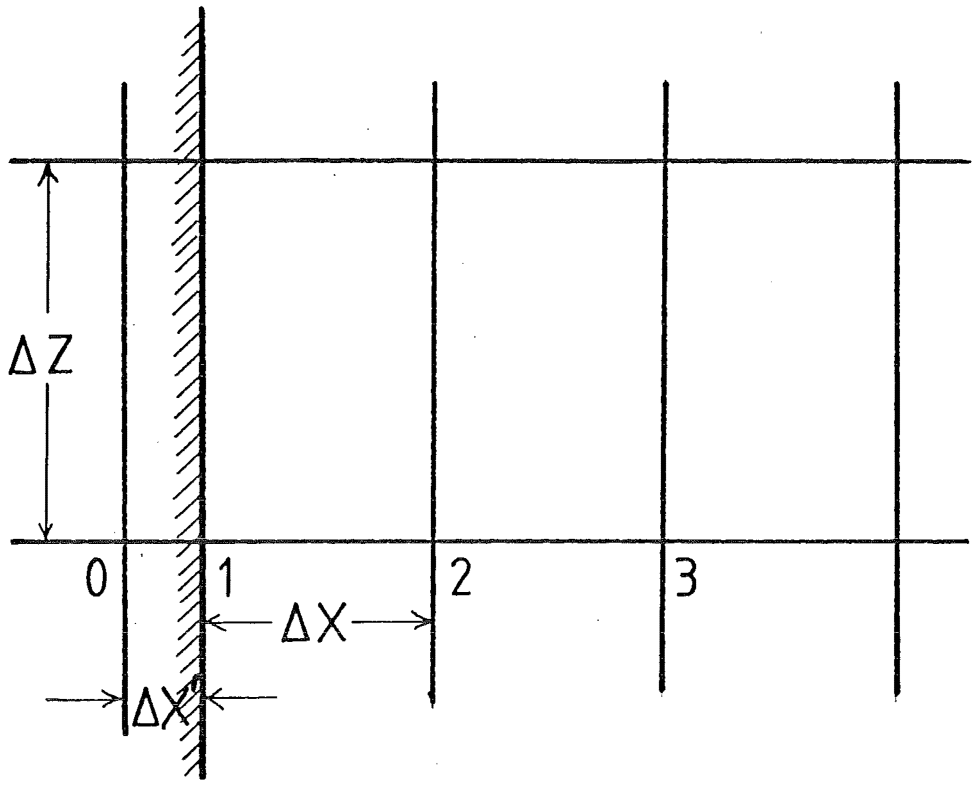

$$\Delta X' << \Delta X$$

FIGURE 3.10 FICTITIOUS BOUNDARY POINT NETWORK

$C_{ij}' = C_{ij}$ involves impractically long computations.

i.e. for $Re = 100$

and $El = 4$

and $\Delta z = 0.25$

requires $\Delta x = 6.25 \times 10^{-4}$

or a grid 3200 steps wide.

Therefore the hybrid method requires correction at each step in order to maintain as mass balance in the z direction during computation.

3.4.3.4 Results: Typical concentration profiles for application of the stated conditions to the two models are shown in Figure 3.11.

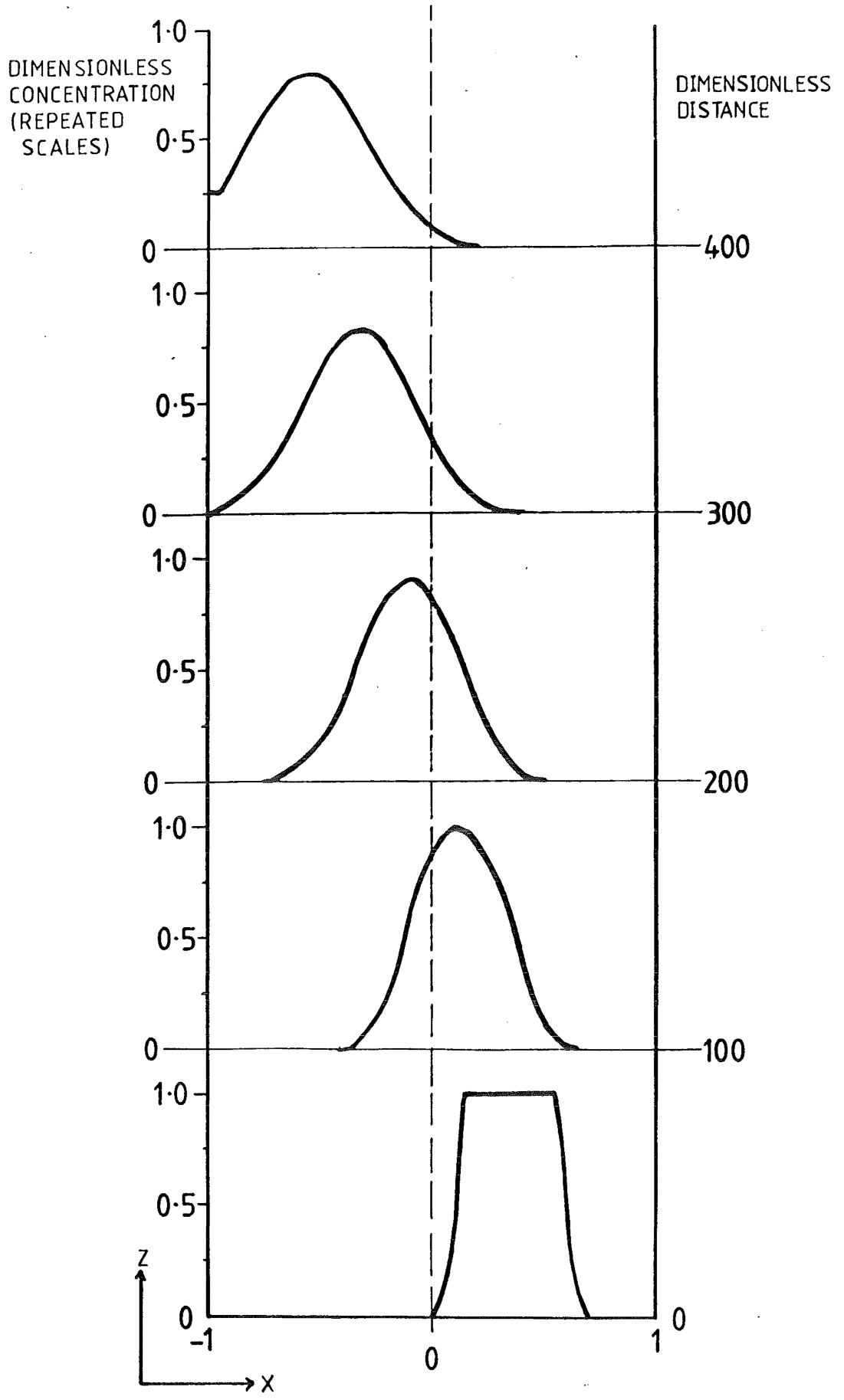

FIGURE 3.11(i) CONCENTRATION PROFILES FOR LINEAR HYBRID MODEL FOR $Re = 100$, $Sc = 10^4$ & $El = 4 \cdot 4$

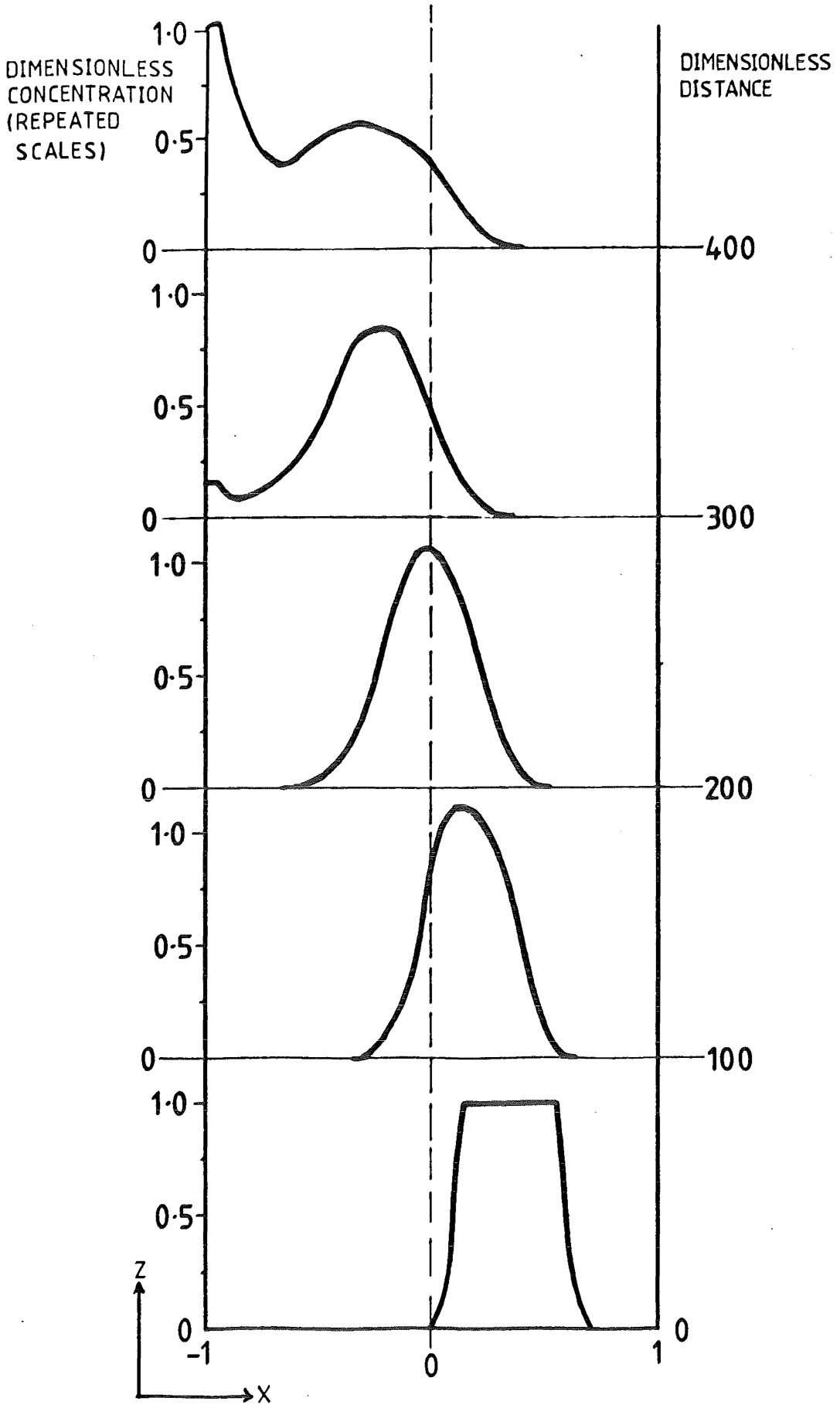

FIGURE 3.11(ii) CONCENTRATION PROFILES FOR CUBIC HYBRID MODEL FOR $Re = 100$, $Sc = 10^4$ & $El = 4 \cdot 4$

4. DESIGN AND COMMISSIONING OF THE PROTOTYPE NARROW-SLOT ELECTROPHORETIC SEPARATOR

4.1 Introduction

The design of a prototype electrophoretic separator to fulfill the requirements of the narrow-slot concept involves planning of both the separating zone and the support services for such a device. The design must necessarily conform to the geometry required by the concept, but there are clearly constraints imposed by the mechanical, structural and electrical properties of materials used to build the separating cell. Ancillary services to provide fluids, electric power and heat transport where necessary must be an integral part of the overall design exercise. Since it is likely that the cell will contain buffers which may be chemically corrosive and that the passage of an electric current will give rise to locally strong oxidising conditions, corrosion resistance of materials will also be of importance. The requirements of these conditions and the design used to meet them is outlined in this chapter. The modifications, found necessary on commissioning, of the initial design are then detailed.

4.2 Physical Structure of the Prototype Cell

4.2.1 General

In order to simplify construction, maintenance, and subsequent possible modification of the separator, its design is in three basic units.

i) The input zone which is designed to promote fully developed laminar flow of the dilute solute in a carrier buffer to the centre or separating zone of the device. The basic form of this section is a converging wedge with internal dividers such that the narrow end of the wedge matches the cross-section of the separating zone. The solutions fed to the separator enter at the bottom of this compartmented wedge and, by the use of a suitable distributor, the flow is made to conform to the geometry of the duct.

ii) The separating zone consists of a long, narrow, rectangular duct with the larger inner surfaces of the duct made of semi-permeable membranes forming barriers which permit an electric field to be developed across the duct by way of the outer electrode compartments which are faced by metal electrode plates. These electrode compartments require ancillary fluid circulated through them, both to remove gases evolved by the passage of electric current and to remove heat generated resistively in these spaces.

iii) The recovery zone is matched to the top of the separating zone and permits splitting off of the separated streams from the separating zone while maintaining laminar flow. This zone has a decreasing cross-sectional area over a diverging wedge, as described in section 2.2.3, and has a series of knife edges in a parallel-sided duct placed at the top of the 'diverging' zone to complete the separation.

These three sections, when bolted together, form the bare prototype separator.

4.2.2 Input Zone

Orthographic projections of the input zone are given in Figure 4.1. The zone consists of a 300 mm high wedge tapering from a width of 110 mm at the bottom to 5 mm at the top with a depth of 100 mm. The wedge is internally divided into 5 compartments with spacers which terminate in knife edges 90 mm from the narrowest point. Each compartment has a separate feed inlet to permit the input of solute to any compartment across the width of the zone. The input zone is constructed in three sections which are flanged and bolted together so that it may be dismantled for cleaning. The material of construction used was Perspex sheet which was machinable to the necessary precision and transparent to permit observation of the flow in the finished section.

4.2.3 Separating Zone

The core of the separating zone (the drawings of which are shown in Figure 4.2) is a rectangular duct, 5 mm wide by 100 mm deep with a length of 1.15 m. This length is governed by the maximum continuous length of semi-permeable membrane available (see section 4.4). This inner duct is bounded on its narrow faces by the Perspex shell of the separating-zone frame and on its wider faces by the semi-permeable membrane and its supports. The narrow Perspex faces are polished to permit observation of the flow in the duct. The membranes are supported by a porous polythene sheet (approximate pore size 80 μm) bonded to a Perspex frame recessed into the main structural frame of the zone. The 316 grade stainless steel plate electrodes are bolted to the flanged outer faces of the main frame forming a cavity 100 mm by 17 mm in cross-section between the electrodes and the support for the porous plastic membrane. This space is connected

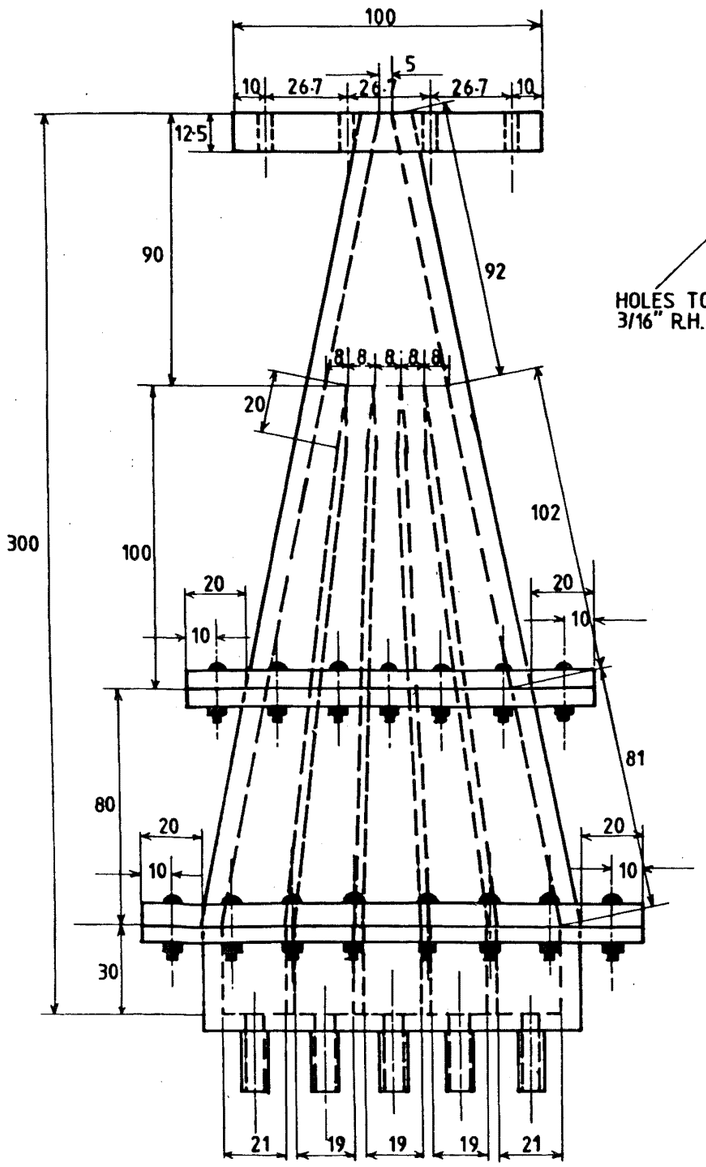

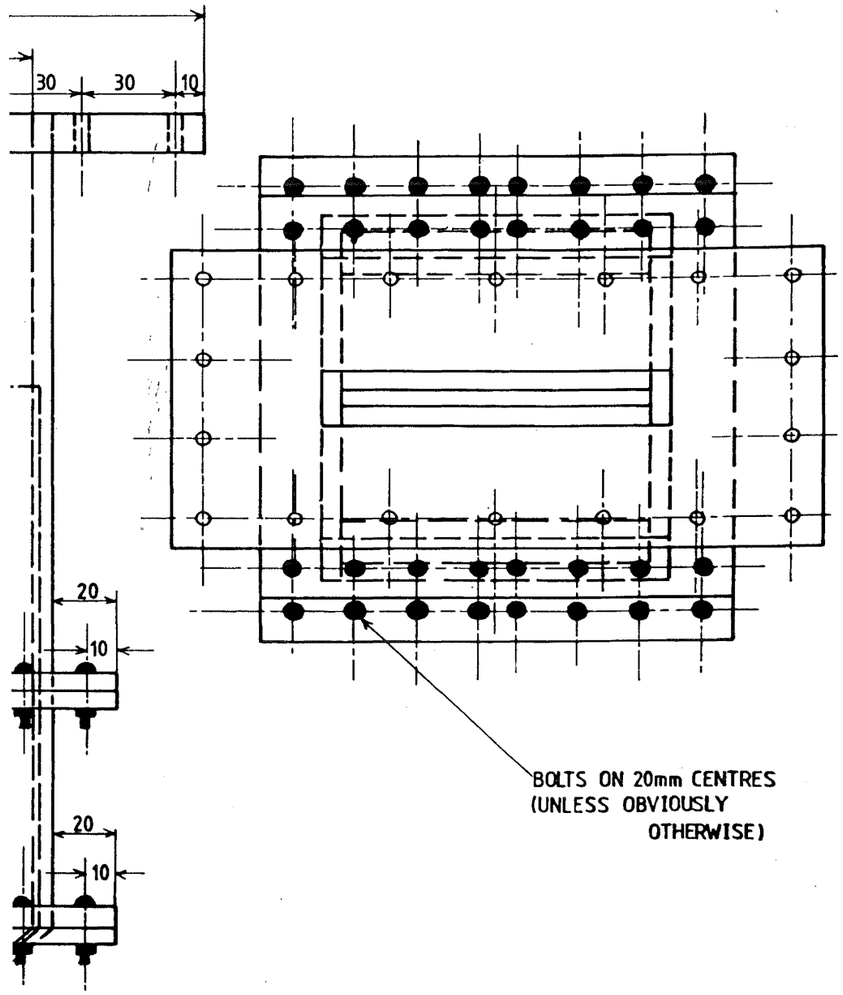

FIGURE 4.1 INPUT ZONE
(DIMENSIONS IN mm)

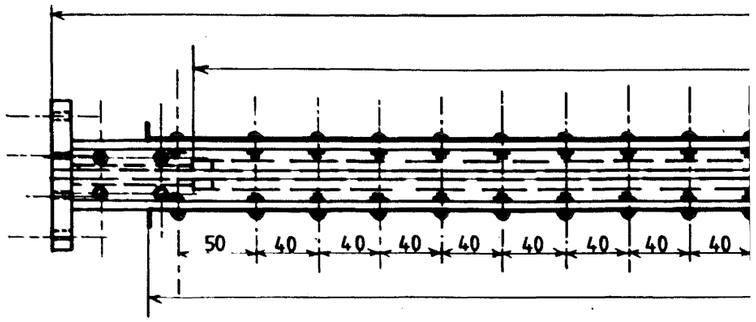

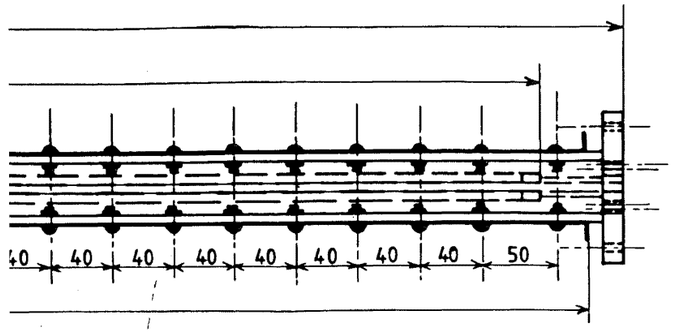

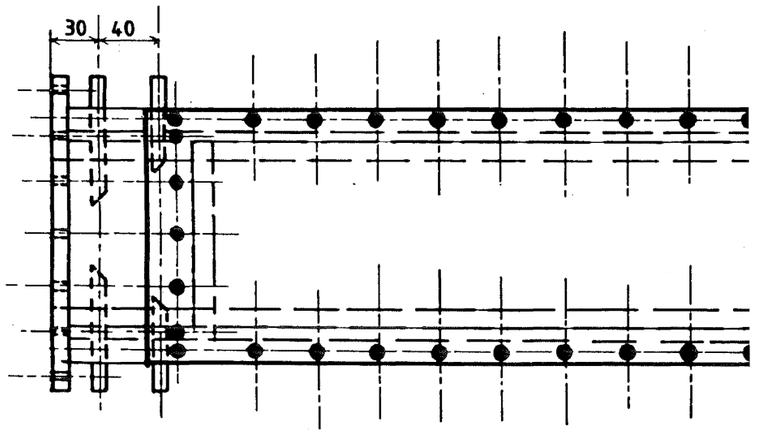

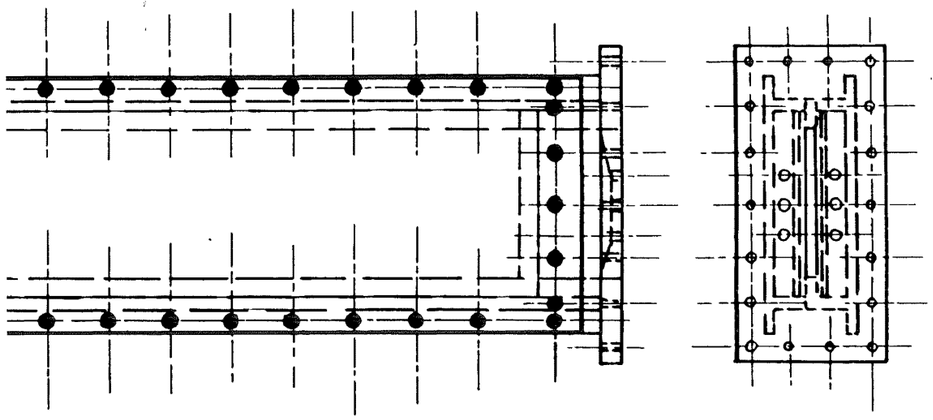

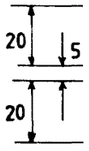

FIGURE 4.2 SEPARATING ZONE
(ALL DIMENSIONS IN mm)

FIGURE 4.3 RECOVERY ZONE

(ALL DIMENSIONS IN mm)

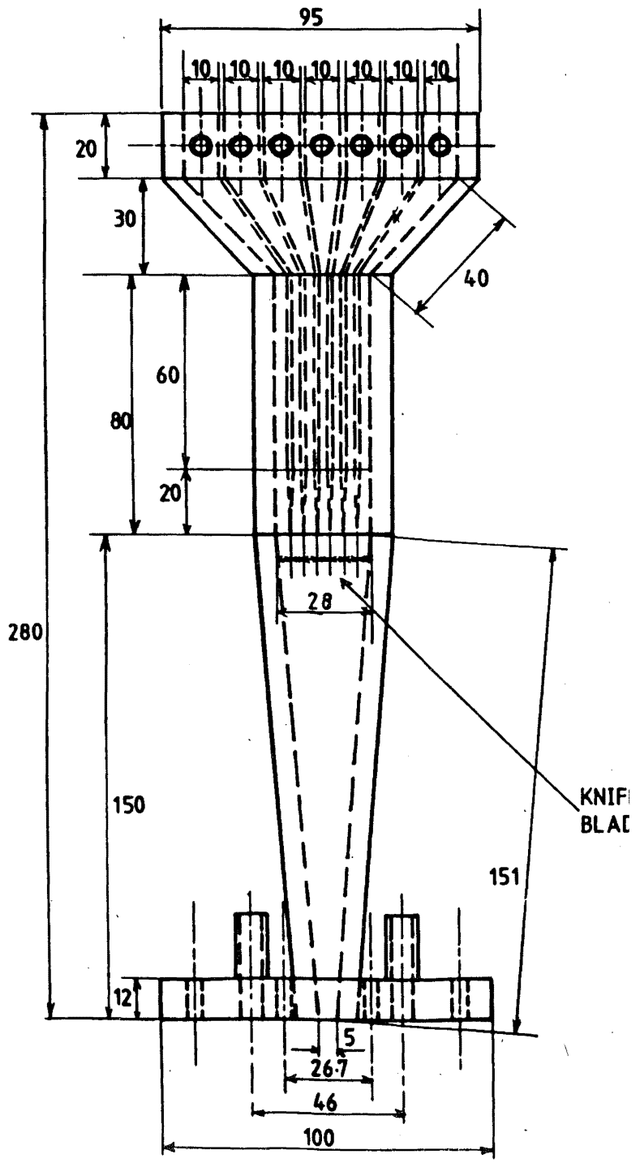

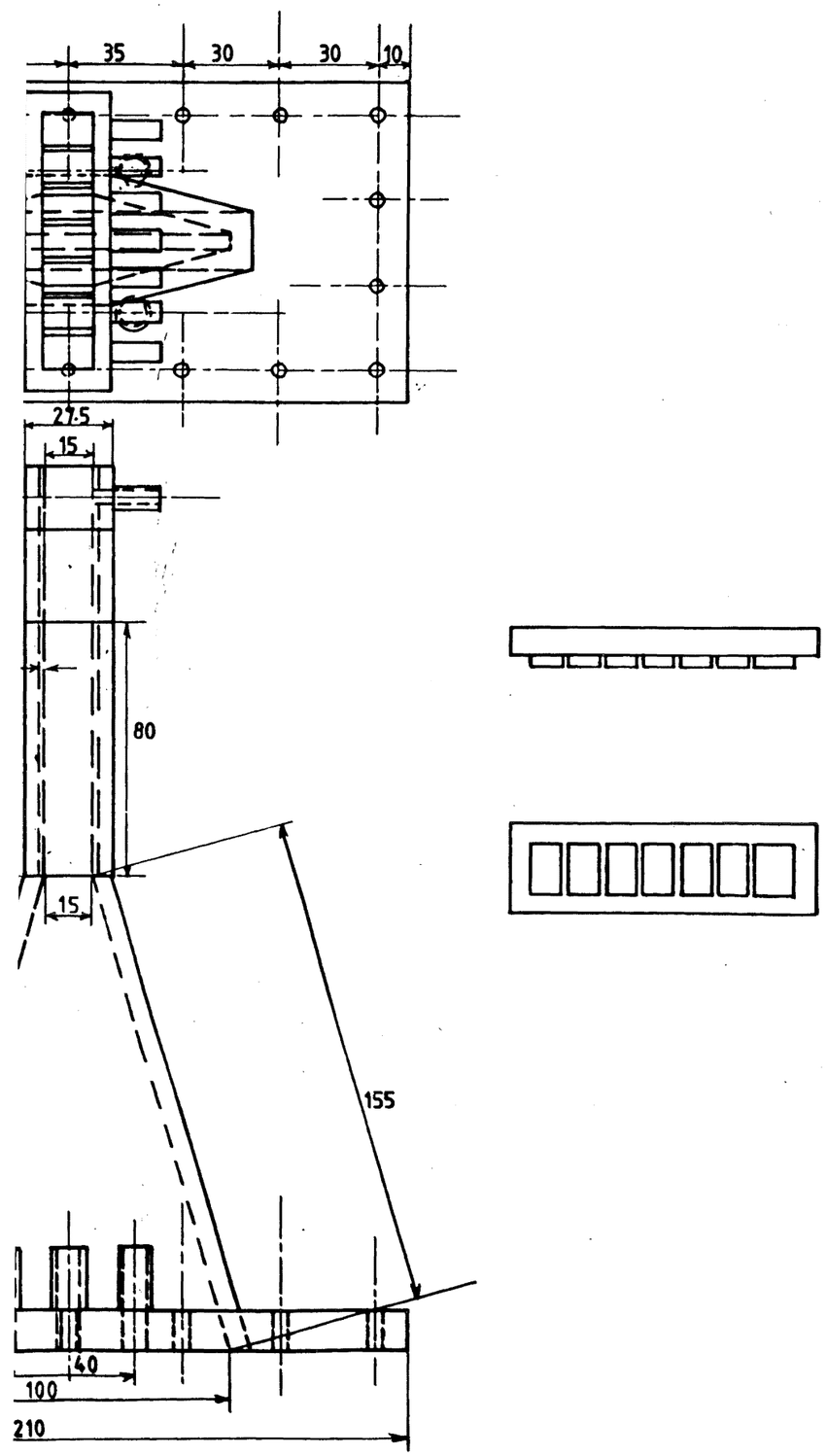

outside the cell by way of built-in pipes entering these compartments at the edges at the bottom of the cavity and holes bored through the top flange.

4.2.4 Recovery Zone

The recovery zone consists of a 150 mm high 'diverging' channel of decreasing cross-sectional area topped by a parallel-sided chamber of cross-section 15 mm by 28 mm and a height of 80 mm. These two sections are topped by a further section diverging to a cross-section of 15 mm by 85 mm. These latter sections are divided into 7 compartments internally with stub pipes leading from the top of each chamber. The entire section is constructed from Perspex and is bolted directly to the top of the separating chamber by way of the Perspex flange through which the outlets from the electrode compartments in the separating chamber pass. Drawings of this zone are shown in Figure 4.3.

4.3 Electrodes and Electrode Spaces

4.3.1 Introduction

The electrode spaces perform several functions in the narrow-slot electrophoretic separator. The metal-solution interfaces necessary to apply an electric field to the solute cause gas evolution when any appreciable current is flowing. (Hydrogen is formed at the cathode and oxygen at the anode by electrolysis of water.) This gas must be removed as it is formed in order to prevent a buildup of gas blocking the electrodes. The electrode spaces also occupy most of the surface area facing the separating zone and thus the electrode fluid can be used to provide cooling for the separating zone by suitable choice of an

electrode fluid temperature. Further, the electrochemical action at the metal-solution interfaces of the anode and cathode will cause local changes in pH and ionic strength which should be isolated from the separating zone.

4.3.2 Current Density

The electrodes and electrode spaces are required to be such that there is negligible change in current density between the top and bottom of the cell - and thus negligible change in electric-field strength with height in the separating zone. The first part of this requirement is that there should be negligible voltage drop along the electrodes themselves.

From the analysis of Tobias and Wijsman (T5), it can be shown that the ratio of local current to average current in a vertical electrode is a function of the parameter ψ where

$$\psi^2 = \frac{\lambda_o + \lambda_d}{\frac{d}{l} + \theta_o + \theta_d} \qquad 4.1$$

and the symbols have the following meanings:

$$\lambda_o = r_o \Lambda l$$

$$\lambda_d = r_d \Lambda l$$

where r_o and r_d represent resistances of a 10 mm wide portion of the electrode for each electrode,

Λ = specific electrical conductance of the solution electrolyte,

and l = electrode length.

Also $\theta_o = \frac{\Lambda b_o}{l}$

and $\theta_d = \frac{\Lambda b_d}{l}$,

where b is the slope of the Tafel line for the appropriate electrode process, i.e.

$$b = \partial V / \partial \log i$$

in which i is the current density

and d = electrode space thickness.

For stainless steel the specific resistivity is given by Perry (P3) as:

$$7 \times 10^{-7} \ \Omega m.$$

Therefore the resistance of a 10 mm wide electrode portion 1.6 mm thick (approximately 1/16") = 0.0004 Ω cm^{-1};

whence $\lambda_o = \lambda_d = (0.0004)(0.01)(50)$

$= 2 \times 10^{-4}$ cm^{-1}

(where $\Lambda = 0.015 Scm^{-1}$, see section 4.3.4).

For the evolution of oxygen (B11)

$$b = 1.2 \ V$$

and for the evolution of hydrogen (P8)

$$b = 0.93 \ V$$

so that $\theta_o = \frac{(0.01)(1.2)}{50}$

$= 2.4 \times 10^{-4}$ A cm^{-2}

and similarly $\theta_d = 1.9 \times 10^{-4}$ A cm^{-2}

On assuming an electrode spacing of 20 mm (see section 4.3.3), one finds by equation 4.1:

$$\psi^2 = 0.01$$

or $\psi = 0.1$

which small value, according to Tobias and Wijsman (T5), implies that there is negligible change in current density with height of the electrode.

4.3.3 Evolution of Gas

The electrode spaces are required to be of sufficient width to enable the evolved gas to be removed without a significant increase in the resistance of the electrode solution due to the presence of gas bubbles. Tobias (T8) has developed a procedure whereby the average volume fraction of gas can be evaluated for a given set of electrode parameters. If a voltage gradient of 3 kV m^{-1} is assumed for the cell and a specific conductance of .1 Sm^{-1} is similarly assumed for the whole cell, then the current density will be

$$i = \nabla\phi\Lambda$$
$$= 300 \text{ A } m^{-2} \qquad 4.2$$

Therefore, for this case (a value for current and voltage twice the maximum expected value), the hydrogen and oxygen evolution rates are given by,

$$\text{number of moles per unit time} = \frac{i\, l\, w}{nF} \qquad 4.3$$

where l = electrode length

w = electrode width

n = number of Faradays required to produce a mole of gas

F = Faraday constant

Equation 4.3 gives for evolution of gases at S.T.P.

12.5 ℓ/hr of hydrogen

and 6.25 ℓ/hr of oxygen

at a current density of 300 A m^{-2}.

If it is further assumed that Stokes law may be applied to the gas bubbles formed by this electrolysis and that these bubbles are of average diameter 2 mm, the speed of rise of these bubbles is given by:

$$U = \frac{g\, D_p^{\,2}\, (\rho_p - \rho_s)}{18\mu} \qquad 4.4$$

where g = acceleration due to gravity,

D_p = bubble diameter,

ρ_p = density of the gas bubble,

ρ_s = density of the solution,

and μ = viscosity of the solution.

On substituting values for the physical properties for water for those of the solution and assuming $\rho_p = 1$ kg m^{-3} equation 4.4, one finds:

$$U \simeq 2\ ms^{-1}$$

for the average speed of rise of the bubbles.

Tobias (ibid) has shown that the average volume fraction of the gas bubbles is given by:

$$f_{av} = K/(K+2) \qquad 4.5$$

where

$$K = \frac{RT\ Eh}{P_m\ F\ n\ \nu\ \delta^2} \qquad 4.6$$

and where R = gas constant,

T = absolute temperature,

h = height of electrode,

P_m = mean pressure in the electrolyte,

n = number of Faradays required for the liberation of one mole of gas,

ν = resistivity of the gas free electrolyte,

and δ = electrode separation.

If ambient temperature is assumed and $\delta = 0.02$ m, then equation becomes:

$$K = \frac{(8.314)(2.93)\ 3 \times 10^3 (1)}{(1.06 \times 10^5)(2)(9.85 \times 10^4)(2)(0.02)^2}$$

$$= 0.44$$

so that

$$f_{av} = 0.18$$

for the evolution of hydrogen.

That is to say, at a current density of 300 A m^{-2} the maximum gas fraction is 0.18 without forced circulation through the electrode spaces. Therefore an electrode space width of 0.02 m is expected to provide sufficient electrode compartment width to prevent the evolved gases from interfering with the electrical conductance of the electrode solution in forced circulation.

4.3.4 Thermal Effects

For all practical purposes, the electrical energy supplied to the separator will all be dissipated as heat. In general, the power dissipated is given by:

$$P = \Delta\phi i A$$

where $\Delta\phi$ = total voltage drop

i = current density

A = electrode area.

If an upper limit of electric field strength of 3.0 kV m^{-1} is used in a cell of average specific conductance 0.1 S m^{-1} with a cell thickness of 65 mm (electrode to electrode), where this thickness is made up of 20 mm for each electrode chamber, 5 mm for the separating channel and 20 mm equivalent for the membrane, then the power dissipation for the cell is given by:

$$P = (30 \times 65)(0.03)(100 \times 10)$$

$$= 5.85 \text{ kW}.$$

However, if the conductance in the electrode compartments is permitted to be different from that in the separating channel (say in the electrode compartments Λ = 1 Sm^{-1}) the total voltage required and hence the power dissipation is greatly reduced. In this case

$$P = [(30 \times 2.5) + (3 \times 4)] \times (0.03) \times (100 \times 10)$$
$$= 2.6 \text{ kW}$$

of which 360 W is dissipated in the electrode compartments.

Two important trends are evident from these calculations:-

i) The quantities of heat evolved in the cell can be significantly reduced by the use of solutions of high electrical conductivity in the electrode compartments.

ii) By the use of a sufficiently high circulation rate for the electrode solutions, the electrode compartments can be used as heat sinks for the membranes and the separating duct.

NOTE: It must be emphasised that the calculations of this section (4.3) were performed to evaluate the upper limits of the loadings of the electrode cavities and real operating values of the parameters used above are expected to be very much (up to an order of magnitude) less than the values used. The purpose of these calculations was to design in large safety factors in the prototype separator.

4.4 Membrane Barriers

The crucial link in the process of applying an externally generated voltage gradient to the flowing solution in the cell is the provision of a suitable type of barrier between the metal-solution interfaces of the electrodes and the separating duct. This barrier must meet the following requirements:-

i) The barrier must be permeable to ions to permit the flow of electric current across the cell.

ii) The barrier substance must present a complete bar to movement of the solutes and so preventing their movement outside the separating duct.

iii) It should be uniform in properties over its entire surface area.

iv) The material of which the barrier is constructed must be chemically inert to the solute and the carrier buffers. It should also withstand a wide pH range.

v) Once in place, the barrier should possess a reasonable degree of mechanical rigidity in order that mechanical and fluid disturbances are not transmitted from the electrode compartments to the separating duct.

The first and second of the above requirements suggest the use of a semi-permeable membrane of the type used in ultra-filtration equipment. In general, these membranes are designed with a molecular-weight cutoff value which enables them to pass soluble substances of up to a given molecular weight while rejecting substances of higher molecular weight. However, until the advent of the De Danske Sukkerfabriker GR series membranes, ultrafiltration membranes were not available with sufficient chemical resistance for this application in sheet form. The D.D.S. GR series membrane, as supplied, is mounted on a polyester fibre paper-like base which is relatively flexible. Thus the membranes used, D.D.S. GR8P type with a cutoff at a molecular weight of 6000, were supported with a sheet of 'Vyon' porous 2 mm thick polythene, which was of sufficient rigidity to provide the necessary protection of the central zone from disturbances in the electrode compartments. These D.D.S. GR8P membranes

were specially manufactured in a continuous 1 m length for this project. This length was the greatest value for which a continuous membrane could be supplied and hence this defined the maximum length of the separating zone.

4.5 Auxilliary Services for the Separator

4.5.1 General

The services required to operate the prototype electrophoretic cell may be conveniently divided into three areas. The first and most fundamental of these is the provision of a supply system for the carrier buffer and solute and a recovery system for the separated components. The cell requires a very slow, stable inflow of the carrier and solute and a number of collection points for the output from the cell. A secondary fluid circuit is required for the electrode solutions. This involves a pump for circulating the electrolyte, degassing vessels for the solutions withdrawn from the electrode compartments, and a reservoir of electrolyte with provision for cooling. The third component of the support system is a d.c.-power supply. This power supply is required to be highly stable and capable of delivering higher currents and voltages than those customarily used for electrophoresis.

4.5.2 Solute and Carrier Buffer Supply

The primary requirement for supply of fluid to the separating zone of the cell is that the flow should be continuous and highly stable as well as being controllable to relatively fine limits. The most practical way in which to accomplish these objectives is to use gravity feed from infinitely-variable head tanks. In order that the flow can be regulated separately to

each inlet to the cell, independently adjustable head tanks with independent supplies from a reservoir are required. The setup is shown schematically in Figure 4.4.

There are however certain practical difficulties in constructing a system of this type. The header tanks must be comparatively small as they are required to be easily and independently adjusted in height. This in turn requires that the supply pumps for each tank should be capable of delivery of small flowrates (of order 10 $cm^3\ s^{-1}$) at a head of approximately 2 m in continuous, rather than pulsed, flow. These requirements were found to be matched by the small centrifugal pumps found in automotive windscreen washer units. This type of pump is, in general, driven by a d.c. motor built onto the pump body and hence their speed is proportional to the voltage applied to them. Therefore they can be controlled by connecting them to a variable voltage d.c. power supply.

The Mitsuba brand windscreen washer kits purchased for this duty were supplied with 1400 ml polyethylene tanks which were found to be suitable for use as header tanks. The pump and motor units in these kits were fully sealed so the motors were dismantled and their cases drilled with air holes to permit air to circulate through the motor to cool it. The reassembled pump and motor units were then connected between the 25 ℓ capacity supply reservoir and the header tanks which were fitted with overflow pipes to maintain a fixed head in each tank. The complete supply system is shown in Plate 4.1.

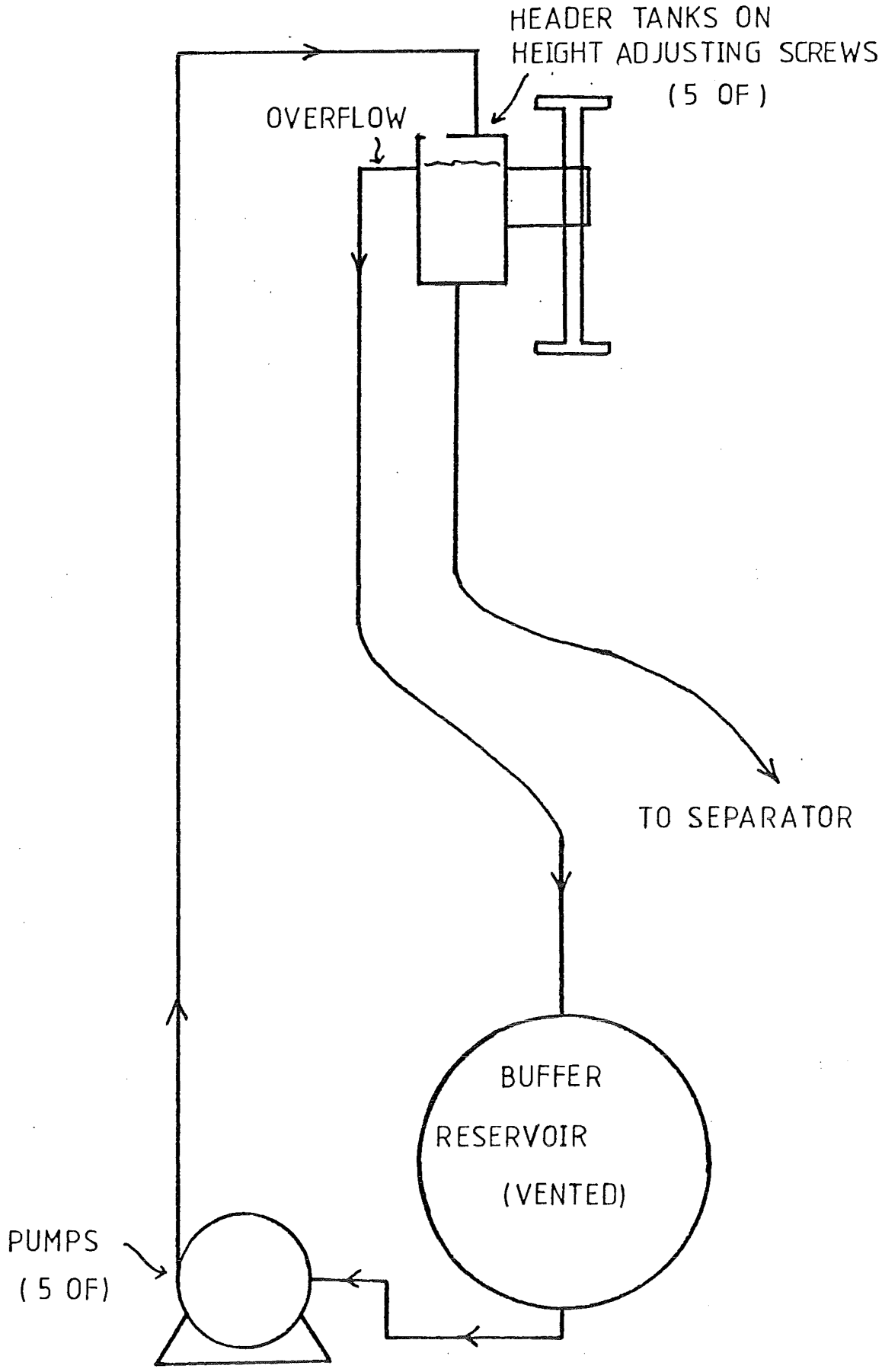

FIGURE 4.4 HEADER TANK SYSTEM FOR BUFFER FEED TO ELECTROPHORETIC SEPARATOR

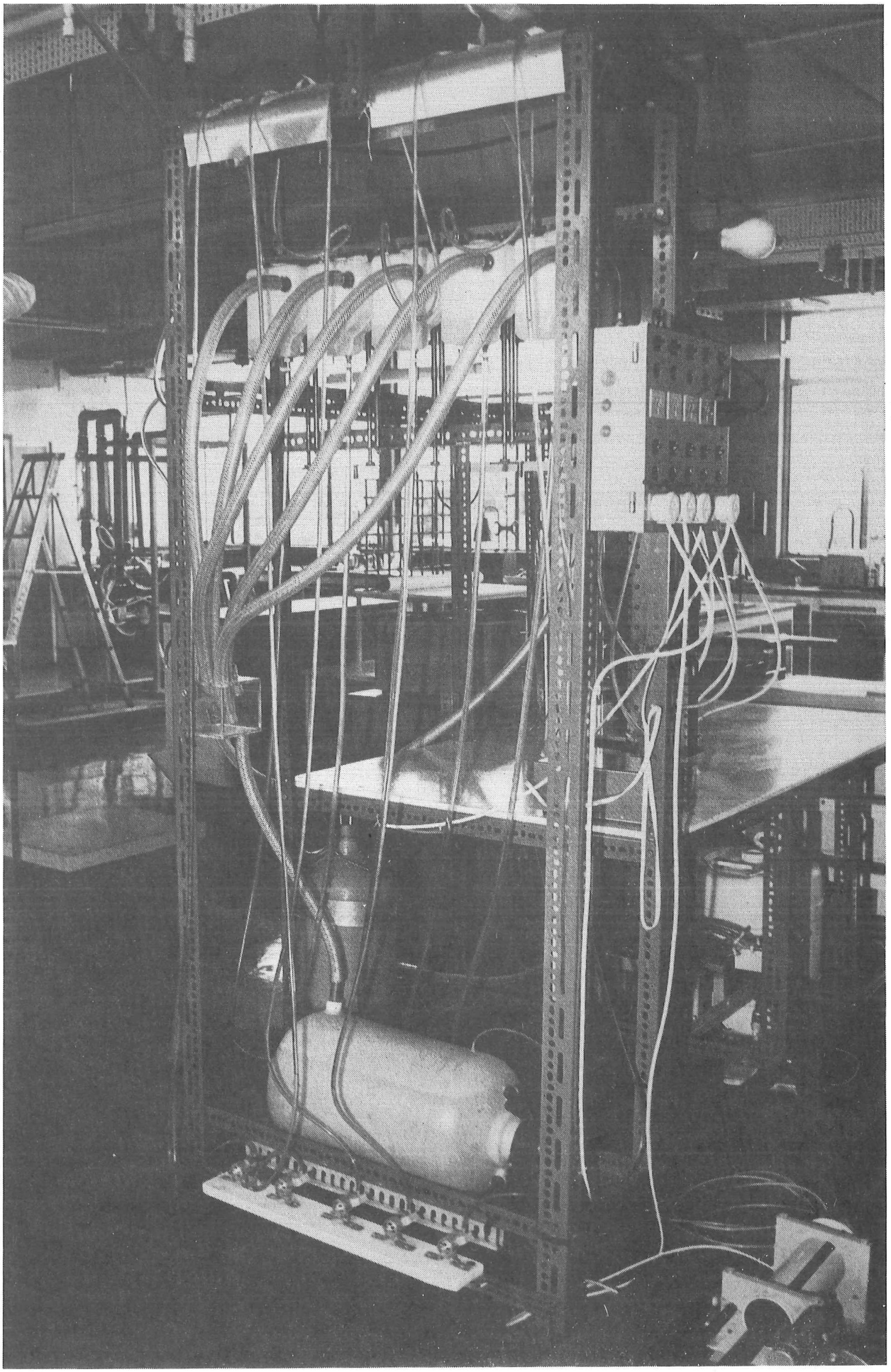

Plate 4.1: General view of solute and carrier buffer supply.

4.5.3 Solute Feeder

The supply of solute to the column must match the requirements of the carrier solute supply (viz, a small constant flowrate). The means chosen to provide this supply is, in essence, a large motor-driven syringe. This consists of a 'Perspex' barrel 76 mm in diameter and 295 mm in length into which a 'Perspex' piston is fitted. This piston is driven by a nut travelling on a screw turned by an a.c. motor through two worm reduction gearboxes. The gearboxes and thread pitch are arranged to provide a constant feed rate of 0.25 $cm^3\ s^{-1}$ from a PVC tube attached to the otherwise blanked end of the barrel. This tube extends to a section of hypodermic tubing which is dipped into the appropriate header tank for a particular feed zone.

As a consequence of the oversized overflow fitted to the header tank, a constant flow is still maintained to each inlet of the cell as the excess carrier solution simply overflows from the header tank. The specific feedrate of the solute can be adjusted by adjusting the concentration of the solute in the feed solution in the feeder barrel. The solute feeder is shown in Plate 4.2. An additional feature of this feeder is that the second gearbox in the drive train can be swung clear of the barrel to permit rapid withdrawal of the piston for reloading of the unit. This latter is accomplished with a specially modified twist drill.

4.5.4 Electrode Fluid Circuit

The evolution of gas in the electrode compartments by electrolysis of water means that the electrode solution must be circulated out of these compartments at a rate sufficient to

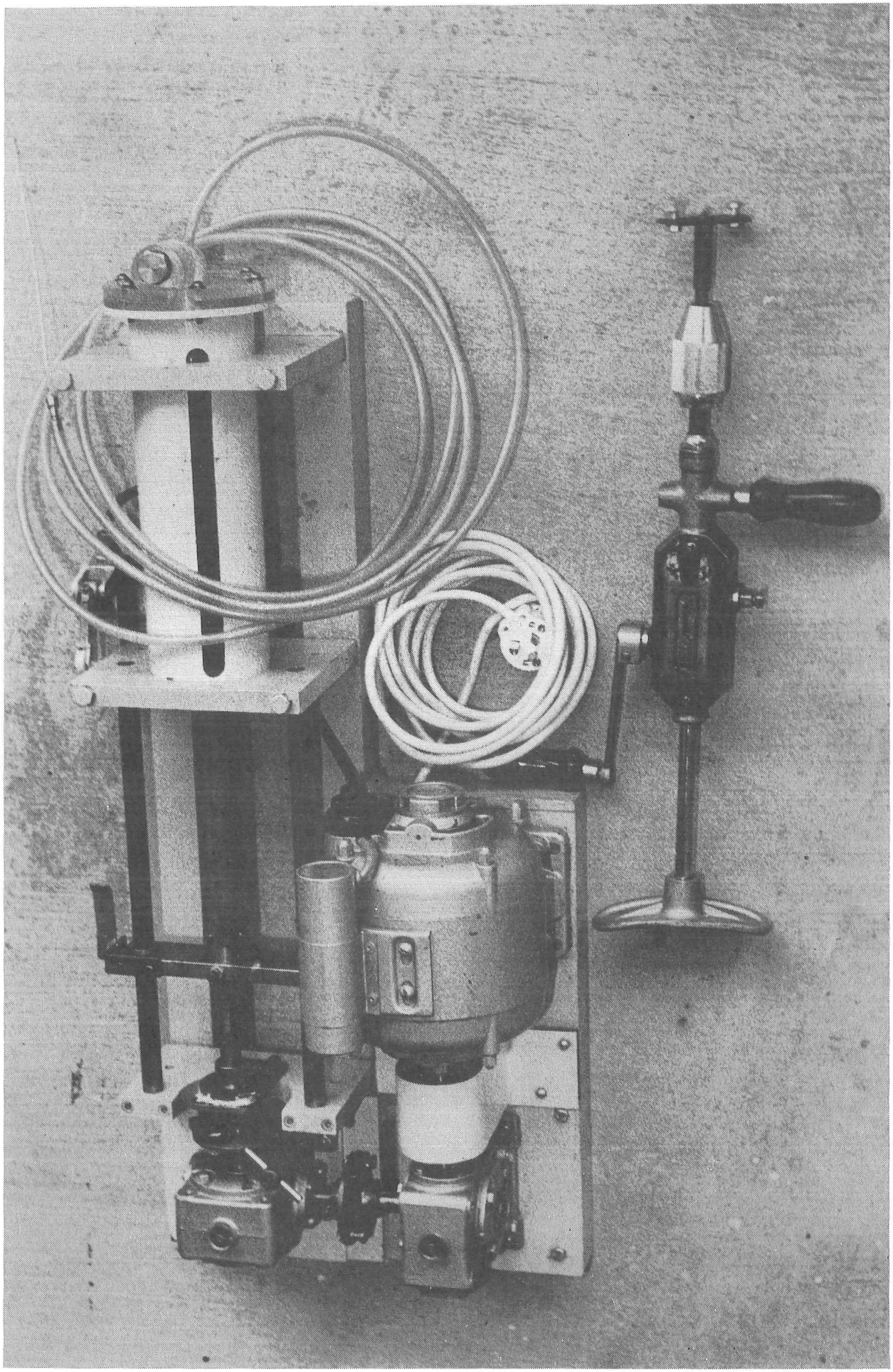

Plate 4.2: Solute feeder.

prevent gas building up in them. The electrode fluid may also be used as a cooling agent for the cell. For these reasons a relatively high circulation rate of 2 ℓ min^{-1} was specified for the electrode solutions.

Since the solution circulated through the anode contains oxygen at the outlet and that from the cathode contains hydrogen, these solutions cannot be degassed in a common chamber as the resulting gas mixture would be explosive. Thus the two outlet streams are piped to separate degassing tanks each of which has a stainless steel gauze fitted around the inlet from the electrode to aid coalescence of the gas bubbles. Holdup was designed as 5 min for the hydrogen-containing stream and 2 min for the oxygen-containing stream to allow sufficient time for full gas-liquid disengagement. Thus the degassing tanks are of volumes 5 ℓ (oxygen) and 10 ℓ (hydrogen). Solutions passed from the degassing tanks are remixed in a 40 ℓ capacity electrolyte storage tank to neutralise any pH changes resulting from the electrode reactions. This tank can be fitted with a refrigerated coil, if required, for cooling the electrode solutions. The complete circuit is shown schematically in Figure 4.5. All tanks, pipework, valves, and the pump are of polyvinylchloride, polythene or glass in order to eliminate problems with corrosion and secondary electrolytic effects.

4.5.5 Power Supply

As previously pointed out, the power supply requirement for electrophoresis in free solution is for extreme stability especially with respect to short duration disturbances (see section 2.3). The narrow-slot separator is unusual in terms of conventional electrophoresis requirements in that the closely spaced but very deep electrodes require a power supply capable

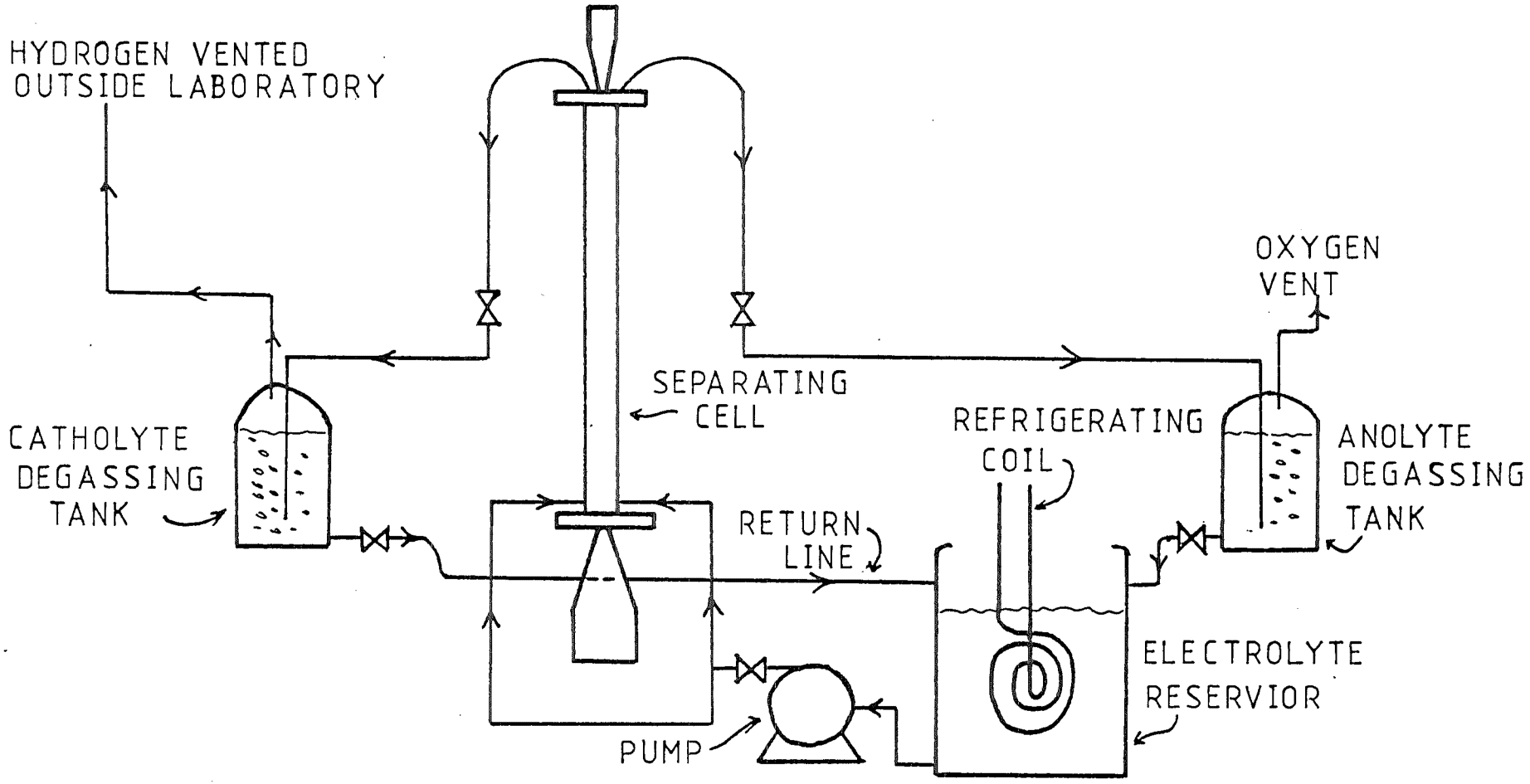

FIGURE 4.5 ELECTRODE FLUID SUPPLY AND DEGASSING CIRCUIT

of supplying a high current at comparatively low voltage. The expected currents were of order 10 A and expected voltages of order 30-50 V. Thus the original power supply envisaged for the cell was a Redfern Radio Services series 51/3, 0-50 V, 0-20 A, continuously variable d.c. unit. This was to have a high-performance smoothing regulator added to it for work at high field strengths. However modifications to the prototype cell as a result of the commissioning experiments led to the requirement for a higher voltage power supply. As a result, the power supply for which the circuit is shown in Figure 4.6 was built to meet this need by the Chemical Engineering Department technical staff.

This power supply is of somewhat unusual design for a modern regulated power supply because of the use of an inductance-capacitance network instead of the more usual resistance-capacitance network for primary regulation. The current is supplied to the bridge rectifier through a 2 kW transformer acorss which the inductance-capacitance network is connected. The final regulation is then supplied by a water-cooled network of transistors and amplifiers to give an output from the regulator of up to 110 V at up to 15 A. Precision regulation (to better than .005%) is provided only at voltages greater than 50 V.

4.6 Commissioning and Design Improvements

4.6.1 Introduction

The device described in sections 4.2-4.4 was built and set up. However a number of problems immediately became apparent. The flow distribution in the entrance zone was found to be inadequate and the zone failed to form fully developed

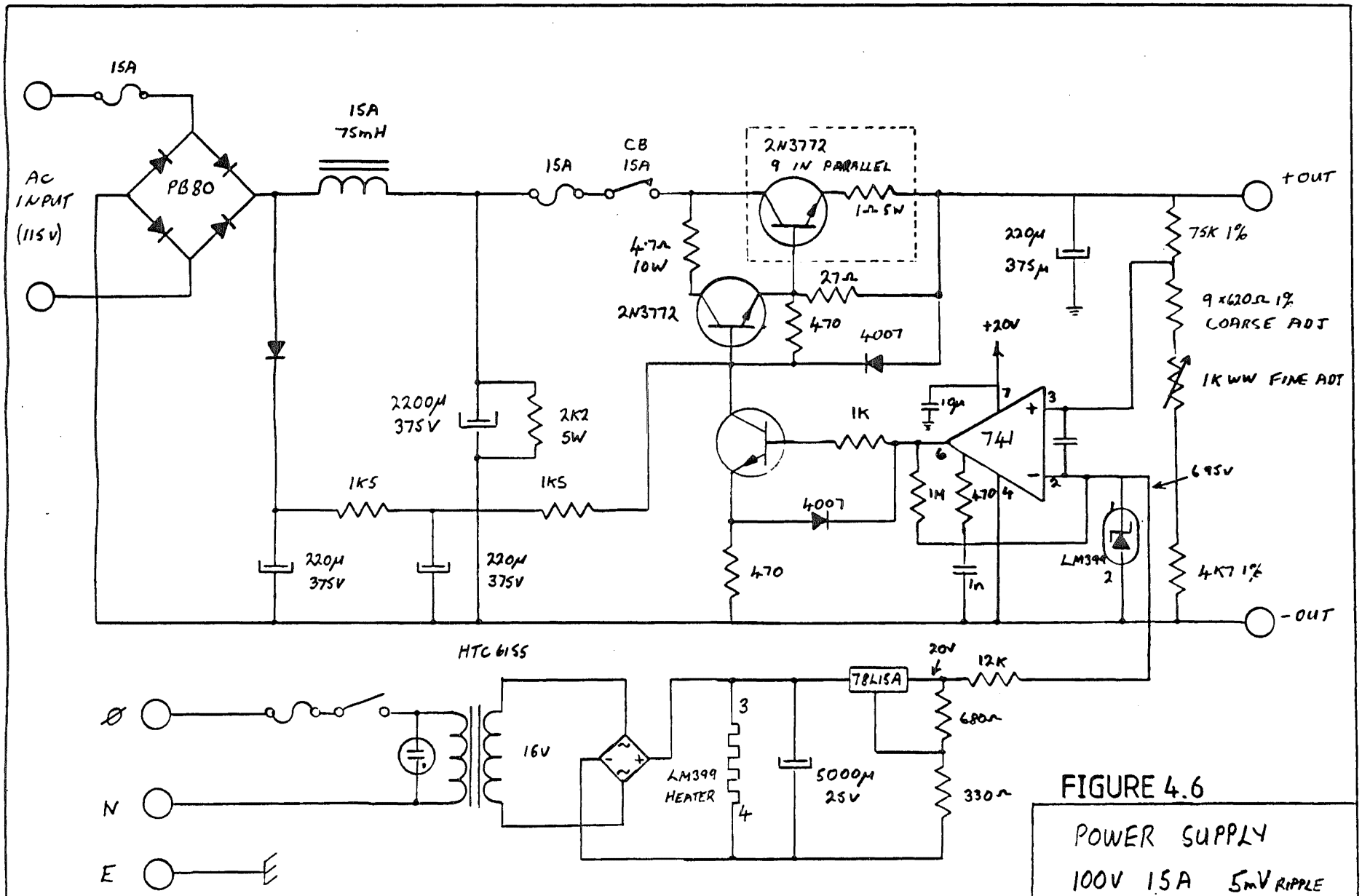

FIGURE 4.6

POWER SUPPLY

100V 15A 5mV RIPPLE

laminar flow. It was also found that flow across the knife edges in this zone gave rise to slow-speed eddying disturbances. This effect was found to be due to a slight enlargement in cross section at the knife edges which was the result of limits placed on the angle of the knife edges as a result of the use of Perspex as a material of construction. It was also found that it was extremely difficult to control the outflow from each of the recovery channels. Flow tended to pass through one output tube at the expense of the others.

The more serious problems occurred in the separating zone. Because of the non-availability of solid Perspex bar the main-frame of the separating zone had been constructed from pre-machined sections of Perspex sheet-bonded together. It proved almost impossible to obtain a satisfactory level of integrity from these joints. Further, the inherent flexibility of the membrane support frames permitted the membrane itself to flex into the separating zone giving a variable cross-sectional area for this duct. After a number of unsuccessful attempts to solve these problems the entire section was rebuilt. The alteration in power-supply requirement resulting from this rebuild has already been discussed (section 4.5.5).

4.6.2 Modifications to the Input Zone

The input zone (shown in detail in Figure 4.1) was modified on the basis of early experiments to provide greater flow stability in this zone and ease of access to the external connecters to the cell. This latter requirement was simply met by the addition of a right-angle bend to each of the tubes providing access to the bottom of the zone. The flow distribution in this zone was found to be initially unsatisfactory and gave rise to large scale eddies in the entrance slots (see Figure 4.7).

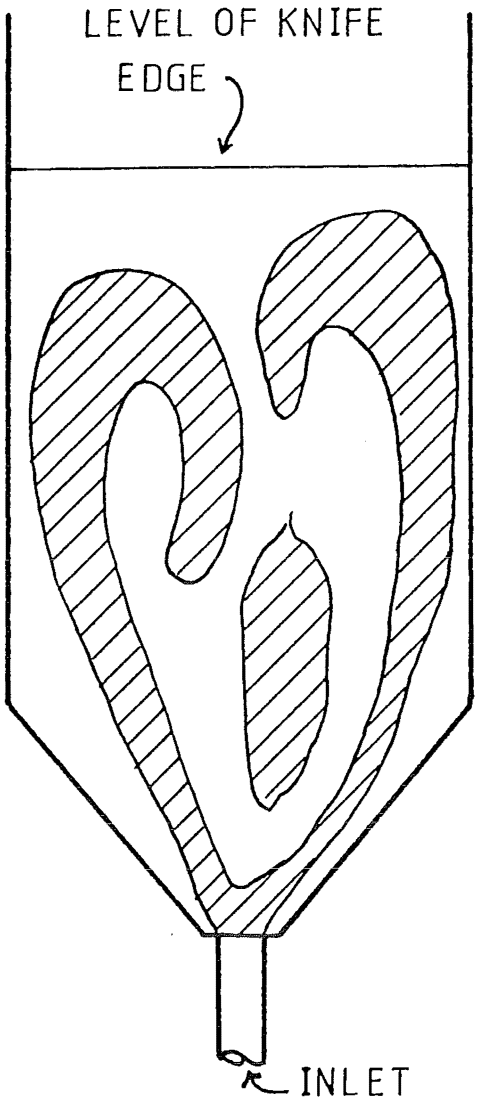

FIGURE 4.7 LARGE SCALE EDDIES IN THE INLET SLOTS BEFORE THE ADDITION OF GLASS BEADS AS FLOW STABILISERS

This problem was corrected by filling the lowest section of the zone with 1 mm diameter glass beads resting on an expanded polythene base. This modification resulted in satisfactory flow distribution across the depth and width of the input slots. However it was found that wavelike disturbances were forming at the knife edges where the input slots merged to form a continuous section (see section 5.2.4).

On inspection, it was found that, because of machining limitations on the Perspex used for the dividers between the input slots, these knife edges had been cut at a steeper angle than originally designed. As a result there was a slight increase in cross-sectional area at the knife edges, this being most pronounced for the central three slots. The cross-sectional area at this level was decreased by the addition of a shallow wedge to the parallel walls of the zone with apex of the wedge at a height corresponding to the tips of the knife edges. The shape of this wedge was so calculated to provide a continuously decreasing cross-sectional area in the zone in the area of the 'thinning' of the spacers to form the knife edges. Tests of the zone after the fitting of this wedge showed that this type of disturbance was no longer present. The completed modified entry zone unit is shown in plate 4.3.

4.6.3 Modifications to Increase Controllability of the Outflow from the Separator

Early tests of the assembled cell showed that, since the top of the outlet section of the cell was a free liquid surface, syphoning effects tended to cause all the liquid output to flow through one or two outlet pipes. This problem was partially solved by capping the channels to isolate them from one another. At a later stage, it was found necessary to refine

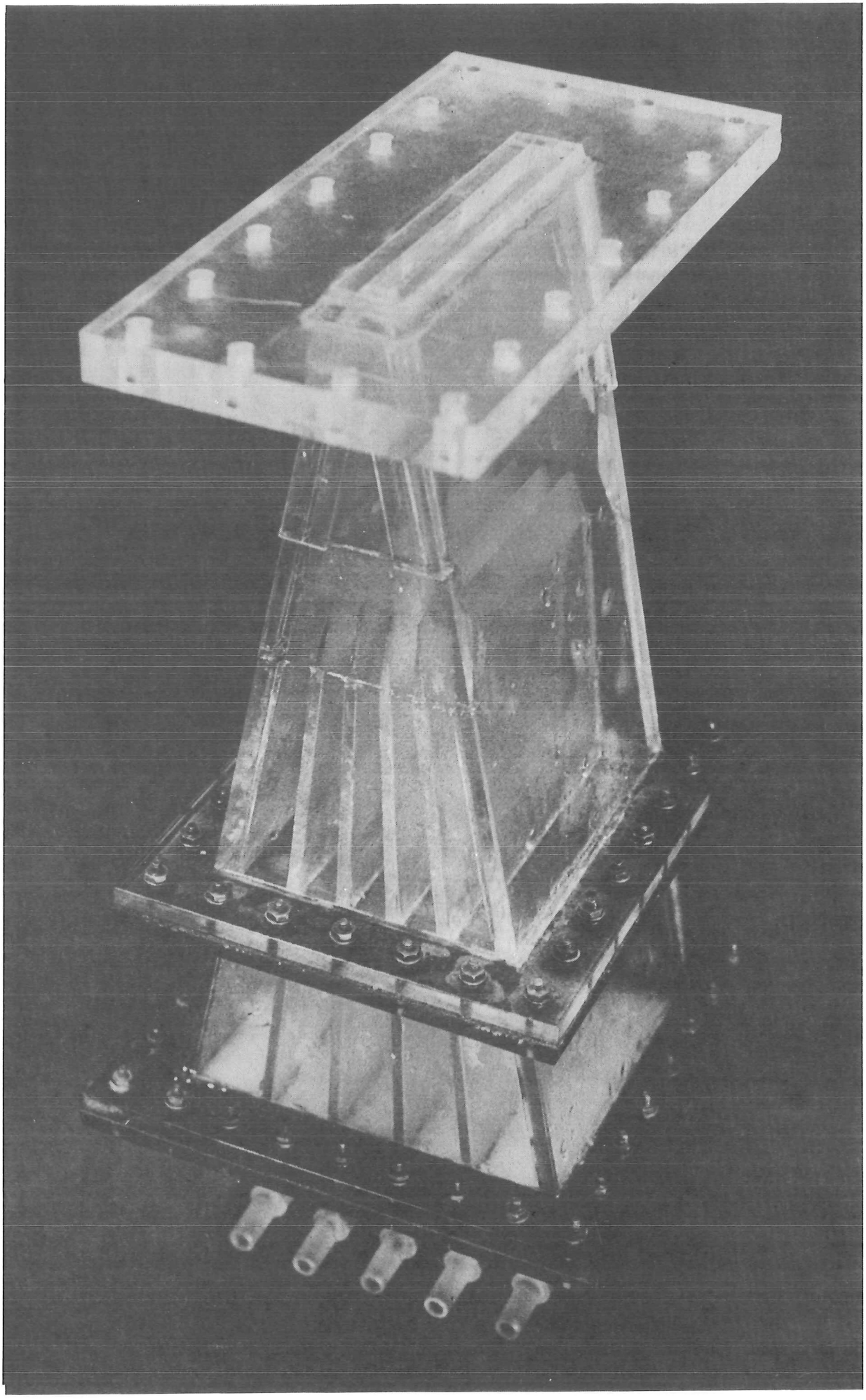

Plate 4.3: Input zone (as modified)

this control by adding needle valves to each of the output pipes. This was done after it was found that Hoffman clips fitted to each of the flexible tubes connected to each outlet gave inadequate control of the outflow. These needle valves were constructed with a Perspex body and a PVC one-piece needle and adjuster. The final form of the output section of the cell is shown in plate 4.4.

4.6.4 Commissioning Modifications to the Separating Zone

4.6.4.1 Defficiencies in the Separating Zone as Originally Designed: The most serious initial problem with the separating zone was the extreme difficulty encountered in maintaining the mechanical integrity of the mainframe of the unit. At the time of the original design of the separator neither Perspex bar nor thick (greater than 12 mm) sheet sections were available in New Zealand. Resultingly, the mainframe of the separator was built of machined sections of 6 mm Perspex sheet bonded together with the recommended adhesive, a methyl chloride 'solvent welding' compound known as Tensol No. 6. This compound proved to be extremely difficult to use for the long continuous bonds required to assemble the mainframe due to its quick-drying nature. The result of this was that the joints in the frame were never entirely satisfactory and leaked frequently when loaded with the over 1 m of hydrostatic head which was imposed on the frame by filling the separator with solution. After considerable efforts on the part of Mr C.R. Campbell, the technician who originally built the cell, to seal this mainframe it was abandoned, and the separating zone was rebuilt using specially imported Perspex bar supplied by Cadillac Plastics Ltd.

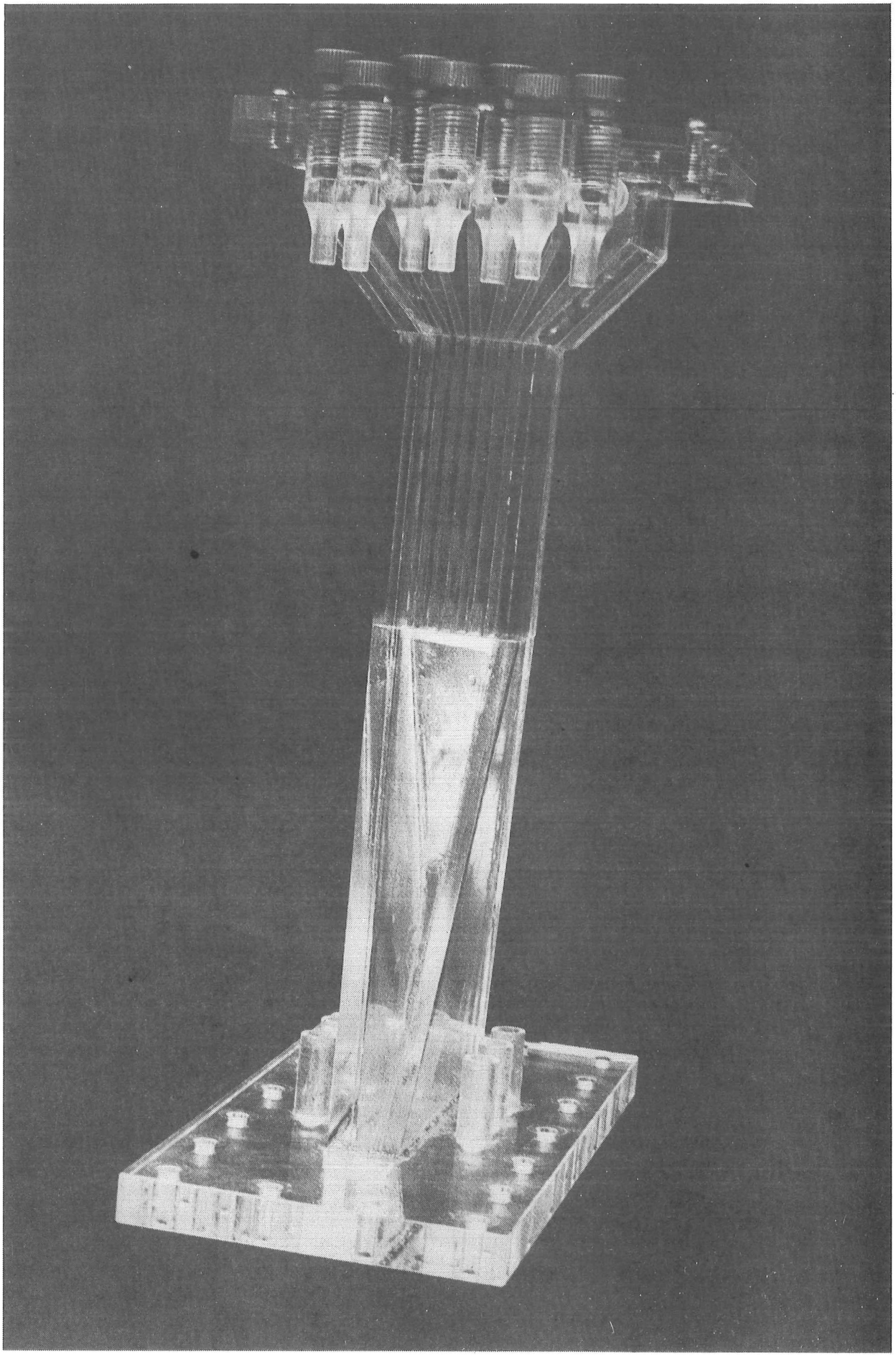

Plate 4.4: Output zone (as modified).

In the course of the experimental work with this first version of the device several other problems arose and the necessity of finding a solution to these contributed to the decision to rebuild the separating zone. The original design used a rectangular Perspex frame with a porous insert to support the membrane barriers used to isolate the separating duct. This essentially free-standing frame was found to be inadequate to support the membranes with the required degree of rigidity. Further, problems were encountered with sealing the faces of the membrane support frames to the main support frame. It was also found on dismantling the separating zone after a series of tests with current flowing in the cell that the 316 grade stainless steel anode was corroding rapidly.

4.6.4.2 The 'Mark II' Version of the Separating Zone: The rebuilt separating zone is essentially of the same dimensions as the version described in section 4.2.3. However, as has already been remarked on, the mainframe was constructed by machining the side walls from two solid Perspex bars and jointing these to 12 mm thick end flanges. The technique removed the necessity for solvent-welded joints extending the full length of the zone, as was previously required. Also, the 'Mark II' version was constructed using meta-cresol as a solvent-welding agent. This substance is much slower drying than the methyl-chloride-based Tensol No. 6 and so allowed considerably more time for the placement of each component in the joint. The joints formed with this compound required treatment at 60^{o}C for at least 6 hours to ensure proper hardening and the resulting bond was found to be most satisfactory in service. The author is greatly indebted to Dr A.C. Arcus of the Christchurch Clinical School for the suggestions leading to the techniques

used to handle this substance. The rebuilt separating zone also used somewhat different membrane support frames. These frames were tapped and screwed directly to the electrode plates to give positive location of the membranes relative to the mainframe of the separating zone. Initially, the membranes were supported in the same manner as in the first version of the cell. That is to say, the sheet of membrane was backed with a layer of porous polythene sheet leaving the surface of the membrane facing the separating channel. However, it was found that this arrangement still permitted the membrane to flex and so alter the cross-section of the separating duct. The membrane was then recessed further into the support frame and a further porous polythene sheet added between the membrane and the separating channel on each side. While this achieved the object of maintaining a constant cross-sectional area in the separating channel, it also greatly increased the electrical resistance of the cell. This latter effect occurs because the inner sheet of porous polythene in this configuration is necessarily filled with solution of the low specific conductance of the carrier buffer solution effectively more than doubling the 'thickness' of the cell at this lower conductance. The resultingly larger power supply required has already been discussed in section 4.5.6.

Difficulties were also experienced creating and maintaining an effective seal around the edges of the membrane frame (between this frame and the mainframe). After some experimentation a satisfactory seal was achieved using a neoprene O-ring around the entire perimeter of the membrane-support frame, with a seal being formed by 'downward' pressure on this O-ring by way of the electrode plates' retaining bolts. Since the joining 'bridges' at the ends of the membrane frames (where the

frames meet the cross-pieces forming the channel in the mainframe) were comparatively thin, the O-ring's retaining slots were enlarged so that no load was placed on the bridges. Instead, the cross-joint was sealed using a silicone adhesive/sealant, Dow-Corning RTV 732, which sets to a rubberlike consistency. Cross-sections of the 'Mark II' separator are shown in Figure 4.8 (not to scale) to illustrate these features. Dow-Corning RTV 732 was also used to locate the membrane and porous polythene supports in the membrane-support frames.

The electrode plates were also rebuilt for this latter version of the separator. In an attempt to reduce and hopefully eliminate anode-corrosion problems, the rebuilt plates were fabricated from Avesta 254 SLX, a high-nickel and chromium stainless steel with 4.5% molybdenum and 1.5% copper added. This was supplied by Sandvik (N.Z.) Ltd as 2 mm thick sheet. Experiments with a sample of this material used as an anode in the buffer solution used for the cell showed that some corrosion could be expected at current densities less than approximately 60 A m^{-2}, so it was thought that this alloy would not entirely eliminate the corrosion of the anode of the prototype cell. Dismantling the cell after some 10 hours of operation showed that there was some corrosion occurring on the anode, but there was no evidence of pitting.

4.6.5 Modifications to the Support Services

It was found that, after the cell had been operating for some time, that the 'non-toxic' grade clear PVC tube used for most of the pipework in the fluid-circulation network had become opaque and was depositing a white fine crystalline material into the circulating fluid. It was hypothesised that the sodium

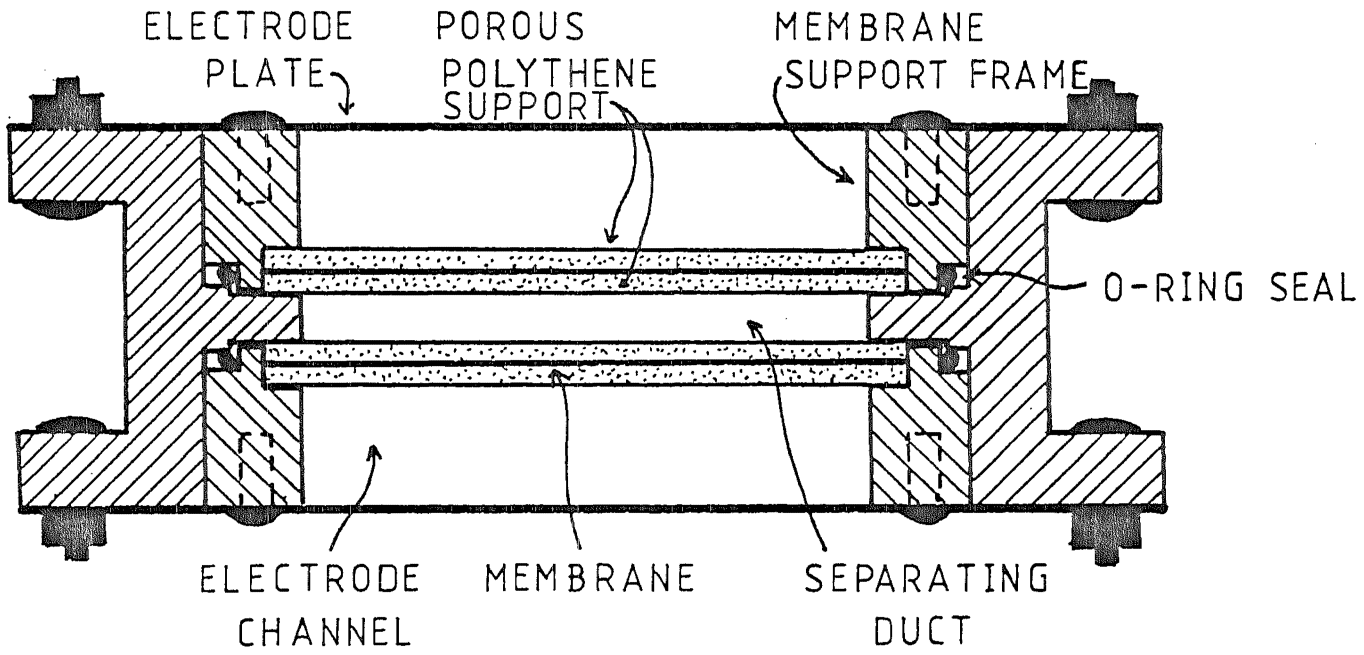

FIGURE 4.8 (i) CROSS SECTION OF SEPARATING ZONE AT RIGHT ANGLES TO THE FLOW AND ELECTRIC FIELD

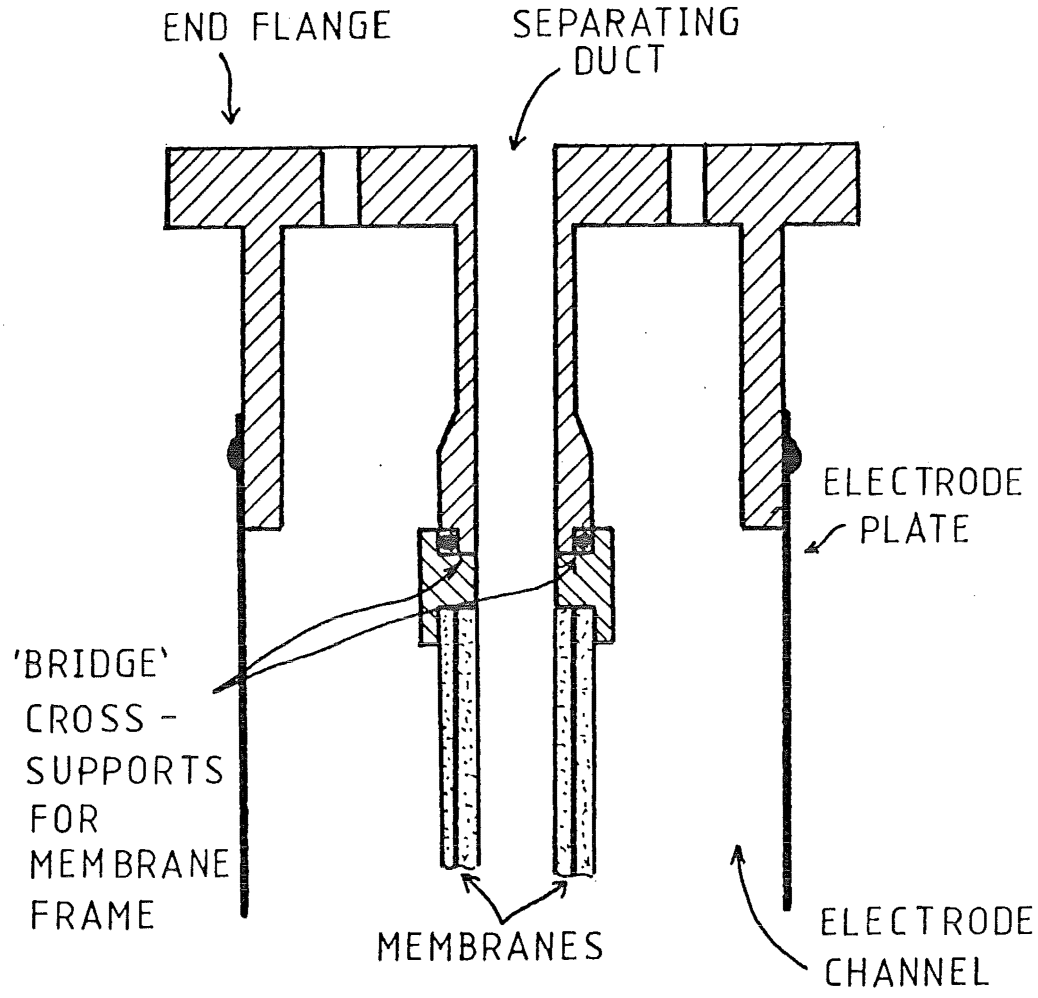

FIGURE 4.8(ii) CROSSSECTION OF THE UPPER END OF THE SEPARATING ZONE PARALLEL TO THE ELECTRIC FIELD

borate/boric acid buffer being circulated was leaching some of the plasticiser from the PVC tube. Therefore, the pipework was changed in its entirety and replaced with 'petrol-resistant' grade PVC tubing which has shown no evidence of this problem.

The alterations to the power supply necessitated by the increased internal resistance of the 'mark II' separator are detailed in section 4.5.6. The other support services performed as designed and were found to have sufficient capacity to enable as wider operating condition limits as required imposed on them.

4.7 The Final Form of the Prototype Electrophoretic Separator

The final configuration of the prototype separator and support services is shown in Plate 4.5. The cell itself is mounted in a frame made of braced Dexion angle in such a way that it stands vertically through the centre of an operating 'table' which enables instruments to be conveniently placed for reading while observing flow in the cell. The separating zone is lit from behind using a 65-W, 1.5 m long, fluorescent tube in a splash-proof housing (see plate 4.5). This arrangement permits a sufficient light intensity in the separating duct to photograph solute tracks in the duct without inducing heating in it. The electrode fluid recirculating pump and solute feeder are each mounted independently of the supports for the cell to ensure it is isolated from the vibrations from the motors in these elements. The power supply is also mounted independently in its own trolley because of the weight of the transformer, variable resistance, and inductance elements of the supply.

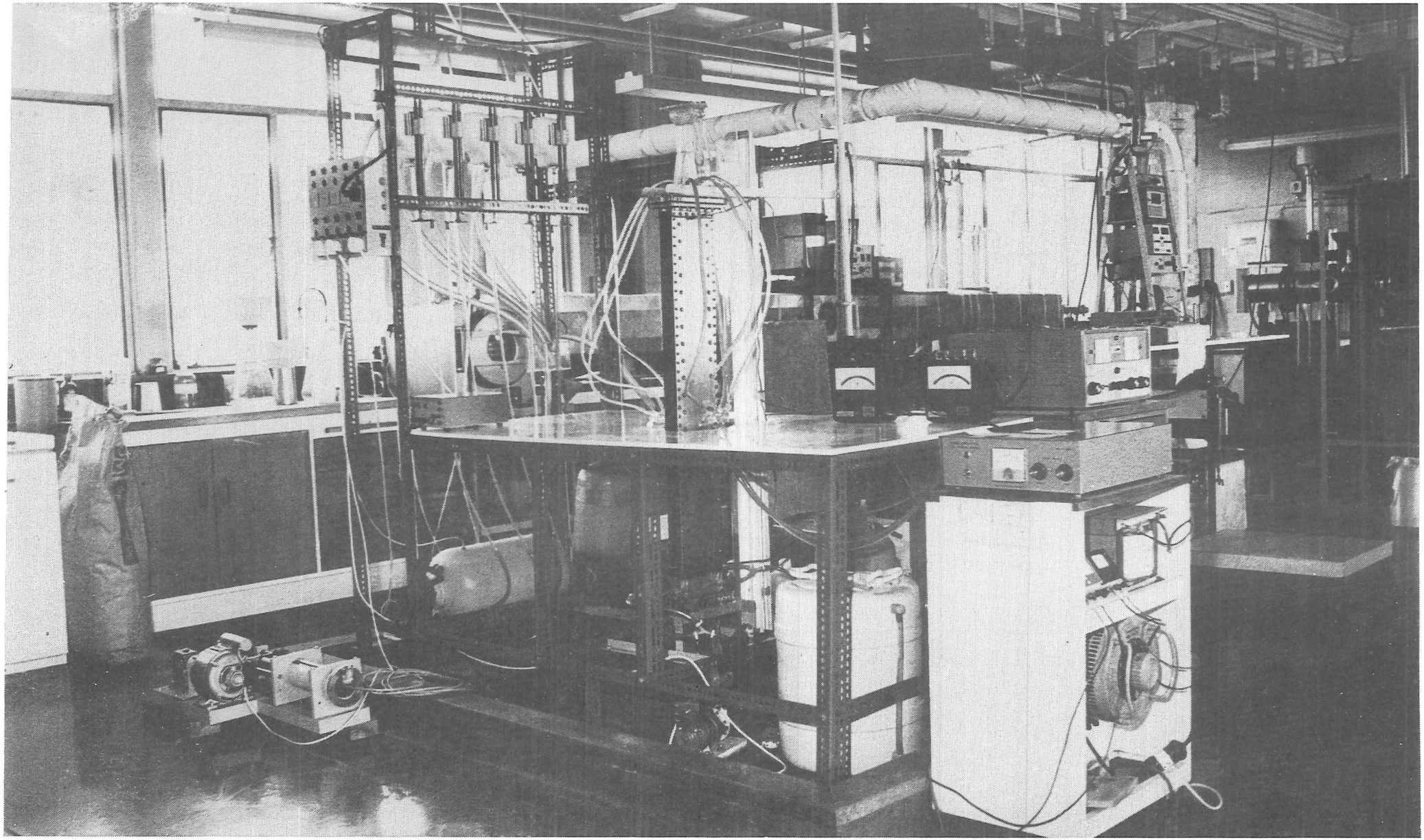

Plate 4.5: General view of the separator set up.

The power supply to the cell is laid out as shown in Figure 4.9. The ammeter and voltmeter are both analog precision moving-iron meters. Coarse voltage control is supplied by a 2 kW Variac attached to the supply transformer while finer control is supplied by the internal controls of the solid-state regulating stage of the power supply (see Figure 4.6).

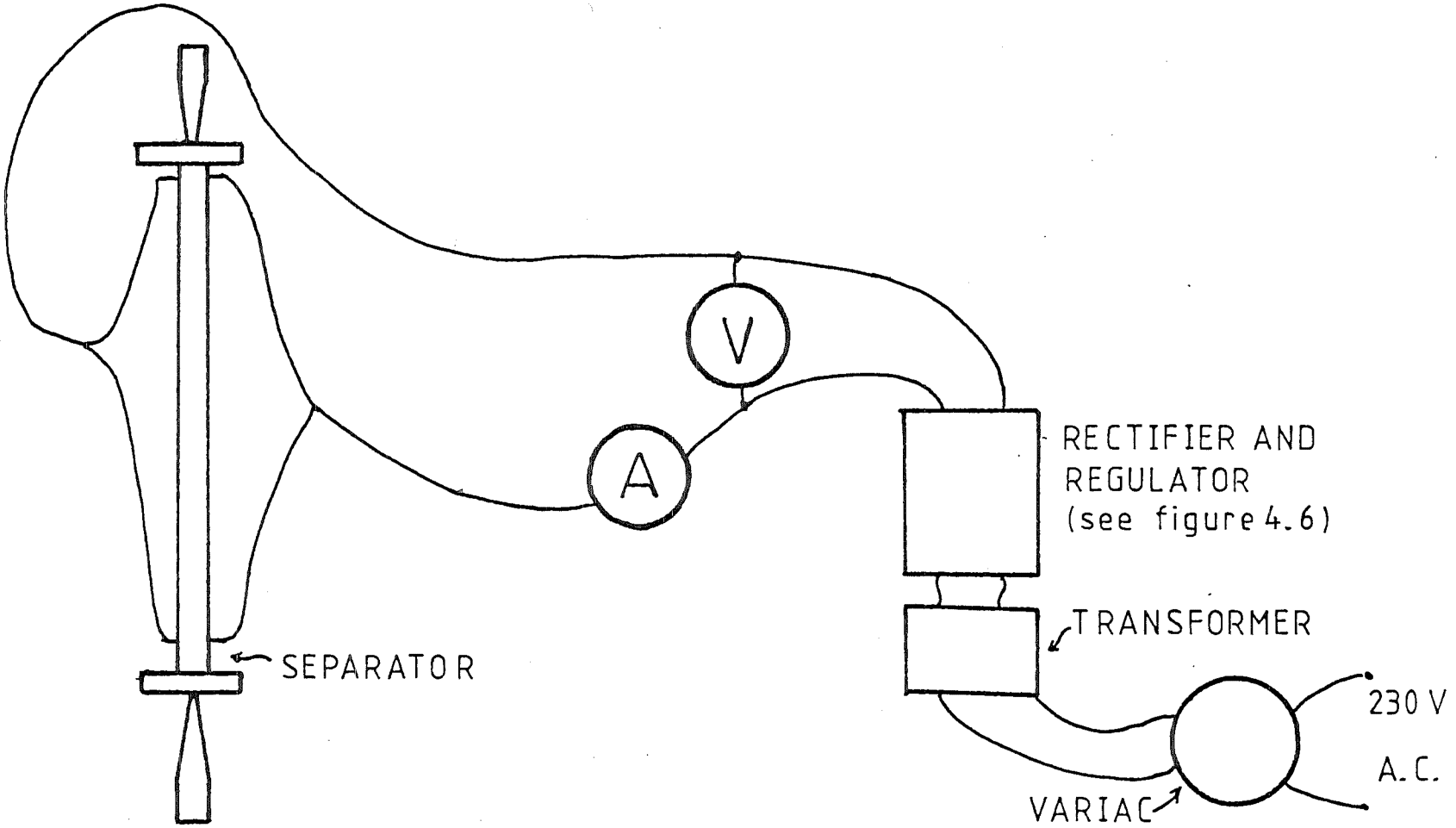

FIGURE 4.9 POWER SUPPLY LAYOUT

5. EXPERIMENTAL WORK

5.1 Introduction

As might be expected with a project concerned with the design of a new device to perform a novel separation, a considerable portion of the experimental work associated with this project has been commissioning work on the device and its associated systems. This included experiments to determine flow-stability limits for the device, with respect to both flow velocity and density differences and in the flow stream resulting from differences between solute and carrier densities. A series of experiments were also required to determine the electrical response of the separator, so that suitable settings for solution conductance and supply voltage could be found. This latter question also involves the selection of a suitable buffer substance for use in the carrier medium.

Further, since free-solution electrophoresis is a comparatively little-studied phenomenon, considerable care was required in the selection of solutes for testing the device. In fact, it was found that measurements of electrophoretic mobility independent of the narrow-slot separator, were required to provide data for the characterisation of the performance of the device. The experiments with the prototype device revealed a number of defects in the equipment and consequently the documentation of these faults and their detection and rectification are part of commissioning experiments for a device of this degree of novelty.

The primary reason for the initial experiments performed with this device was to determine the validity of the theoretical model developed for the narrow-slot separator. Accordingly, the

experiments were performed with single-component solutes to facilitate comparison with the calculated single-component profiles.

5.2 Hydraulic Experiments

5.2.1 General

Hydraulic experiments with the prototype separator in its original form showed that the limits on the flow stability in the cell are connected with the flows in the inlet and outlet zones. On the one hand, low flowrates* (of order Re = 100) and relatively high solute concentrations (density differences of order 0.01% between carrier and solute) gave rise to disturbances in the flow in the inlet zone. On the other hand, high flowrates (of order Re = 300) promoted turbulence in the outlet zone. It appears from these experiments that the parameters of density difference and flowrate through the cell are interlinked in the definition of a stable operating envelope for the device. The original version of the cell suffered problems with variation in the cross-section of the separating zone due to the flexing of the membranes at the sides of the zone (see section 4.6.4) which somewhat complicated these experiments.

5.2.2 Low Flowspeed and High Density Difference Limiting Behaviour

At low flowspeeds (approximately Re = 100 in the separating zone) and density differences between solute and

---

* All flowrates are shown as Reynolds numbers based on the mean hydraulic diameter of the separating zone and calculated using the transport properties of water (see section 2.2).

carrier solutions of order 0.01% the flow was observed to be unstable at the input section. (The solute used for these experiments was 'designer' - grade cobalt blue watercolour pigment - see section 5.4). At these conditions the flow was observed to form a 'smokey' plume of solute at the knife edges where the input streams are merged (plate 5.1). The eddies resulting from this are propagated into the separating zone so that stable laminar flow is not observed in the separating zone at these conditions.

The above density difference should be regarded as determined to an order of magnitude, as it was measured by comparing weights of specific gravity bottles; a process for which, at this level, the errors are of the same magnitude as the measured differences.

5.2.3 High Flowspeed Limiting Behaviour

At flowspeeds corresponding to Reynolds numbers in the region of 400 it was observed that, while stable flow was found in the inlet and separating zones (as evidenced by sharply defined time stable pigment traces), the flow in the recovery zone was no longer laminar. From observation of the pigment trace in this zone (see plates 5.2(i) and 5.2(ii)) the flow appeared to be suffering a hydrodynamic breakdown to the transition or mixed turbulent flow regime. Note that from plate 5.2(ii) (photographed with the plane of the film parallel to the electrodes, or at right-angles to the other plates in this section) there are turbulent eddies forming in the centre of the collector throat. This flow condition destroys the effectiveness of the recovery zone and so represents an upper limiting flowspeed through the cell. This limit does not appear

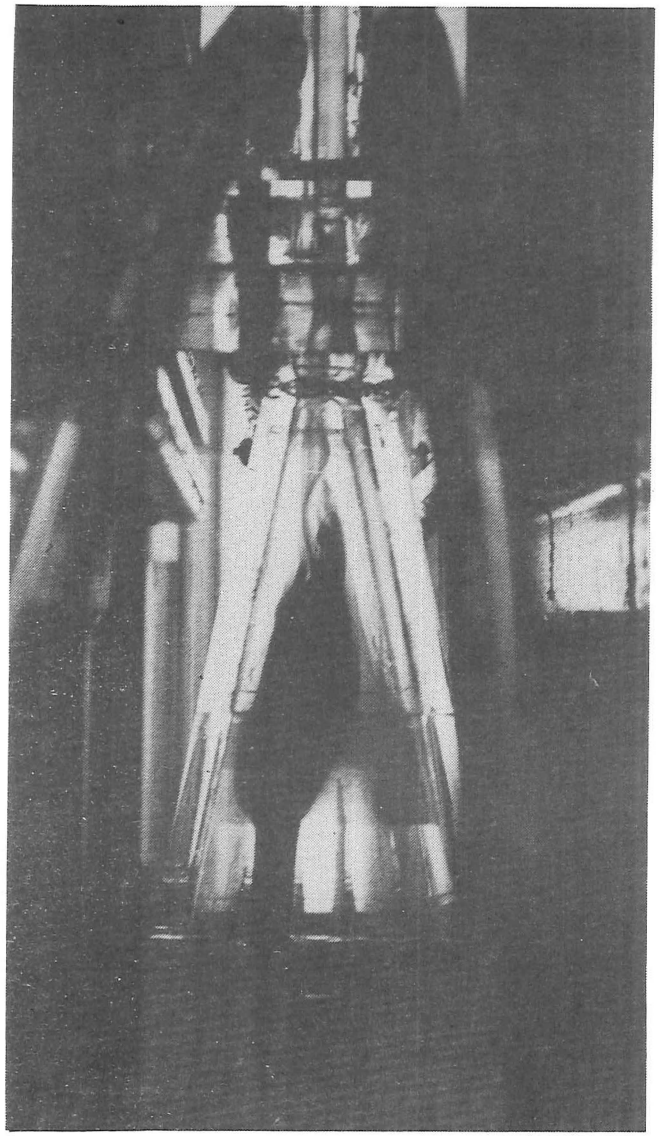

Plate 5.1: Low flow high concentration instability at the inlet ($Re \simeq 100$)

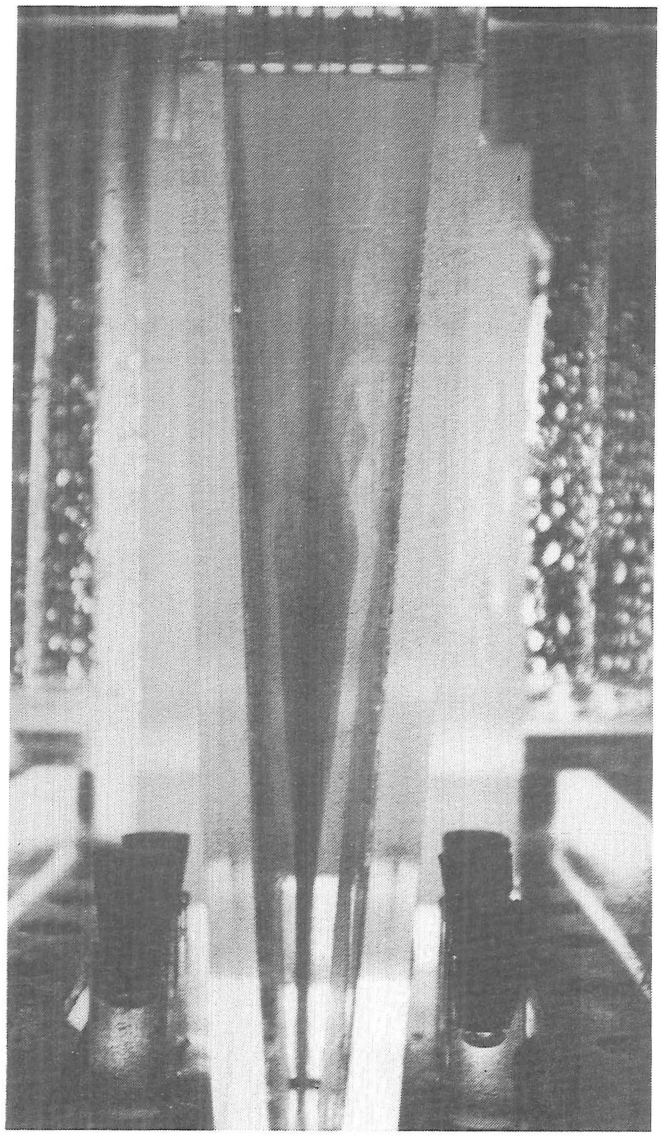

(i)

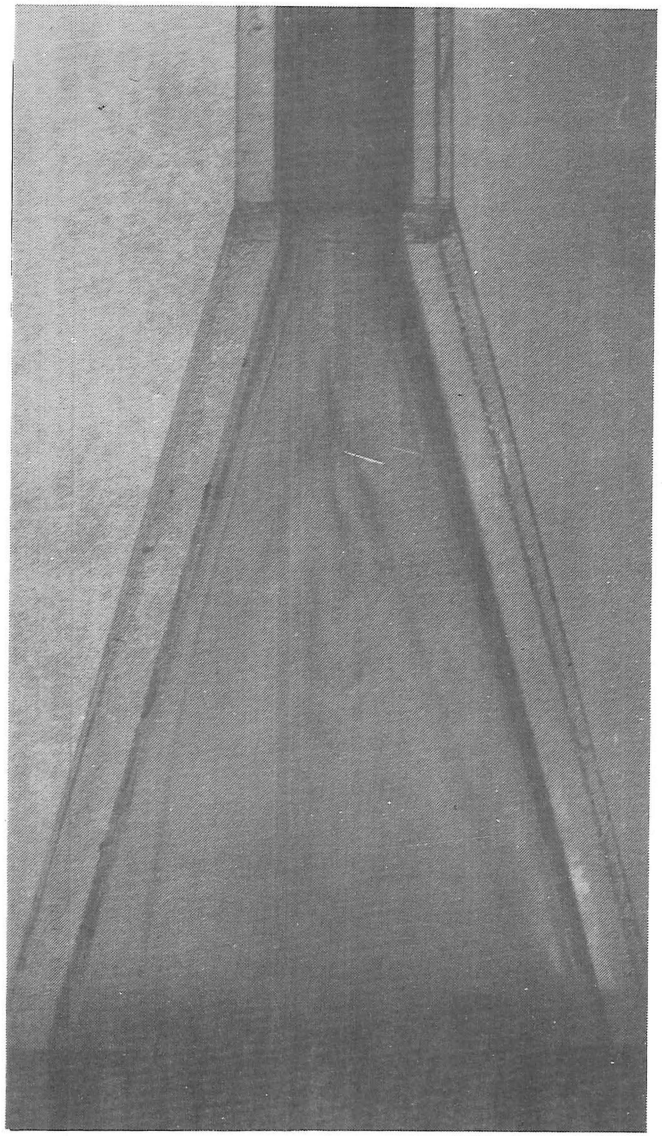

(ii)

Plate 5.2: High flow speed instability at the outlet ($Re \simeq 400$)

to be affected by density differences between the solute and carrier.

5.2.4 Stable Operating Region

Between the above two extremes the observations show that there exists a stable operating region where stable laminar flow (as shown by the solute pigment tracks through the cell) may be established and maintained. Initial investigations in this flow region (approximately $150 < Re < 250$) showed waves, with their amplitudes at right-angles to the direction of flow, forming at the knife edges in the input zone (plate 5.3). Inspection of this part of the separator showed that, because of the limits imposed by the materials of construction, there was a slight increase in cross-sectional area at this point. As a result, the shallow wedges shown in plate 4.3 were fitted, which satisfactorily overcame this problem (see plate 5.4(i) for which $Re = 180$). The flow at speeds of this order was observed to continue in stable fashion through the separating zone and emerged to follow the expected path through the recovery zone (plate 5.4(iii)). At this stage in the evolution of the apparatus the problems of retaining a uniform cross-sectional area in the separating zone had not been solved, so the stream of pigment tended to follow the irregularities of the separating zone walls caused by distortions of the membrane (see section 4.6.4), as shown in plate 5.4(ii).

5.2.5 Comparison Between the Hydraulic Stability Experiments and the Results of the Preliminary Investigations

Comparison of the above results with those of section 2.2 shows a somewhat narrower range of stable flowrates as compared with the preliminary hydraulic model. This result is not particularly surprising for the following reasons.

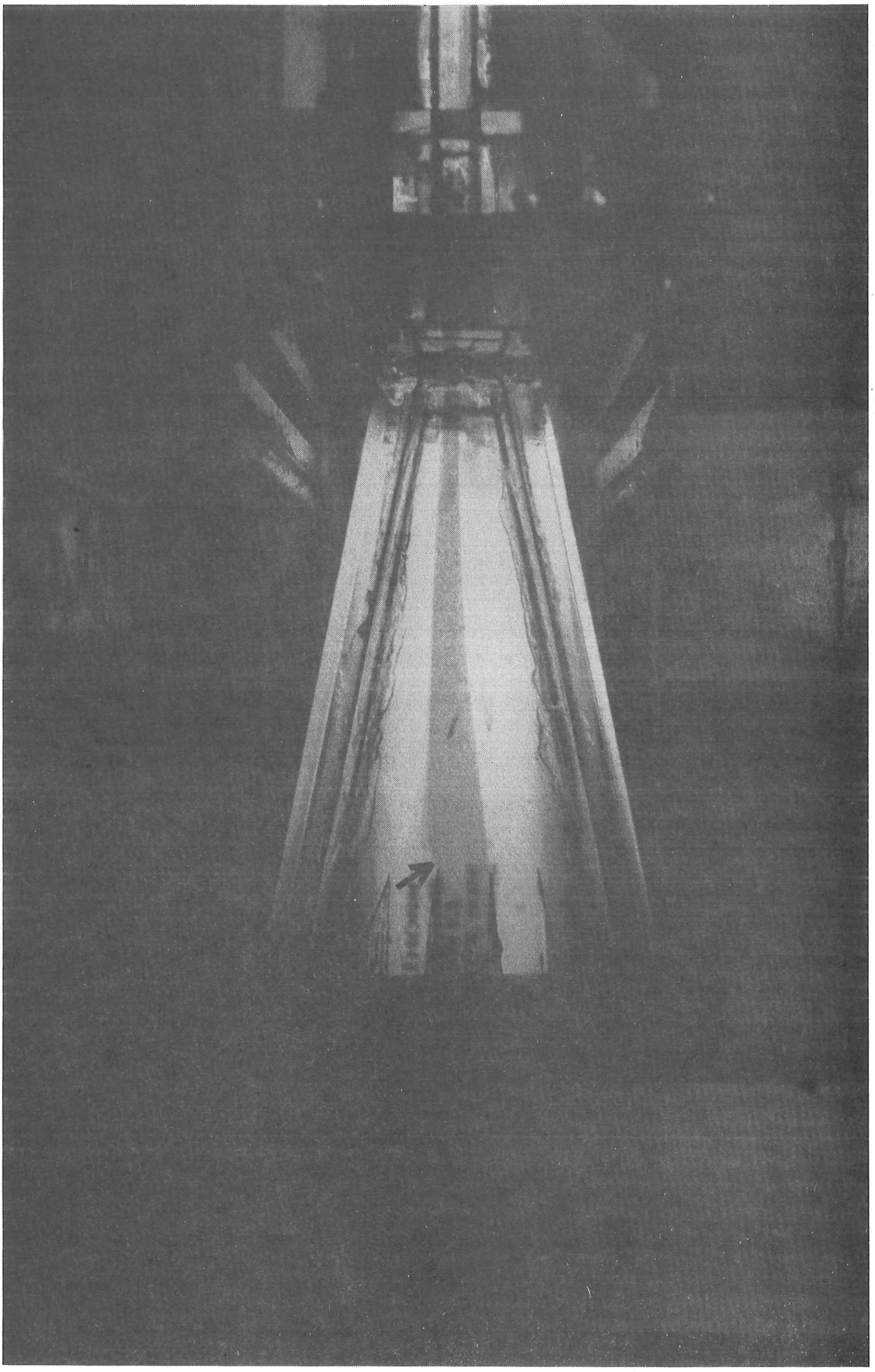

Plate 5.3: Wave at knife edge before inlet modifications.

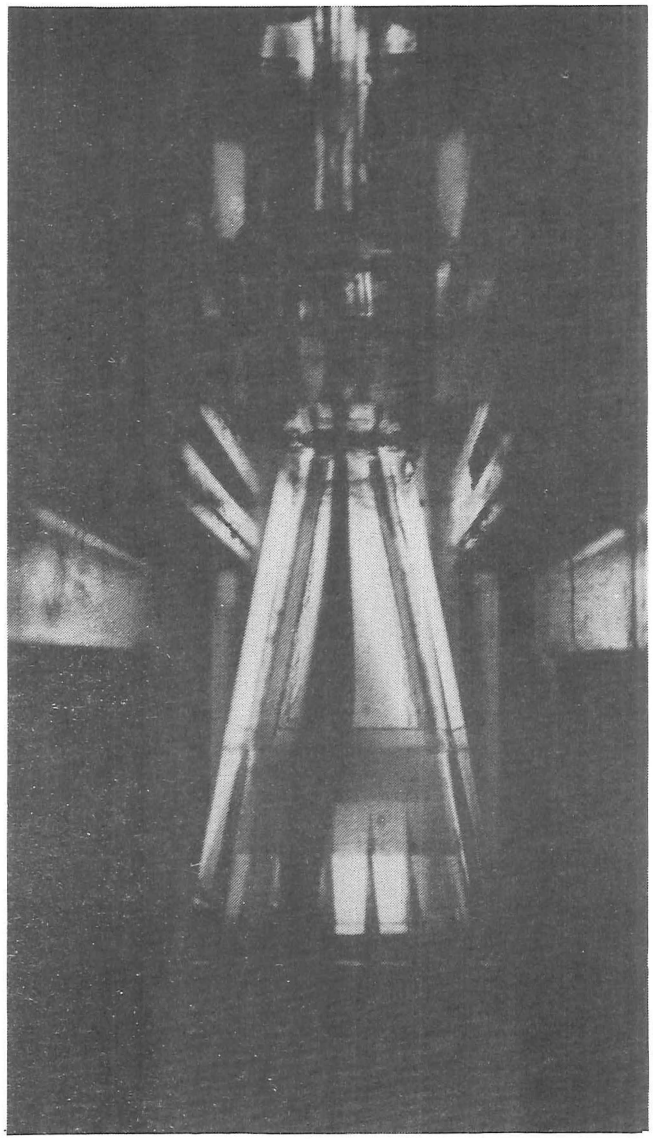

(i) INLET

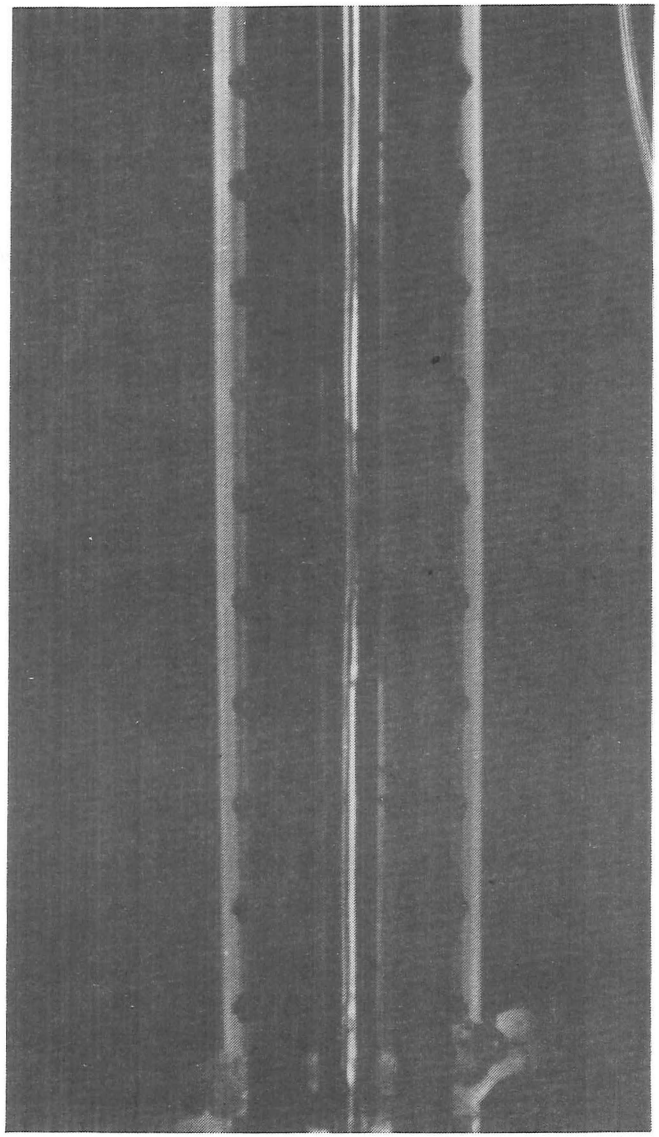

(ii) CENTRE

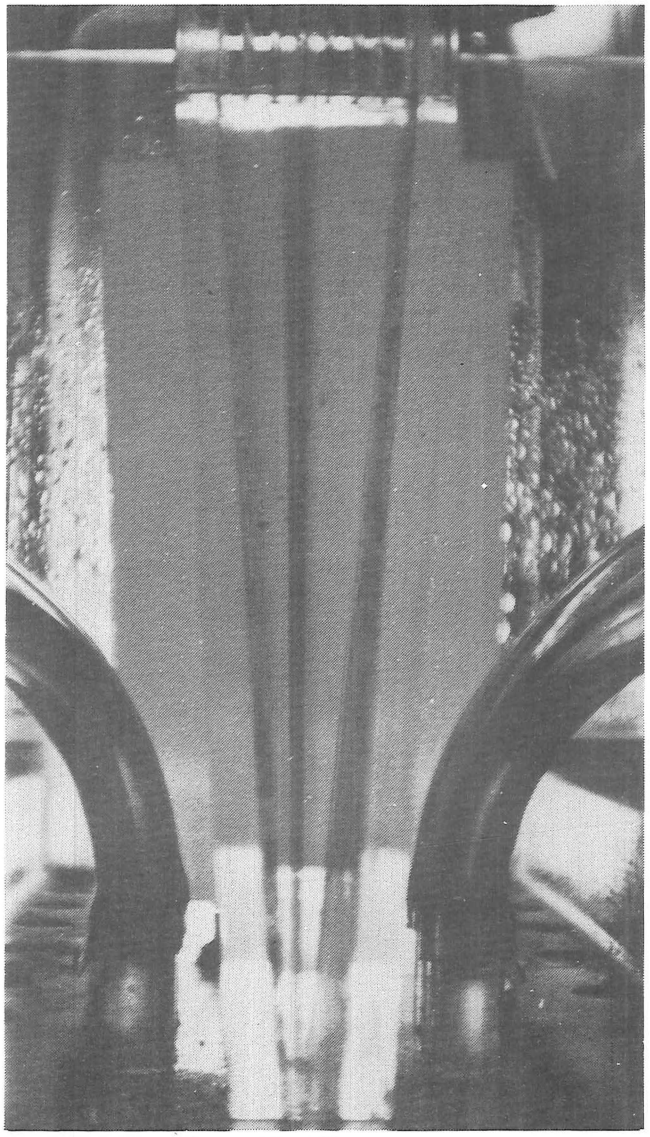

(iii) OUTLET

Plate 5.4: Stable flow through the prototype cell

i) The changes in cross-section between the input, 'core' and collecting zones of the device are considerably more extreme than those in the preliminary hydraulic model (see figures 2.4 and 4.1, 4.2, and 4.3).

ii) The imperfectly rectangular form of the cross-section of the separating zone, initially caused by the flexing of the membrane and later by a slight tendency for the porous polythene walls to 'bow' (see figure 5.1), caused a difference in cross-section of the separating zone with length.

iii) A second irregularity in the cross-sectional area was caused at the junction between the membrane frame and the 'bridges' in the mainframe (see figure 4.8(ii)), as a result of loading the mainframe in order to seal the O-rings.

From the above, it can be seen that the limiting behaviour of the device from a hydraulic standpoint is the result of limits imposed by the materials of construction and is further governed by the ratio of cross-sectional areas between the zones of the cell.

5.3 Choice of the Carrier Buffer

The requirements for the carrier-buffer solutions in the narrow-slot electrophoresis cell are to a certain extent conflicting. On the one hand, the conductance of the buffer used as the carrier for the solute components should have a relatively low value to permit a large voltage gradient across the separating duct without excessive current drain and the resulting resistive heating. On the other hand, the same buffer should have a high specific conductance at higher concentrations, so that the electrode solution does not show a large voltage drop.

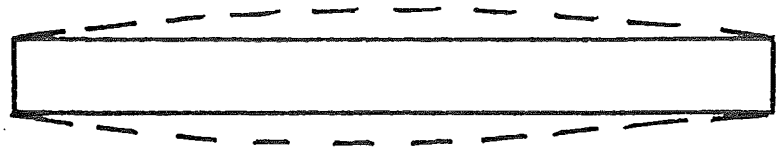

FIGURE 5.1 CROSS SECTIONAL SKETCH OF THE SEPARATING DUCT SHOWING 'BOWING' IN THE POROUS POLYTHENE.

(Clearly these two solutions must be of the same compounds as the electric field will carry component ions across the barriers between the electrodes and the separating duct.) Also inherent is the requirement common to all electrophoresis buffers that the buffering action of the substance chosen should be large at low concentrations - this requirement itself being a conflict in terms of standard buffer theory (P2). A final requirement is that the buffer substances should be readily available at reasonable cost and relatively easy to handle, as considerable quantities are required.

The buffer chosen must, of course, be of the correct pH for the separation to be performed. With a view to the eventual separation of biological substances, a pH of about 8.5 was regarded as the optimum as previous work (H3) shows that this value is the most generally useful for handling proteins. After consideration of the buffers previously used in free-flow electrophoresis, the choice of substances fulfilling most of the above requirements, while lying in the appropriate pH range, was reduced to two: sodium barbitol/barbituric acid and sodium borate/boric acid. The latter mixture has advantages in terms of cost, availability, and handleability and so it was chosen.

The basic recipe used was that of Perrin and Dempsey (P2), consisting of 4.65 g of H_3BO_4 and 8.8 g of $Na_2B_4O_7.10H_2O$ per litre of solution. The conductances and pH values of multiples of this base solution are given in Figures 5.2(i) and 5.2(ii) respectively. As can be seen, solutions of conductance 0.1 S m^{-1} and 1.0 S m^{-1} for the solute carrier and electrode solution respectively can be readily selected from Figure 5.2(i) (compare section 4.3.4).

FIGURE 5.2(i) CONDUCTANCE VARIATION WITH CONCENTRATION FOR SODIUM BORATE/BORIC ACID BUFFER

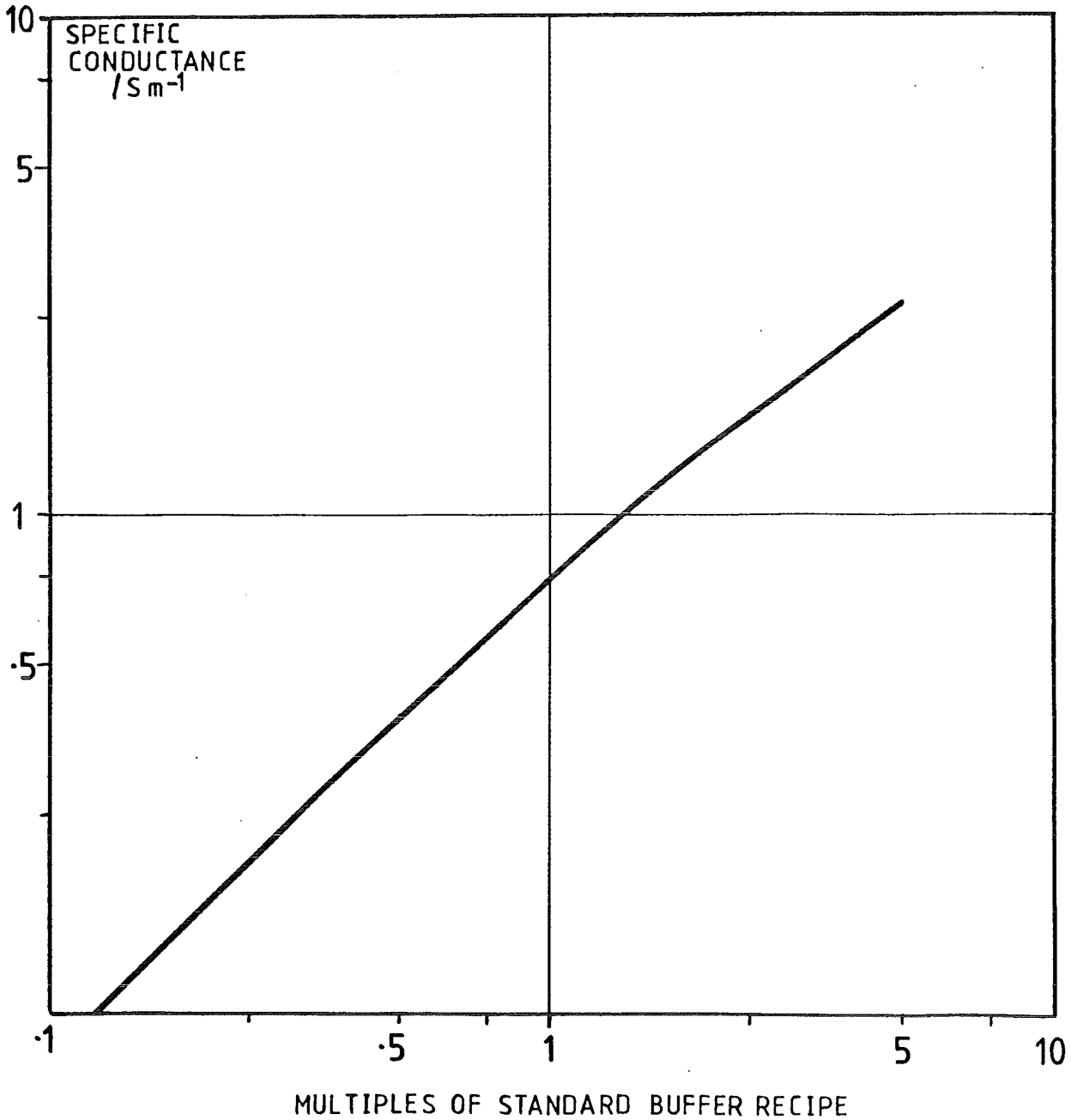

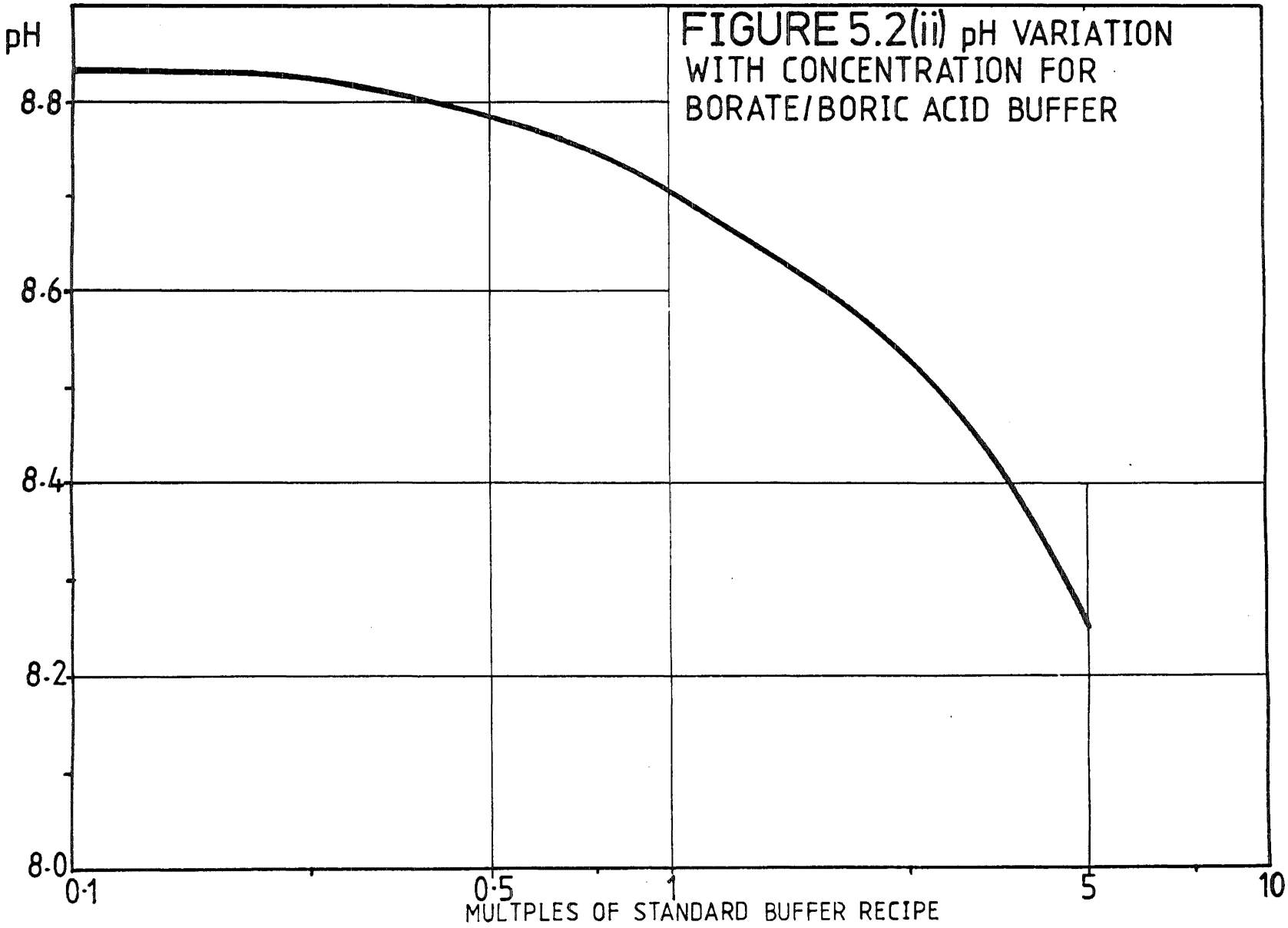

FIGURE 5.2(ii) pH VARIATION WITH CONCENTRATION FOR BORATE/BORIC ACID BUFFER

5.4 The Choice of a Test Substance for the Prototype Separator

In order to evaluate the separator, particularly in terms of the models described in Chapter 3, a test substance is required. The material used for this purpose is required to satisfy a number of conditions. It should be a dissolved or dispersed substance with a density, in dilute solution, not significantly different from that of the carrier buffer. The substance is required to form a coloured or at least visible suspension or solution to enable the solute path to be tracked in the separating cell. The substance should be relatively chemically and thermally insensitive for ease of handling during the initial trials of the cell. Further, the material chosen should be relatively cheap and disposable or easily recoverable from the test solution. Most importantly, the substance(s) chosen must have a well-defined or readily and independently measurable electrophoretic mobility and diffusivity in free solution.

This last requirement is a difficult condition to fulfil as the number of substances for which accurately measured, free-solution electrophoretic mobilities have been published is comparatively small. Hjerten (H7) and Hannig (H3) have published some data for proteins and similar substances; but, in general, these materials are expensive and difficult to handle on a large scale. The work of Strickler, Kaplan and Vigh (S10) shows the relative mobility differences of a series of pigments; however, absolute mobility measurements are a function of separator geometry and electro-osmotic effects in their equipment, so independent values of absolute mobility cannot be extracted from this data. Similar data are available from Dow Chemicals for their uniform polystyrene latex particles (M4), but these particles are

extremely expensive and not readily recoverable from the carrier solution.

Recent work by Tison (T4), with modifications to this equipment by Visca, Ardizzone, and Formaro (V5), gives a method whereby electrophoretic mobilities of suspensions can be measured by direct weighing. This technique enables the electrophoretic mobilities of pigments to be measured relatively easily. Therefore the selection of a suitable pigment which fulfils the other requirements listed above would appear to be a reasonable course. In practice, two such pigments were chosen: cobalt blue & titanium white, both Rowney 'designer'-grade artists' watercolours. These substances, chemically, are respectively: cobalt aluminate and titanium dioxide which are chemically and thermally stable with respect to the experimental conditions in the separator. The technique used to perform these mobility measurements is outlined in section 5.5. It was further found that dilute suspensions of these substances could be cleaned by vaccum filtration with a standard filteraid, thus permitting the carrier buffer solution to be reused.

However, no definite values for the diffusion coefficient of these pigments could be found. The most reasonable approach appears to be to assume a mean particle diameter for the pigment particles and use this as a basis for evaluating the likely diffusion coefficient from published tables. On using this approach, a particle diameter approximately equal to that of colloidal silica was chosen giving a diffusion coefficient of 10^{-10} m^2 s^{-1} (W2). The precision of this parameter is not as important as that of the electrophoretic mobility, as is shown by the computations of Chapter 3.

5.5 Determination of Pigment Electrophoretic Mobilities by the Method of Tison and Visca et al.

5.5.1 Technique

The technique used to measure the electrophoretic mobility of these pigments essentially consists of collection of a quantity of electrically transported pigment and relating this quantity to the electric-field strength. As shown in Figure 5.3, the apparatus consists of a collector placed in a suspension of the substance to be measured in the appropriate buffer with an electric circuit through the collector and solution by way of an ammeter. Inspection of Figure 5.3 shows that the suspended solute transported by the electric field between the cathode and anode must pass through the orifice of the collector cell. This fact enables the evaluation of the rate of transport of the substance and the field used to drive it. In accordance with the equations developed by Ross and Long (R4), the mobility of a given suspended species may be calculated by use of the following formula:

$$m_i = \frac{\Delta m}{\Delta t\ E\ C\ A\ (1 - \chi)} \qquad 5.1$$

where m_i = electrophoretic mobility

Δm = change in mass of solute in the collector

E = electric field strength

Δt = time of current passage

C = concentration of solutes per unit volume of suspension

A = cross-sectional area of the orifice

and χ = volume fraction of solids in the suspension,

so that $1/(1 - \chi)$ is the factor to correct for the counterflow of liquid forced out of the collector by the accumulating solids (significant only for highly concentrated suspensions). The

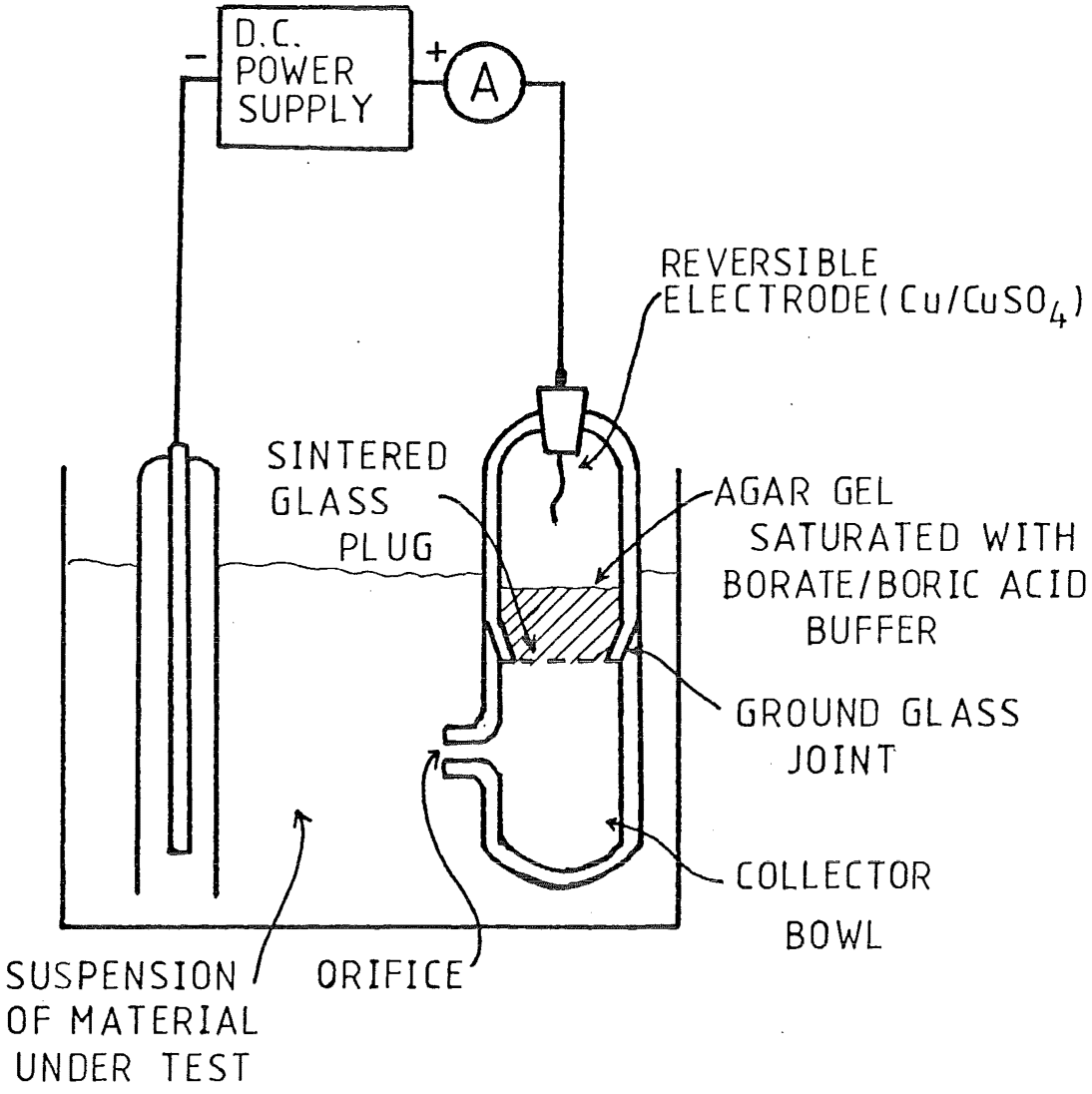

FIGURE 5.3 THE VISCA ET AL MODIFICATION OF THE TISON COLLECTOR TYPE MOBILITY CELL

electric field strength required by equation 5.1 can be evaluated by the expression:

$$E = \frac{I}{A\Lambda} \qquad 5.2$$

where I = current

A = orifice area

and Λ = solution specific conductance.

The measurement technique was then as follows.

i) A suspension of known solute concentration was made up with oven-dried pigment and the borate/boric acid buffer.

ii) The cell was placed in this suspension and a 'collector bowl' full of suspension was removed and placed into an evaporating basin for oven drying.

iii) The collector cell was placed back into the suspension and the current switched on for a fixed time, after which the collector bowl was again emptied into an evaporating basin for oven drying.

iv) The two samples were oven dried at $80^{o}C$ for 48 hours and allowed to return to room temperature and weighed to determine Δm.

v) Equations 5.1 and 5.2 were used to evaluate m_i.

5.5.2 Results

After some initial runs to establish a 'feel' for the operation of the apparatus, a series of runs was performed to evaluate the electrophoretic mobilities of titanium white and cobalt blue, at a pH of 8.5. The results obtained for titanium white were not consistent from one run to the next

and it was thought that this inconsistency may have been due to the prescence of other substances in the supplied pigment (e.g. optical brighteners etc.). However, consistent results were obtained for cobalt blue solutions under the following conditions.

Orifice area

$$A = 2.52 \times 10^{-5} \ m^2$$

Solute concentration

$$C = 0.0158 \pm 0.0005 \ g \ ml^{-1}$$

Solution pH

$$pH = 8.50 \pm .01$$

Current

$$I = 30 \pm .5 \ mA$$

Time interval

$$\Delta t = 30 \ min.$$

Solution conductance

$$\Lambda = 5.0 \times 10^{-1} \ S \ m^{-1}$$

For five runs under these conditions, a mean mobility value of

$$3.0 \times 10^{-8} \ m \ s^{-1}/V \ m^{-1}$$

with a standard deviation of $0.3 \times 10^{-8} \ m \ s^{-1}/V \ m^{-1}$ was obtained for cobalt blue assuming that the volume fraction correction factor $1/(1 - \chi)$ was negligible (justifiable in terms of the initial concentration value for the suspension).

It was therefore decided that cobalt blue would be used in the initial series of test experiments with the prototype separator to determine the response of the cell and compare this behaviour with the theoretical models of Chapter 3.

5.6 Commissioning Trials

5.6.1 Introduction

The commissioning trials for the separator brought together the hydraulic experiments with a series of tests to determine the response of the cell and the behaviour of single solutes as increasing electric fields were applied across the separating zone. These trials illuminated a series of problems, not only with the physical structure of the cell, but also with the membrane materials. Inspection of the stainless steel electrodes after a number of these trials showed that the anode was still corroding in the severe oxidising conditions present at this metal-solution interface.

5.6.2 Preliminary Tests with the Electric Field

The first series of experiments carried out with voltages of between 20V and 40V applied across the cell, as originally designed (see section 4.2), gave current flows of between 3.5 A and 8 A. This gave a nett resistance of the cell in this configuration of approximately 8 Ω which was confirmed by direct measurement of the resistance between the electrode plates. However, computation of the expected resistance of the electrode channels and separating duct based on the specific conductance of the solutions in these zones gave:

i) for the electrode channels,

$$\Lambda = 1.6 \text{ S m}^{-1}$$

so that resistance = 0.14 Ω or total resistance = 0.28 Ω for both channels;

ii) for the separating duct

$$\Lambda = 0.2 \text{ S m}^{-1}$$

so that resistance of the separating duct = 0.3 Ω. Thus, even allowing for a voltage drop due to polarisation at each metal-solution interface of 1 V to 2 V, approximately 90% of the resistance of the cell was in the membrane and porous polythene plate. Moreover, there were a number of other problems with the cell in this configuration.

It was observed that, to maintain the membrane flat against the porous polythene supports, a pressure difference between the inner (separating) duct and the electrode compartments sufficient to cause an outward leak of a magnitude approximately equal to the flow through the duct (i.e. ca. 10 $cm^3\ s^{-1}$) was required. Over a period of time this diluted the electrode solution, so increasing the resistance still further. It was also observed that this leakage caused solute to flow around the edges of the membrane support and into the electrode chambers. Adding the electric field to this situation complicated matters still further as the membranes were found to bulge into the separating duct under the influence of the electric field. This not only caused a variable cross-sectional area in the separating zone with its attendant hydraulic problems, but also caused oscillations in the current flow through the cell as the effective cell resistance altered with time and the local resistance varied with distance along the cell. These effects are diagrammed in Figure 5.4. As a result of this experience the redesigned cell, shown in cross-section in Figure 4.8, was built.

5.6.3 Trials with the Mark II Separator

The separating zone, modified as described in Section 4, was tested in a similar manner to that discussed

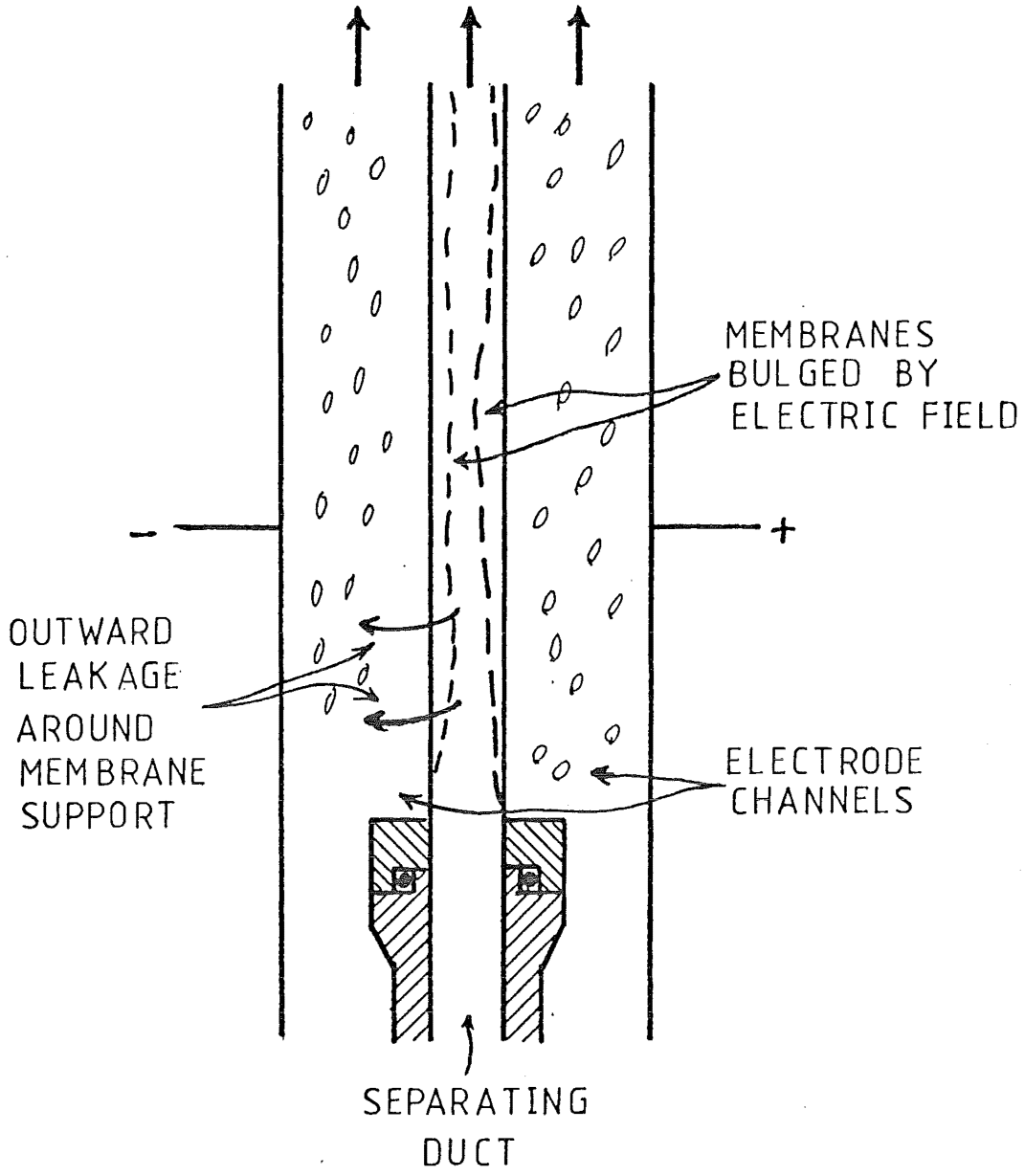

FIGURE 5.4 BULGING OF MEMBRANES BY ELECTRIC FIELD

above. The cross-leakage rate was now found to be of the order of 10% of the flow through the separating duct, while the cell resistance had increased to approximately 20 Ω (for the same order of conductance in the electrode channels and separating duct as quoted above). However, attempts to run a single solute in the separator gave the expected behaviour at an electric field strength of 0.64 kV m^{-1} (see section 5.7), and this result was not repeatable. For other runs, the observed trace of the cobalt blue solute is represented by plates 5.5 and 5.6. Compare in particular plate 5.5 with the trace in the absence of an electric field (plate 5.4(ii)). (Electric-field strengths were calculated from the current flow through the cell using the specific conductance of the carrier buffer in the separating duct, i.e. using equation 5.2).

The dispersed flow behaviour of the solute trace shown in plate 5.5 was observed to grow more pronounced with each succeeding run with the cell. It was therefore decided to dismantle the cell and inspect the membranes and supports for any sign of leakage. On dismantling the cell it was found that leakage was still occurring around the edges of the membrane-support plates. This leak was shown clearly by the trace of pigment left on the edges of the porous polythene support plates as shown in plate 5.7. The membrane's porous polythene support assembly was dismantled and reglued. Also the O-ring seal around the membrane-support frame was adjusted by lessening the tension on the O-ring, so lessening the 'thinning' of the O-ring causing it to fill with grove more readily. These modifications reduced the cross-leakage between compartments in the cell to virtually zero.

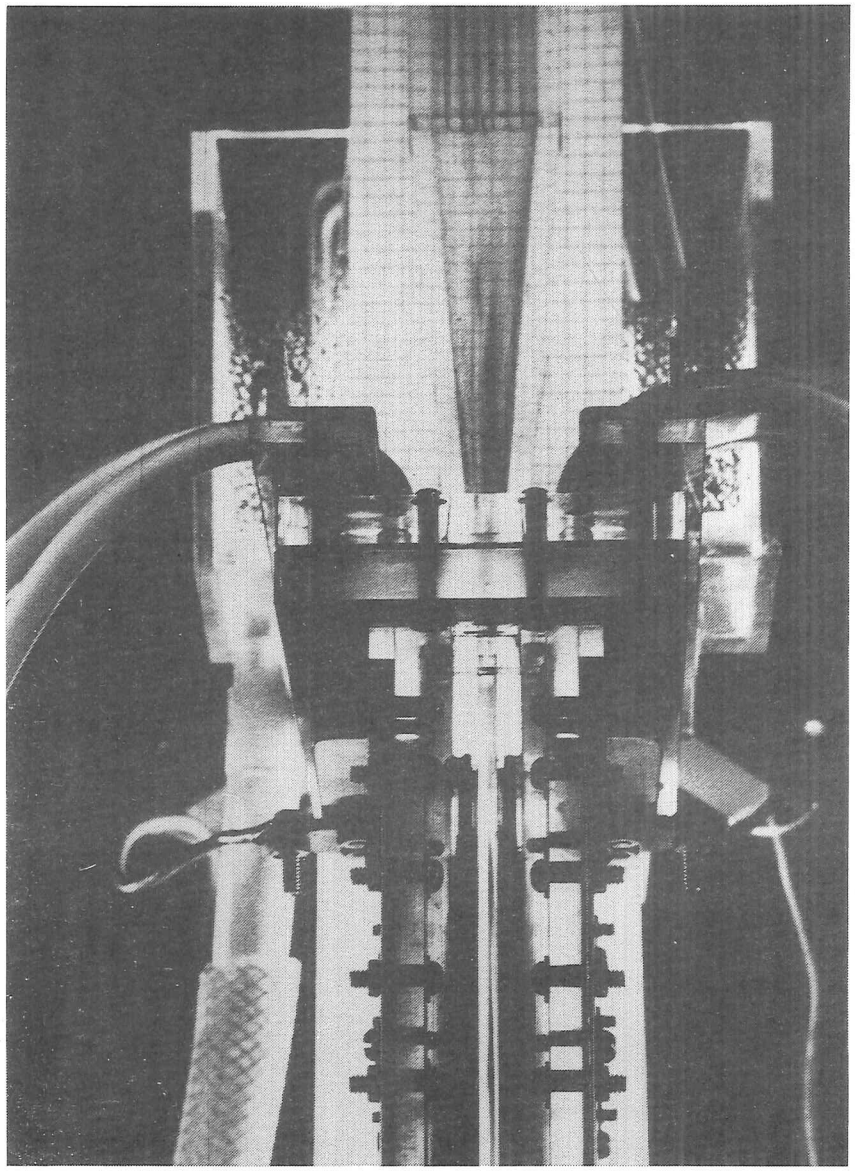

Plate 5.5: Cell behaviour at $Re \simeq 200$
$E = 4\ V\ cm^{-1}$

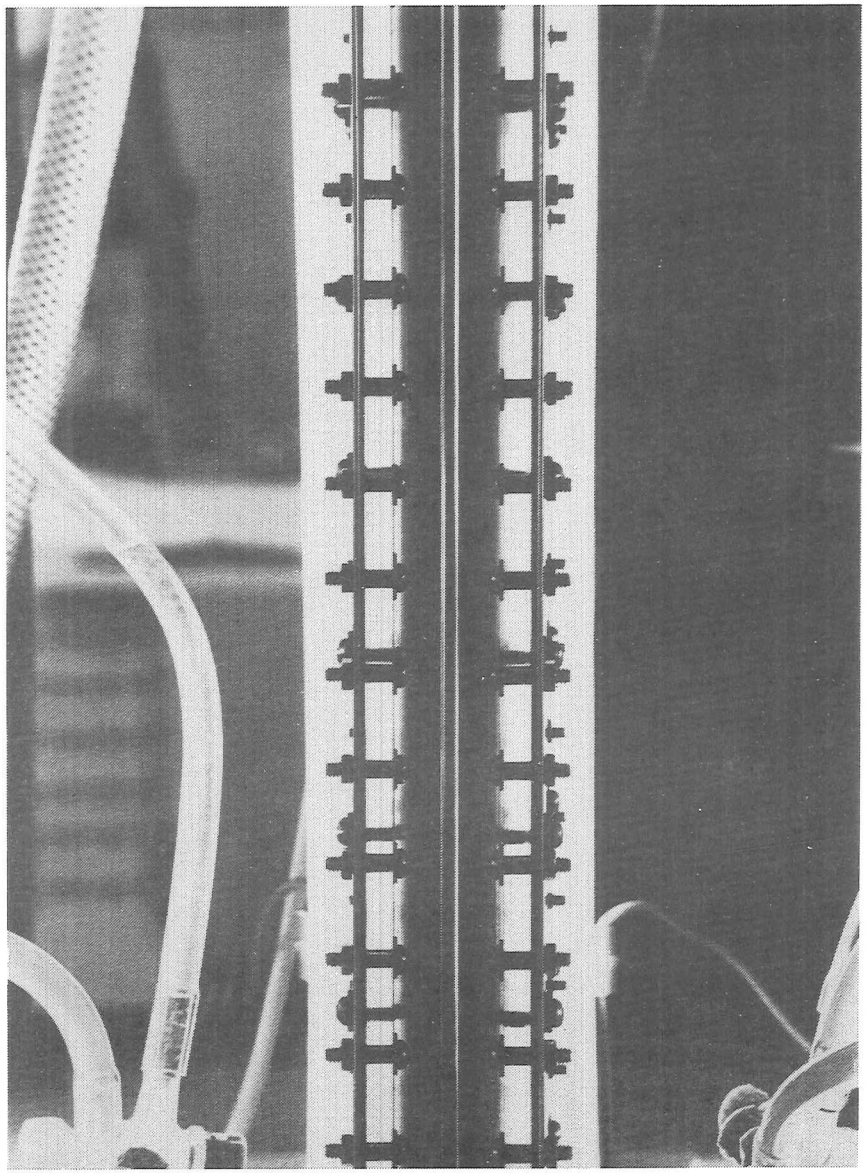

Plate 5.6: Cell behaviour at $Re \simeq 200$
$E = 4\ V\ cm^{-1}$

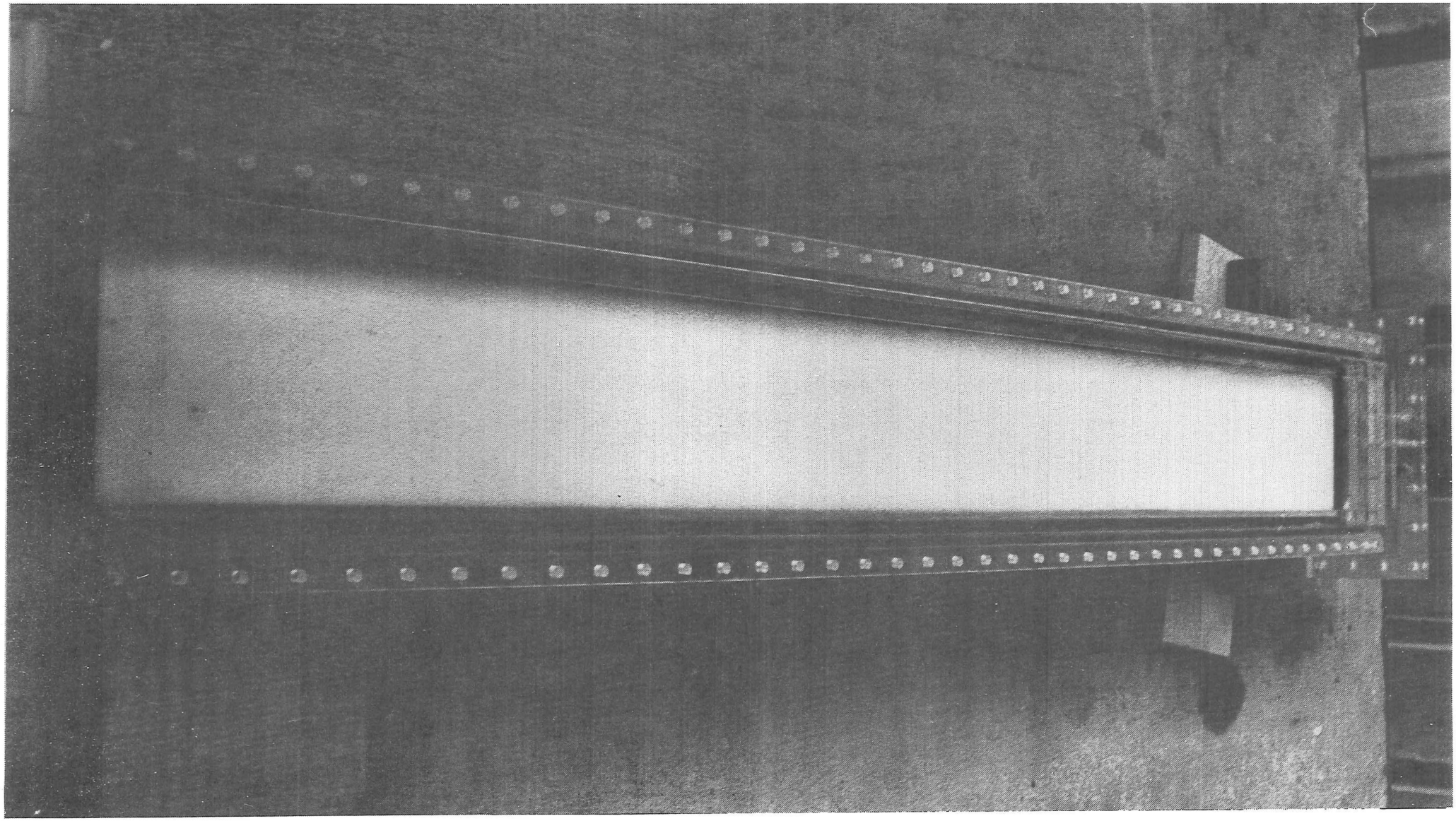

Plate 5.7: Staining of porous polythene due to leakage at edges

However, it appeared that at this point one membrane failed in service. The resulting pinhole in the membrane permitted passage of the concentrated solution into the separating duct causing a disturbance to the flow in this zone due to the density difference between the two solutions (see plates 5.8 and 5.9). The resultingly destabilised flow mixed the carrier buffer and the solute across the full width of the duct, so masking observation of the expected deflection of the solute trace. Further evidence of this pinhole was found when the membrane was again removed from the supporting porous polythene and it was found that the solute cobalt blue had discoloured the porous polythene sheet on the side of the electrode compartment, at a point opposite the observed position of the disturbance arising from the pinhole (see figure 5.5). An attempt was made to circumvent this problem by partially blanking the membrane, but further failures of the membrane became evident when this was done. As a result, the membranes were scrapped, and replacements ordered.

The available replacements were 'improved' DDS GR81P-type which were, according to the New Zealand agents for DDS (Niro Atomizer (N.Z.) Ltd), of exactly the same chemical resistance as the GR8P-type previously used. This later series was, however, quoted as having a higher permeability than the GR8P-type. The roll of this membrane was found on receipt to have been crushed flat in transit from Denmark and extreme difficulty was encountered in locating the membranes correctly in the support frames. When this was finally done and the current switched on in the reassembled separator, it was found that after approximately 20 minutes in service the membrane facing the anode again exhibited evidence of failure similar

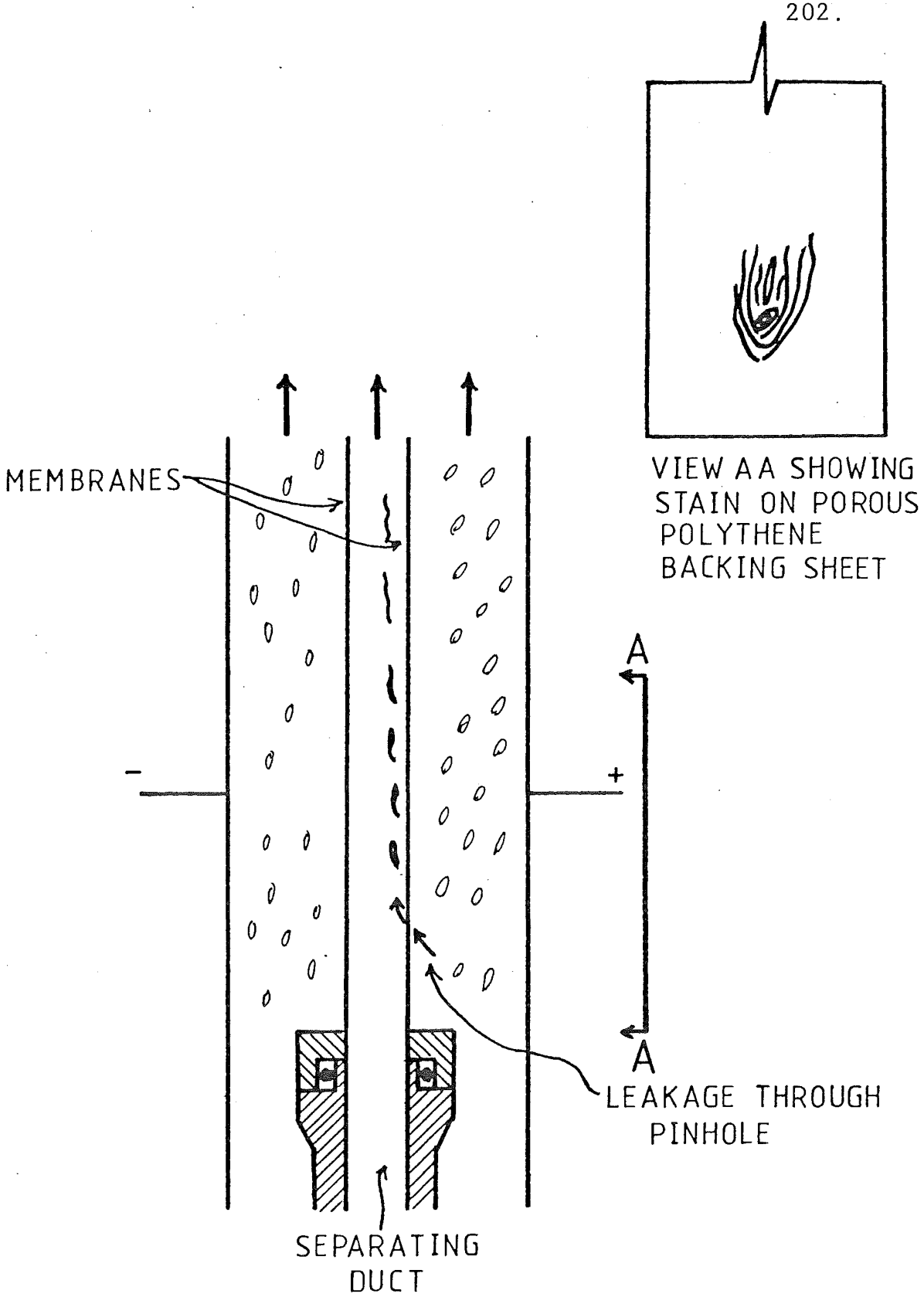

FIGURE 5.5 DIAGRAMATIC VEIW OF THE EFFECTS OF PINHOLING OF THE MEMBRANE

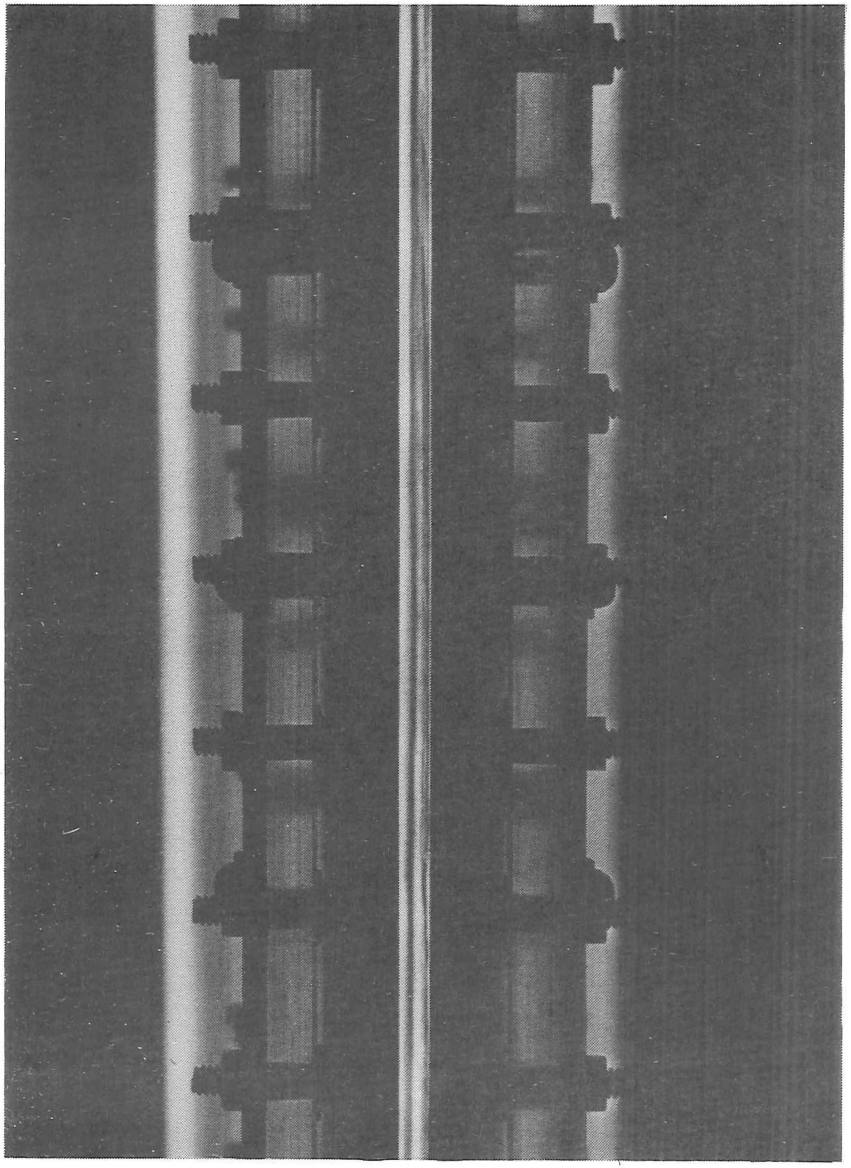

Plate 5.8: Effect of pinhole in membrane on flow.

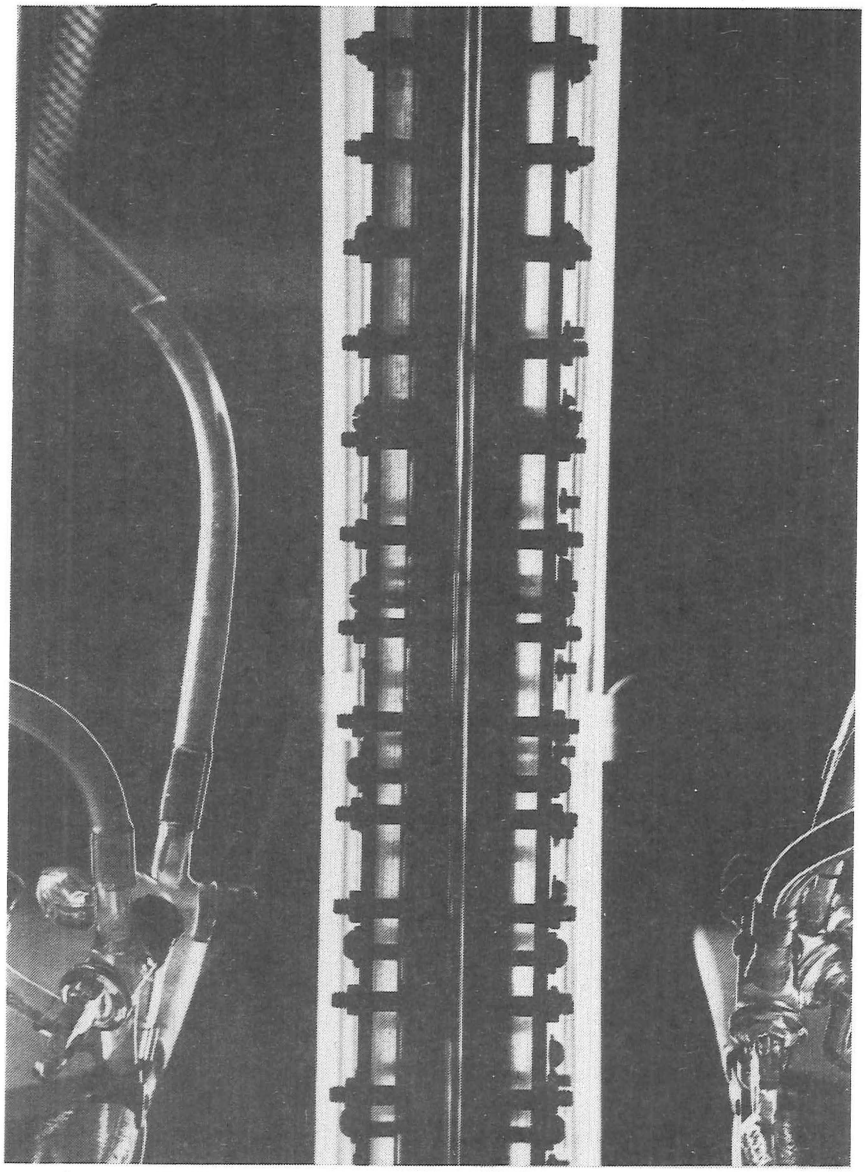

Plate 5.9: Effect of pinhole in membrane on solute stream.

to that shown in plates 5.8 and 5.9. It was therefore concluded that further fundamental work was required in the area of the behaviour of these and similar membranes in the presence of electric fields in ionic solutions to determine the cause of these failures.

While likely causes of these problems are discussed in Chapter 6, the fundamental investigation of membrane performance required to determine the reasons for these failures is beyond the scope of the present work.

5.7 A Result Indicative of the Expected Performance of the Narrow-Slot Electrophoretic Separator

During the experiments described in section 5.6.3 a single result showing the type of behaviour expected of the separator under test with a single solute component was observed. As shown in plates 5.10 and 5.11 the cobalt blue solute used for this test was deflected by approximately 1/7 of the total duct width by a field strength of 0.64 kV m^{-1} at a bulk flowrate corresponding to a Reynolds number of 200 in the separating zone. Plate 5.10 shows the undeflected stream and plate 5.11 shows the pigment stream under the action of the electric field. The electric field was evaluated, using the observed current and specific conductance in the separating duct, by way of equation 5.2. The Reynolds number was evaluated using the method of section 2.2.5.

The significance of this result is discussed in detail in section 6.2.

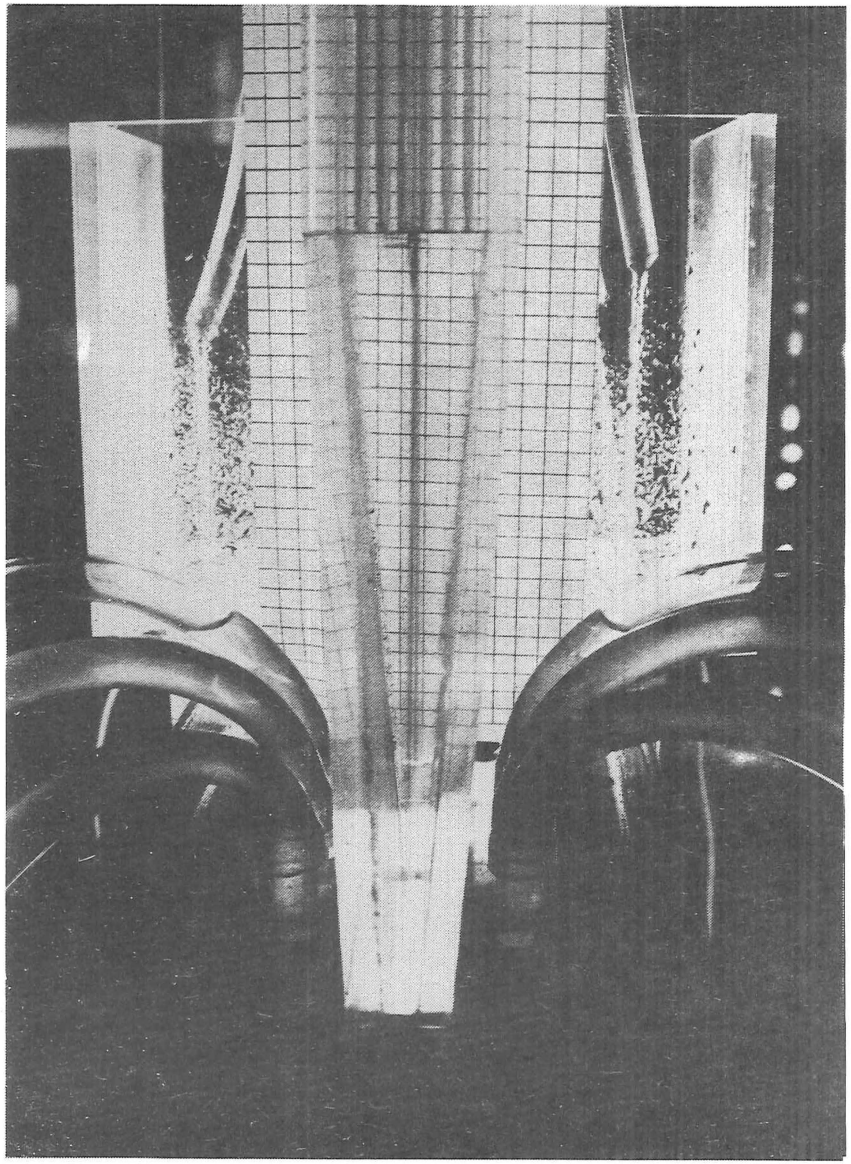

Plate 5.10: Pigment stream at $Re \simeq 200$ and E = 0

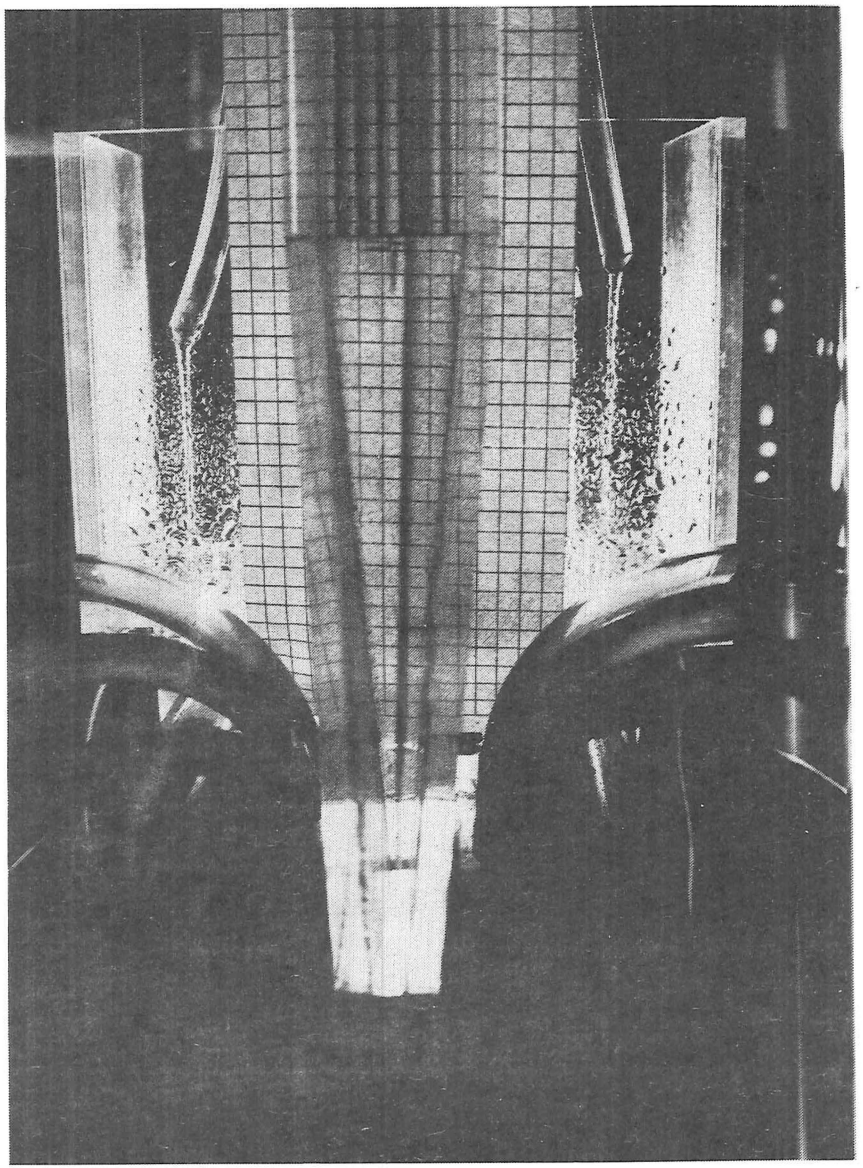

Plate 5.11: Pigment stream at $Re \simeq 200$ and E = 6.4 V cm^{-1}

6. DISCUSSION

6.1 Flow Stability

As has been previously remarked, the stability of flow through the narrow-slot electrophoretic separator is fundamental to the operation of this device. The observations recorded in section 5.2 show essentially two possible factors limiting the stability of flow in the separator: the absolute speed of flow through the cell, and the irregularities in the cross-section of the separating zone caused by the mechanical limits of the materials of construction.

From the presently accepted picture of the mechanism of transition from laminar to turbulent flow, it is reasonable to interlink these factors. This picture (L2, R1, B2) regards the transition as occurring when oscillations within the flow grow to a level at which they can no longer be damped by viscous forces within the fluid. In terms of this picture, factors which increase the magnitude of the oscillations present or impose further secondary oscillations on the flow will tend to force the breakdown of laminar flow. In the case of a homogeneous fluid flowing through a smooth duct, the analyses quoted above show that this state of affairs is reached when the Reynolds number of the flow reaches a characteristic value, dependent on the duct type.

However, in the case of the present version of the narrow-slot separator, there are complications to this picture. The small irregularities in the walls of the cell described in section 5.2 lead to small variations in the local Reynolds number

and tend to distort the steamlines in the flow across them. For instance, if the 'bowing' effect described in section 5.2 can be regarded as changing the channel thickness by 0.5 mm, then the Reynolds number for flow at this point, when compared with that for the flow through the 'normal' 5 mm by 100 mm section of the separating duct, is decreased by 1%. The effect of a series of small changes of this type combined with the small negative pressure gradients (see section 2.2.3) resulting from expansions in the duct cross-sectional area can be qualitatively regarded as destabilising the flow and lowering the threshold for the onset of hydraulic turbulence.

The matter is further complicated by the small density difference between the solute and carrier components of the solution. From the analysis of section 2.3, the eventual effect of this density difference will cause the 'column' of solute flowing through the cell to 'fall over'. This type of behaviour was in fact found to be triggered at the knife edges in the entrance zone (see section 5.2.2). This is reasonable in the light of the greater proneness of this area to disturbances as a result of the boundary-layer separation which occurs as the fluid flows off the ends of the knife edges (see Figure 6.1). However, in more general terms, the additional (unavoidable) destabilising effect of this density difference will tend to contribute to the breakdown of laminar flow if this is instigated from any of the above-mentioned sources.

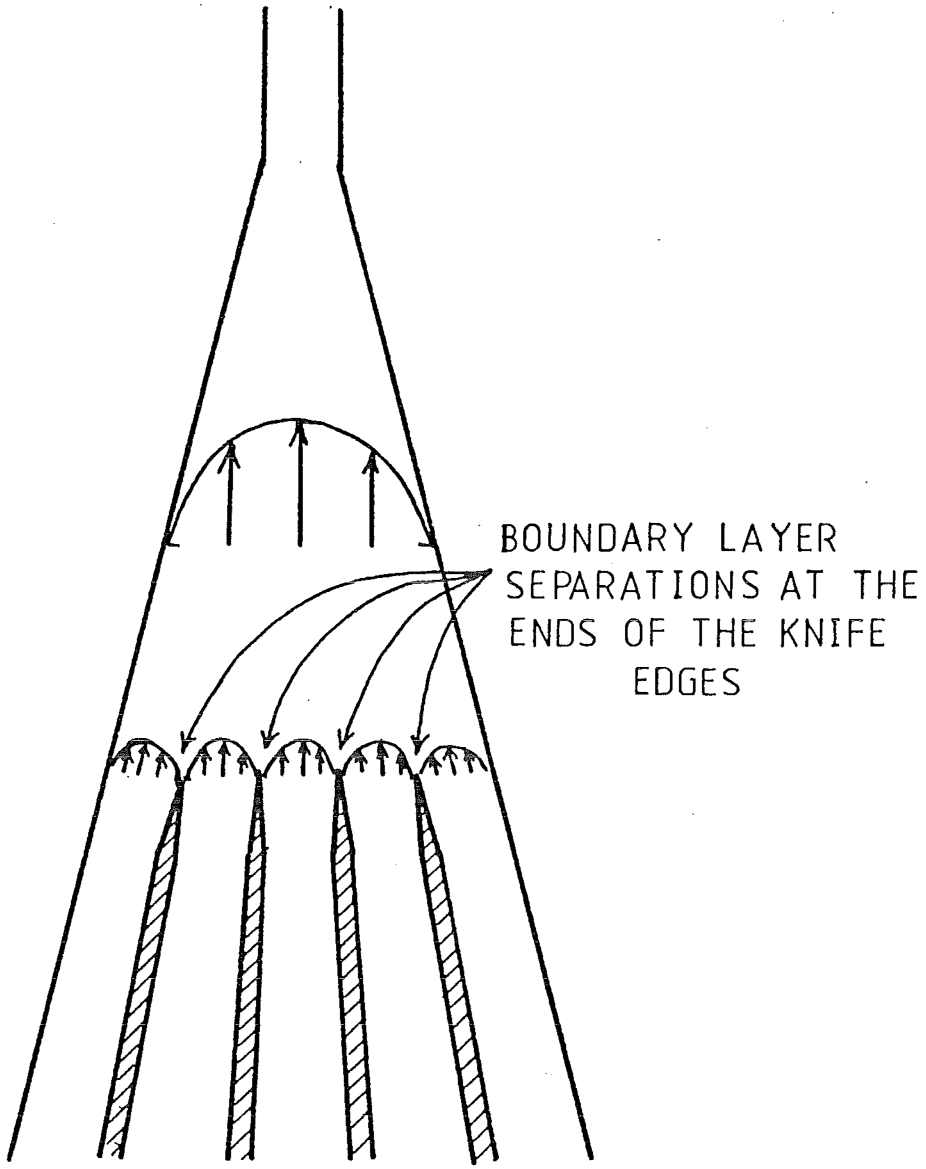

FIGURE 6.1 BOUNDARY LAYER SEPARATIONS IN THE ENTRANCE ZONE

6.2 Comparison Between the Linear and Cubic Theoretical Models and the Observed Result

The single observed solute track obtained in the prototype separator was obtained in circumstances in which the conditions of flow and electric field were not precisely controlled. The track of the cobalt blue test substance, shown in plates 5.10 and 5.11, was photographed when there was evidence of cross leaks between the separating duct and the electrode spaces (see section 5.6). Under these circumstances, the assumptions used in formulating the models described in chapter 3 were, at least in part, invalid.

For the run, during which plates 5.10 and 5.11 were obtained, a bulk leakage rate of approximately 10% of the flow through the separating duct was observed. This figure was evaluated by running the carrier-buffer solution, in the absence of solute, from the outlet to the separating zone back into the carrier buffer reservoir. The change in level with time in the reservoir was then measured enabling the loss rate of carrier into the electrode compartments to be evaluated. This method, while somewhat crude, yielded figures which agreed within 15% with those obtained, in separate tests, by direct collection of the outflow from the separator over a measured time. However, that former technique could not be used during the operation of the separator with solute for obvious reasons. It is however likely that the cross-leakage during the run photographed in plates 5.10 and 5.11 was of the same order as that measured above by this technique.

From the above, it is clear that the assumption of perfect isolation of the separating duct (i.e. impervious duct walls)

used in the derivation of the theoretical profiles is invalid. The specific effects of this bulk leakage on the performance of the cell (in terms of a single solute track) are dependent on the location and direction of these leaks. If the leaks are uniform with distance along the cell and in both directions (i.e. towards the anode and cathode), the effects could be expected to be small, provided no leak was sufficiently severe that pigment was drawn from the separating duct into the electrode spaces. (There is evidence of this action shown in plate 5.5 since cobalt blue was recovered from the electrode solution by filtration at this stage.) However, provided no flow of pigment occurred out of the separating duct into the electrode spaces, if the leakage was biased in one direction (either towards anode or cathode) then the effect would be to bulk 'shift' the solute trace in the direction of either anode or cathode. Such a shift should occur when the electric field across the duct is switched off. However plate 5.10 shows no evidence of a shift of this type. It may therefore be concluded that the leakage effect was uniformly bi-directional.

From the evidence of section 5.6.3, the leakage was around the edge of the membrane (see plate 5.7). This suggests that there exists a low resistance current path at the edges of the membranes. It is reasonable to suppose that this would cause a variation of electric field with depth in the cell. However this effect would be most severe at the extreme edges of the duct where both the bulk flow and the solute concentration are expected to be small as a result of the stagnant zone present in this area (see section 3.1.1 and Figure 3.2). If such a field distortion was present, the effect, when viewed 'edge-on' (as the plates 5.10 and 5.11 are), would be to apparently broaden the

deflected pigment stream by comparison with that viewed in the absence of no electric field. This effect would occur as a result of the distortion of the 'sheet' of pigment flow by the nonuniform electric field (see Figure 6.2). This effect is not observed in plate 5.11. However this hypothesis may provide some explanation for the unstable flow behaviour shown in plates 5.5 and 5.6.

A plot of the expected concentration profiles for the models of chapter 3 with the observed deflection of the pigment stream taken from plate 5.11 (corrected to match the input conditions of the models) superimposed is shown in Figure 6.3. The value of Reynolds number used is calculated from the volumetric flow from the outlets to the separating duct during the run which produced plates 5.10 and 5.11. The value of the electrophoretic transport number is calculated using the measured electric field strength from the above run (by the method of section 5.6.3) and the electrophoretic mobility of cobalt blue evaluated by the mass collection method of Tison (T4) (see section 5.5). As can be seen, the somewhat uncertain nature of the transposed result from plate 5.11 coupled with the position of the profile in the flow does not distinguish between the two models. The plot does tentatively suggest that the linear model might be more appropriate, if only because plate 5.11 shows no evidence of the 'tail' exhibited by the profile generated by the cubic model. However, since neither profile is a particularly good fit to the observation, this is inconclusive.

The trend which is apparent however is that the models both predict a larger transition for a single component than that shown by plate 5.11. The linear model was computed with El values

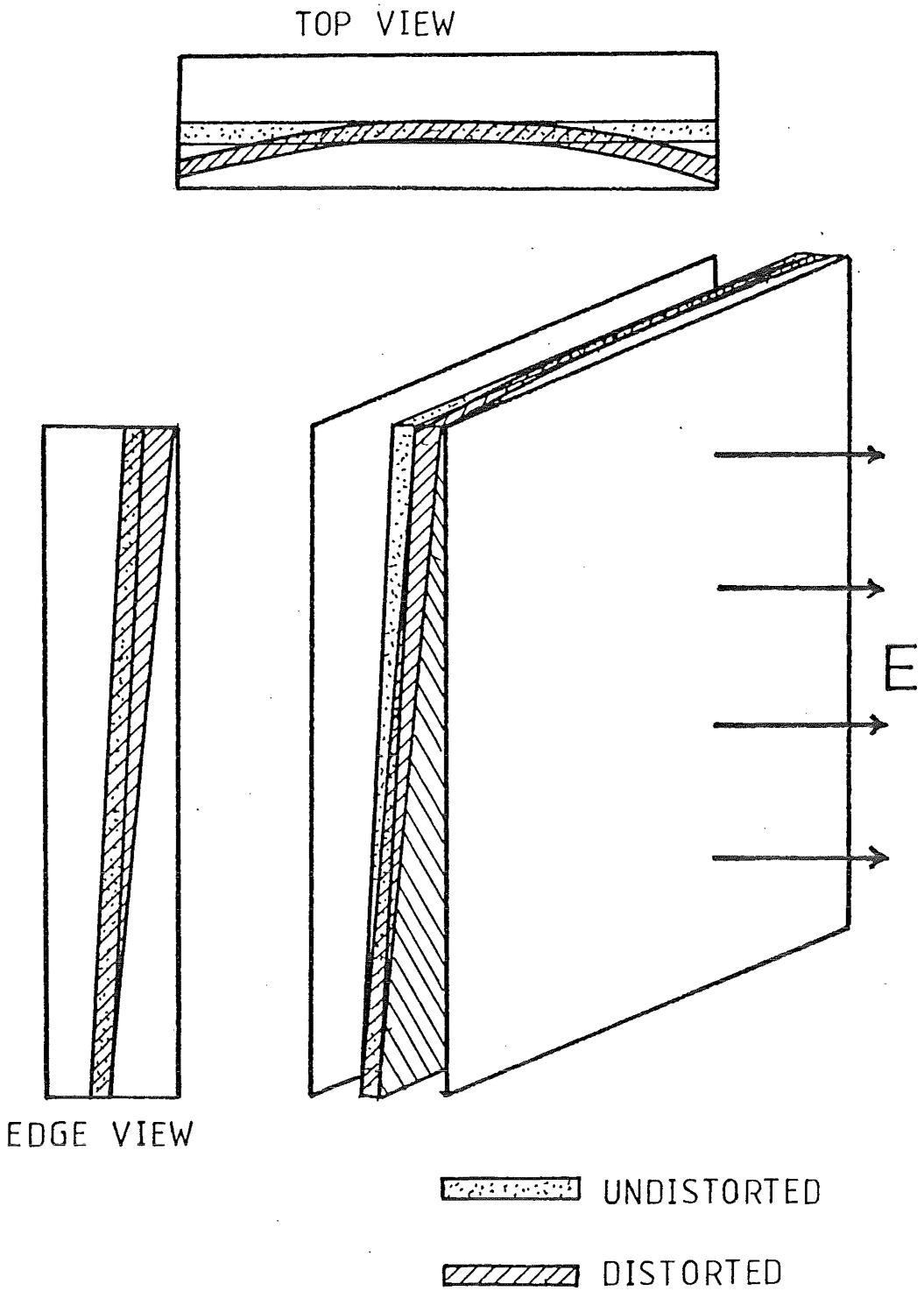

FIGURE 6.2 DISTORTION OF THE SOLUTE FLOW EXPECTED FROM A NON-UNIFORM ELECTRIC FIELD

FIGURE 6.3 COMPARASON OF OBSERVED RESULT WITH MODEL PROFILES

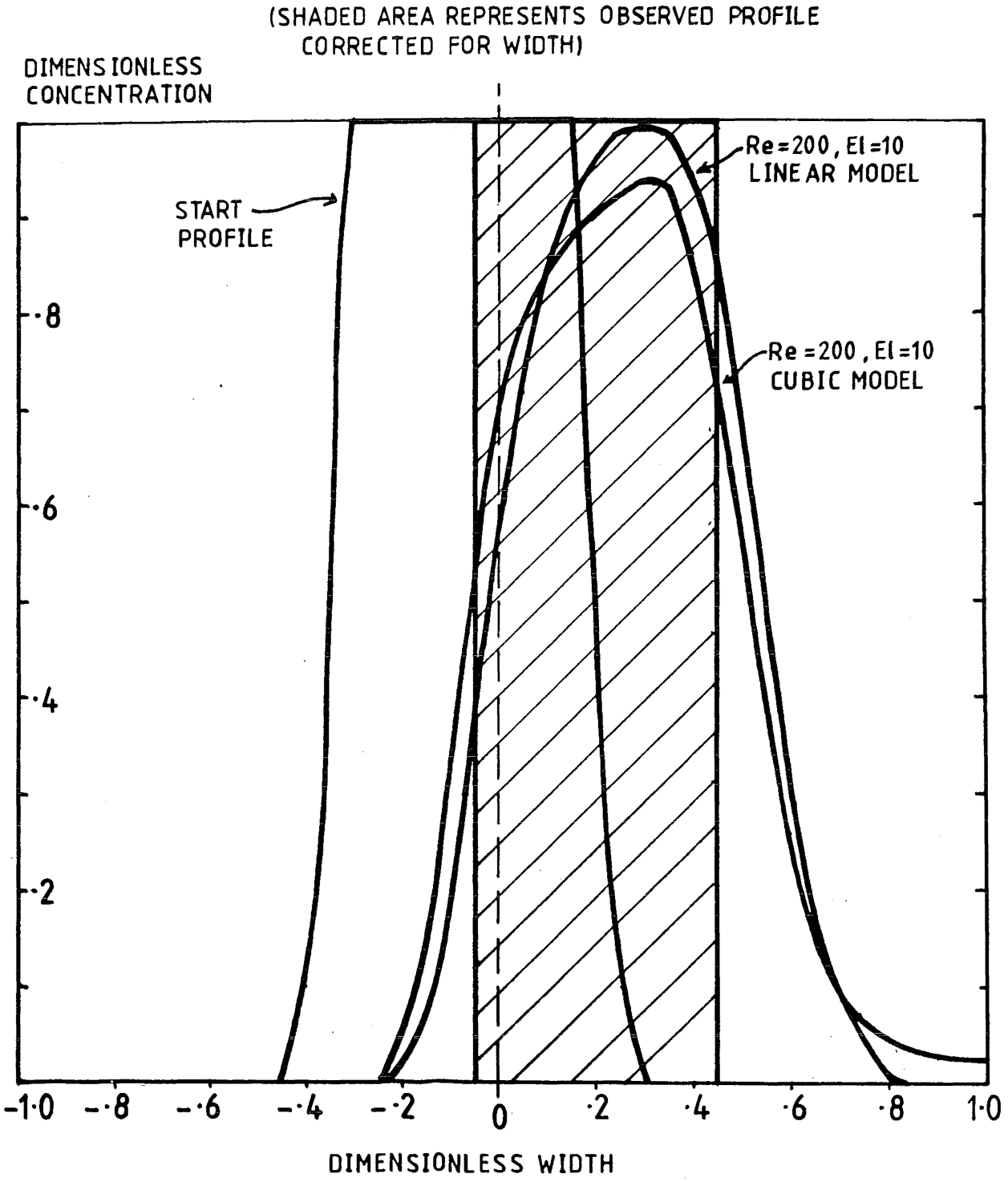

FIGURE 6.4 BEST FIT OF LINEAR MODEL TO OBSERVED RESULT

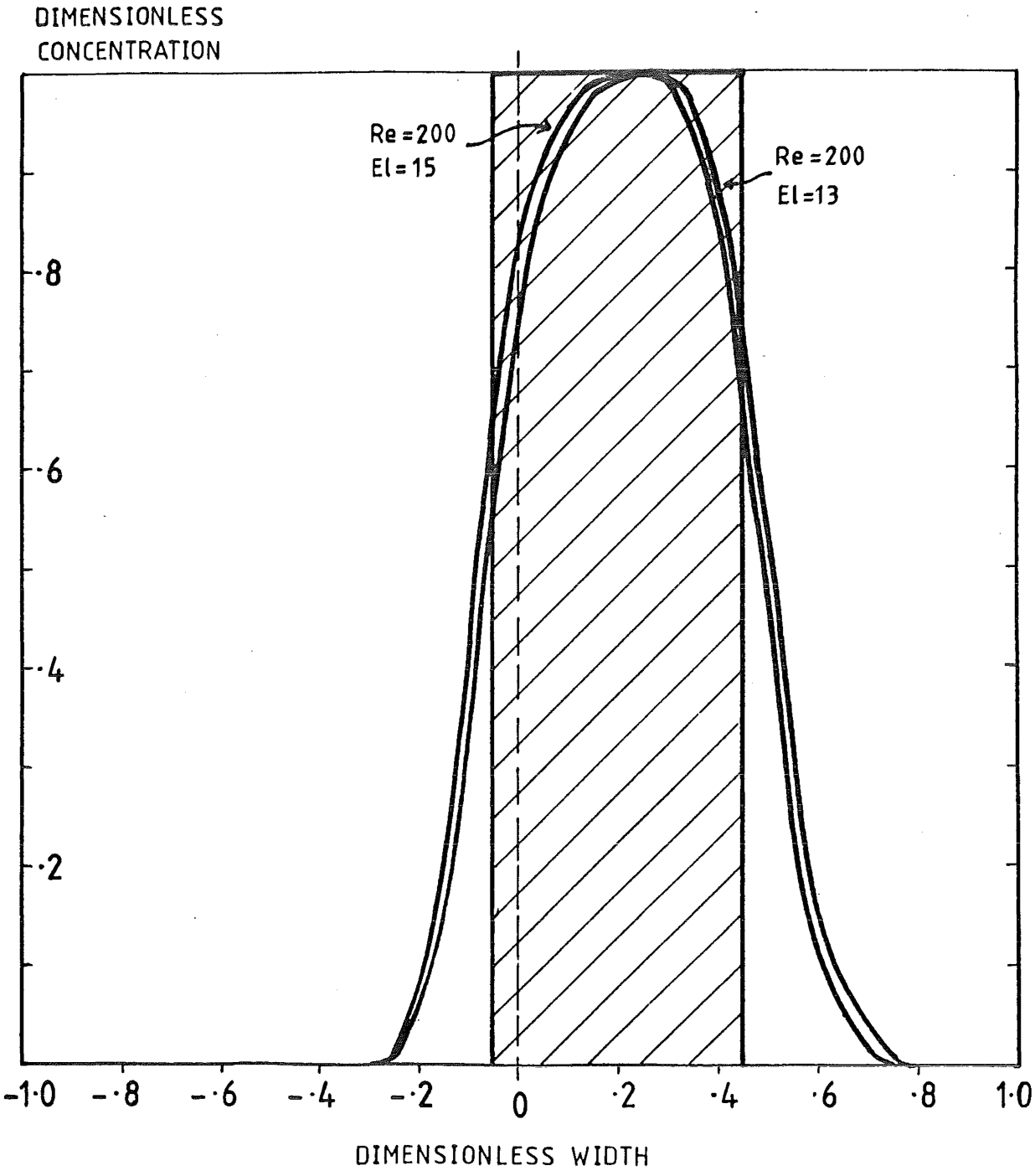

of 13 and 15 for the same Reynolds number. As shown by Figure 6.4 these profiles more closely approximate the observed deflection. This suggests that there may be an electro-osmotic effect present and that this effect is practically uniform across the depth of the duct. This is the expected form of any electro-osmotic effect for a duct of the aspect ratio of the narrow-slot separator (see section 1.4 and in particular section 1.4.5). Calculation of the effective mobilities from the values of El used to generate the curves in Figure 6.4 shows that this electro-osmotic effect provides a retardation or decrease in effective electrophoretic mobility of between 40% and 50% of the independently measured electrophoretic mobility of cobalt blue.

Bearing in mind the state of the separator prototype, especially with regard to the cross-leakage problems, it would be unwise to place a high level of significance on these conclusions.

6.3 Membranes

Both from the observed behaviour of the replacement D.D.S. GR81P membranes and from the evidence of pinholding in the original GR8P membranes (see section 5.6.3) it would appear that there exists some fundamental problems with the use of ultrafiltration membranes of this type in this service. From the observations documented in section 5.6.3 it can be seen that this pinholing effect occurs first on the membrane facing the anode of the separator at a point approximately 4 cm from the bottom edge of the membrane. Further, no problems were encountered with the membranes until the electrode cavities were efficiently sealed off from the separating duct (refer section 5.6). It would therefore appear that this problem arises only when a

comparatively high electric field (an estimated 15 V per membrane when the applied voltage is 50 V across the cell) is applied directly across the membrane. However the presence of two different concentrations of borate solution on either side of the membrane may be a complicating factor.

While very little information is available about the chemical nature and structure of the D.D.S. GR-series membranes, Madsen (M1) states that the GR6 series are polysulphone-type membranes. Other sources (S7, B1) describe this class of membranes even more vaguely as 'copolymer' membranes. If it is assumed that the GR8 series membranes are chemically similar to the GR6 series membranes described by Madsen (M1), then they may be assumed to consist of one or more of the polysulphone-group polymers with a slightly 'tighter' pore structure than the GR6 series (GR8 membranes have a molecular weight cutoff at a solute molecular weight of 6000 instead of the 22000 value quoted for GR6 membranes). Polysulphones, as a general class are polymers of the form -R-SO_2-R- where the R groups may be linear or cyclic hydrocarbons (or in some cases a mixture of these). This generic group of compounds has widely differing properties depending on the structure of the R group (B5). For olefinic R groups the polymers are soluble in strong concentrated acids and are broken down by strong alkalis, whereas polymers with cyclic R groups are resistant to alakalis and soluble only in concentrated sulphuric acid.

In the chemical environment of the narrow-slot electrophoretic separator, the above extremes of chemical condition are unlikely to be present. There are not expected to be sulphate ions in the solution at all and the buffering action of the

borate/boric acid buffer is expected to limit pH in the region of the membranes to values around the buffered 8.5. However, there is expected to be ionic drift through the membranes under the action of the electric field (at the anode these might be expected to be principally hydrated sodium ions). Madsen (M1) remarks in his discussion of the GR6 membrane that this membrane, when mounted upside down, is almost impervious to distilled water. Upside down in this sense is equivalent to viewing the membrane from the electrode side (i.e. looking inward at the separating duct). If a comparison is drawn between Madsen's situation and the narrow-slot separator in normal operation then the electric field will tend to force hydrated sodium ions 'backwards' through the membrane on the anode side. If the GR8 membranes are in a similar manner resistant to water flow 'backwards' then this may explain the bulging of the membranes into the separating duct observed in the Mark I separator (see section 5.6.2).

Furthermore, electron micrographs presented by Madsen show that the bottom surface of the GR6 membranes appear smooth but with a series of distinct irregularly spaced holes dotted across the surface. From the scale given these holes are of order 10^{-7} m in diameter, considerably larger than the diameter of solvated ions (order 10^{-10} m). It therefore appears possible that solvated ions in the buffer solution are being driven through these holes and forced against the denser front surface of the membrane from behind by the electric field. There may then develop sufficient local tension on the structure of this denser 'molecular diode' section of the membrane to cause a local break in its structure. However, the exact mechanics of this tension, or what form the

breakdown might take, are not at all clear and could not be elucidated without a deeper understanding of the chemical and structural nature of the membrane.

The above hypothesis hinges on the (unproven) assumption of structural and chemical similarity between the GR8 and GR6-series membranes. It also assumes a 'molecular diode' model for these membranes such that the transmission of any substance is unidirectional (from the 'front' to the 'back' of the membrane) and then only up to the molecular weight cutoff limits of the membrane. Also this hypothesis does not account for the reverse osmotic pressure effect of the placement of the membrane with more concentrated ionic solution on the back face of the membrane than that on the front face.

In view of these limitations, at best, the above hypothesis should be regarded as speculative and a possible basis for the design of further experiments testing the suitability of these and other membrane types for use in the narrow-slot electrophoretic separator.

6.4 Materials of Construction for the Cell

Experience with the Mark I and Mark II versions of the narrow-slot separator has shown that construction of the cell mainframe from Perspex or an equivalent acrylic polymer is a reasonable choice in the light of the requirements for electrical insulating properties, machinability to close tolerances, and transparency placed on the cell material. The only viable alternative at present appears to be the use of polycarbonate. However it is likely that a similar learning process to that undergone in the jointing of machined Perspex sections would be

required with this material. Thus the use of Perspex solvent welded with meta-cresol, as described in section 4.6, is the more viable alternative. However it appears that Perspex is subject to a small degree of expansion when immersed in the sodium borate/boric acid buffer solution used in the cell. Hence the possibility of using another polymer, less susceptible to swelling in the presence of this solution for the membrane support frames, bears investigation. Furthermore, experience in handling the mainframe of the separating zone would suggest that this would benefit in terms of dimensional stability if it were designed so that the mainframe was considerably more massive (i.e. of greater cross-section).

The use of 'Vyon' porous polythene for the membrane support, while in some respects satisfactory, also bears further consideration. If a porous polymeric material could be found which is more dimensionally stable, rigid and readily machinable (preferably with a higher porosity) it should be used to replace this sintered polythene. Experience with the operation of the cell with the current switched on showed, on subsequent dismantling of the cell, that the Avesta SLX 254 stainless steel used for the electrodes was slowly corroding on the anode side, particularly at low current densities. A more oxidation-resistant metal is therefore required for use as an anode in the cell.

7. DIRECTIONS FOR FURTHER WORK

7.1 Investigation of the Performance of Ultrafiltration Membranes in Electric Fields

From the observations recorded in section 5.6, fundamental work on the evaluation of the performance of ultrafiltration membranes in electric fields is the first requirement for the continuation of the development of the narrow-slot electrophoretic separator. From these observations it would appear that, at least in the case of the membrane adjacent to the anode in the cell, the imposed electric field in the separator is causing pinholing in the membrane. Therefore, the first priority for continued work on this project is to isolate and find a solution to this problem. A suggested course of action designed to investigate the membrane behaviour under these conditions is given below.

It is proposed that a test cell of the general form shown in Figure 7.1 be constructed to enable a systematic study of the membrane performance in various electric fields to be undertaken. In this cell the membrane is mounted between the anode and cathode which form the end walls of the cell. The cell should be of sufficient thickness to prevent the gases evolved at the electrodes from coming in contact with the membrane. Initially, the cell should be filled with buffer at the same concentration on both sides of the membrane and the specific surface resistance of the membrane calculated from current/voltage measurements over a range of conditions. This set of observations may possibly give indirect evidence of the onset of membrane breakdown. However a more satisfactory approach might be to add a low

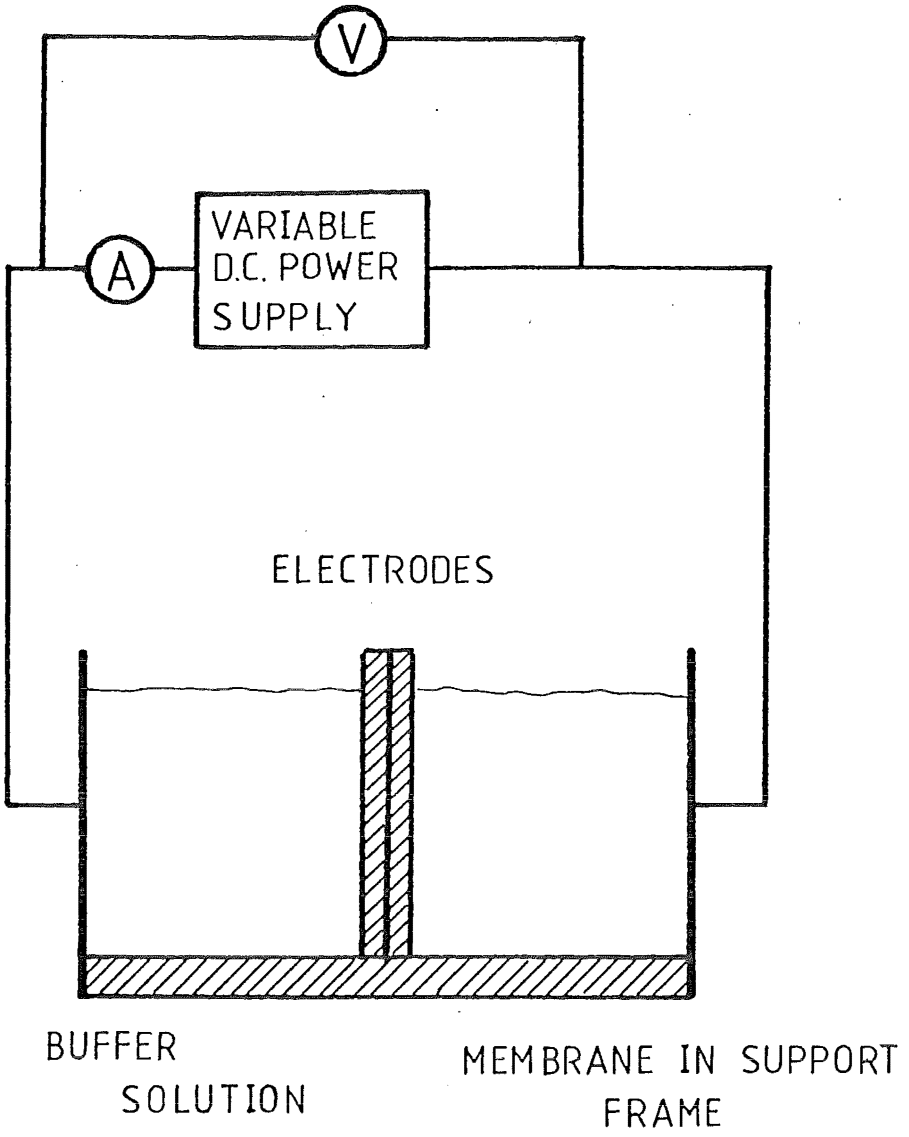

FIGURE 7.1 PROPOSED MEMBRANE TEST CELL

molecular-weight dye to the solution on one side of the membrane and observe the migration of the dye through the membrane. Pinholes should, under these conditions, be expected to be revealed by a locally faster rate of migration through the membrane. A more definite test of membrane integrity, however, would be to use an electrophoretically mobile pigment, which would not be passed by a sound membrane, and observe any evidence of passage of pigment through the membrane.

These experiments should be performed with the membrane facing both the anode and cathode of the test cell and any differences in membrane behaviour noted. The experiments should also be performed with different concentrations of buffer on each side of the membrane and the observed behaviour again noted. In particular, evidence of diode-like behaviour (for example a higher electrical resistance in one direction than the other) would be significant in determining the kinds of actions occurring as solvated ions travel through the membrane. In this way, a test of the hypothesis of section 6.3 of inhibition of hydrated ion flow 'backwards' through the membrane should be possible.

If, as is suspected from the evidence of section 5.6, the D.D.S. GR8-series membranes are failing under the conditions of service imposed by the configuration of the narrow-slot electrophoretic separator, then the above experiments should be repeated with other types of membrane. The selection of such other membranes must be made on the basis of the requirements given in section 4.4. These conditions are somewhat limiting and the only other immediately obvious kind of membrane for this service is the Millipore Corporation PTGC membrane, which appears to

have the necessary chemical resistance and is available in sheet form (M7). However, the technology of synthetic membranes is rapidly changing and other membranes to fit these specifications may become available. A more technically advanced option is to obtain a membrane specifically tailored for this service from a membrane manufacturer. The possibility of locally synthesising such a membrane is ruled out by the complex nature of the manufacture of modern synthetic membranes of high chemical resistance (S7), particularly in large sheets. If this approach is possible, the membrane should preferably be coated directly onto a rigid porous support to enable easier mounting of the membrane in the separator.

7.2 Towards a Mark II Narrow-Slot Continuous Electrophoretic Separator

7.2.1 General Structure

As has been remarked in section 6.4, in general, the use of Perspex for the construction of the main components of the separator frame was found to be satisfactory. However, in order to provide a higher degree of structural rigidity for a mark III version of the separator, the main walls of both the inlet and separating zones should be constructed of, or machined from, thicker sections. In the light of experience in handling the mainframe in particular, it is recommended that a version of this frame should be designed such that the minimum cross-section of any load bearing section of the frame exceeds 10 mm in thickness wherever possible. In some cases, this may not be possible (due to constraints imposed by electrode spacing for example) and in these cases, especially where very thin sections are necessary, the possibility of reinforcement with stainless

steel should be considered.

A particular example of an application of this procedure would be to the bridging sections at the ends of the membrane support frames (see Figure 4.8(ii)). In a case such as this, where the section is in direct contact with the electric field, care would be needed to ensure that the metal itself did not come into direct contact with the electrolyte in the presence of the field, otherwise secondary electrodes could be formed by these metal sections.

As can be seen by the description of the sealing problems encountered with the mark I separator prototype (see section 4.6), the avoidance of long lengths of jointed Perspex is desirable, if not necessary. The techniques evolved to bond the components of the mark II separator (section 4.6.4.2) using meta-cresol as a solvent-welding agent, followed by a six-hour curing procedure at 60^{o}C, was superior to any other jointing technique tried. However, it is recommended that, wherever possible, long sections of the separator be machined from continuous sections of solid material.

7.2.2 Entrance Zone

In general the entrance zone, as modified, performed satisfactorily. As mentioned in the above section, if rebuilt, this zone would benefit in terms of structural stability if thicker external walls were used. It appears that, if Perspex is retained as a material for the internal dividers in this section, the use of a shallow wedge projecting into the stream at right-angles to these dividers will be necessary to ensure accelerating flow throughout this zone. However, since there is no need for these dividers to be transparent, other materials

could be considered for them, allowing these dividers to be thinner, and so reducing the effective change of cross-section caused by 'sharpening' them to a knife edge. The use of stainless steel may possibly lead to problems with stray electric currents causing secondary electrode effects. One of the more modern fibre-reinforced polycarbonate materials would probably be better in this application although some experimentation with the machinability of such substances would be required.

The use of thinner dividers in the entrance zone would also allow a greater number of entry channels, permitting a greater number of streams to be introduced, or allowing the position of the solute input to be more finely controlled. A further consequence of this option is that less of the total duct width is initially filled with the solute stream, giving a larger permissible horizontal transit distance in the cell, to yield finer separations at a single pass.

The glass beads used as a distributing medium at the bottom of each inlet channel have been effective for this purpose. However, these beads are not self-cleaning at the flowspeeds at which the cell operates, so a distributor material less prone to fouling would be an improvement on them. A possible alternative material for this purpose would be solid PTFE spheres or a grid of this same material.

7.2.3 Separating Zone

The use of a thicker cross-section for the Perspex frame for this section has already been discussed in some detail, as has the possibility of selective reinforcement of parts of the structure with stainless steel. These comments also apply to the membrane-support frames. Since at present the only type

of sheet membrane useable as a barrier between the separating duct and the electrode channels is highly flexible, some type of support for the membrane will be essential. In this respect, 'Vyon' porous polythene is less than ideal, and a more rigid and readily machinable, porous membrane support would be desirable. Such a material should be highly and uniformly porous, thin, rigid, machinable to close tolerances and electrically non-conducting as well as not being subject to creep.

This list of conditions is an extremely difficult set to meet and obtaining such a material, particularly in sheets of sufficient size for the separator, would require an extensive survey of the available porous materials. An alternative approach would be to coat the membrane directly onto a rigid porous polymer sheet which could then be directly fixed to the membrane-support frame. This approach would considerably lessen the problems involved in retaining a rigid flat surface facing the separating duct. A second alternative is to redesign the membrane supports and the mainframe of the separating zone to enable the membrane to be clamped around its entire edge (in a similar manner to that used in the D.D.S. plate-and-frame ultrafiltration unit). In practice, this approach would be difficult for a number of reasons. Such a clamping system would necessarily obstruct viewing of the flow through the separating duct which would increase the difficulty of observing the progress of separations. Also, the mechanics of obtaining a satisfactory clamped seal across the ends of the membrane support (the location of the present bridging sections) would be extremely difficult, particularly without obstructing either the electrode solution or solute and buffer flows. It is also by no means certain that a clamped membrane would not flex, as did the

original membrane in the mark I separator.

Ultimately, the design of the membrane supports requires information about the type of membrane used and the conditions of use. Therefore the final design of membrane supports for a mark III separator will depend on the results of the investigation into membrane behaviour.

The corrosion observed on the anode indicates that, for long-term use, the Avesta SLX 254 stainless steel incorporated in the mark II separator is insufficiently oxidation-resistant for this application. The prime requirement for an anode material for the cell is oxidation resistance or passivity of the metal surface at low current densities (of order 30 A m^{-2}). To achieve this type of passive resistance at such low current densities, a relatively inert metal is required; that is, a metal well towards the 'cathodic' end of the Galvanic series. While practical tests would be required to evaluate the performance of particular metals or alloys for this duty, likely metals for service as anodes include titanium-containing alloys and the special electrode formulations such as the rhodium-treated alloys employed in modern chlorine-producing cells (K2). However, since these metals are relatively expensive, it may be better to employ a cheaper anode which is replaced from time to time, bearing in mind that the anode is part of the cell structure and so is required to be machined to a high standard.

7.2.4 Recovery Zone

The recovery zone as modified (see section 4.6.2 and plate 4.4) has performed as expected in tests of the separator so far. It therefore is expected to be satisfactory

for use in a mark III version of the narrow-slot separator.

7.3 Support Services

The support services have been found to perform satisfactorily for the experimental work performed so far. It is therefore expected that these services would work for the operation of a mark III version of the narrow-slot electrophoretic separator.

Implicit in the design of the cell is that it is a continuous-flow device, while the solute carrier buffer and solute supplies are by nature essentially batch devices. Thus, at some point in the further development of this device, continuous-flow solute injection and separated solute recovery from the carrier buffer will be required. This latter would enable recycling of the carrier buffer as well as the electrode solutions, enabling the cell to be operated in a continuous fashion.

POSTFACE

THE POTENTIAL FUTURE FOR THE NARROW-SLOT ELECTROPHORETIC SEPARATOR

The substantial advances in the understanding and manipulation of natural systems, particularly in the areas of biochemistry and microbiology, of the last decade appear to be almost certain to lead to equally large advances in the industrial production of biochemically produced items. The most promising areas for such work appear to be applications in medicine, particularly in the control or correction of genetic disorders. A characteristic aspect of this branch of medical science appears to be the need for specific cellular and biochemical substances in a state of high purity with their biological activity retained. However, medicine is by no means the only area likely to benefit from the availability of specific biochemical substances in a state of high purity. The culture of microorganisms for the production of specific chemical substances under much milder conditions than those normally associated with chemical synthesis is another field likely to advance under the twin forces of advances in the knowledge of biological systems on the one hand and the increasing cost of high-grade energy on the other.

When considering this potential for growth in biologically and biochemically based production, it is clear that, as in the evolution of almost every major facet of industrial development, suitable separation processes will be required. For the reasons given in chapter 1, the separation processes required for biological substances need unusually mild conditions. As previously discussed, electrophoresis is operated under such chemically and physically mild conditions.

Of the electrophoresis techniques reviewed at the outset of this work only two appear to offer reasonable opportunities for continuous separations on the medium to large scale. These are the velocity-gradient stabilised cell developed by Mattock, Aitcheson and Thomson at Harwell (M3) and the narrow-slot cell herein described. A recent publication (X1) shows that the Harwell work has reached an advanced stage and, in spite of the inherent complexity of the device, it appears to offer good separations on a scale not previously available. As demonstrated by this recent analysis, however, the Harwell cell is mechanically complex and requires advanced engineering techniques for its design and construction. Nevertheless it does appear to offer high resolution and, after correct setting up, relatively simple operation.

By contrast, the narrow-slot cell is mechanically simple and easy to scale up, but may not offer as higher resolution as that of the Harwell velocity-gradient stabilised (VGS) unit. There are two possible approaches to this question of resolution in the narrow-slot cell. One is to construct a bank of such cells so that separations are performed on a cascade basis with finer resolutions being provided later in the cascade. Such a cascade would enable interstage adjustment of separating conditions to optimise a particular separation at each stage (for instance by adjustment of pH so that the isoelectric point of one component is reached in a given stage). An alternative and more radical proposal by Strickler (X2) is that the narrow-slot cell should be used in a micro-gravity environment such as an orbiting space laboratory, thereby removing potential thermal disturbances which are density-difference and hence gravity based. Such a

cell would still be subject to electrically induced disturbances to the free flow however.

However, a more rational view is that the two techniques (VGS and narrow-slot) are complementary rather than competitive. The VGS cell should find application where high-resolution, free-flow electrophoresis is required while the narrow-slot cell is better suited to lower resolution applications of higher throughput.

Therefore, considering that the VGS cell has been 10 years in the development since the issue of a patent for the device, it is recommended that work on the narrow-slot cell should be continued in order to resolve the remaining problems with the mechanics of the system and, in particular, the performance of free-span membranes. It appears likely that these problems with membranes can be solved as the electropolarisation chromatography work of Ries and Lightfoot (X3) and Chiang et al (X4) shows that some classes of ultrafiltration membranes can be successfully used in the presence of an electric field without damage. The continuation of this work on the narrow-slot separator is especially significant as the device shows promise of high throughput separations at a relatively low development and construction cost.

SYMBOLS

a	radius (of spherical particle)
A	area
b	slope of the Tafel line
Br	Brinkman number $(\frac{\mu U^2}{k(T_1-T_0)})$
C_i	concentration of component i
C_p	heat capacity at constant pressure
d	depth of duct (also special use in equation 1.36)
D	characteristic length or mean hydraulic diameter
$\frac{D}{Dt}$	total derivative
D_p	particle diameter
D_i	diffusion coefficient of component i
e	electronic charge
E	electric field strength
El	electrophoresis number $(\frac{\mu}{m_i \Delta\phi\rho})$
f	friction force
F_1, F_2, F_3	forces
$f( )$	function of
$\underset{\sim}{f}_e$	electric force
Fr	Froude number $(\frac{U}{gD^2})$
F	Faraday constant
f_{av}	average volume fraction of gas bubbles
g	acceleration due to gravity
$\underset{\sim}{g}$	vector acceleration due to gravity
Gr	Grashoff number $(\frac{\rho^2 \beta g D^3 \Delta T}{\mu^2})$

H_i enthalpy of component i

H_E electrical heating number $\left(\frac{(\Sigma_i K_i x_i)(\Delta\phi)^2 D}{\rho U^3}\right)$

H_{MT} mass flux heat flow number $\left(\frac{H_i(C_1 - C_0)}{\rho U^2}\right)$

h surface heat transfer coefficient

h height of electrode

i current density

I current

$\underset{\sim}{J}$ electric current vector

$\underset{\sim}{j}_i$ mass flux relative to mass averaged velocity

$\underset{\sim}{J}_i$ molar flux relative to mass averaged velocity

j $\sqrt{-1}$

k Boltzman constant

K ratio of channel width to depth (equation 1.38)

K parameter in equation 4.5

k thermal conductivity

K wavelength

K_i specific volumetric conductance of component i

l electrode length

m mobility

m_i mobility of species i

m mass

N_i number of ions of species i

$N_{i\infty}$ number of ions of species i at a large distance

n number of Faradays

Nu Nusselt number $\left(\frac{hD}{k}\right)$

$\underset{\sim}{N}_i$ flux of component i

P pressure

P_m	mean pressure
P	power dissipation
P_v	viscous power dissipation
P_e	electric power dissipation
Pr	Prandtl number $(\frac{C_p \mu}{k})$
Q	total surface charge
Q_x	nett flow in electro-osmosis
$\underset{\sim}{q}$	energy flux
q	heat generation rate
r	radius
R	gas constant
Re	Reynolds number $(\frac{DU\rho}{\mu})$
Ra_{el}	electrical Raleigh number $(\frac{\varepsilon \Delta \phi}{\mu m_i})$
R_i	reaction rate of component i
r_o, r_d	specific electrode resistances
Sc	Schmidt number $(\frac{\mu}{\rho D_i})$
St	Stanton number $(\frac{DU}{D_i})$
T	absolute temperature
t	time
U	velocity
$\underset{\sim}{U}$	vector velocity
U_{el}	electrophoretic velocity
U_{os}	electro-osmotic velocity
V	volume
w	width of duct
w	width of electrode
x, y, z	coordinates

Z_i	charge number of ionic species i
β	coefficient of volume expansion
Δ	difference in
ε	electric permitivity
ζ	electric potential at surface of shear (zeta-potential)
Θ_o, Θ_d	voltage slope terms (equation 4.1)
κ	inverse thickness of the double layer
Λ_i	specific conductance of component i
λ_o, λ_d	resistance terms in equation 4.1
μ	dynamic viscosity
ν	resistivity of gas free electrolyte
ρ	density
ρ_e	space charge density
ρ_p	particle density
ρ_s	solution density
σ_0	surface charge density
$\underset{\approx}{\tau}$	fluid stress tensor
ϕ	electric potential
Φ_v	stress energy component for Newtonian fluid (terms like $(\frac{\partial U_x}{\partial x})^2$
χ	volume fraction of solids in suspension
Ψ	stream function
ψ	parameter for determining current density on electrode (equation 4.1)
ω	frequency

REFERENCES

A1 ABRAMSON H.A. Journal of General Physiology, 12: 469, 1929.

A2 ARCUS A.C. Continuous Zone Electrophoretic Analysis in Free-Flowing Liquid Systems - Towards Large Scale Operation. 1973 (Unpublished).

A3 ATTEN P. and MOREAU R. Acadamie of Sciences, Paris 270 Serie A: 415. 9 Fevrier 1970.

B1 BELL D., BUISSON D.H. and KELSEY J.G. Reverse Osmosis - Ultrafiltration Technology Part 1, N.Z. DSIR 1977 (N.Z. DSIR Report C.D. 2251).

B2 BETCHOV R. and CRIMINALE W.O. Stability of Parallel Flows. New York, Academic Press, 1967.

B3 BIER M. U.S. Patents 2878178 and 3079318.

B4 BIER M. and ALLGYER T.T. Isotachophoresis. In RIGHETTI P.G. VAN OSS C.J. and VANDERHOFF J.W. Eds.Electrokinetics Separation Methods, Amsterdam, Elsevier/ North Holland 1979, p.443.

B5 BIKALES N.M., MARK, H.F. and GAYLORD N.G. Eds. Encyclopedia of Polymer Science and Technology, New York, Wiley, 1968.

B6 BIRD R.B., STEWART W.E. and LIGHTFOOT E.N. Transport Phenomena. New York, Wiley, 1960, Ch.18.

B7 Ibid Section 4.1

B8 Ibid p.62

B9 BLANK F. and VALKO E. Biochemie Zeitung, 195: 220, 1928.

B10 BLOEMENDAL H. High Resolution Techniques In BIER M. Eds. Electrophoresis, Theory, Methods and Applications Vol. II, New York, Academic Press, 1967, p.379.

B11 BOKRIS J.O'M.and CONWAY B.E. Eds. Modern Aspects of Electrochemistry, Vol 5. New York, Plenum Press, 1969.

B12 BOLTZ R.C. and TODD P. Density Gradient Electrophoresis of Cells in a Vertical Column. In RIGHETTI P.G. VAN OSS C.J. and VANDERHOFF J.W. Eds. Electrokinetics Separation Methods, Amsterdam, Elsevier/North Holland 1979, p.229.

B13 BOOTH F. Proceedings of the Royal Society, London, A203: 514, 1950.

B14 BRINTON C.C. and LAUFFER M.A. The Electrophoresis of Viruses, Bacteria and Cells and the Microscope Method of Electrophoresis. In BIER M. Ed. Electrophoresis, Theory, Methods, and Applications Vol. 1, London, Academic Press, 1959, p.427.

B15 BROWN D.R. Nature, 202: 68, 1964.

B16 BUCKENHAM N.R. Investigation into Thermal Instability of Electrophoretic Cells, Christchurch 1977 (University of Canterbury B.E. Project Report 1977).

C1 CARNAHAN B., LUTHER H.A. and WILKES J.O. Applied Numerical Methods. New York, Wiley, 1969, Ch.7.

C2 CHAPMAN D. Philosophical Magazine 25: 475, 1913.

C3 CHRAMBACK A. and NGUYEN N.Y. Preparative Electrophoresis, Isotachophoresis and Electro-focussing on Polyacrylamide Gel. In RIGHETTI P.G., VAN OSS C.J. and VANDERHOFF J.W. Eds. Amsterdam, Elsevier/ North Holland 1979, p.275.

C4 CRANK J. and NICHOLSON P. Proceedings of the Cambridge Philosophical Society 43: 50, 1947.

D1 DE DANSKE SUKKERFABRIKER Sales Literature, 1977.

D2 DORN E. Wieder Annals, 10: 70, 1880.

D3 DUPONT E.I. de NEMOURS & CO. British Patent 642025, 1950.

G1 GIANAZZA E. and RIGHETTI P.G. Electrophoresis in Gels of Graded Porosity and Two Dimensional Techniques. In RIGHETTI P.G., VAN OSS C.J. and VANDERHOFF J.W. Eds. Electrokinetic Separation Methods, Amsterdam, Elsevier/North Holland, 1979, p.293.

G2 GRAHAME D.C. Journal of Chemical Physics, 18: 903, 1950.

G3 GRASSMAN W. and HANNIG K. Hoppe-Seylors Zeitschrift Physiologie Chemie, 292: 32, 1953.

G4 GOUY G. Annals of Physics, 7(9): 129, 1917.

G5 GOUY G. Journal of Physics, 9(4): 457, 1910.

H1 HANNIG K. Preparative Electrophoresis. In BIER M. Ed. Electrophoresis Theory, Methods and Applications, Vol. II. New York, Academic Press, 1967, p.423.

H2 HANNIG K. et al. Hoppe-Seylors Zeitschrift Physiologie Chemie, 356: 1209, 1975.

H3 HANNIG K. et al. Hoppe-Seylors Zeitschrift Physiologie Chemie, 358: 753, 1977.

H4 HARDY W.B. Proceedings of the Royal Society, London, 66: 110, 1900.

H5 HENRY D.C. Proceedings of the Royal Society, London, A133: 106, 1931.

H6 HEWISH J.R. and BRIGNELL J.E. Journal of Physics & Applied Physics, 5: 746, 1972.

H7 HJERTEN S. Free Zone Electrophoresis, Upsalla, Almquist & Wiksells, 1967. (Also in, Chromatographic Reviews, 2: 122, 1967.)

H8 HUKEL E. Physik Zeitschrift 28: 277, 1924.

K1 de KEIZER A., VAN DER DRIFT W.P.J.T. and OVERBEEK J.Th.G. Biophysical Chemistry, 3: 107, 1975.

K2 KIRK-OTHENIER Encyclopedia of Chemical Technology (3rd Ed) Vol. I, New York, Wiley, 1978, p.806.

K3 KOENIG P. Actas III, Congress Sudam. Chima 2: 334, 1937.

K4 KOLIN A. Kinematic Stabilisation of Continuous Flow Electrophoresis Against Thermal Convection. Proceedings of the National Academy of Science, 51: 1110, 1964.

K5 KOLIN A. Continuous Electrophoretic Fractionation Stabilised by Electromagnetic Rotation. Proceedings of the National Academy of Science, 46: 509, 1960.

K6 KOLIN A. Endless Belt Continuous-Flow Deviation Electrophoresis. In RIGHETTI P.G., VAN OSS C.J. and VANDERHOFF J.W. Eds. Electrokinetics Separation Methods. Amsterdam Elsevier/North Holland, 1979, p.169.

K7 KUNKEL H.G. and TISELIUS A. Journal of General Physiology, 35: 89, 1952.

K8 KUNKEL H.G. and TRAUTMAN R. Zone Electrophoresis in Various Types of Supporting Media. In BIER M. Ed. Electrophoresis, Theory, Methods and Applications, Vol. I, New York, Academic Press, 1959, p.225.

L1 LACROIX J.C., ATTEN P. and HOPFINGER E.J. Journal of Fluid Mechanics, 69(3): 539, 1975.

L2 LANDAU L.D. and LIFSHITZ E.M. Fluid Mechanics, London, Pergamon Press, 1959, Chapter 3.

L3 LOEB A.L., OVERBEEK J.Th.G. and WIERSEMA P.H. The Electrical Double Layer Around a Spherical Colloidal Particle. Cambridge Massachusetts, Massachusetts Institute of Technology Press, 1961.

L4 LONGSWORTH G. Moving Boundary Electrophoresis Theory and Practice. In BIER M. Ed. Electrophoresis Theory, Methods and Applications, Vol. I, London, Academic Press, 1959, p.91.

L5 LYKLEMA J. Journal of Colloid and Interfacial Science, 58: 242, 1977.

M1 MADSEN, R.F. Hyperfiltration and Ultrafiltration in Plate and Frame Systems. Amsterdam, Elsevier, 1977.

M2 MALKUS W.V.R. and VERONIS G. Physics of Fluids, 4: 13, 1961.

M3 MATTOCK P., AITCHESON G.F. and THOMSON A.R. The Development of Electrophoresis for Production Scale Use. Institution of Chemical Engineers Symposium Series 51: 55, 1978.

M4 McCAN G.A. et al. Separation of Latex Particles According to Size by Continuous Electrophoresis. Separation and Purification Methods, 2(1): 153, 1973.

M5 METHIS B. and ECKERT E.R.G. Journal of Heat Transfer, 86: 295, 1964.

M6 MICALE F.J., VANDERHOFF J.W. and SNYDER R.S. Analysis of the Apollo 16 Free-Fluid Electrophoresis Experiment. Separation and Purification Methods 5(2): 361, 1976.

M7 MILIPORE Catalogue and Purchasing Guide 1978/1979. Bedford Massachussetts, Milipore Intertech. Inc.

M8 MURPHY E.A. Transactions of the Institution of the Rubber Industry, 12: 173, 1942.

N1 NEE T.W. Journal of Chromatography 105: 231, 1975.

N2 NIELSEN W.K. and WAGNER J. Novel Developments in Ultra- and Hyperfiltration as Applied to the Biochemical Industries. Naksov. D.D.S. Ro. Division Publication, 1976.

O1 OVERBEEK J.Th.G. and BIJSTERBOSCH B.H. The Electrical Double Layer and the Theory of Electrophoresis. In RIGHETTI P.G., VAN OSS C.J. and VANDERHOFF J.W.Eds Electrokinetic Separation Methods. Amsterdam, Elsevier/North Holland, 1979, p.1.

O2 OVERBEEK J.Th.G. and LIJKLEMA J. Electric Potentials in Colloidal Systems. In BIER M. Ed. Electrophoresis Theory, Methods and Applications, Vol. I, London, Academic Press, 1959, p.1.

O3 OVERBEEK J.Th.G. Kolloid Beiheft 54: 287.

O4 OVERBEEK J.Th.G. Philips Research Reports, 1: 315, 1946.

O5 OVERBEEK J.Th.G. Electrokinetic Phenomena. In KRUYT H. Ed. Colloid Science, Vol. I, Amsterdam, Elsevier, 1952.

P1 PAULI W. Biochemie Zeitung, 152: 365, 1924.

P2 PERRIN D.D. and DEMPSEY B. Buffers for pH and Metal Ion Control, London, Chapman and Hall, 1974.

P3 PERRY R.H. Chemical Engineers Handbook, 5th Ed., New York McGraw-Hill, 1973, Ch.23.

P4 PHILIP J.R. and WOODING R.A. Journal of Chemical Physics. 52: 953, 1970.

P5 PHILPOT J.St.L. The Use of Thin Layers in Electrophoretic Separation. Transactions of the Faraday Society, 36: 38, 1940.

P6 PHILPOT J.St.L. British Patents 1150722, 1969, and 1186184, 1970.

P7 PICTON H. and LINDER S.E. Journal of the Chemical Society, 71: 568, 1897.

P8 POURBAIX M. Atlas of Electrochemical Equilibria in Aqueous Solutions, Oxford, Pergamon Press, 1966.

Q1 QUINKE G. Poggendorff's Annalen der Physik, 113: 513, 1861.

R1 RANDKIVI A.J. and CALLANDER R.A. Advanced Fluid Mechanics: An Introduction, London, Edward Arnold, 1975 Ch.4.

R2 REUSS M. Memories de la Societe Imperiale des Naturalistes des Moscou, 2: 327, 1809.

R3 RIGHETTI P.G. Isoelectric Focussing. In RIGHETTI P.G., VAN OSS C.J. and VANDERHOFF J.W. Eds. Electrokinetic Separation Methods, Amsterdam, Elsevier/North Holland, 1979, p.389.

R4 ROSS S. and LONG R.F. Electrophoresis as a Method of Investigating the Double Layer. Industrial and Engineering Chemistry, 61(10): 58, 1969.

S1 SCHNEIDER J.M. and WATSON P. Physics of Fluids, 13(8): 1948, 1970.

S2 SHEPPARD M.P. Investigation of Electro-hydrodynamic Stability of Electrophoretic Buffer Solutions. Christchurch 1975 (University of Canterbury B.E. Project Report, 1975).

S3 SIEDER E. and TATE G. Industrial and Engineering Chemistry, 28: 1429, 1936.

S4 SMITH G.D. Numerical Solutions of Partial Differential Equations: Finite Difference Methods. Oxford, Oxford University Press, 1978, Ch4.

S5 Ibid, Ch.2.

S6 SMITH I. Zone Electrophoresis on Paper, Thin Layers, Pevikon Block. In RIGHETTI P.G., VAN OSS C.J. and VANDERHOFF J.W. Eds. Electrokinetic Separation Methods, Amsterdam, Elsevier/North Holland, 1979, p.33.

S7 SOURIRAJAN S. Ed. Reverse Osmosis and Synthetic Membranes. Ottawa, National Research Council of Canada, 1977.

S8 STERN O. Zeitschrift Electrochemie, 30: 508, 1924.

S9 STIGTER D. Journal of Physical Chemistry, 82(12): 1417, 1978.

S10 STRICKLER A., KAPLAN A. and VIGH E. Microchemical Journal, 10: 529, 1966.

S11 STRICKLER A. and SACKS T. Annals of the New York Academy of Science, 209: 497, 1973.

T1 TAYLOR G.I. Dispersion of Soluble Matter in Solvent Flowing Slowly Through a Tube. Proceedings of the Royal Society, London, A219: 186, 1953.

T2 TILLMAN M.S. Electro-hydrodynamic Stability in Conducting Solutions. Christchurch, 1976 (University of Canterbury B.E. Project Report, 1976).

T3 TISELIUS A. Transactions of the Faraday Society, 33: 524, 1937.

T4 TISON R.P. A Simple Transport Apparatus for Electrophoresis Journal of Colloidal and Interfacial Science, 52(3): 611, 1975.

T5 TOBIAS C.W. and WIJSMAN R. Journal of the Electrochemical Society, 100: 459, 1953.

T6 TOBIAS C.W. Journal of the Electrochemical Society, 106(9): 833, 1959.

T7 TURNBULL R.J. Physics of Fluids, 11(12): 2589, 1968.

V1 VANDERHOFF J.W. and VAN OSS C.J. Electrophoretic Separation of Biological Cells in Microgravity. In RIGHETTI P.G., VAN OSS C.J. and VANDERHOFF J.W. Eds. Electrokinetic Separation Methods, Amsterdam, Elsevier/North Holland, 1979, p.257.

V2 VANDERHOFF J.W., MICALE F.J. and KRUMRINE P.H. Continuous Flow Electrophoresis. In RIGHETTI P.G., VAN OSS C.J. and VANDERHOFF J.W. Eds., Electrokinetic Separation Methods, Amsterdam, Elsevier/North Holland, 1979, p.121.

V3 VAN OSS C.J. and FIKE R.M. Simplified Cell Microelectrophoresis with Uniform Electro-osmotic Backflow. In RIGHETTI P.G., VAN OSS C.J. and VANDERHOFF J.W. Eds., Electrokinetic Separation Methods. Amsterdam, Elsevier/North Holland, 1979, p.111.

V4 VERMULEN T. et al. Design of Theory and Separations in Preparative-Scale Continuous-Flow Electrophoresis. Industrial and Engineering Chemistry: Process Design and Development, 10(1): 91, 1971.

V5 VISCA M., ARDIZZONE S. and FORMARO L. Journal of Colloidal and Interfacial Science, 66(1): 95, 1978.

V6 VON SMOLUCHOWSKI M. Physik Chemie, 92: 129, 1918.

V7 VANDERHOFF J.W. and MICALE F.J. Influence of Electro-osmosis. In RIGHETTI P.G., VAN OSS C.J. and VANDERHOFF J.W. Eds. Electrokinetic Separation Methods, Amsterdam Elsevier/North Holland, 1979, p.81.

W1 WALDROP Interferon Production Off to a Good Start. Chemical and Engineering News, August 13, 1979, p.24.

W2 WEAST, R.C. Ed. Handbook of Chemistry and Physics, 52nd Edn. Cleveland, The Chemical Rubber Co., 1972, p.F218.

W3 WEIRSEMA P.H., LOEB A.L. and OVERBEEK J.Th.G. Journal of Colloidal and Interfacial Science, 22: 78, 1966.

W4 WELTY J.R., WILSON R.E. and WICKS C.E. Fundamentals of Momentum, Heat and Mass Transfer, New York, Wiley, 1969.

W5 WUNDERLY C.H. Paper Electrophoresis. In BIER M. Ed. Electrophoresis Theory, Methods and Applications Vol. I, London, Academic Press, 1959, p.179.

X1 MATTOCK P., AITCHISON G.F. and THOMSON A.R. Velocity Gradient Stabilised Continuous Flow Electrophoresis. Separation and Purification Methods 9(1): 1 (1980).

X2 STRICKLER A. Deflected Lamina Electrophoresis: High Performance Separation of Biologicals in Space. A.I.A.A. Journal 16(5): 463 (1978).

X3 RIES J.F.G. and LIGHTFOOT E.N. Electropolarisation Chromatography. American Institution of Chemical Engineers Journal, 22(4), 779 (1976).

X4 CHIANG A.S. et al. Preliminary Experimental Survey of Hollow-Fibre Electropolarisation Chromatography (Electrical Field Flow Fractionation) for Protein Fractionation. Separation Science and Technology, 14(6), 453 (1979).

```
B6700/B7700  F O R T R A N  C O M P I L A T I O N  M A R K  2.6.001  THURSDAY, 12/23/76  11:36 AM

C     SOLUTION OF HEAT TRANSFER EQUATION  DUFORT-FRANKEL METHOD USING                C  000:0000:5
C     RECURSIVE ALGORITHM OF CARNAHAN LUTHER &WILKES                                C  000:0000:5
                                                                                     START OF SEGMENT 002
      DIMENSION XAC(41),TEMP(2,41),BETA(41),GAMA(41)                                 C  002:0000:0
C     CELL EXTENDS FROM X=-1 TO X=+1.                                                C  002:0000:0
C     VALUES FOR INCREMENTS & COORDINATES.                                           C  002:0000:0
      Z=0.                                                                           C  002:0000:0
      DELX=.05                                                                       C  002:0000:4
      DELZ=.25                                                                       C  002:0002:3
      RE=100                                                                         C  002:0004:3
      PR=6.8                                                                         C  002:0005:2
C     TEMP. DIFF=10    COND=.001     VOLT DIFF=7.5 V                                 C  002:0007:3
      HE=1406                                                                        C  002:0007:3
      BR=3.33E-6                                                                     C  002:0008:3
      NU=0.                                                                          C  002:000A:3
      TB=0.                                                                          C  002:000B:2
C     CALCULATION ASSUMES 5MM WIDE 2DIMENSIONAL CELL                                 C  002:000C:0
C     BASE LENGTH=2.5 MM                                                             C  002:000C:0
C     SETS UP & WRITES CELL WIDTH REFERENCE                                          C  002:000C:0
      XAC(1)=-1.                                                                     C  002:000C:0
      DO 10 I=2,41                                                                   C  002:000D:1
   10 XAC(I)=XAC(I-1)+DELX                                                           C  002:000E:0
      WRITE(6,100)                                                                   C  002:0013:1
                                                                                     FIB IS 0006 LONG
      WRITE(6,101)(XAC(I),I=1,41,2)                                                  C  002:0017:2
      DO 20 J=1,41                                                                   C  002:0023:2
   20 TEMP(1,J)=0.                                                                   C  002:0024:0
      WRITE(6,102)Z,(TEMP(1,J),J=1,41,2)                                             C  002:0028:2
   25 Z=Z+DELZ                                                                       C  002:0036:2
      VEL=1.5/DELZ                                                                   C  002:0037:4
      REPRI=1./(RE*PR*DELX*DELX)                                                     C  002:003A:0
      ELHE=BR*HE/PR                                                                  C  002:003C:4
C     BOUNDARY AT X=-1                                                               C  002:003E:3
   29 BETA(1)=VEL*(1-.820*.820)-REPRI                                                C  002:003E:3
      TEMP(2,1)=((4*TEMP(1,2)-TEMP(1,3))/(2*DELX)+NU*TB)/(3/(2*DELX)+NU)             C  002:0044:1
      GAMA(1)=(.5*REPRI*TEMP(1,1)+(VEL*(1-XAC(2)*XAC(2))-REPRI)*TEMP(1,2             C  002:004B:0
     9)+.5*REPRI*TEMP(1,3)+TEMP(2,1)*.5*REPRI+ELHE)/BETA(1)                          C  002:0050:4
      DO 50 J=2,40                                                                   C  002:0059:1
   50 BETA(J)=(VEL*(1-XAC(J)*XAC(J))+REPRI)-REPRI*REPRI*.25/BETA(J-1)                C  002:005A:0
      BETA(41)=(VEL*(1-XAC(40)*XAC(40))+REPRI)-REPRI*REPRI*.25/BETA(40)              C  002:0065:0
      DO 51 J=2,40                                                                   C  002:006C:2
   51 GAMA(J)=(TEMP(1,J-1)*.5*REPRI+TEMP(1,J)*(VEL*(1-XAC(J)*XAC(J))-REP            C  002:006E:0
     9RI)+TEMP(1,J+1)*.5*REPRI+ELHE+.5*REPRI*GAMA(J-1))/BETA(J)                      C  002:0077:2
C     BOUNDARY AT X=1                                                                C  002:0083:3
      TEMP(2,41)=((4*TEMP(2,40)-TEMP(2,39))/(2*DELX)+NU*TB)/(3/(2*DELX)+             C  002:0083:3
     9NU)                                                                            C  002:0089:4
      DO 52 J1=1,39                                                                  C  002:006A:3
      J=41-J1                                                                        C  002:008C:0
   52 TEMP(2,J)=GAMA(J)+(.5*REPRI*TEMP(2,J+1))/BETA(J)                               C  002:0080:3
      TEMP(2,1)=((4*TEMP(2,2)-TEMP(2,3))/(2*DELX)+NU*TB)/(3/(2*DELX)+NU)             C  002:0097:5
      WRITE(6,102)Z,(TEMP(2,J),J=1,41,2)                                             C  002:009E:4
      Z=Z+DELZ                                                                       C  002:00AD:2
      IF(Z.GE.250) GO TO 99                                                          C  002:00AE:4
C     RESETS ARRAY FOR NEXT STEP                                                     C  002:00AF:4
      DO 35 J=1,41                                                                   C  002:00AF:4
      J1=42-J                                                                        C  002:00B1:0
   35 TEMP(1,J)=TEMP(2,J1)                                                           C  002:00B2:3
      GO TO 29                                                                       C  002:00B8:1
   99 WRITE(6,101)(XAC(I),I=1,41,2)                                                  C  002:00B8:4
      STOP                                                                           C  002:00C5:2
  100 FORMAT(30X,'NORMALISED DISTANCE ACROSS CELL',///)                              C  002:00C6:1
  101 FORMAT(5X,21F6.3,//)                                                           C  002:00C6:1
  102 FORMAT(1X,F5.1,21F6.4,///)                                                     C  002:00C6:1
      END                                                                            C  002:00C6:1
                                                                                     SEGMENT 002 IS 00D4 LONG
```

B6700 FORTRAN COMPILATION MARK 3.0.180 TUESDAY, 10/21/80 10:58 AM

MASS TRANSFER

```
C     ********                                                          C  000:0000:5
C     SOLUTION OF MASS TRANSFER TRANSPORT PHENOMENA TYPE EQUATIONS      C  000:0000:5
C     FOR CONTINUOUS FLOW ELECTROPHORESIS USING FINITE DIFFERENCE       C  000:0000:5
C     METHODS & THOMAS ALGORITHM                                        C  000:0000:5
C     *********                                                         C  000:0000:5
                                                                        START OF SEGMENT 002
      DIMENSION XAC(203), CONC(2,203), VEL(203), A(203), B(203), C(203),C  002:0000:0
     9D(203), VA(203)                                                   C  002:0000:0
C     ********                                                          C  002:0000:0
C     INITIALISATION OF INCREMENTS, COORDINATES & ASSIGNMENT OF         C  002:0000:0
C     DIMENSIONLESS GROUPS                                              C  002:0000:0
C     CALCULATION ASSUMES 5MM WIDE CELL, BASE LENGTH = 2.5MM            C  002:0000:0
C     *********                                                         C  002:0000:0
      Z=0.                                                              C  002:0000:0
      XAC(2)=-1.                                                        C  002:0000:4
      DELZ=0.25                                                         C  002:0001:5
      DELX=0.05                                                         C  002:0003:1
      N=2/DELX+3                                                        C  002:0005:3
      SC=1.0E4                                                          C  002:0007:3
      PE=10.                                                            C  002:0008:3
      RE=200                                                            C  002:0009:2
      DIMENSION ZRED(40)                                                C  002:000A:1
      READ(5,110)(ZRED(J),J=1,90)                                       C  002:000A:1
                                                                        FIB IS 0006 LONG
  110 FORMAT(8F10.7)                                                    C  002:0017:2
      WRITE(6,107)(ZRED(J),J=1,N-3)                                     C  002:0017:2
                                                                        FIB IS 0006 LONG
  107 FORMAT(1X,8F10.8,///)                                             C  002:0024:2
C     **********                                                        C  002:0024:2
C     EL= VISCOSITY/(MOBILITY*ELECTRIC FEILD*DENSITY)                   C  002:0024:2
C     **********                                                        C  002:0024:2
C     ********                                                          C  002:0024:2
C     SETS UP CELL WIDTH REFERENCE, VELOCITY PROFILE & INITIAL          C  002:0024:2
C     CONCENTRATION PROFILE                                             C  002:0024:2
C     **********                                                        C  002:0024:2
      DO 10 I=3,N-1                                                     C  002:0024:2
   10 XAC(I)=XAC(I-1)+DELX                                              C  002:0028:3
      K1=2*(N-4)/5                                                      C  002:002C:0
      DO 20 J=2,K1-4                                                    C  002:002E:2
   20 CONC(1,J)=0.0                                                     C  002:0032:4
      CONC(1,K1-3)=0.01                                                 C  002:0035:2
      CONC(1,K1-2)=0.1                                                  C  002:0039:1
      CONC(1,K1-1)=0.5                                                  C  002:003D:1
      K2=3*(N-1)/5                                                      C  002:0041:1
      DO 17 J=K1,K2                                                     C  002:0043:3
   17 CONC(1,J)=1.0                                                     C  002:0045:0
      CONC(1,K2+1)=0.5                                                  C  002:0049:2
      CONC(1,K2+2)=0.1                                                  C  002:004C:1
      CONC(1,K2+3)=0.01                                                 C  002:0050:1
      DO 15 J=K2+4,N-1                                                  C  002:0054:1
   15 CONC(1,J)=0.0                                                     C  002:0058:3
      SUM1=0.5*(CONC(1,2)+CONC(1,N-1))                                  C  002:005B:1
      DO 16 J=3,N-2                                                     C  002:0060:1
   16 SUM1=SUM1+CONC(1,J)                                               C  002:0064:4
      SUM1=SUM1*DELX                                                    C  002:0067:5
      DO 30 J=2,N-1                                                     C  002:0069:1
   30 VEL(J)=1.5*(1.-XAC(J)*XAC(J))                                     C  002:006D:3
      WRITE(6,100)RE,EL,SC                                              C  002:0073:2
      WRITE(6,101)                                                      C  002:0076:2
      K3=N/20.+.5                                                       C  002:0081:2
      WRITE(6,102)(VEL(I),I=2,N-1,K3)                                   C  002:0084:5
      WRITE(6,102)(XAC(I),I=2,N-1,K3)                                   C  002:0091:2
      WRITE(6,104)Z                                                     C  002:009E:2
      WRITE(6,105)(CONC(1,J),J=2,N-1)                                   C  002:00A5:2
      DO 35 J=2,N-1                                                     C  002:00B2:2
   35 VEL(J)=VEL(J)/DELZ                                                C  002:00B6:3
      ALFA=0.0001                                                       C  002:00B9:1
      BALFA=1.+ALFA*ALFA                                                C  002:00BB:3
      RSD=RE*SC*DELX*DELX                                               C  002:00BD:0
      Z=Z+DELZ                                                          C  002:00BF:2
      ICOUNT=1                                                          C  002:00C0:4
C     **********                                                        C  002:00C1:2
C     CRANK-NICHOLSON FINITE DIFFERENCE METHOD FOR DIFFUSION            C  002:00C1:2
C     *******                                                           C  002:00C1:2
      A(1)=0.0                                                          C  002:00C1:2
```

```
      A(2)=-2./(RSD*BALFA*(1.+ALFA))                                    C  002:00C2:2
      A1=-0.5/RSD                                                       C  002:00C5:3
      DO 43 J=3,N-2                                                     C  002:00C8:1
   43 A(J)=A1                                                           C  002:00CC:4
      A(N-1)=-2.*ALFA/(RSD*BALFA*(1.+ALFA))                             C  002:00CE:5
      A(N)=1.                                                           C  002:00D3:1
      B(1)=-1.0                                                         C  002:00D4:4
      B(2)=VEL(2)+2./(RSD*BALFA)                                        C  002:00D5:5
      DO 53 J=3,N-2                                                     C  002:00D8:4
   53 B(J)=VEL(J)+1./RSD                                                C  002:00DC:4
      B(N-1)=VEL(N-1)+2./(RSD*BALFA)                                    C  002:00E0:2
      B(N)=-1.                                                          C  002:00E4:3
      C(1)=1.0                                                          C  002:00E6:1
      C(2)=-2.*ALFA/(RSD*BALFA*(1.+ALFA))                               C  002:00E7:1
      C1=-0.5/RSD                                                       C  002:00EA:5
      DO 63 J=3,N-2                                                     C  002:00ED:1
   63 C(J)=C1                                                           C  002:00F1:4
      C(N-1)=-2./(RSD*BALFA*(1.+ALFA))                                  C  002:00F3:5
      C(N)=0.0                                                          C  002:00F7:4
   82 CONTINUE                                                          C  002:00F9:1
C     **********                                                        C  002:00F9:1
C     **********                                                        C  002:00F9:1
C     METHOD OF CHARACTERISTICS BASED CALCULATION TO PROVIDE            C  002:00F9:1
C     ELECTROPHORESIS SHIFT                                             C  002:00F9:1
C     **********                                                        C  002:00F9:1
      CONC(1,2)=CONC(1,2)+CONC(1,3)*ZRED(1)                             C  002:00F9:1
      DO 46 J=3,N-2                                                     C  002:00FC:0
   46 CONC(1,J)=CONC(1,J)*(1.-ZRED(J-1))+CONC(1,J+1)*ZRED(J-2)          C  002:0100:4
      CONC(1,N-1)=CONC(1,N-1)*(1.-ZRED(N-3))                            C  002:0107:5
      CONC(1,1)=CONC(1,2)                                               C  002:010B:5
      CONC(1,N)=CONC(1,N-1)                                             C  002:010D:2
C     ABOVE ARE LHS TERMS OF EQUATION                                   C  002:0111:0
C     BELOW ARE RHS TERMS OF EQUATION                                   C  002:0111:0
C     **********                                                        C  002:0111:0
      D(1)=CONC(1,1)=CONC(1,2)                                          C  002:0111:0
      D(2)=CONC(1,1)*2./(RSD*BALFA*(1.+ALFA))+CONC(1,2)*(VEL(2)-2./     C  002:0113:1
     9(RSD*BALFA))+CONC(1,3)*2.*ALFA/(RSD*BALFA*(1.+ALFA))              C  002:0118:1
      DO 73 J=3,N-2                                                     C  002:011D:3
   73 D(J)=0.5*CONC(1,J-1)/RSD+(VEL(J)-1./RSD)*CONC(1,J)+0.5*CONC(1,J+1)C  002:0121:4
     9/RSD                                                              C  002:0120:1
      D(N-1)=CONC(1,N-2)*2.*ALFA/(RSD*BALFA*(1.+ALFA))+CONC(1,N-1)*     C  002:012E:4
     9(VEL(N-1)-2./(RSD*BALFA))+CONC(1,N)*2./(RSD*BALFA*(1.+ALFA))      C  002:0136:1
      D(N)=CONC(1,N)=CONC(1,N-1)                                        C  002:013D:3
      CALL THOMAS(N,A,B,C,D,VA)                                         C  002:0142:2
      DO 75 J=1,N                                                       C  002:0146:5
   75 CONC(2,J)=VA(J)                                                   C  002:014B:0
      SUM2=0.5*(CONC(2,2)+CONC(2,N-1))                                  C  002:0140:0
      DO 78 J=3,N-2                                                     C  002:0152:1
   78 SUM2=SUM2+CONC(2,J)                                               C  002:0156:4
      SUM2=SUM2*DELX                                                    C  002:0159:4
      RATIO=SUM1/SUM2                                                   C  002:015B:0
      DO 85 J=2,N-1                                                     C  002:015C:2
   85 CONC(2,J)=CONC(2,J)*RATIO                                         C  002:0160:3
      IF(ICOUNT.NE.20) GO TO 91                                         C  002:0163:4
      WRITE(5,104) Z                                                    C  002:0165:0
      WRITE(5,105)(CONC(2,J),J=1,N)                                     C  002:016B:2
      SUM=0.5*(CONC(2,2)+CONC(2,N-1))                                   C  002:0178:2
      DO 79 J=3,N-2                                                     C  002:017D:1
   79 SUM=SUM+CONC(2,J)                                                 C  002:0181:4
      SUM=SUM*DELX                                                      C  002:0184:4
      WRITE(5,106)SUM                                                   C  002:0186:0
  100 FORMAT(1X,F7.3////)                                               C  002:018C:2
      ICOUNT=0                                                          C  002:018C:2
   91 Z=Z+DEL_Z                                                         C  002:0190:0
      ICOUNT=ICOUNT+1                                                   C  002:018E:2
      DO 80 J=1,N                                                       C  002:01AF:4
   80 CONC(1,J)=CONC(2,J)                                               C  002:0191:0
         IF(Z.GE.3.01) GO TO 99                                         C  002:0196:4
      GO TO 82                                                          C  002:0198:1
   99 WRITE(5,103)(XAC(I),I=2,N-1,K3)                                   C  002:01A8:4
  100 FORMAT(1HX,'LARGE SCALE ELECTROPHORESIS SIMULATION  RE = ',F4.0,   C  002:01A5:2
     9' EL = ',F5.2,' SC = ',F7.2////)                                  C  002:01A5:2
  101 FORMAT(20X,'NORMALISED VELOCITY PROFILE ',//)                     C  002:01A5:2
  102 FORMAT(5X,21F6.3,/////)                                           C  002:01A5:2
  103 FORMAT(5X,21F6.3,/)                                               C  002:01A5:2
  104 FORMAT(1X,F5.1)                                                   C  002:01A5:2
  105 FORMAT(6X,15F8.5,//)                                              C  002:01A5:2
      STOP                                                              C  002:01A5:2
      END                                                               C  002:01A6:1
                                                                  SEGMENT 002 IS 01C2 LONG
```

```
                                                                        START OF SEGMENT 006
      SUBROUTINE THOMAS(N,A,B,C,D,VA)                                 C  006:0000:0
C     **********                                                      C  006:0000:0
C     SUBROUTINE PROVIDES THOMAS ALGORITHM SOLUTION(VA) OF N*N        C  006:0000:0
C     TRIDIAGONAL MATRIX WITH LHS TERMS A,B,C & RHS TERM D            C  006:0000:0
C     **********                                                      C  006:0000:0
      DIMENSION A(N),B(N),C(N),D(N),VA(N),BETA(203),GAMA(203)         C  006:0000:0
      BETA(1)=B(1)                                                    C  006:0000:0
      DO 10 J=2,N                                                     C  006:0001:3
   10 BETA(J)=B(J)-A(J)*C(J-1)/BETA(J-1)                              C  006:0003:0
      GAMA(1)=D(1)/BETA(1)                                            C  006:000C:5
      DO 20 J=2,N                                                     C  006:000F:0
   20 GAMA(J)=(D(J)-A(J)*GAMA(J-1))/BETA(J)                           C  006:0010:0
      VA(N)=GAMA(N)                                                   C  006:0019:1
      DO 30 J1=1,N-1                                                  C  006:001C:0
      J=(N-J1)                                                        C  006:0020:3
   30 VA(J)=GAMA(J)-C(J)*VA(J+1)/BETA(J)                              C  006:0022:0
      RETURN                                                          C  006:0029:3
      END                                                             C  006:002A:0
                                                                   SEGMENT 006 IS 0032 LONG
```